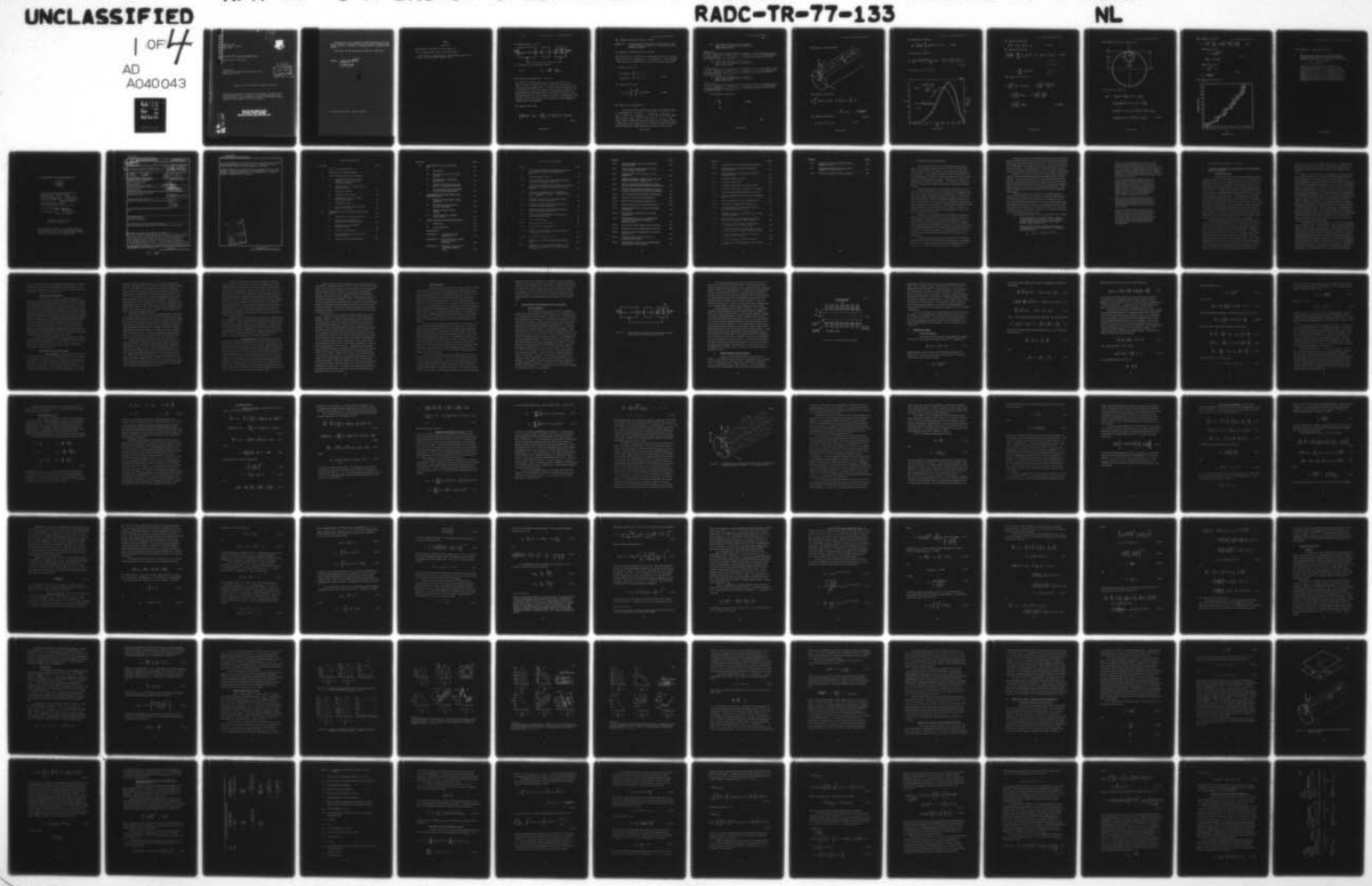
AD-A040 043 HUGHES RESEARCH LABS MALIBU CALIF F/G 9/5
MILLIMETER WAVE UBITRON DEVELOPMENT PHASE I.(U)
APR 77 J M BAIRD, S SENSIPER, K AMBOSS F30602-76-C-0215
UNCLASSIFIED RADC-TR-77-133 NL

1 OF 4
AD
A040043

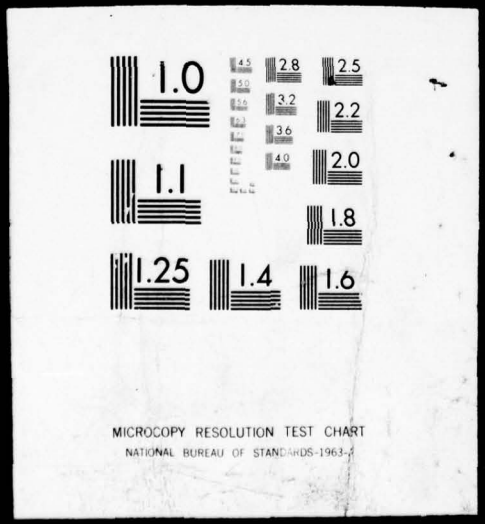


SIFIED

1 OF 4

AD

A040043



AD A040043

RADC-TR-77-133
Final Technical Report
April 1977

MILLIMETER WAVE UBITRON DEVELOPMENT PHASE I

Hughes Research Laboratories

DDC
RECEIVED
JUN 1 1977
A

Sponsored by
Defense Advanced Research Projects Agency (DoD)
ARPA Order No. C192

Approved for public release; distribution unlimited.

The views and conclusions contained in this document are those of the authors and should not be interpreted as necessarily representing the official policies, either expressed or implied, of the Defense Advanced Research Projects Agency or the U. S. Government.

**ROME AIR DEVELOPMENT CENTER
AIR FORCE SYSTEMS COMMAND
GRIFFISS AIR FORCE BASE, NEW YORK 13441**

AD No.____
DDC FILE COPY

MILLIMETER WAVE UBITRON DEVELOPMENT PHASE I

This report has been reviewed by the RADC Information Office (OI) and is releasable to the National Technical Information Service (NTIS). At NTIS it will be releasable to the general public, including foreign nations.

This report has been reviewed and approved for publication.

APPROVED: R. Hunter Chilton

R. HUNTER CHILTON
Project Engineer

Do not return this copy. Retain or destroy.

ERRATA

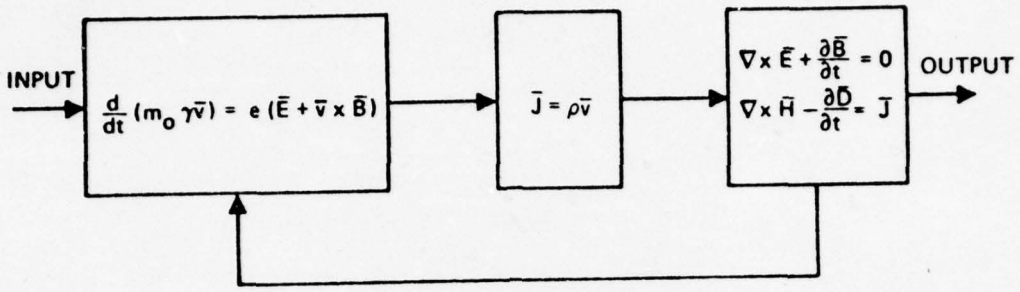
May 1977

Errata pages for RADC-TR-77-133, dated April 1977

Title: Millimeter Wave Ubitron Development Phase I

The corrections contained in the attached ERRATA pages should be made to Technical Report, RADC-TR-77-133.

P13 Replace Figure II-1 with:



P21 Replace the 2nd line above 2-19a with:

$$\Theta = \theta \qquad V_\Theta = R\frac{d\Theta}{dT} = \frac{\beta_m}{\omega R_b} v_\theta$$

P22 Replace the paragraph under 2-19b with:

r_a is the r.f. waveguide tube radius, r_b the beam radius at the entrance plane (see Figure II-2), B_o is the average or dc value of the axial z directed magnetic field, ω_c the usual cyclotron frequency, and γ_c the ratio of the cyclotron frequency to the operating frequency. A few additional normalizing parameters will appear shortly and will be defined as introduced. As is evident, lower-case symbols apply to the physical variables while upper-case ones apply to their normalized nondimensional counterparts.

P23 Replace Eq 2-21 with:

$$\frac{1}{R}\frac{d}{dT}(RV_\Theta) + F_r V_\Theta = -\frac{\eta\beta_m}{\gamma\omega^2 R_b} E_\theta - \frac{\eta}{\gamma}\frac{1}{R_b}(V_Z B_r - R_b V_R B_z) \qquad (2\text{-}21)$$

P28 Replace the caption of Figure II-3 with:

Figure II-3. Cyclotron orbits of electrons in a hollow beam in constant axial magnetic field only. The initial Θ directed velocity is positive.

P36 Replace the sentence under Eq. 2-52 with:

We assume that $E_\theta = 0$ but make no other approximations or assumptions at this point. Multiplying eq. (2-52) through by r and noting that in the usual way the flux enclosed in a circle of radius r given by[28]

P37 Replace Eq 2-57 with:

$$\begin{aligned} \gamma_{e_1} r_{e_1} v_{\theta e_1} &= \frac{\eta}{2\pi} (\psi_{e_1} - \psi_{c_1}) , \\ \gamma_{e_2} r_{e_2} v_{\theta e_2} &= \frac{\eta}{2\pi} (\psi_{e_2} - \psi_{c_2}) . \end{aligned} \qquad (2\text{-}57)$$

P44 Replace Eq 2-81 with:

$$P_z = \frac{1}{2} \int_0^{r_a} \int_0^{2\pi} E_\theta H_r^* r dr d\theta \qquad (2\text{-}81)$$

P49 Replace last paragraph with:

A somewhat more stringent test resulted from the two cases for input conditions given by $R_e = 1$, $\Theta_e = 0$, $Z_e = 0$, $V_{Re} = 0$, $V_{\Theta e} = +0.0075$, $V_{Ze} = dZ/dT_{T=Z=0} = 0.397$, and for the same conditions except for $V_{\Theta e} = -0.0075$. Here, too, $B_a = 0$ or $F_1 = 1$ was taken. This is equivalent to launching electrons with either positive or negative directed θ velocities into a constant magnetic field, taken here as 7000 gauss. Other parameters of choice or derived are:

P53 Label graphs from top left to right a,b,c.
Label graphs from bottom left to right d,e,f
Replace caption with:

Figure II-6.
Computer solutions for DC only equations of motion for Ubitron conditions: B_1/B_0 = 0.1, B_0 = 5000 gauss V = 300 Kv, $v_{\theta e}/v_{ze}$ = 0.018, v_{re}/v_{ze} = 0.0 (cathode beam compression ratio) = 0.91, R = 2.0, Z_e = $\pi/2$ magnetic period for synchrorons operation at 94 GHz = L ≈ 0.6 cm.

P54 Label graphs from top left to right a,b,c.
Label graphs from bottom lef to right d,e,f.
Replace caption with:

Figure II-7.
Computer solutions for DC only equations of motion for Ubitron conditions: B_1/B_0 = 0.1, B_0 = 7000 gauss V = 300 Kv, $v_{\theta e}/v_{ze}$ = 0.029, v_{re}/v_{ze} = 0.0, (cathode beam compression ratio) = 0.89, R = 2.0, Z_e = $\pi/2$ magnetic period for synchrorons operation at 94 GHz = L ≈ 0.6 cm.

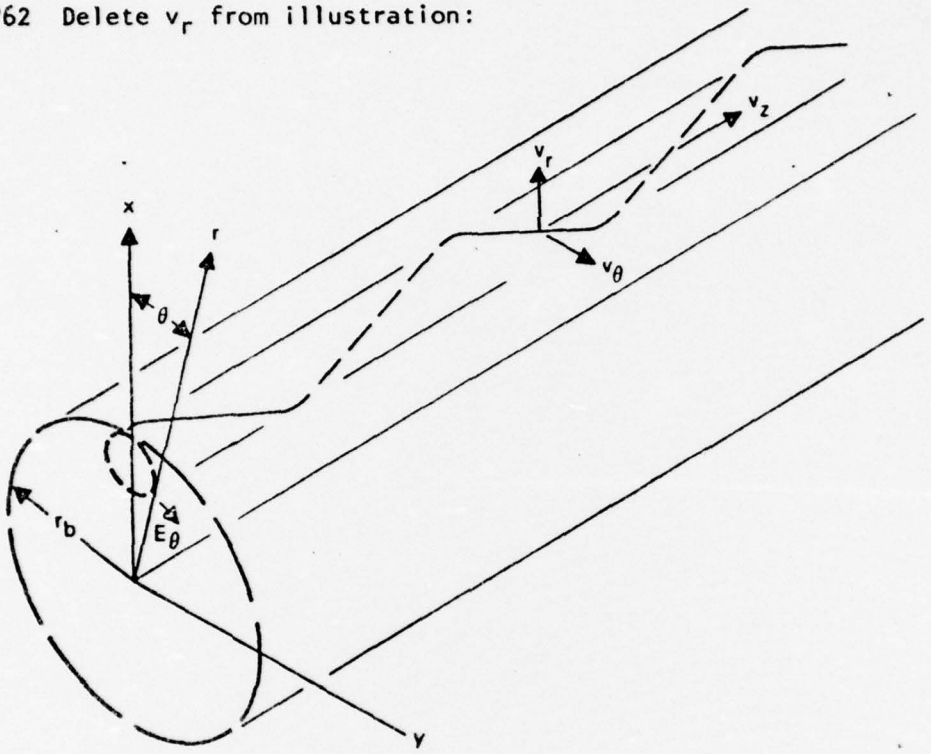
P55 Label graphs from top left to right a,b,c.
Label graphs from bottom left to right d,e,f.
Replace caption with:

Figure II-8.
Computer solutions for DC only equations of motion for Ubitron conditions: B_1/B_0 = 0.1, B_0 = 7000 gauss, V = 300 Kv, $v_{\theta e}/v_{ze}$ = 0.044, v_{re}/v_{ze} = 0, (cathode beam compression ratio) = 0.89, R = 1.33, Z_e = $\pi/2$ magnetic period for synchrorons operation at 94 HGz = L ≈ 0.6 cm.

P60 Replace Eq 2-98c with:

$$\Lambda = \frac{\dot{y}_o}{v_o} \qquad (2\text{-}98c)$$

P62 Delete v_r from illustration:



P68 Replace Eq 2-105 with:

$$\frac{1}{Z}\int_0^Z f(Z)\, f(Z+Z')\, dZ = a_o^2 + \frac{a_1^2}{2}\cos Z' + \frac{a_2^2}{2}\cos Z'$$

$$+ \cdots \frac{a_2^2}{2}\cos 2Z' + \cdots + \frac{\text{Remainder}}{Z} \qquad (2\text{-}105)$$

P69 Replace Eq 2-108 with:

$$I_o \simeq 2\pi r_b \left[\delta r\right]_e \rho_e v_{ze} \qquad (2\text{-}108)$$

P75 Replace Eq 2-102 with:

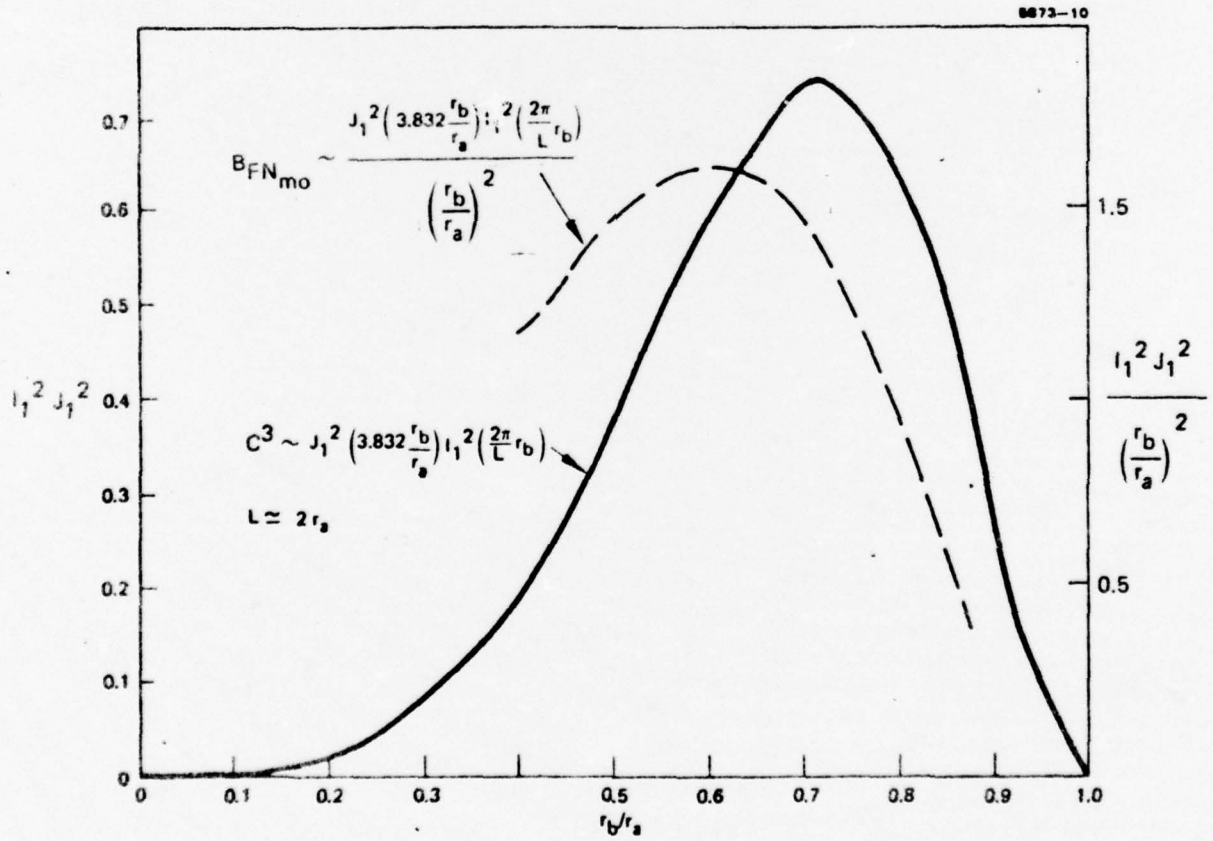
$$V_{\otimes 1} = \frac{\gamma_c}{\gamma_e} \frac{1}{R_b} \frac{B_1}{B_0} I_1(R_b) \sin (Z - \theta_1) \qquad (2\text{-}120)$$

75

P78 Replace Eq 2-123 with:

$$C_u^3 \sim \frac{1}{\mathscr{R}^2} \bar{R} J_1^2\left(\frac{3.832}{\mathscr{R}} \bar{R}\right) \frac{1}{R_b^2} I_1^2(R_b) \sim J_1^2\left(3.832 \frac{r_b}{r_a}\right) I_1^2\left(\frac{2\pi}{L} r_b\right) \qquad (2\text{-}123)$$

P79 Replace Figure 11-13 with:



P81 Replace Eq 2-124 with:

$$\gamma R V_{\Theta} - \gamma_e V_{\Theta_e} = \frac{\gamma_c}{2} (\Psi - \Psi_e) \qquad (2\text{-}124)$$

P90 Replace Eq 2-154 with:

$$\left(\frac{\gamma_e}{\gamma_c}\right)\frac{d\Theta}{dT} = \sum_{m=0}^{\infty} (P'_{i\ 2}B_r)\,\mu^m = P'_o + (P'_{o2}B_1 + P'_{12}B_o)\,\mu \qquad (2\text{-}154)$$

$$i + r = m$$

$$i \geq 0,\ r \geq 0$$

$$+ \sum_{m=2}^{\infty} (P'_{i\ 2}B_r)\,\mu^m \qquad i + r = m$$

etc.

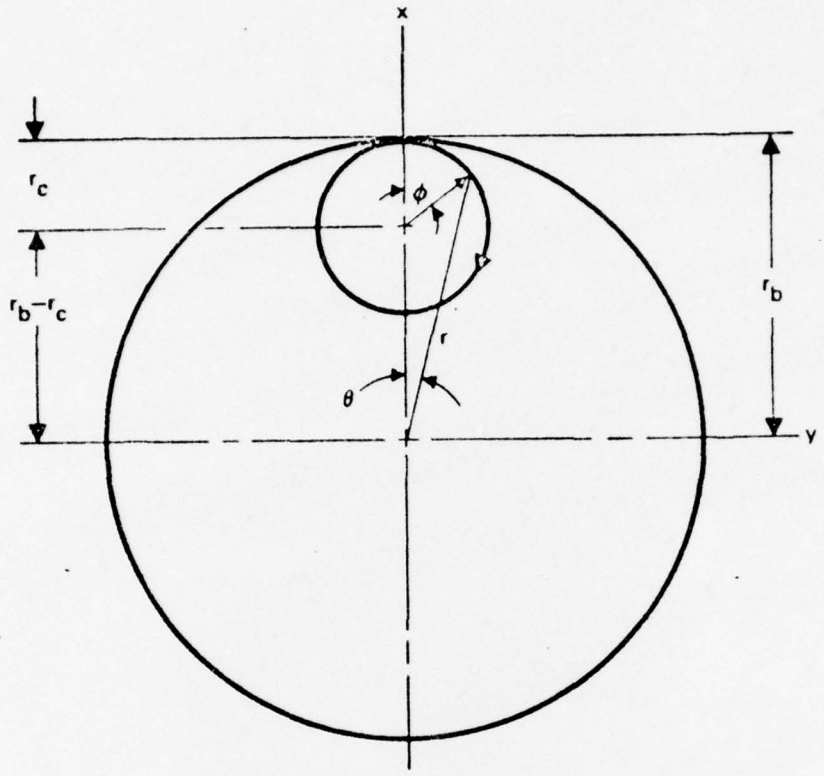
P96 Replace Eq 2-167d with:

$$b_0 = \left(\frac{B_1}{B_0}\right)^2 \frac{1}{R_b} I_1(R_b)I_0(R_b) + \cdots + \frac{1}{2}\left(\frac{B_1}{B_0}\right)^2 \frac{I_0(R_b)I_1(R_b)}{R_b} + \cdots$$

$$- \frac{1}{2}\left(\frac{B_1}{B_0}\right)^2 I_1^2(R_b) + \cdots - \frac{3}{2}\left(\frac{B_1}{B_0}\right)^2 \frac{I_1^2(R_b)}{R_b^2} + \cdots$$

$$- \frac{1}{2}\left(\frac{B_1}{B_0}\right)^2 I_0^2(R_b) + \cdots \qquad (2\text{-}167d)$$

P101 Replace V_c with r_c in Figure 11-14.



P119 Replace Eq 2-226 with:

$$R_{b\circledast} = -Z\left[\mathcal{A}_{\theta 1}(1+\mathcal{R}^2_{V\circledast Z})\cos Z_e - \mathcal{R}_{V\circledast Z}\right.$$

$$\left. - \mathcal{R}_{V\circledast Z}\mathcal{A}^2_{\theta 1}\left(1+\cos Z_e + \frac{3}{4}\cos 2Z_e\right)\right]$$

$$+ \mathcal{A}_{\theta 1}\left[\sin(Z - Z_e) + \sin Z_e\right]\left[1 + \frac{9}{8}\mathcal{A}^2_{\theta 1} + \mathcal{R}^2_{V\circledast Z}\right.$$

$$\left. - 3\mathcal{A}_{\theta 1}\mathcal{R}_{V\circledast Z}\cos Z_e + \frac{3}{4}\mathcal{A}^2_{\theta 1}\cos 2Z_e\right] + \cdots \qquad (2\text{-}226)$$

P204 Replace Eq 5-2 with:

$$k = \sqrt{\gamma^2 - 1}\left[\beta_m\gamma \pm \sqrt{\beta_m^2\gamma^2 - \left(\beta_m^2 + \gamma_{01}^2\right)}\right] \qquad (5\text{-}2)$$

Replace Eq 5-3 with:

$$k = \beta_m\gamma\sqrt{\gamma^2 - 1}$$

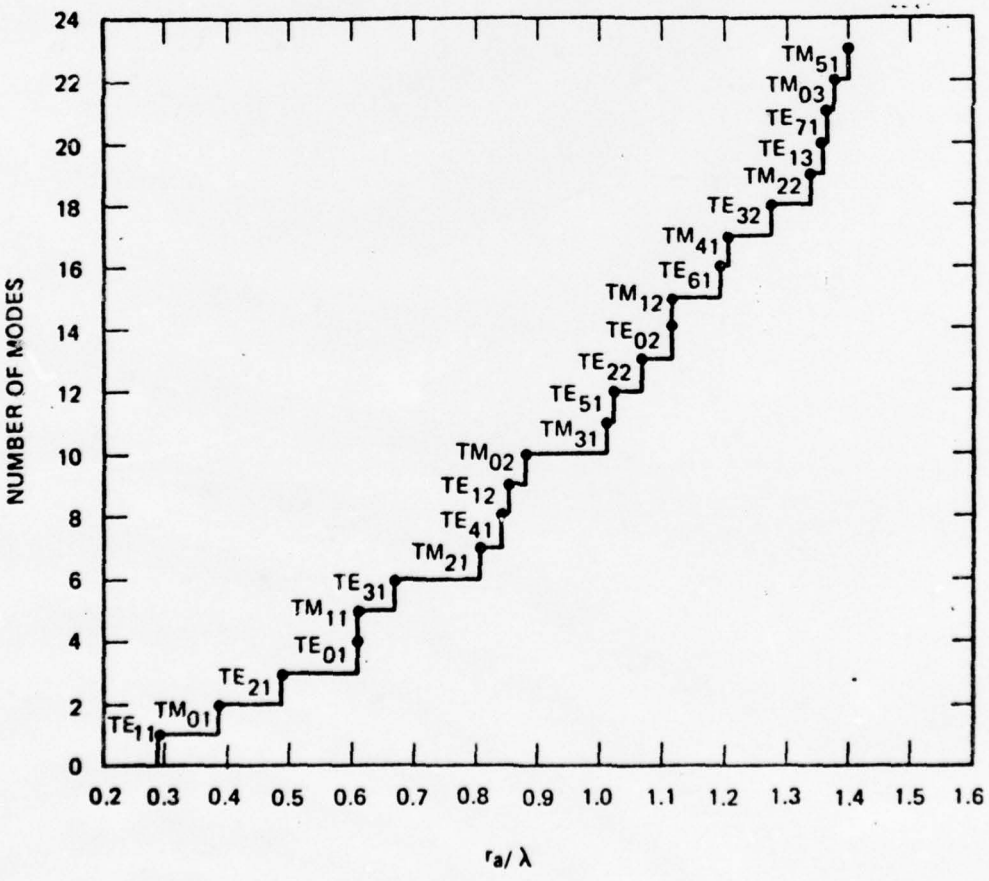
$$\gamma^2\beta_m^2 = \gamma_{01}^2 + \beta_m^2 \qquad (5\text{-}3)$$

Replace Eq 5-4 with:

$$L = \gamma\sqrt{\gamma^2 - 1}\,\lambda_o$$

$$r_a = \frac{q_{01}\,\gamma\,\lambda_o}{2\pi} \qquad (5\text{-}4)$$

P215 Replace Figure V-3 with:



P231 Replace No. 2 under conclusions with:

2. Under the small-signal assumption that efficiency is proportional to the gain parameter, the following relationships occur for a wideband Ubitron design.

$$\eta_e = B_\eta C_u \sim B_\eta^{3/4} P^{1/4} f^{-1/2} h$$

where η_e is the electronic efficiency; B_η is the assumed efficiency parameter; C_u is the Pierce type small-signal gain parameter for the Ubitron; P is the rf power; and f is the operating frequency. The factor hs is a relatively complex function of the voltage, the beam-to-waveguide diameter ratio, and the magnetic polepiece i.d.-to-waveguide diameter ratio. This function decreases with increasing voltage primarily due to the effects of relativity.

MILLIMETER WAVE UBITRON DEVELOPMENT PHASE I

J. M. Baird
S. Sensiper
K. Amboss
J. F. Heney

Contractor: Hughes Research Laboratories
Contract Number: F30602-76-C-0215
Effective Date of Contract: 8 March 1976
Contract Expiration Date: 28 February 1977
Short Title of Work: Millimeter Wave Ubitron Development Phase I
Program Code Number: 6E20
Period of Work Covered: Mar 76 - Dec 76

Principal Investigator: John Heney
Phone: 213 456-6411
Project Engineer: R. Hunter Chilton
Phone: 315 330-4381

Approved for public release;
distribution unlimited.

This research was supported by the Defense Advanced Research Projects Agency of the Department of Defense and was monitored by R. Hunter Chilton (OCTP), Griffiss AFB NY 13441 under Contract F30602-76-C-0215.

UNCLASSIFIED

SECURITY CLASSIFICATION OF THIS PAGE (When Data Entered)

REPORT DOCUMENTATION PAGE

READ INSTRUCTIONS BEFORE COMPLETING FORM

1. REPORT NUMBER: RADC-TR-77-133	2. GOVT ACCESSION NO.
3. RECIPIENT'S CATALOG NUMBER	
4. TITLE (and Subtitle): MILLIMETER WAVE UBITRON DEVELOPMENT PHASE I	5. TYPE OF REPORT & PERIOD COVERED: Final Technical Report, 8 Mar 76 – 31 Dec 76
	6. PERFORMING ORG. REPORT NUMBER: N/A
7. AUTHOR(s): J. M. Baird, J. F. Heney, S. Sensiper, K. Ambross, John F. Heney	8. CONTRACT OR GRANT NUMBER(s): F30602-76-C-0215
9. PERFORMING ORGANIZATION NAME AND ADDRESS: Hughes Research Laboratories, 3011 Malibu Canyon Road, Malibu CA 90265	10. PROGRAM ELEMENT, PROJECT, TASK AREA & WORK UNIT NUMBERS: 62301E, C1920001
11. CONTROLLING OFFICE NAME AND ADDRESS: Defense Advanced Research Projects Agency, 1400 Wilson Blvd, Arlington VA 22209	12. REPORT DATE: April 1977
	13. NUMBER OF PAGES: ~~292~~ 309 p.
14. MONITORING AGENCY NAME & ADDRESS (if different from Controlling Office): Rome Air Development Center (OCTP), Griffiss AFB NY 13441	15. SECURITY CLASS. (of this report): UNCLASSIFIED
	15a. DECLASSIFICATION/DOWNGRADING SCHEDULE: N/A

16. DISTRIBUTION STATEMENT (of this Report)
Approved for public release; distribution unlimited.

17. DISTRIBUTION STATEMENT (of the abstract entered in Block 20, if different from Report)
Same

18. SUPPLEMENTARY NOTES
RADC Project Engineer:
R. Hunter Chilton (OCTP)

19. KEY WORDS (Continue on reverse side if necessary and identify by block number)
Ubitrons, Relativistic beams, High power, Millimeter wave, Amplification

20. ABSTRACT (Continue on reverse side if necessary and identify by block number)
The theory of Ubitrons (Undulating Beam Interactions) for high power millimeter wave amplification is reviewed and extended. Relativistically correct dc and small-signal theories are developed and applied to a 94-GHz, 50-kW Ubitron amplifier. This amplifier employs the fast-wave interaction between the cylindrical TE_{01} waveguide mode and the -1 beam harmonic mode derived from a stationary periodic magnetic field. A numerical integration technique is used to correct the small-signal theory for the effects of radial variations in the dc electron beam. Relativistic corrections to the gain per unit wavelength are

DD FORM 1 JAN 73 1473 EDITION OF 1 NOV 65 IS OBSOLETE

UNCLASSIFIED

SECURITY CLASSIFICATION OF THIS PAGE (When Data Entered)

172 600 SS

shown to be significant for voltages above 50 kV. Design principles for hollow-beam magnetron injection guns are also given, and techniques for producing periodic magnetic fields in cylindrical geometry are evaluated.

Electronic efficiencies for 94-GHz, 50-kW Ubitron amplifiers will most likely be between 1 and 2% for wide bandwidth (~50%) and between 4 and 6% for narrow bandwidth. Overall efficiencies will still be high, however, if collector depression is demonstrated to be effective.

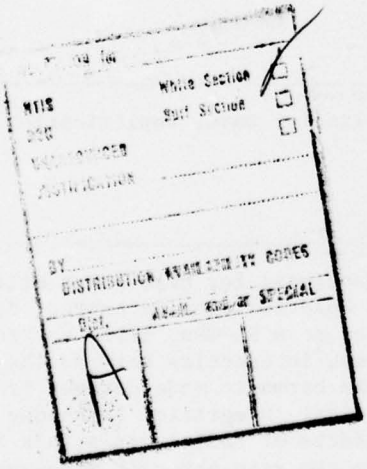


TABLE OF CONTENTS

SECTION			PAGE
	LIST OF ILLUSTRATIONS		v
I	INTRODUCTION AND SUMMARY		1
II	ELECTRON BEAM AND RF ANALYSIS		5
	A.	Background, Objectives, Brief Summary, Future Directions and Section Contents	5
	B.	Electron Beam – Electromagnetic Wave Interaction	12
	C.	Equations of Motion	16
	D.	Computer Code Results	48
	E.	Equivalence Theory – Hybrid Small Signal Approach	59
	F.	Analytical Results	80
	G.	Review and Conclusion of Electron Beam – rf Analysis	121
III	PERIODIC MAGNETIC FIELD STRUCTURES STUDY		123
	A.	Introduction and Summary of Task	123
	B.	Periodic Magnetic Structures Immersed in a Solenoidal Field	128
	C.	Periodic Permanent Magnet (PPM) Structures	142
	D.	Periodic Electromagnets	154
	E.	Superconducting Current-Carrying Ring Structure	156
	F.	Immersed Superconducting Rings	160

SECTION			PAGE
IV	THE DESIGN OF THE ELECTRON GUN		163
	A.	Introduction	163
	B.	The Relativistic Lorentz Force Equation	167
	C.	The Motion in the Magnetron Injection Gun	169
	D.	Boundary Conditions for the DC Beam — The Adiabatic Invariant	177
	E.	The Paraxial DC Electron Motion in the RF Interaction Region	180
V	PRELIMINARY UBITRON DESIGN AND CONFIGURATION		201
	A.	Relativistic Small-Signal Design Equations	202
	B.	RF Modes and Attenuation in Circular Waveguide	213
	C.	Design Trade-Offs Versus Voltage	218
	D.	300-kV Design of a 94-GHz, 50-kW Ubitron	225
VI	CONCLUSIONS AND RECOMMENDATIONS		231
	A.	Conclusions	231
	B.	Recommendations	232
	REFERENCES		235
	APPENDIX A —	Computer Program Description	241
	APPENDIX B —	Derivation of Small Signal Relativistic Gain Parameter	269
	APPENDIX C —	Mathematical Description of Periodic Magnetic Fields	283

LIST OF ILLUSTRATIONS

FIGURE		PAGE
II-1	Self-consistent system for solution of electron beam-electromagnetic wave interaction devices	13
II-2	Physical model of Ubitron	15
II-3	Cyclotron orbits of electrons in hollow beam in constant axial magnetic field only	28
II-4	Proof runs for program-2; DC relativistic electron equations of motion - cyclotron circles, V_{Θ_e} = +0.0075	52
II-5	Proof runs for program-2; DC relativistic electron equations of motion - cyclotron circles, V_{Θ_e} = -0.0075	52
II-6	Computer solutions for DC only equations of motion for Ubitron conditions	53
II-7	Computer solutions for DC only equations of motion for Ubitron conditions	54
II-8	Computer solutions for DC only equations of motion for Ubitron conditions	55
II-9	Equivalence between planar sheet beam and hollow cylindrical beam	62
II-10	Proof run for B_{FNm}	76
II-11	B_{FNm} from run of Figure II-7	76
II-12	B_{FNm} from run of Figure II-8	76
II-13	Factors relating to optimizing zeroth-order C^3 and B_{FNmo} for Ubitron	79
II-14	End view of cyclotron circles	101
III-1	Techniques for producing a periodic magnetic field	124
III-2	Application of the five periodic magnetic field techniques to the design of a 94 GHz, 360 kV Ubitron device	126

FIGURE		PAGE
III-3	Periodic magnetic structure immersed in solenoidal field	129
III-4	Direct-current magnetization curves for various magnetic materials	131
III-5	Comparison of B-H curves for iron and Hiperco-50	132
III-6	Simplified boundary conditions for first order analysis of periodic magnetic field	133
III-7	Plot of first harmonic amplitude B_1 versus average solenoidal field B_o with G/L parameter .	135
III-8	Plot of second harmonic amplitude B_2 versus average solenoidal field B_o with G/L parameter .	136
III-9	Plot of B_1/B_0 versus B_0 with G/L parameter . .	137
III-10	Plots of B_1 versus B_0 for parameter θ	138
III-11	Plots of B_2 versus B_0 for parameter θ	139
III-12	Plots of B_1/B_0 versus B_0 for parameter θ . . .	140
III-13	Nonsaturated values of B_1/B_0 versus gap/period ratio	143
III-14	Saturated peak values of B_1 versus gap/period ratio	144
III-15	Demagnetization curves for common high coercive PM materials compared to samarium cobalt	145
III-16	Periodic permanent magnet (PPM) structure . .	147
III-17	Doubly periodic permanent magnet structure . .	148
III-18	Samarium cobalt demagnetization curve and shifted curve	150
III-19	PPM equivalent magnetic structure for computer aided analysis	152
III-20	Axial magnetic field versus dissipated power using periodic electromagnets	155

FIGURE		PAGE
III-21	Characteristics of superconducting materials . .	157
III-22	Axial magnetic field using periodic superconducting rings.	159
III-23	Axial magnetic field using immersed superconducting rings.	161
IV-1	Convergent hollow beam gun	164
IV-2	Magnetron injection gun	165
IV-3	*Coordinate system* used in analysis of gun . . .	171
IV-4	Projection of electron trajectory in $\theta = 0$ plane .	176
IV-5	The form of the magnetic field in the Ubitron . .	179
IV-6	Velocity components of the beam in the magnetic field	186
IV-7	Perturbed trajectory in the undulating field. . .	193
IV-8	Trajectories in magnetron injection gun. . . .	194
IV-9	Computed trajectory in magnetron injection gun with large ratio of $\ell / r_{c,m}$	197
V-1	Dispersion diagram for wideband TE_{01} circular waveguide Ubitron	203
V-2	Guide diameter $2r_a$ and magnetic undulation period L as a function of beam voltage	206
V-3	Circular waveguide modes versus (radius/wavelength) ratio and design voltage	215
V-4	Circular waveguide TE_{01} mode losses versus waveguide radius and design voltage at 94 GHz. .	216
V-5	Calculated relativistic efficiencies versus voltage for 94 GHz Ubitron	219
V-6	Enhanced interaction circuit for Ubitron . . .	220
V-7	Variation of Ubitron parameters versus voltage for case I	221

FIGURE		PAGE
V-8	Variation of Ubitron parameters versus voltage for case 2	222
V-9	Calculated relativistic efficiency versus voltage for 35-GHz Ubitron	223
V-10	Outline of high-power Ubitron amplifier	229

I. INTRODUCTION AND SUMMARY

This final report covers work accomplished during a nine-month study program ending December 31, 1976. The long-range objective of this effort is to develop a very-high-power millimeter-wave amplifier. The emphasis during this initial study program has been on the study and analysis of a Ubitron-type device for the realization of 50-kW output power at 94 GHz. This work was sponsored by DARPA and was funded through RADC. The body of this report contains four sections which reflect the program tasks that were implemented.

Section II describes the work related to electron beam and rf analysis. Most of the effort during this program was expended on this task. The section contains a review of prior related work both in the USA and the USSR. A thorough treatment and analysis is then given of the dc beam motion within the undulating magnetic field and a technique is described by which the net effective interaction impedance and small-signal gain can be calculated. A relativistically corrected small-signal gain theory which shows a decrease in gain as voltage is increased is also described. This small-signal theory is in the same form as Pierce's TWT analysis.

In Section III we present the results of analysis on periodic magnetic structures which can be used in the design of millimeter-wave Ubitrons. The goal of this work has been to identify the techniques, materials, and configurations which maximize the amplitude of the desired periodic component of the field. Five types of structures were identified and analyzed. A superconducting periodic ring structure proved to be the most effective, as might be expected, but the desirability and practicality of implementing such a structure are questionable.

Periodic soft magnetic pole pieces immersed in a solenoidal field proved to be the next best method for producing a strong undulating field. The configuration and geometry that optimize this structure are given. This is the easiest structure to implement.

Periodic permanent magnet (PPM) structures were also investigated in the hopes that the new samarium cobalt magnets now available would make this type of structure competitive. The results show that the available field will be about half of that attainable by the immersed-pole-piece method. The PPM approach will still be useful, however, in applications where weight and prime power are major considerations.

Section IV gives the results of electron gun design studies leading to the design of magnetron injection guns applicable to a 94-GHz Ubitron. The principles of relativistic magnetron injection guns are derived. The design parameters of this type of gun are then investigated with respect to how they affect the specific and the average beam motion within the rf circuit and its undulating magnetic field. Some typical design parameters are presented for the desired magnetron injection gun.

The results of this study program are brought together in Section V and are applied to the design of a 94-GHz, 50-kW Ubitron. A basic trade-off of the tube parameters versus voltage is given. This trade-off shows that gain and efficiency are decreasing functions of voltage due to relativistic effects. An electronic design for a 300-kW Ubitron is presented and a preliminary sketch of the overall tube envelope is given. Section VI, the final section, provides conclusions and recommendations for future work.

The principal conclusions of this study program are as follows:

1. The development of a 94-GHz, 50-kW cw Ubitron amplifier appears to be feasible, using a 7000-Gauss solenoid and a waveguide circuit with imbedded periodic magnetic pole pieces.

2. Under the small-signal assumption that efficiency is proportional to the gain parameter, the following relationships occur.

$$\eta_e = B_\eta C_u \sim B_\eta^{3/4} P^{1/4} f^{-1/2} h$$

where: η_e is the electronic efficiency, B is the assumed efficiency parameter, C_u is the Pierce-type small-signal gain parameter for the Ubitron, P is the rf power, f is the operating frequency. The factor h is a relatively complex function of the voltage, the beam-to-waveguide diameter ratio, and the magnetic polepiece i.e.-to-waveguide diameter ratio. This function decreases with increasing voltage primarily due to the effects of relativity.

3. Using the small-signal assumptions described above, a 300-kV Ubitron design would have an inherent efficiency just under 2%. The estimated bandwidth would be on the order of 50%, since f/f_{co} is 1.6 at 300 kV. At a lower design voltage of 100 kV, the efficiency would rise to between 3 and 4% but the bandwidth would decrease to about 10%. The lower efficiency at higher voltage is mainly due to relativistic effects contained in the factor h above.

4. There will be a slight degradation of gain and efficiency due to the radial variations which must exist in the undulating electron beam, but with proper design these effects are shown to be on the order of 10% or less in the rf small-signal regime.

5. Because of the low inherent efficiency of the Ubitron, it will be necessary to take advantage of every available means to both enhance the electronic efficiency and recover the energy in the spent beam through collector depression. Because the spent beam and the rf power exit the Ubitron at the same place, collector depression needs further feasibility study and demonstration.

II. ELECTRON BEAM AND RF ANALYSIS

A. Background, Objectives, Brief Summary, Future Directions, and Section Contents

1. Prior Related Work

Early analytical work related to the Ubitron was shown by Phillips[1] and by Bacon, Phillips, and Enderby.[2] In the former the principles of operation were explained on a kinetic basis, and the synchronous gain velocity relationships were illustrated. Results were also shown for an analog computer run for a planar geometry with a constant rf drive. Although quite illustrative, particularly for large signal conditions, and suggesting efficiencies of about 20%, the model suffered from several deficiencies. Among others, it was nonrelativistic although approximate means were suggested for correction, it was planar whereas the geometry of prime interest is most likely cylindrical, and it ignored the influence of space charge. In the second of the above references, the authors developed a small-signal theory that ended in design equations defining tube performance in standard traveling-wave tube parameters essentially identical to the Pierce form. However, it too had several shortcomings; it was planar and nonrelativistic but permitted inclusion of space charge effects in the traditional traveling-wave tube manner via ω_q, ω_p, and QC.

Work on and analysis of the performance of Ubitron type devices seems to have been dormant in this country since the early work of Phillips and associates until recently. Then several articles by workers at the Naval Research Laboratory and Cornell appeared. Only a few of the most relevant ones are noted here. The work by Mannheimer and Ott[3] concerned a beam in a rippled magnetic field and compared the various gain mechanisms available. Although planar, the model included small beam perturbations, space charge, and relativistic effects. It was not cast in the usual traveling-wave tube parameter form making comparisons with other theories indirect. Also describing some theory, but primarily experimental, is the paper by Granatstein[4] and others, on the gain performance of a

relativistic beam tube with a rippled magnetic field. Another paper of analytical interest is a recent one by Sprangle[5], although it is not concerned with the effect of rippled magnetic fields of the Ubitron variety.

Rather differently than in the United States, work and publications on Ubitron devices seems to have continued in Russia over the past several years. Indeed, although only recently noted by us, several publications in the open literature have appeared. Seemingly, the most recent on mostly experimental results, is one by Krementsov, Reiser, and Smorgonskii.[6] From this, one can trace back to a large number of significant Russian papers. Of these, only a few are those of Petelin and Smorgonskii[7] on a nonlinear theory of the Ubitron suggesting possible efficiencies of up to 50%; by Gaponov and Petelin[8] on the linear theory of periodic static field electron beam interaction; by Gaponov, Petelin, and Yulpatov[9] on a general analysis of various types of related microwave devices; and by Petelin[10] on a similarity principle which appears to relate the performance of different types of relativistic beam devices. Time did not permit a thorough study of these and related papers in the Russian literature, but it appears that even aside from working experimental devices they have developed methods of analysis, procedures, and points of view which may be unique and may permit ready calculation and prediction of tube performance and parameter relationships.

In addition to the above references, a few others of a general nature should be noted. Particularly the work by Bobroff[11] and other reports mentioned there, are noteworthy. He demonstrated how the choice among the different independent space variables, the Eulerian, polarization, and hose systems, for small-signal analysis, leads to different relationships among the continuity, dynamical, and power exchange equation, and he also defined the equations permitting interchange among these systems. The importance of a firm knowledge of the correct dc motion of the electrons was emphasized. Bobroff did not consider relativistic effects which would modify his equations somewhat. As an example of the use of the polarization variable

system, the work by Durney and Johnson[12] is noteworthy. It demonstrated how, even in the relatively simple nonrelativistic case of a constant axial magnetic field and in the presence of space charge, the well-known multiplicity of modes exists.

2. Objectives of Current Work

The above brief review is hardly comprehensive. It merely touches on the truly voluminous literature on devices related to various aspects of Ubitron performance. It may not even include the most pertinent, particularly in the Russian literature. Nevertheless, at the start of the program, it appeared on review that several specific items regarding Ubitron performance were unknown or poorly understood, and that these could only be resolved by a more complete analysis. Information for preliminary design purposes on at least the following seemed necessary, particularly as they influenced small-signal gain: (1) The influence of a nonplanar model, i.e., an axisymmetric cylindrical geometry, on the electron motion; (2) the influence of cathode flux and other entrance conditions on electron motion; (3) the interrelationships between electron beam radius, the electromagnetic field configuration, and the dc magnetic field; and (4) the influence of operation in the relativistic regime.

The objectives of this program were to consider an analytical model more nearly representative of an operating tube and to resolve, to the maximum extent possible, the above items. Further, it was desired to so construct the analysis that the influence of various assumptions could be examined.

3. Brief Summary, Future Directions

a. Brief Summary – During the course of the analysis effort on this program, several computer codes were developed. Two major ones, closely related, are considered most relevant and are reported here. One describes the non-rf exact relativistic electron motion in an axisymmetric geometry under the influence of a cylindrical constant plus a space periodic magnetic field. The other is identical but includes the influence of a constant power TE_{01} mode

rf signal of arbitrary phase with all the rf mode field components included. The latter code is the same as the former with the rf power zero. In both codes as written to date, the small dc radial space charge force is excluded on the basis that the devices of most immediate interest are Ubitron devices in the perveance range of 10^{-7} to 10^{-8} or less where this force is generally significantly less than the applied magnetic forces. Also so far excluded is the small force resulting from the self-magnetic field of the beam. Expressions for these forces, however, are shown and they could be included in later modifications of these codes. The codes have been checked for some cases, with simple known solutions, and have shown excellent accuracy, three to four significant figures.

Included in the codes are several plotting routines which permit display of various characteristics of the Ubitron type beam, particularly coordinate and velocity variables as a function of tube length. Also included are several checking routines which permit review of the accuracy of calculation, and some stop commands if nonphysical situations should be encountered. In operation, the codes require only the physical parameter inputs of voltage, frequency, magnetic field characteristics, etc. and permit examination of beam performance as these variables are altered around some initially chosen mean values which fix the dimensions of the physical structure.

Another developed code which chains with the dc code is one which determines a beam factor applicable to the Phillips small-signal theory in the cylindrical Ubitron configuration. This code computes the weighted square of the circumferential electric rf field of the TE_{01} mode and the velocity harmonic of interest, from the computer-calculated electron orbits. This permits calculation of the traditional C^3 traveling-wave tube small-signal factor in the theory developed by Phillips[2] for the Ubitron, but in this case, corrected for the relativistic nonplanar case. This hybrid small-signal theory approach is essentially based on an equivalence concept and is not uncommon in traveling-wave tube work.

In parallel with the computer code development, a strictly analytic effort was undertaken. The same assumptions were made regarding space charge and beam self-field forces as taken for the computer code development. Relativistic conditions were taken which are particularly simple in the nonspace charge situation. An early effort in which only very small radial motion was assumed and other truncation assumptions taken led to integrable equations for all the coordinate variables. Although the axial and circumferential solutions were reasonably manageable, the radial solution was unwieldy and seemingly precluded the iteration process planned to improve all the coordinate solutions. All the solutions, particularly the axial and circumferential solutions, showed reasonably qualitative and even quantitative agreement with the computer solutions, particularly for small radial perturbations.

As an alternative near the close of the program, again from the basic equations, a form was obtained which permits exact expansion to any order of the radial deviation from the nominal beam radius, and to any order of the magnetic field harmonic components. Although not yet solved to any order, it appears that when truncated to first order, the equations will take the form of Hills equation or some related modification.[13] The advantage of having the differential equations of motion in some such standard form would be substantial.

b. Future Directions – The computer codes can be advanced in the direction of providing substantially complete design information on Ubitron devices by several steps. Among these are the inclusion of dc space charge forces and the self-magnetic field of the beam to permit more accurate trajectory determination and application to high-perveance devices. Inclusion of beam thickness effects resulting from practical electron gun designs and, possibly, inclusion of thermal velocity effects, are refinements which would be required eventually. Improvements in the magnetic field definition to permit improved entrance conditions and even tapering, are possible future refinements. Additionally, the possible influence of the input and output rf transducers, and particularly any collector depression geometry on the electron motion, would need to be programmed.

Before some of the above additions to the dc computer code are considered, a modification of the dc-plus-rf drive code should be undertaken. In this, the beam charge elements would be used as inputs to the field equations and the dynamical equation and field equations coupled. This would result in a complete definition of the Ubitron, and permit description, not only through the small-signal regime, but also into the large-signal saturation region. The influence of other modes, propagating but purposefully lossy and cutoff, could be included. Rf space charge and possibly magnetic field effects would most likely need to be included. Still further refinements might be necessary depending on the outcome of the above and any requirements from actual tube design activity.

In many respects, the steps required to advance the strictly analytical approach would parallel the computer code advancement. Initially, however, a further examination of the most recent form of the equations of motion is warranted to determine if convenient analytical solutions are possible. Quite possibly a recasting of these equations in the form of perturbations from the cyclotron circle radii rather than from the hollow beam radius would be most useful. On the assumption that analytically convenient and sufficiently accurate dc equations of motion can be obtained, preferably with space charge and self-magnetic field included, the next step includes the definition of the resulting rf charges and currents from a TE_{01} mode driving field using the relativistic form of the Ubitron, polarization, hose, or possibly Lagrangian variables system. Coupling of these equations with the electromagnetic wave equation in terms of these currents and charges leads to the complete definition of the small-signal performance of the Ubitron. A mode wave solution, in the usual traveling-wave tube manner, would follow, with growing and decaying waves resulting from complex roots and amplitudes resulting from defined boundary conditions. Again, the refinements noted above for the computer code description might be included, but might be analytically intractable or impractical. Extension to some approximation into the large signal regime might be possible, but again the computer code approach may be more practical.

4. Section Contents

The development given below proceeds as follows. After some initial general comments regarding the solution of electromagnetic wave-electron beam interaction problems, the relativistic equations of motion applicable to the Ubitron are derived. These are shown in two forms and are then normalized into expressions particularly convenient for application here. This is accompanied by a discussion of the assumptions made, the validity of these assumptions, and the means for eliminating such assumptions in further development. Various aspects of the relativistic equations with these assumptions are noted, particularly in relation to energy invariants. The significance of the entrance conditions on the dc beam performance is then pointed out and some useful relationships are derived. The equations of motion with constant rf TE_{01} mode drive are then noted and discussed briefly.

A review of the computer code work follows, with comments on the general approach and the results of some proof runs. After this some results of computer runs with typical Ubitron parameters are shown and discussed. The concept of equivalence theory is then described and application to a hybrid small-signal theory is noted. This is followed by the derivation of the beam factor expression in terms of the computer-obtained dc electron orbit results. The use of the beam factor is illustrated and various aspects of its characteristics are noted. The effect of relativistic corrections to the small-signal theory of Ubitrons is shown and the gain degradation predicted by the beam factor is illustrated. Some comments regarding Ubitron gain optimization are made at this point.

The last major portion of this section deals with the work performed to obtain solely analytic closed-form solutions to the dc equations of motion for the Ubitron. From the same equations used in the computer codes, differential equations in series expansion form valid to any desired order of the radial perturbations and the dc periodic magnetic field harmonic amplitudes are derived. The method whereby the series coefficients can be obtained exactly are prescribed. Although

complete closed-form solutions are not obtained, various characteristics of these equations and correspondence to possible known forms are noted. This is followed by a description of earlier work based on a truncated form of the equations from which closed-form solutions were obtained. These are discussed and compared briefly with the computer results. The section closes with some further discussion and comments regarding possible future directions for the analytic work.

B. Electron Beam – Electromagnetic Wave Interaction

1. General Approach

The considerable complexity involved in a complete solution of an electron beam – electromagnetic wave interaction device can be appreciated from the diagram in Figure II-1. This expresses the relationship in traveling-wave terminology between the circuit and the electronic equations. The procedure requires the solution of the electron motion force/field relationship in the geometry of interest leading to the coordinate and velocity components x_1, x_2, x_3 and d/dt (x_1, x_2, x_3) as a function of time or an equivalent parameter. From these the relevant vector current and related charge density $\overline{J}(t, x_1, x_2, x_3)$ and $\rho(t, x_1, x_2, x_3)$, can be found. These are the driving terms on Maxwell's equations leading to solutions of $\overline{E}(t, x_1, x_2, x_3)$ and $\overline{B}(t, x_1, x_2, x_3)$ in the force equation. Closing the loop as shown and solving the set for selfconsistent solutions completes the problem. The constitutive relationship between the $\overline{E}, \overline{D}, \overline{H}, \overline{B}$ field vectors which are particularly simple for the usual case of free space, $\overline{D} = \epsilon_o \overline{E}$, and $B = \mu_o \overline{H}$, are also required. The divergence relationships follow from Maxwell's equations. Figure II-1 shows the general problem in all its complexity. Even so, computer codes and machine capabilities are near the point that such very general problems can be handled. For example, the code CYLRAD, particularly, appears to be approaching or is already at the point where it could handle the general Ubitron problem.[14] Unfortunately, this code was not available to us during the course of this program.

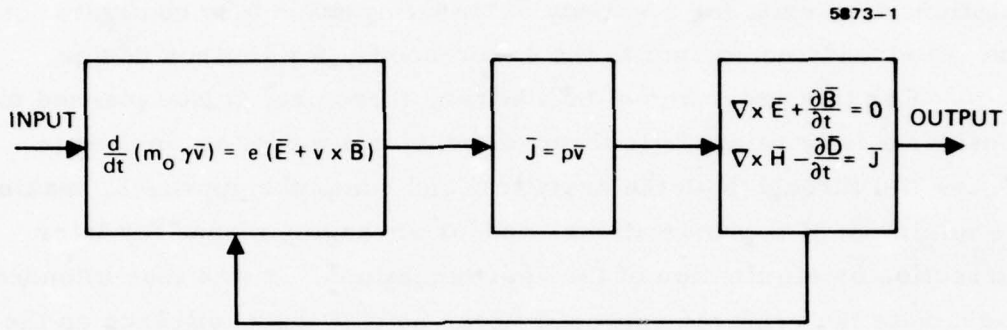


Figure II-1. Self-consistent system for solution of electron beam-electromagnetic wave interaction devices.

The usual procedure for solving this system for a particular geometry is to reduce the problem to one or two dimensions and to make such other approximations as can be justified or seem reasonable. Analytic solutions of varying degrees of complexity and completeness and for various geometries abound. Computer-generated solutions, particularly for the cases where nonlinearities enter or where the two- or three-dimensional character of the geometry preclude useful or tractable analytic solutions, are the other alternative. Many such solutions also exist for a variety of traveling-wave tube configurations, but, as already noted, not to the extent needed for Ubitron design.

For this program on the Ubitron, therefore, it was planned to consider a fully relativistic three-dimensional model as implied in Figure II-1 through both the analytical and computer approach, making the minimum of approximations, and/or arranging means for later correction or elimination of the approximations. It was also intended to evaluate the required approximations so that their influence on the end results could be evaluated. It was recognized that achievement of a final design version might have to proceed in several steps and that improvement of the small-signal theory would be required first. It was recognized from previous experience[15] that the usefulness of the results regarding rf performance would depend heavily on a knowledge of the dc performance of the beam. Indeed, in the small-signal polarization variable approach, or equivalently in any of the other approaches, accurate knowledge regarding the dc parameters of the beam, position, and velocity are required as starting points. We therefore start our development at this point, that is to determine these dc parameters to adequate accuracy.

2. Physical Model, Some Definitions

Figure II-2 shows the geometry of interest for the Ubitron. A thin hollow beam of radius r_b is launched with known radial circumferential and axial velocities into a cylindrical waveguide of radius r_a propagating a TE_{01} mode waveguide. It is assumed that only this mode is propagating, although a round waveguide capable of

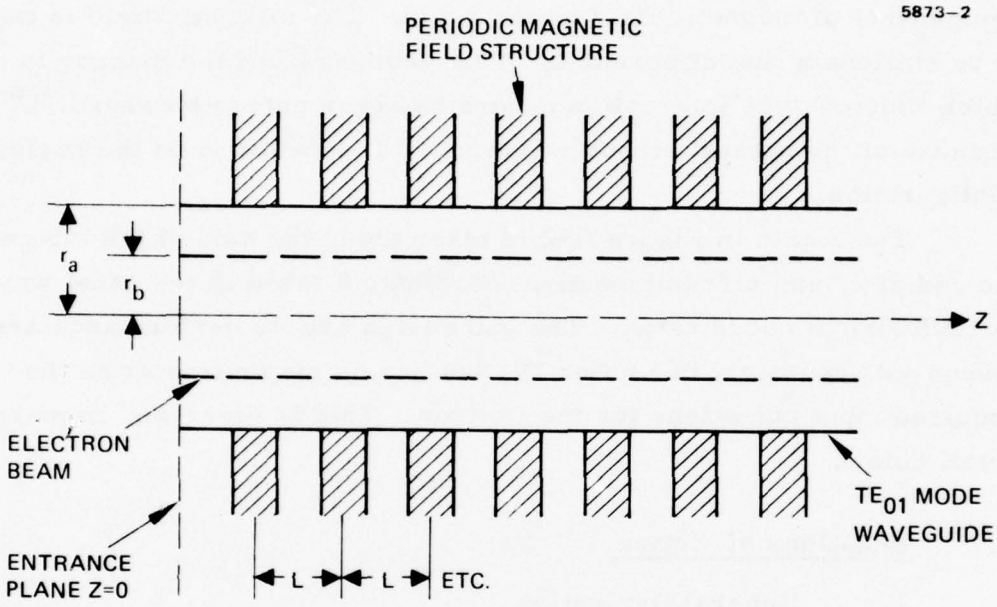


Figure II-2. Physical model of Ubitron.

propagating the TE_{01} mode would generally also propagate the TE_{11}, TM_{01}, TE_{21}, and TM_{11} modes. (See Section V.) It is assumed these other modes are either very highly damped or are not excited by the electron beam and input and output transducers. The electron beam-waveguide system is immersed in a magnetic field configuration (described in Section III) which imposes a constant axial plus periodic components of magnetic field on the beam. The magnetic field is taken to be stationary and of period L. This geometry and the manner in which Ubitron-type interaction occurs has been noted elsewhere.[1, 2] Because of the natural circular symmetry it appears to be the preferred configuration.

The z axis in Figure II-2 is taken along the axis of the tube with the radial r, and circumferential coordinate θ taken in the usual way for cylindrical coordinates. The gun design and its performance are discussed separately in Section IV, but have a major impact on the required input conditions for the Ubitron. This is discussed in more detail below.

C. Equations of Motion

1. General Derivation

From the generally accepted form relating the change of momentum to the Lorentz force on the electron[16, 17] in MKS units,

$$\frac{d}{dt}\,(m_o \gamma \bar{v}) = e(\bar{E} + \bar{v} \times \bar{B}) \qquad (2\text{-}1)$$

with $\bar{E}$ and $\bar{B}$ the vector electric field intensity and magnetic flux density vector, $\bar{v}$ the vector velocity, m_o the rest mass, e the electronic charge, γ the relativistic factor

$$\gamma = \left(1 - \frac{\bar{v} \cdot \bar{v}}{c^2}\right)^{-1/2},$$

and c the velocity of light, there results on expansion in cylindrical coordinates

$$\frac{dv_r}{dt} - \frac{v_\theta^2}{r} + \frac{\gamma^2}{c^2} f(\bar{v}) v_r = - \frac{\eta}{\gamma} (E_r + v_\theta B_z - v_z B_\theta) \qquad (2\text{-}2)$$

$$\frac{1}{r} \frac{d}{dt} \left(r^2 \frac{d\theta}{dt} \right) + \frac{\gamma^2}{c^2} f(\bar{v}) v_\theta = - \frac{\eta}{\gamma} (E_\theta + v_z B_r - v_r B_z) \qquad (2\text{-}3)$$

$$\frac{dv_z}{dt} + \frac{\gamma^2}{c^2} f(\bar{v}) v_z = - \frac{\eta}{\gamma} (E_z + v_r B_\theta - v_\theta B_r) \qquad (2\text{-}4)$$

Here $\eta = |e|/m$ and we show the signs explicitly. The common factor

$$f(\bar{v}) = \frac{1}{2} \frac{d}{dt} (\bar{v}^2) = \frac{1}{2} \frac{d}{dt} (\bar{v} \cdot \bar{v}) = v_r \frac{dv_r}{dt} + v_\theta \frac{dv_\theta}{dt} + v_z \frac{dv_z}{dt} \qquad (2\text{-}5)$$

comes from carrying out the d/dt operation in eq. (2-1), which introduces the term

$$\frac{d\gamma}{dt} = \frac{\gamma^3}{c^2} f(\bar{v}) = \frac{\gamma^3}{c^2} \bar{v} \cdot \frac{d\bar{v}}{dt} . \qquad (2\text{-}6)$$

Since

$$v_r = \frac{dr}{dt} , \quad v_\theta = v \frac{d\theta}{dt} , \quad v_z = \frac{dz}{dt} \qquad (2\text{-}7)$$

the first term of the lhs of eq. (2-3) can be written as

$$\frac{1}{r}\frac{d}{dt}(rv_\theta) = \left(\frac{v_r v_\theta}{r} + \frac{dv_\theta}{dt}\right) = \left(2\frac{dr}{dt}\frac{d\theta}{dt} + r\frac{d^2\theta}{dt}\right) \qquad (2\text{-}8)$$

and similarly the other equations can be written in terms of time derivatives of the coordinate positions rather than the velocities. Equations (2-2) through (2-4) are in a form also shown by Bergmann.[18] For small values of $\bar{v}/c$, γ approaches unity, $f(\bar{v})$ approaches zero, and the nonrelativistic form of the equations of motion result.

Equations (2-3) through (2-4) were the ones used in the computer codes to be described shortly. A possibly simpler form which can be derived either from them or more directly from eq. (2-1) might have been more suitable. Herrmannsfeldt[19] demonstrated how by simultaneous equation solution of the set of three equations a form can be obtained in which only second derivatives of position or first derivatives of velocity occur on the lhs of the equations. This is particularly convenient for both computer code and analytical solutions. The results can also be obtained more simply as follows. From eq. (2-1) with the d/dt operation shown explicitly

$$m_o\left(\bar{v}\frac{d\gamma}{dt} + \gamma\frac{d\bar{v}}{dt}\right) = e(\bar{E} + \bar{v} \times \bar{B}) \qquad (2\text{-}1)$$

and on operating with $\bar{v}$., there results

$$m_o\left(\bar{v}\cdot\bar{v}\frac{d\gamma}{dt} + \bar{\gamma}\cdot\frac{d\bar{v}}{dt}\right) = e\bar{v}\cdot\bar{E}\ ; \qquad (2\text{-}9)$$

or on substituting from eq. (2-6) for

$$v\cdot\frac{d\bar{v}}{dt} = \frac{c^2}{\gamma^3}\frac{d\gamma}{dt}$$

and the definition of γ as

$$\gamma = \left(1 - \frac{\overline{v} \cdot \overline{v}}{c^2}\right)^{-1/2} \tag{2-10}$$

there results

$$m_o\left(\overline{v} \cdot \overline{v}\,\frac{d\gamma}{dt} + \frac{c^2}{\gamma^2}\,\frac{d\gamma}{dt}\right) = m_o c^2\,\frac{d\gamma}{dt} = e\overline{v} \cdot \overline{E} \quad . \tag{2-11}$$

With this expression for $d\gamma/dt$ on substituting in eq. (2-1) we obtain

$$\frac{d\overline{v}}{dt} = \frac{1}{\gamma}\frac{e}{m_o}\left[\overline{E} + \overline{v} \times \overline{B} - \frac{1}{c^2}\,\overline{v}(\overline{v} \cdot \overline{E})\right] \tag{2-12}$$

Again in circular cylindrical coordinates this becomes

$$\frac{dv_r}{dt} - \frac{v_\theta^2}{r} = -\frac{\eta}{\gamma}\left[E_r + v_\theta B_z - v_z B_\theta - \frac{v_r}{c^2}(\overline{v} \cdot \overline{E})\right] \tag{2-13}$$

$$\frac{1}{r}\frac{d}{dt}(rv_\theta) = -\frac{\eta}{\gamma}\left[E_r + v_z B_r - v_r B_z - \frac{v_\theta}{c^2}(\overline{v} \cdot \overline{E})\right] \tag{2-14}$$

$$\frac{dv_z}{dt} = -\frac{\eta}{\gamma}\left[E_z + v_r B_\theta - v_\theta B_r - \frac{v_z}{c^2}(\overline{v} \cdot \overline{E})\right] \tag{2-15}$$

The common factor $\overline{v} \cdot \overline{E}$ is given by

$$v \cdot E = v_r E_r + v_\theta E_\theta + v_z E_z \quad . \tag{2-16}$$

As evident from (2-1) and (2-9) this times e is equal to the work done per unit time by the forces on the electron, i.e., the change in kinetic energy, so that from eq. (2-11) if

$$e\bar{v} \cdot \bar{E} = \frac{d(K.E.)}{dt} \tag{2-17}$$

with K.E. = 0 at $\bar{v} = 0$

$$(K.E.) = m_o c^2 (\gamma - 1) \tag{2-18}$$

From eqs. (2-1), (2-9), and (2-10), it is readily seen that if the force is solely parallel to the velocity so that $\bar{v} \cdot \bar{F} = |v||F|$ the quantity "effective mass" multiplying $d\bar{v}/dt$ to obtain the force is $m_o \gamma^3$, whereas if the force is solely perpendicular to the velocity, the "effective mass" is $m_o \gamma$.

As evident from eq. (2-16) through (2-18) if $\bar{E} = 0$ everywhere along the electron path (K.E.) = constant which implies γ constant or $\bar{v} \cdot \bar{v}$ constant. This states the well-known point that with only magnetic forces acting, the direction, i.e., velocity components, but not the total velocity of the electrons will change. This fact will prove useful as a check in some of the computer calculations. The extra relativistic terms on the lhs of eqs. (2-2) through (2-4) are related to the extra terms on the rhs in eqs. (2-13) through (2-15), as evident from the derivation and eqs. (2-6) and (2-11).

With the substitutions $x = r - r_o$, $y = (r - r_o)\theta$, $z = z$ in eqs. (2-2) to (2-4) or eqs. (2-13) to (2-15), then letting r_o approach infinity and the related cylindrical coordinate field components approach their counterparts in Cartesian coordinates, these equations become exactly the relativistic equations in the Cartesian coordinate system. The latter are of course derivable directly from eq. (2-1). This well known concept is used later in discussing the equivalence between Ubitron theory in cylindrical and planar coordinates and in understanding the computer displays.

Although none of the above is new, this textbook material is inserted here as a reminder and review, and to indicate the starting point for further development.

2. Normalization Factors

For computer application as well as for the analysis it is most convenient to scale the equations of motion into a normalized nondimensional form. A normalization system was chosen and the equations and related computer codes were written and verified in normalized form. A precursor program was then established which accepts physical variable inputs and transforms them into the normalized nondimensional forms. The combination also was verified.

The scale factor system we have used here is given as follows:

$$R = \frac{r}{r_b} \qquad V_R = \frac{dR}{dT} = \frac{\beta_m}{\omega R_b} v_r$$

$$\Theta = \theta \qquad V_\Theta = R\frac{d\Theta}{dT} = \frac{\beta_m}{\omega R_b} v_\theta$$

$$Z = \beta_m z = \frac{2\pi}{L} z \qquad V_Z = \frac{dZ}{dT} = \frac{\beta_m}{\omega} v_z$$

$$T = \omega t \qquad (2\text{-}19a)$$

In the above, r, θ, z, v_r, v_θ, v_z are the usual physical cylindrical coordinate and velocity coordinates, ω is the tube operating radian frequency, t is the time variable, and L is the magnetic period from Figure II-2. In eq. (2-19a) R_b appears, and this as well as some other normalization parameters are defined as follows

$$R_b = \beta_m r_b \quad , \quad R_a = \beta_m r_a \qquad \mathcal{R} = \frac{r_a}{r_b} = \frac{R_a}{R_b}$$

$$\omega_c = \eta B_o \qquad \gamma_c = \frac{\omega_c}{\omega} \qquad (2\text{-}19b)$$

r_a is the r.f. waveguide tube radius, r_b the beam radius at the entrance plane (see Figure II-2), B_o is the average or dc value of the velocity which generally differs only negligibly (perhaps 1%) from γ_c the ratio of the cyclotron frequency to the operating frequency. A few additional normalizing parameters will appear shortly and will be defined as introduced. As is evident, lower-case symbols apply to the physical variables while upper-case ones apply to their normalized nondimensional counterparts.

A possible disadvantage of the normalization system noted above is that it normalizes the r variable to the beam entrance radius. This has the disadvantage of measuring the radial coordinate in terms of a base, r_b, which in turn is a variable design parameter. Also, for a fixed frequency, as the voltage is increased to maintain the usual Ubitron synchronous condition[1] the normalized axial velocity V_Z decreases. An alternate normalization system is to define $Z = z/r_a$ leaving all the other definitions as in eq. (2-19). This still leaves the r/r_b normalization problem, but does make the normalized axial velocity almost independent of voltage in the 100- to 500-kV range. Still another choice is to define $R = r/r_a$ leaving all the other definitions as in eq. (2-19). Again, because of the precursor program noted above the impact of a change in the normalization factors on the computer codes is negligible except for the plotting or display routines, and, perhaps more importantly, for the case where thick electron beams may be considered. The influence of the normalization factors on the analytical expressions is more significant in terms of convenient handling, and a review would be suggested in further work.

3. Normalized Forms

a. General – All Cases – Substitution of eq. (2-19) in eqs. (2-2) through (2-4) yields

$$\frac{dV_R}{dT} + F_r V_R = \frac{V_\Theta^2}{R} - \frac{\eta}{\gamma}\frac{\beta_m}{\omega^2 R_b} E_r - \frac{\eta}{\gamma\omega}\left(V_\Theta B_z - \frac{1}{R_b} V_Z B_\theta\right) \quad (2\text{-}20)$$

$$\frac{1}{R}\frac{d}{dT}(RV_\Theta) + F_r V = -\frac{\eta\beta_m}{\gamma\omega^2 R_b} E_\theta - \frac{\eta}{\gamma}\frac{1}{R_b}(V_Z B_r - R_b V_R B_z) \quad (2\text{-}21)$$

$$\frac{dV_Z}{dt} + F_r V_Z = -\frac{\eta}{\gamma}\frac{\beta_m}{\omega^2} E_z - \frac{\eta}{\gamma}\frac{R_b}{\omega}(V_R B_\theta - V_\Theta B_r) \quad (2\text{-}22)$$

where

$$F_r = \frac{\gamma^2}{2}\left(\frac{L}{\lambda_o}\right)^2 \frac{dE}{dT} = \frac{d}{dT}\ln\gamma = \frac{1}{\gamma}\frac{d\gamma}{dT} \quad (2\text{-}23)$$

and explicitly in normalized parameters

$$\gamma = \left[1 - \left(\frac{L}{\lambda_o}\right)^2 E\right]^{-1/2} , \quad (2\text{-}24)$$

$$E = R_b^2\left(V_R^2 + V_\Theta^2\right) + V_Z^2 \quad (2\text{-}25)$$

and

$$\frac{1}{2}\frac{dE}{dT} = R_b^2\left(V_R\frac{dV_R}{dT} + V_\Theta\frac{dV_\Theta}{dT} + V_Z\frac{dV_Z}{dT}\right) . \quad (2\text{-}26)$$

In the above and elsewhere λ_o is the free-space wavelength. The normalized velocities and their derivatives can in turn be expressed in terms of the coordinates, and of their first and second derivatives.

The alternative forms of the normalized relativistic equations of motion from eqs. (2-13) through (2-15) are

$$\frac{dV_R}{dT} = \frac{V_\Theta^2}{R} - \frac{\eta}{\gamma}\frac{\beta_m}{\omega^2 R_b} E_r - \frac{\eta}{\gamma\omega}\left(V_\Theta B_z - \frac{1}{R_B} V_Z B_\theta\right) + \mathcal{F}_r V_R \tag{2-27}$$

$$\frac{1}{R}\frac{d}{dt}(RV_\Theta) = -\frac{\eta\beta_m}{\gamma\omega^2 R_b} E_\theta - \frac{\eta}{\gamma}\frac{1}{\omega R_b}(V_Z B_r - R_b V_R B_z) + \mathcal{F}_r V_\Theta \tag{2-28}$$

$$\frac{dV_Z}{dT} = -\frac{\eta}{\gamma}\frac{\beta_m}{\omega^2} E_z - \frac{\eta}{\gamma}\frac{R_b}{\omega}(V_R B_\theta - V_\Theta B_r) + \mathcal{F}_r V_Z \tag{2-29}$$

where

$$\mathcal{F}_r = \frac{\eta}{\gamma}\frac{1}{c^2\beta_m}(R_b V_R E_r + R_b V_\Theta E_\theta + V_Z E_z) \tag{2-30}$$

As evident in a comparison of eqs. (2-20) through (2-22) with their counterparts of eqs. (2-27) through (2-29), for these to be identical it is necessary that $F_R = -\mathcal{F}_r$. In the following steps using eqs. (2-23), (2-26), (2-11) the definitions of the normalizing parameters eq. (2-19) and eq. (2-30) we see that

$$F_r = \gamma^2 \left(\frac{L}{\lambda_o}\right)^2 R_b^2 \left(V_R \frac{dV_R}{dT} + V_\Theta \frac{dV_\Theta}{dT} + V_Z \frac{dV_Z}{dT}\right) = \frac{1}{\gamma} \frac{d\gamma}{dT}$$

$$= \frac{1}{\omega} \frac{e}{\gamma m_o c^2} \overline{v} \cdot \overline{E} = -\frac{\eta}{\omega\gamma} \frac{1}{c^2} \frac{\omega}{\beta_m} (R_b V_R E_r + R_b V_\Theta E_\theta + V_Z E_z)$$

$$= -\mathcal{F}_r \qquad (2\text{-}31)$$

and the identity is confirmed.

b. Applied and Self Fields – DC Case – Equations (2-20) through (2-22) or (2-27) through (2-29) are the exact general normalized relativistic equations of motion resulting from the total field on the electrons for all cases, both dc and rf, applied and self (from the electron beam) and no approximations or assumptions have so far been taken. To normalize these further, and to put them in a useful form for writing the computer codes as well as for analysis, some initial approximations and assumptions about the applied fields are required. Further, since we are integrating three coupled differential equations, the values and derivatives of R, Θ, and Z, must be set. These matters are now discussed for the dc case.

For the simple Ubitron, the applied dc fields are the constant axial magnetic field (if any) and the periodic axial and transverse fields. No tapering or jumps which might be useful in an operating tube are considered here. Means for producing periodic magnetic fields are discussed in Section III. For the computer code and analysis they are given as

$$B_z = B_o + \sum_{m=1}^{\infty} B_m \cos\left[m \frac{2\pi}{L} (z - z_e)\right] I_o\left(m \frac{2\pi}{L} r\right) \qquad (2\text{-}32)$$

$$B_r = \sum_{m=1}^{\infty} B_m \sin m\left[\frac{2\pi}{L} (z - z_e)\right] I_1\left(m \frac{2\pi}{L} r\right) \qquad (2\text{-}33)$$

or in normalized form as $B_z = B_o F_1$ (2-34a) and $B_r = B_o F_2$ (2-34b)

$$F_1 = 1 + \sum_{m=1}^{\infty} \frac{B_m}{B_o} \cos m(Z - Z_e)\, I_o(mR_b R) \qquad (2\text{-}35a)$$

$$F_2 = \sum_{m=1}^{\infty} \frac{B_m}{B_o} \sin m(Z - Z_e)\, I_1(mR_b R) \qquad (2\text{-}35b)$$

I_1 and I_o are the usual modified Bessel functions, z_e (normalized to Z_e) is an entrance "phase" parameter, and the B_m are the harmonic field amplitudes in the series representation of the space periodic field. Generally $Z_e = \pi/2$ corresponds reasonably well to the physical situation of the beam entering an end pole piece with an aperture. Minor variations from this situation can be accounted for by varying Z_e somewhat from $\pi/2$. A more accurate specification would require multiplying F_1 and F_2 by a function of Z which modifies them in the neighborhood of $Z = 0$ but nowhere else. This could be handled easily in the computer code, although probably not so easily in an analytic solution. We have not included this additional factor here. Also note: if F_1 is defined without the initial "1" term, F_1 and F_2, or sums of such functions, apply to a strictly periodic dc magnetic field which may prove useful in some Ubitron configurations. B_o then merely becomes a useful normalizing constant.

An often-used approximation is to consider the dc axial flux density to be represented by a square wave of average value B_o and peak-to-peak amplitude of $2B_a$ at $r = r_a$, with $B_a \leq B_o$, generally much less. In this instance

$$\frac{B_m}{B_o} = \frac{4B_a}{\pi B_o} \frac{(-1)^{\frac{m-1}{2}}}{m} \frac{1}{I_o(mR_a)} \quad , \quad m = 1, 3, 5 \ldots$$

$$= 0, \; m = 2, 4, \ldots \tag{2-36}$$

This approximation was used in the computer calculations to date since it was a part of the early computer code development which has not yet been changed. It is believed adequate for cases where $\mathcal{R} = r_a/r_b \simeq 4/3$ to 2. However at this lower limit for $\mathcal{R}$ and for smaller values, the more precise values of B_m/B_o now available (see Section III) should be used for calculations because of the increasing sensitivity of the electron motion to the higher harmonic values of B_m/B_o for smaller values of $\mathcal{R}$. Finally, for the configurations of interest, the applied dc component B_θ is taken to be zero.

It remains to consider the magnetic and electric fields established by the electron beam itself. To do this we must note some results obtained elsewhere, and anticipate some results to be shown shortly. We recall that electrons injected essentially axially into a constant axial magnetic field but with some nonzero circumferential and/or radial velocity will travel in a helical fashion along the axial magnetic field lines spiraling about them.[22] If space charge forces are neglected, the axis of the electron helical paths are coincident with the axial magnetic field lines. This is illustrated in Figure II-3 where a few of the electron trajectories are shown for this case. Note that the hollow cylindrical beam of infinitesimal thickness with initial radius r_b remains cylindrical and of infinitesimal thickness at any z cross section. However, its radius varies by the cyclotron circle diameter as the electrons move down the tube. For positive initial V_θ, the initial radius r_b remains the maximum beam radius. For negative initial V_θ, r_b is the minimum radius. For a less idealized model, where the injected beam would have a finite radial thickness as well as include the effects of varying θ- and r-directed

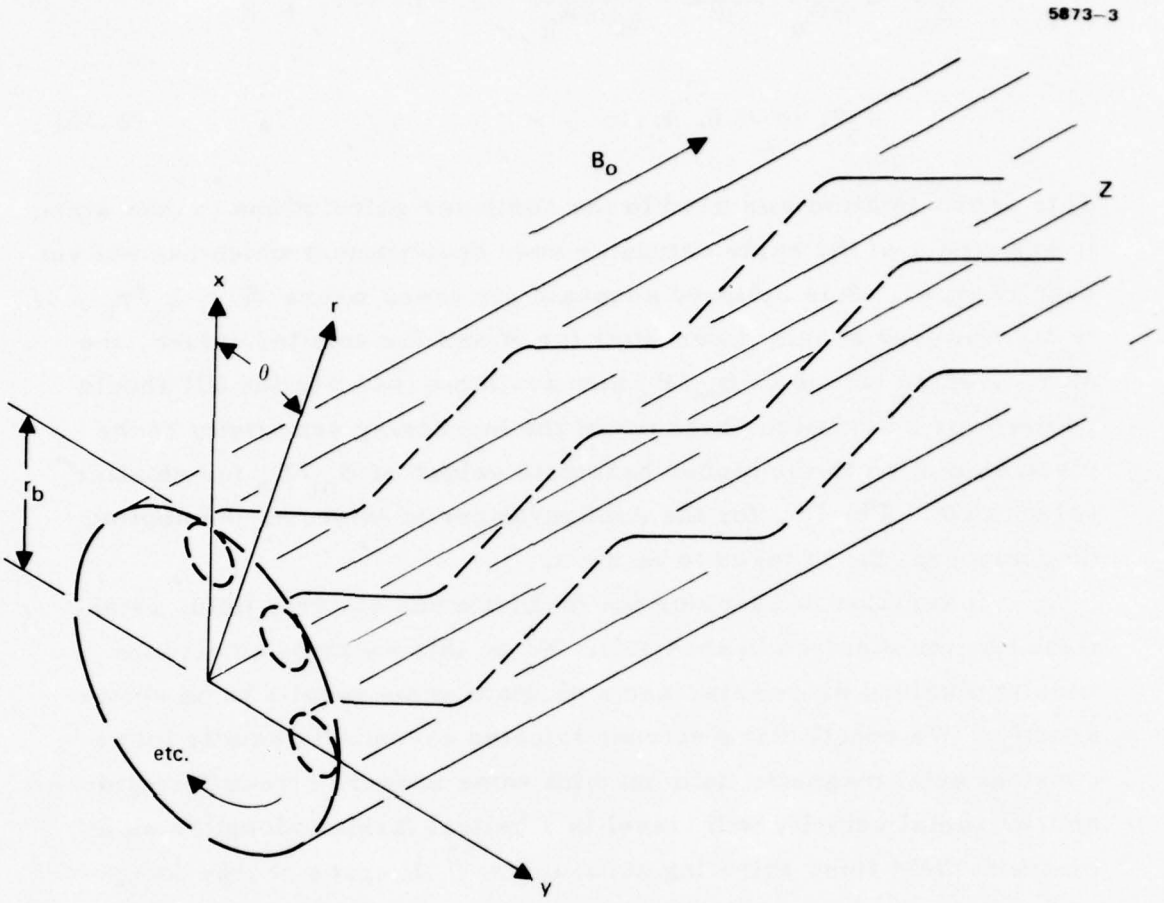


Figure II-3. Cyclotron orbits of electrons in hollow beam in constant axial magnetic field only. Initial Θ = +1.6 directed velocity.

velocities, thermal and space charge effects, the beam would have radial thickness at any z cross section. It is assumed here that the field and beam parameters are such that the cyclotron circle diameters are less than the hollow beam radius.

If space charge forces are included, even in the idealized case the centers of the cyclotron orbits or circles move slowly around the periphery of the initially defined hollow beam.[23] If space charge forces are neglected but the constant plus periodic magnetic field of eqs. (2-32) and (2-33) is applied, the cyclotron orbits are distorted from their circular shape and a precession of their centers also occurs. In the presence of both space charge and the magnetic fields one expects a combination of these motions to occur.

In the usual way it is assumed that the orbit distortions are small and that the beam can be considered essentially the equivalent of a long cylindrical hollow beam. Since the slope of the trajectories with respect to the z axis can be shown to be approximately 1^{o} to 2^{o} or less over a wide range of the parameters of interest, this approximation is quite suitable. Also, the dc axial magnetic field resulting from this motion for beams with total currents in the range of 10 A is of the order of 10^{-3} or less of applied axial fields of interest (~5000 Gauss). Thus this magnetic component of the self field and its resulting forces appear negligible. Similarly, the self B_r field is as small or smaller and its velocity interaction forces are negligible. However, although the self B_θ field is small, because it is multiplied by v_z in the r equation its force term must be considered at least there. Again, for the range of parameters of interest here, this force term turns out to be small compared to the dominant one of $v_\theta B_z$, of the order of 5%. This term should probably be included if the finer details of the electron motion are to be determined.

As for the electric field intensity forces, E_θ is zero because of symmetry and the long beam assumption. There will be an E_z component because of the cyclotron orbit periodicities as well as other axial variations. As will be seen, small standing waves of charge

exist on the beam because of the influence of the periodic magnetic field on the axial velocity. However, estimates of these effects show that both yield force terms several orders of magnitude smaller than the major ones and thus appear quite negligible.

The radial dc electric field force resulting from the beams' space charge is not quite so small. Indeed, for currents of the order of 4 A, at 300 kV and a beam diameter of 3 mm, the electric force term is comparable in magnitude to the $v_z B_\theta$ term already noted, and should be treated in a similar manner, i.e., included for finer detail determinations. In other than the radial equation, the E_r forces are again generally quite small compared to others.

With the long beam approximation we write

$$B_\theta = \frac{\mu_o I}{2\pi r} \tag{2-37}$$

and

$$E_r = \frac{I}{2\pi r\, v_{z_{av}}\, \epsilon_o} \tag{2-38}$$

where the fields to this approximation really apply to the electrons on the outer periphery of the beam. For beams of finite thickness, B_θ and E_r are both zero at the inner radius, although in reality the beam edges have no sharp cut-off. Between the inner and outer beam radii B_θ and E_r vary between these limits and can be calculated based on the assumptions taken for the current and charge density. In eqs. (2-37) and (2-38) I is the average or dc beam current, μ_o and ϵ_o the usual free-space quantities, and $v_{z_{av}}$ is the average dc beam axial velocity which is generally differs only negligibly (perhaps 1%) from the entrance axial velocity. If an approximate beam thickness Δr is

assumed or known eq. (2-38) can be expressed in terms of the usual plasma frequency

$$E_r \simeq \frac{\omega_p^2}{\eta} \Delta r \tag{2-39}$$

with

$$\omega_p^2 \simeq \frac{\eta}{\epsilon_o} \frac{I}{2\pi r \Delta r \, v_{z_{av}}} \tag{2-40}$$

Without the self-field terms the beam trajectories determined from the equations of motion are those of the inner edge of the beam. With the terms included, the trajectories are for the outer edge (to this order of approximation). It will be recognized that in order to define some self-field terms, we have made assumptions about the beam characteristics for which we now wish to solve. A common way of proceeding is to treat these terms as first approximation terms, to solve the equations, and then use this information to improve the self field etc., continuing this iterative process with the assumption (or proof) that it converges until a satisfactory self-consistent solution results. For the low-perveance devices of major present interest little if any iteration may be required for adequate trajectory prediction. Indeed, because of the low perveance, we have so far in our computer and analytic results chosen to take these self-field terms as negligible.

During the writing of this report we became aware of two very recent references[24,25] which show essentially closed-form solutions for the self-consistent trajectories of relativistic cylindrical electron

beams, both solid and hollow, immersed in constant axial magnetic fields. Although the author assumes constant sharp cutoff radii for the beam envelopes and considers the extreme high perveance regime, the solutions shown and the methods used to obtain them may be applicable to the problem here. Also very recently noted is reference 26, which examines the influence of the cyclotron orbits and different models of space charge distribution on electron motion in hollow beams.

As a still further indication of the small effect of space charge in our range of interest we obtain from the exact expression for the maximum potential depression in the beam in an idealized model of a hollow-beam in an equipotential tube[27] the following easily used expression

$$\frac{V_{min}}{V_o} \approx \left\{ 1 - \frac{3.03 \times 10^4 \mathscr{P}}{2} \left[\ln \frac{r_a^2}{r_b^2} - \frac{1}{12} \left(\frac{\Delta}{r_b} \right)^2 \right] \right\} \qquad (2\text{-}41)$$

where $\mathscr{P}$ is the beam perveance $I/V_o^{3/2}$, r_a as before, r_b is now the mean beam radius and Δ the beam radial thickness. For a case of interest, $r_a = 0.3 \times 10^{-2}$ m $= 2r_b = 30/4\,\Delta$ and $\mathscr{P} = 2.5 \times 10^{-3}$, $V_{min}/V_o = 0.9995$. At least by this measure the beam is substantially unipotential and space charge potential depression is very small indeed.

c. Final Form, DC Equations — In view of the relative magnitudes of the force terms we can now simplify the dc equations of motion for a reasonably broad range of parameters and write eqs. (2-20) to (2-22) in the following final form.

$$\frac{dV_R}{dT} + F_r V_R = \frac{V_\Theta^2}{R} - \frac{1}{\gamma}\frac{A_1}{R} - \frac{\gamma_c}{\gamma}\left[V_\Theta F_1 - \frac{A_2}{V_b}\frac{V_Z}{R}\right] \tag{2-42}$$

$$\frac{1}{R}\frac{d}{dT}(RV_\Theta) + F_r V_\Theta = -\frac{\gamma_c}{\gamma}\frac{1}{R_b}(V_Z F_2 - R_b V_R F_1) \tag{2-43}$$

$$\frac{dV_Z}{dT} + F_r V_Z = -\frac{\gamma_c}{\gamma} R_b V_R \frac{A_2}{R} + \frac{\gamma_c}{\gamma} R_b V_\Theta F_2 \tag{2-44}$$

In addition to previous definitions we also have

$$A_1 = \frac{I}{I_n}\left(\frac{\lambda_o}{R_b L}\right)^3 \frac{R_b}{V_{Z_{av}}} \tag{2-45a}$$

with

$$I_n = \frac{2\pi\epsilon_o c^3}{\eta} = 8.52 \times 10^3 \text{ A} \tag{2-45b}$$

I_n is a normalization current constant which appears here. The middle term on the right hand side in eq. (2-42) and similarly in eq. (2-47) and others later, can also be written as

$$\frac{1}{\gamma}\frac{A_1}{R} = \frac{1}{\gamma}\Delta R\,(\omega_p/\omega)^2$$

based on eqs. (2-39), (2-40), and the discussion there. ΔR is defined as $\Delta r/r_b$. $V_{Z_{av}}$ is the average normalized axial-directed velocity for which V_{Ze}, the normalized entrance velocity, is probably an adequate approximation. Also A_2 is defined as

$$A_2 = \frac{\mu_o I}{R_b L B_o} \tag{2-46}$$

and is a dimensionless constant. Comparison of eqs. (2-42) to (2-44) with eqs. (2-20) to (2-22) will indicate the field force terms dropped based on the previous discussion.

A similar treatment of eqs. (2-27) to (2-29) yields

$$\frac{dV_R}{dT} = \frac{V_\Theta^2}{R} - \frac{1}{\gamma}\frac{A_1}{R}\left[1-\left(\frac{L}{\lambda_o}\right)^2 R_b^2 V_R^2\right] - \frac{\gamma_c}{\gamma}\left[V_\Theta F_1 - \frac{A_2}{R_b}\frac{V_Z}{R}\right] \tag{2-47}$$

$$\frac{1}{R}\frac{d}{dT}(RV_\Theta) = -\frac{\gamma_c}{\gamma R_b}(V_Z F_2 - R_b V_R F_1) + A_3 \frac{1}{\gamma}\frac{V_R V_\Theta}{R} \tag{2-48}$$

$$\frac{dV_Z}{dT} = -\frac{\gamma_c}{\gamma} R_b V_R \frac{A_2}{R} + \frac{\gamma_c}{\gamma} R_b V_\Theta F_2 + A_3 \frac{1}{\gamma}\frac{V_R V_Z}{R} \tag{2-49}$$

where

$$A_3 = \left(\frac{R_b L}{\lambda_o}\right)^2 \quad A_1 = \frac{I}{I_n}\left(\frac{\lambda_o}{L}\right)\frac{1}{V_{Z_{av}}} \tag{2-50}$$

A comparison with eqs. (2-27) to (2-29) indicates the terms dropped.

Although the force terms resulting from the radial space charge force are shown in eqs. (2-48) and (2-49) little error will generally result if A_3 is taken equal to zero in both eq. (2-48) and (2-49) particularly in eq. (2-48) where the $V_R V_\Theta$ product occurs. For perveance values in the range 10^{-7} to 10^{-6} this is still substantially true for eq. (2-48) but the term should perhaps be included in eq. (2-49) where the product $V_R V_Z$ occurs, although its effect would appear quite small. This implies similar comments regarding the $F_r V_\Theta$ and $F_r V_Z$ terms in eqs. (2-43) and (2-44). The $V_R B_\theta$ terms from eqs. (2-22) and (2-29) are included in eqs. (2-44) and (2-49) respectively, since these can be of the order of the other beam self-field terms retained, but still small compared to the dominant terms.

Neglecting the self magnetic field terms in the above two sets of equations (i.e., setting A_1, A_2, and $A_3 = 0$) makes both sets identical in form. As noted following eq. (2-18), this would imply $E_r = 0$, as well as the E_θ and E_z components already taken zero. In this case $d\gamma/dt = 0$ and this results in E, as defined in eq. (2-25), remaining constant at its entrance value independent of the electron position. Thus, the value of the quantity

$$\delta = \frac{E(Z) - E(0)}{E(0)} \qquad (2\text{-}51)$$

is a measure of the accuracy of the computer or analytic solutions for the non-space charge assumption. This is discussed briefly again when some of the computer results are discussed.

d. Entrance Conditions – Because of the θ symmetry of the Ubitron analytical model it is evident that $\Theta = 0$, $R = 1$, and $Z = 0$ are the coordinate initial values. Other choices of Θ merely displace the trajectories by this amount in Θ. However, since electrons enter the Ubitron interaction space from a gun focusing configuration, for example a magnetron injection gun or a convergent hollow-beam

gun, they must cross magnetic field lines and will have finite values of V_Θ and V_R as well as the major velocity V_Z imparted by the anode voltage. A completely immersed cathode gun might also be used, but this configuration does not appear a likely candidate for a Ubitron device. Since these initial velocity values have very significant influence on electron trajectories and on Ubitron performance, their values, bounds, and inter-relationships must be established. That the gun design has such major influence on traveling-wave tube performance is well known (see for example references 15, 23 and 28), but the required relationships do not seem to have been stated in relativistic form or in the convenient normalized manner we desire here. Further details regarding the electron gun design for the Ubitron are described in Section IV.

From the unnormalized form for θ motion in eq. (2-3) with the relationship noted in eq. (2-6) the former can be stated as follows:

$$\frac{\gamma}{r}\frac{d}{dt}(rv_\theta) + v_\theta\frac{d\gamma}{dt} = -\eta\left(B_r\frac{dz}{dt} - B_z\frac{dr}{dt}\right). \qquad (2\text{-}52)$$

We assume that $E_\theta = 0$ but make no other approximations or assumptions of this point. Multiplying eq. (2-52) through by r and noting that in the usual way the flux enclosed in a circle of radius r given by[28]

$$\psi = \int_0^r B_z\, 2\pi r dr \qquad (2\text{-}53a)$$

so

$$d\psi = -2\pi r(B_r dz - B_z dr) \qquad (2\text{-}53b)$$

Equation (2-52) can be written as

$$d(\gamma r v_\theta) = \frac{\eta}{2\pi}\, d\psi \tag{2-54}$$

or

$$\gamma_2 r_2 v_{\theta_2} - \gamma_1 r_1 v_{\theta_1} = \frac{\eta}{2\pi}(\psi_2 - \psi_1) \tag{2-55}$$

on integrating between positions 1 and 2. The subscripts refer to the values of the quantities at the respective z coordinate positions. Equation (2-55) is the well known Busch's theorem in relativistic form. It should be recalled that γ contains all the velocity components.

Equation (2-55) applies between any two points along the electron beam in the Ubitron and, of particular interest here, between the emitting cathode at $z < 0$ and the entrance plane at $z = 0$. If we assume that at the cathode $v_{\theta_c} = 0$ eq. (2-55) becomes

$$\gamma_e r_e v_{\theta e} = \frac{\eta}{2\pi}(\psi_e - \psi_c)\,. \tag{2-56}$$

The subscripts e and c refer to the values at the entrance plane at $z = 0$ and at the cathode for $z < 0$. By assuming $v_{\theta c} \simeq 0$, we are for the present neglecting the emission thermal velocities. This must eventually be considered if a precise determination of the beam characteristics, thickness or radial extent, velocity distribution, noise, etc. is to be obtained. Since any practical cathode will have an emission surface extending over a range of r and/or z depending on the type of gun, we should really write for every circular differential ring of emission

$$\begin{aligned} \gamma_{e_1} r_{e_1} v_{\theta e_1} &= \frac{\eta}{2\pi}(\psi_{e_1} - \psi_{c_1})\,, \\ \gamma_{e_2} r_{e_2} v_{\theta e_1} &= \frac{\eta}{2\pi}(\psi_{e_2} - \psi_{c_2})\,. \end{aligned} \tag{2-57}$$

On the assumption that by careful design and construction $r_{e_1} \cong r_{e_2} \cdots r_{e_{n\to\infty}} = r_b$ and $r_{emax} - r_{emin} \ll r_b$ i.e., a thin beam enters the tube at the entrance plane, after summing both sides of the relationship in eq. (2-57) and averaging we have

$$\gamma_e r_b v_{\theta_e} = \frac{\eta}{2\pi} (\psi_e - \psi_c) \tag{2-58}$$

$$\psi_e = \int_0^{r_b} B_z(z = 0)\, 2\pi r dr \tag{2-59}$$

$$\psi_c = \int_0^{\bar{r}_c} B_z(z, r)\, 2\pi r dr \cong \pi \bar{r}_c^2 \bar{B}_{z_c} \tag{2-60}$$

Actually all the derived parameters in eq. (2-58) are average values but this is only emphasized for ψ_e as defined by $\bar{r}_c$ and $\bar{B}_{z_c}$. $\bar{B}_{z_c}$ is some average flux density at the cathode and $\bar{r}_c$ is some average cathode radius. These are somewhat arbitrary parameters, however, depending on the type of cathode. The significant parameter is really ψ_c.

It is convenient to cast eq. (2-58) in normalized form using the definitions in eqs. (2-19), and (2-32) to (2-35). With these we obtain

$$\gamma_e V_{\Theta_e} = \frac{\gamma_c}{2} (\Psi_e - C) \tag{2-61}$$

with

$$\Psi_e = 2 \int_0^1 F_1(Z = 0)\, R dR \tag{2-62}$$

$$C = \left(\frac{\bar{B}_{z_c}}{B_o} \right) \left(\frac{\bar{r}_c}{r_b} \right)^2 \tag{2-63}$$

(not to be confused with other C's in traveling wave tube theory) and from eqs. (2-24) and (2-25)

$$\gamma_e = \left\{ 1 - \left(\frac{L}{\lambda_o} \right)^2 \left[R_b^2 \left(V_{R_e}^2 + V_{\Theta_e}^2 \right) + V_{Z_e}^2 \right] \right\}^{-1/2} \tag{2-64}$$

where again the e subscript refers to values at Z = 0. C is a measure of the flux threading the cathode and the convergence factor or their equivalents whatever the type of gun. From eqs. (2-17) and (2-18) we see that

$$\text{K.E.} = m_o c^2 (\gamma - 1) = |e| V \tag{2-65}$$

where V is the line integral of the electric field from the cathode where the emission velocities are all assumed to be zero, to an electron with a K.E. of the value given by eq. (2-65) and related γ.

Because of our interest in low-perveance thin beams and average velocity values, we now assume that the potential depression in the beam is small. This is equivalent to the assumption that the space charge force is small compared to the other forces acting on the electrons. We also make the additional assumption that the equivalent cathode beam compression ratio is not too high. This allows us to solve equation 2-65 for γ at the entrance plane

$$\gamma_e = 1 + \frac{\eta}{c^2} V \tag{2-66}$$

where V is the cathode-to-anode voltage.* Then combining equations 2-64 and 2-66 we get

$$V_{\Theta e} = \frac{\gamma_c}{2\gamma_e} [\Psi_e - C] = \frac{\gamma_c}{2} [\Psi_e - C] \frac{1}{1 + \frac{\eta}{c^2} V} \tag{2-67}$$

and

$$\left(\frac{L}{\lambda_o}\right)^2 \left[R_b^2 \left(V_{R_e}^2 + V_{\Theta_e}^2\right) + V_{Z_e}^2\right] = 1 - \frac{1}{\gamma_e^2} = 1 - \frac{1}{\left(1 + \frac{\eta}{c^2} V\right)^2} \tag{2-68}$$

It is convenient to define the ratios of the radial and circumferential velocities to the axial velocity as

$$\mathscr{R}_{V\Theta Z} = \frac{v_{\theta e}}{v_{ze}} = \frac{R_b V_{\Theta_e}}{V_{Z_e}} \tag{2-69}$$

$$\mathscr{R}_{VRZ} = \frac{v_{re}}{v_{ze}} = \frac{R_b V_{R_e}}{V_{Z_e}} \tag{2-70}$$

---

*Taking V as the anode voltage is an approximation. The radial electric fields in the gun region will also do some work on the electrons and V should be slightly different from the anode voltage. However in a typical case of 300 kV, 4A, and 5-to-1 compression ratio, an estimate showed that the proper V differed from 300 kV by about 0.2%. Other situations will change this, but if V in eq. 2-66 and beyond is considered an equivalent voltage only slightly different from the anode voltage, the equations will apply exactly. Also, they will probably be sufficiently accurate at the tube entrance if V is taken as just the anode voltage.

With these from eqs. (2-67) and (2-68) we find after some manipulation

$$C = \Psi_e - \frac{\mathscr{R}_{V\Theta Z}}{\left[1 + \mathscr{R}^2_{V\Theta Z} + \mathscr{R}^2_{VRZ}\right]^{1/2}} \frac{1}{R_b \frac{L}{\lambda_o} \frac{\gamma_c}{2}} \left[\left(1 + \frac{\eta}{c^2} V\right)^2 - 1\right]^{1/2} \tag{2-71}$$

Another expression of interest is

$$\mathscr{R}_{V\Theta Z} = \pm (1 + \mathscr{R}^2_{VRZ})^{1/2} \left[\frac{\left(1 + \frac{\eta}{c^2} V\right)^2 - 1}{(\Psi_e - C)^2 \left(R_b \frac{L}{\lambda_o} \frac{\gamma_c}{2}\right)^2} - 1\right]^{-1/2} \tag{2-72}$$

where the sign is determined from eq. (2-67). The above equations express the interrelationships among some of the tube parameters and the entrance velocities. For example, the bounds on C can be readily established. From eq. (2-63), one limit is $C \geq 0$ on the assumption that the cathode flux is in the same direction as the entrance flux.* The other limit occurs when the voltage and gun configuration results in only $V_{\Theta e}$ with $V_{R_e} = V_{Ze} = 0$ at $Z = 0$. From eqs. (2-67) and (2-68) this upper limit is readily established resulting in

$$0 \leq C \leq \Psi_e + \frac{2}{\gamma_c} \frac{\lambda_o}{L} \frac{1}{R_b} \left[\left(1 + \eta \frac{V}{c^2}\right) - 1\right]^{1/2} \tag{2-73}$$

This is obviously a very high upper limit and clearly much smaller values must be used. We believe a better upper limit bound can only

---

*Reference 15 suggests a field reversal arrangement in which a different limit than the one derived here would apply.

come from computer or analytic solutions to the full equations of motion which relate V_{Θ_e}, V_{R_e}, V_{Z_e}, C, etc. to the useful range of Ubitron performance. Incidentally, from the definition of Ψ_e it can be shown that generally $\Psi_e \simeq 1$ (it is identically 1 for the usual case of $Z_e = \pi/2$ and the idealized model of eq. (2-36)). The limited experience we have had with the computer solutions of the equations of motion for Ubitron performance indicate that values for C in the neighborhood of 1 are most useful. This may have some implications regarding possible gun compression ratios and permissible cathode loading.

Some examination of Figure II-3 and consideration of the trajectories from the cathode at $Z < 0$ to the entrance plane at $Z = 0$ demonstrates that in a certain sense V_{R_e} and V_{Θ_e} are interchangeable. For any given initial values, there are positions along the trajectories at which the transverse component of electron velocity is only radial or only circumferential. These positions will be at different radii. In our work we have only assumed initial conditions which make the cyclotron radii smaller than r_b, the normal beam radius. In the computer runs to be described later, we have taken $V_R = 0$ at $Z = 0$ although nonzero values can be used for input. As already noted, we have ignored thermal effects on the basis that at least in the model this is consistent with some choice of cathode-anode spacing, magnetic field configuration, etc.

The above equations are relativistically correct and so also apply in the non-relativistic approximation but in somewhat simplified form. Nonrelativistic forms result from setting $\gamma_e = 1$ in equation (2-61) and using

$$\left(1 + \frac{\eta}{c^2} V\right)^2 - 1 = \frac{2\eta V}{c^2}\left[1 + \frac{\eta V}{2c^2}\right] \simeq \frac{2\eta V}{c^2}$$

in equations (2-71) and (2-72). Note that $c^2/\eta = 511.006 \times 10^3$ volts, or $\eta/c^2 = 1.95692 \times 10^{-6}$ volts^{-1}.

e. Final Form-DC Plus Constant RF Drive – In order to determine the effect of the presence of the TE_{01} mode rf fields on Ubitron electron motion we have written the equations of motion for the case where a constant rf power TE_{01} mode propagates down the tube containing the electron beam. Solution of these equations would yield information about the magnitude of the parameters for which a small-signal theory applies, would give a useful picture of the bunching mechanism, and would permit some estimate of possible efficiency in the large-signal regime. It would also be a step in the direction of a complete system of equations leading to growing waves describing the energy exchange between the dc beam and the interacting TE_{01} mode wave over the entire small- to large-signal regime.

The TE_{01} mode field components can be written as follows where their amplitudes are defined in terms of the power, P_z, which would be transmitted in the absence of the electron beam[29]

$$E_\theta = DJ_1(k_c r)\, e^{j(\omega t - 2\pi/\lambda_g z - \theta_i)} \tag{2-74}$$

$$H_r = -\frac{\sqrt{1 - \left(\frac{\lambda_o}{\lambda_{oc}}\right)^2}}{\sqrt{\frac{\mu_o}{\epsilon_o}}} DJ_1(k_c r)\, e^{j(\omega t - 2\pi/\lambda_g z - \theta_i)} \tag{2-75}$$

$$H_z = j\,\frac{\lambda_o}{\lambda_{oc}}\,\frac{1}{\sqrt{\frac{\mu_o}{\epsilon_o}}}\, DJ_o(k_c r)\, e^{j(\omega t - 2\pi/\lambda_g z - \theta_i)} \tag{2-76}$$

where

$$D = \sqrt{\frac{2}{\pi}}\ \frac{1}{r_a}\left(\frac{\mu_o}{\epsilon_o}\right)^{1/4}\ \frac{\sqrt{P_z}}{\left|J_o(k_c r_z)\right|}\ \frac{1}{\left[1 - \left(\frac{\lambda_o}{\lambda_{oc}}\right)^2\right]^{1/4}} \qquad (2\text{-}77)$$

Additionally, λ_{oc} is the free space cutoff wavelength for a tube of radius r_a, where $J_1(k_c r_a) = 0$. Thus

$$k_c = \frac{3.832}{r_a}, \quad \lambda_{oc} = \frac{2\pi}{k_c} = 1.640\ r_a \qquad (2\text{-}78)$$

and

$$\left|J_o(k_c r_a)\right| = 0.4028 \qquad (2\text{-}79)$$

Further

$$\lambda_g = \frac{\lambda_o}{\sqrt{1 - \left(\frac{\lambda_o}{\lambda_{oc}}\right)^2}} \qquad (2\text{-}80)$$

The entrance phase of the TE_{01} mode wave is θ_i which has been momentarily described in the usual complex notation. With the fields defined as in eqs. (2-74) to (2-78)

$$P_z = \frac{1}{2}\int_0^{r_a}\int_0^{2\pi} E_\theta H_r^* r\,dr\,d\theta \qquad (2\text{-}81)$$

with * the usual complex conjugate. All the units are in the MKS system with P_z in watts, E_θ in V/m, H_r and H_z in A/m, and all other symbols are as previously defined.

Insertion of the TE_{01} mode field components from eqs. (2-74) to (2-76) into eqs. (2-20) to (2-22) including the applied and self dc field results in the following:

$$\frac{dV_R}{dT} + F_r V_R = \frac{V_\Theta^2}{R} - \frac{1}{\gamma}\frac{A_1}{R} - \frac{\gamma_c}{\gamma}\left[V_\Theta F_1 - \frac{A_2}{R_b}\frac{V_Z}{R}\right]$$

$$+ \frac{a}{\gamma}\tau V_\Theta \sqrt{P_z}\, J_0(\beta R)\sin\Phi \qquad (2\text{-}82)$$

$$\frac{1}{R}\frac{d}{dT}(RV_\Theta) + F_r V_\Theta = -\frac{\gamma_c}{\gamma}\frac{1}{R_b}(V_Z F_2 - R_b V_R F_1)$$

$$- \frac{a}{\gamma}\left(\frac{\lambda_{0c}}{L}\right)\frac{1}{R_b}\tau\sqrt{P_z}\, J_1(\beta R)\cos\Phi$$

$$+ \frac{a}{\gamma}\left(\frac{\lambda_{0c}}{\lambda_0}\right)\frac{1}{R_b}\left(\frac{\lambda_0}{r_a}\right)^4 \frac{1}{\tau} V_z\sqrt{P_z}\, J_1(\beta R)\cos\Phi$$

$$- \frac{a}{\gamma}\tau V_R \sqrt{P_z}\, J_0(\beta R)\sin\Phi \qquad (2\text{-}83)$$

and

$$\frac{dV_Z}{dT} + F_r V_Z = -\frac{\gamma_c}{\gamma} R_b V_R \frac{A_2}{R} + \frac{\gamma_c}{\gamma} R_b V_\Theta F_2$$

$$- \frac{a}{\gamma}\left(\frac{\lambda_{0c}}{\lambda_0}\right) R_b\left(\frac{\lambda_0}{r_a}\right)^4 \frac{1}{\tau} V_\Theta \sqrt{P_z}\, J_1(\beta R)\cos\Phi \qquad (2\text{-}84)$$

where

$$a = \left[\frac{\eta}{2\pi c^2} \sqrt{\frac{2}{\pi}} \left(\frac{\mu_0}{\epsilon_0} \right)^{1/4} \frac{1}{1.64 \left| J_0 (k_c r_a) \right|} \right]$$

$$= 7.3 \times 10^{-6} \text{ (watts)}^{-1/2} \tag{2-85}$$

$$\tau = \left(\frac{\lambda_0}{r_a} \right)^2 \left[1 - \left(\frac{\lambda_0}{\lambda_{0c}} \right)^2 \right]^{-1/4} \tag{2-86}$$

$$\beta = \frac{3.832}{\mathscr{R}} \tag{2-87}$$

and

$$\Phi = T - \frac{L}{\lambda_g} - \Phi_i \tag{2-88}$$

Alternatively the equations for the combined rf and dc fields can be expressed from eqs. (2-27) to (2-28) as

$$\frac{dV_R}{dT} = \frac{V_\Theta^2}{R} - \frac{1}{\gamma} \frac{A_1}{R} \left[1 - \left(\frac{L}{\lambda_0} \right)^2 R_b^2 V_R^2 \right] - \frac{\gamma_c}{\gamma} \left[V_\Theta F_1 - \frac{A_2}{R_b} \frac{V_Z}{R} \right]$$

$$+ \frac{a}{\gamma} \tau V_\Theta \sqrt{P_z} J_0(\beta R) \sin \Phi$$

$$+ \frac{a}{\gamma} \left(\frac{\lambda_{0c}}{\lambda_0} \right) \left(\frac{L}{\lambda_0} \right) R_b \tau V_R V_\Theta \sqrt{P_z} J_1(\beta R) \cos \Phi \tag{2-89}$$

$$\frac{1}{R}\frac{d}{dT}(RV_\Theta) = -\frac{\gamma_c}{\gamma}\frac{1}{R_b}(V_Z F_2 - R_b V_R F_1) + \frac{A_3}{\gamma}\frac{V_R V_\Theta}{R}$$

$$-\frac{a}{\gamma}\left(\frac{\lambda_{0c}}{L}\right)\frac{1}{R_b}\left[1-\left(\frac{L}{\lambda_0}\right)^2 R_b^2 V_\Theta^2\right]\tau\sqrt{P_z}\,J_1(\beta R)\cos\Phi$$

$$+\frac{a}{\gamma}\left(\frac{\lambda_{0c}}{\lambda_0}\right)\frac{1}{R_b}\left(\frac{\lambda_0}{r_a}\right)^4\frac{1}{\tau}V_z\sqrt{P_z}\,J_1(\beta R)\cos\Phi$$

$$-\frac{a}{\gamma}\tau V_R\sqrt{P_z}\,J_0(\beta R)\sin\Phi \qquad (2\text{-}90)$$

and

$$\frac{dV_Z}{dT} = -\frac{\gamma_c}{\gamma}R_b V_R\frac{A_2}{R} + \frac{\gamma_c}{\gamma}R_b V_\Theta F_2 + \frac{A_3}{\gamma}\frac{V_R V_Z}{R}$$

$$-\frac{a}{\gamma}\left(\frac{\lambda_{0c}}{\lambda_0}\right)\left(\frac{\lambda_0}{r_a}\right)^4\frac{1}{\tau}R_b V_\Theta\sqrt{P_z}\,J_1(\beta R)\cos\Phi$$

$$+\frac{a}{\gamma}\left(\frac{\lambda_{0c}}{\lambda_0}\right)\left(\frac{L}{\lambda_0}\right)\tau R_b V_\Theta V_Z\sqrt{P_z}\,J_1(\beta R)\cos\Phi \qquad (2\text{-}91)$$

In the above Φ_i varies from 0 to 2π.

The above equations are in a certain sense unbalanced in that with rf drive some field terms taken to be negligible will become important. Particularly because of axial rf bunching the E_z and perhaps the E_r field forces must be considered. No attempt was made here

to add these terms which might be included to sufficient order by the ring model common in large-signal traveling-wave tube theory, at least for computer models.[30,31] Additionally the magnetic fields resulting from the rf motion of the electrons, again probably B_θ, and possibly B_z, may become of sufficient magnitude to warrant including for precision.

D. Computer Code Results

1. General

Because of the nature of the differential equations which must be solved and since it was anticipated that any analytic solution might be limited by required approximations even aside from the problem of obtaining numerical and easily displayed results from analytic solutions, two major sets of equations of motion for initial investigation of Ubitron performance were coded for computer application. One set is defined by eqs. (2-42) to (2-44) for dc fields and the other by eqs. (2-82) to (2-84) for dc plus constant power rf TE_{01} mode fields. So far the codes do not include the self fields of the beam shown in the equations, space charge etc., but these could be included easily in the next generation.

As presently established the codes require only the physical parameter inputs, i.e., voltage, frequency, electron gun entrance parameter, magnetic field modulation parameter and entrance phase, average magnetic field, and beam/tube ratio. The nominal tube radius is determined for Ubitron synchronous performance at the stated voltage and the entrance velocities are then determined. All these are then normalized and used as input to the integration program. At the operator's choice the program can then be run for variations in voltage, frequency, etc. on the assumption that the physical parameters in a tube, such as the tube radius, magnetic period, gun parameters, etc. remain fixed. For the dc-plus-rf code additional inputs are the power, P_z, and the wave phase, Φ_i. A plotting routine is part of these programs and can be used to plot, R, Ⓗ, Z, etc. as a function of axial position.

In addition to the codes for integrating the equations of motion, two additional ones are available which use the output of these integrations. In one case the code directs plotting R vs Ⓗ as a function of the electron's position; in the other a beam factor, the weighted first harmonic velocity squared for use in the cylindrical/planar equivalence model, is computed via a correlation integral. All of the codes are described in further detail in Appendix A.

2. Proof Tests

To establish some confidence in the computer-generated results two types of simple proof tests were made. In one type the entrance conditions were $R_e = 1$, $Ⓗ_e = 0$, $Z_e = 0$ and $V_{Re} = 0$, $V_{Ⓗe} = 0$, and $V_{Ze} = dZ/dT\big|_{T=Z=0} = V_{Ze}$. The periodic magnetic field was also set to zero but not the average axial field, i.e., $B_a = 0$ in eq. (2-36) or $F_1 = 1$. This is equivalent to launching the electrons strictly axially into the magnetic field parallel to the magnetic field lines. The electrons should travel axially in straight lines with the initial input velocity with solutions $R = 1$, $Ⓗ = 0$, $Z = V_{ze}T$, $V_R = 0$, $V_Ⓗ = 0$, and $V_Z = dZ/dT = V_{Ze}$. Exactly these solutions resulted to the eight significant figures available from the computer printout. In view of the straight-line character of these results they are not displayed here.

A somewhat more stringent test resulted from the two cases for input conditions given by $R_e = 1$, $Ⓗ_e = 0$, $Z_e = 0$, $V_{Re} = 0$, $V_{Ⓗe} = +0.0075$, $V_{Ze} = dZ/dT_{T=Z=0} = 0.397$, and for the same conditions except for $V_{Ⓗe} = -0.0075$. Here, too, $B_a = 0$ or $F_1 = 1$ was taken. This is equivalent to launching electrons with either positive or negative directed velocities into a constant magnetic field, taken here as 7000 gauss. Other parameters of choice or derived are:

$$\frac{L}{\lambda_0} = 1.96,\ \gamma = 1.5931,\ \gamma_c = 0.2080,\ R_b = 1.55$$

These are equivalent to electrons with an entering energy of slightly over 300 keV with a z directed velocity of nearly 0.8c and a θ directed velocity of nearly 0.03c. It can be shown that electrons so launched follow helical paths which in our notation have a radius of[22]

$$r_{c_{\mp}} = \frac{|v_{\theta e}|}{\omega_c/\gamma} = \frac{\gamma}{\gamma_c}\,\frac{1}{\beta_m}\,R_b\,\left|V_{\Theta e}\right| \tag{2-92}$$

where the $\mp$ indicates that for $V_{\theta e} > 0$ the paths are inside the launching radius (r_{c-}) whereas for $v_{\theta e} < 0$ the paths are outside (r_{c+}). The normalization notation of eq. (2-19) is used here. As further normalization with $2r_c$ the diameter, d_c, of the projected cyclotron circles we have

$$\frac{d_c}{r_b} = 2\,\frac{\gamma}{\gamma_c}\,\left|V_{\Theta e}\right| \tag{2-93}$$

Further with $d_c \leq r_b$ it can be shown that the maximum total angular excursion of the projected cyclotron circle is given by

$$\theta_{max} = 2\cos^{-1}\left\{\frac{\left[1 - \frac{2\gamma}{\gamma_c}\,V_{\Theta e}\right]^{1/2}}{1 - \frac{\gamma}{\gamma_c}\,V_{\Theta e}}\right\} \tag{2-94}$$

and here the actual sign of $V_{\Theta e}$ must be used. Finally, since the velocities are invariant it follows in normalized parameters that the time per cycle is given by

$$\underset{\text{per cycle}}{T} = \frac{2\pi}{\frac{\gamma_c}{\gamma}} \tag{2-95}$$

Figures II-4 and II-5 show results of the two test cases run with the parameter values indicated above. As read from the computer plotted graphs, the diameters, maximum angular excursions, and normalized times per cycle agree with theoretical predictions from the given input data to within 3 or 4 significant figures. Z vs T is a straight line and is consequently not shown. The circles are physically the same size but appear of different size in the graphs because of the manner of scale choice by the plotting routine.

Note that in Figures II-4 and II-5) the R versus Θ plots may not appear as true circles because R and Θ are plotted as rectangular coordinates similar to a logarithmic transformation. Actually the plots do not completely indicate the available accuracy from the codes. Examination of some printout data showed that for the step size used in these examples an accuracy of 4-to-5 significant figures was achieved, and greater accuracy may be available.

3. Ubitron Type Fields - DC only

Many computer runs for electron motion in a Ubitron-type magnetic field for dc conditions only were made. Generally these were for conditions equivalent to 300 kV with a magnetic period of 0.6 cm and an eventual operating frequency of 94 GHz. Most of the runs were for the condition $\mathcal{R} = 2.0$ i.e., the beam radius half the tube radius but a few were made for $\mathcal{R} = 1.33$, the beam radius 3/4 of the tube radius. The parameters usually varied were B_a/B_0, or equivalently B_1/B_0, and $V_{\Theta e}$. Time did not permit an exhaustive examination of the influence of the various parameters, but from the available runs, the theory in the latter part of this section and elsewhere in this report, some general trends are quite evident.

Figures II-6, II-7, and II-8 show some examples of the results obtained. The conditions which pertain to each case are indicated in the figures. In all cases the electron motion was determined for $20\pi \geq Z \geq 0$ equivalent to 10 magnetic periods, i.e., 10 L. This seemed sufficient to determine the major characteristics of electron

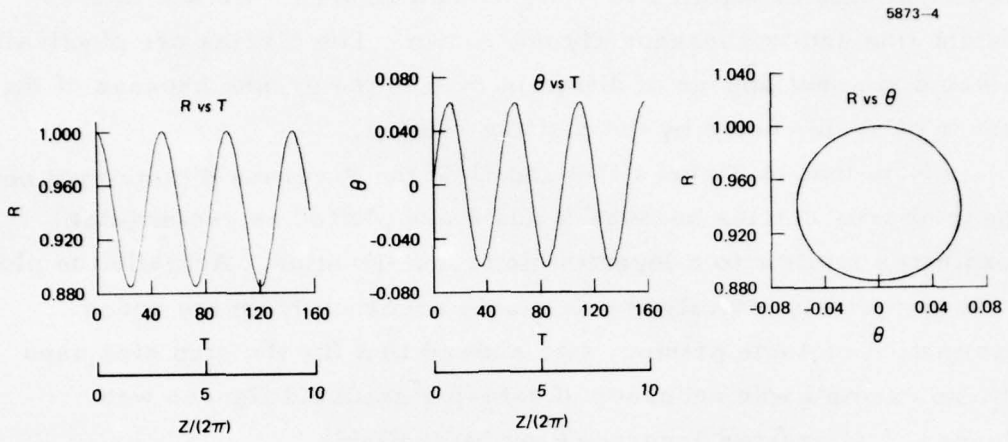


Figure II-4. Proof runs for program 2 DC relativistic electron equations of motion - cyclotron circles, V_{Θ_e} = + 0.0075.

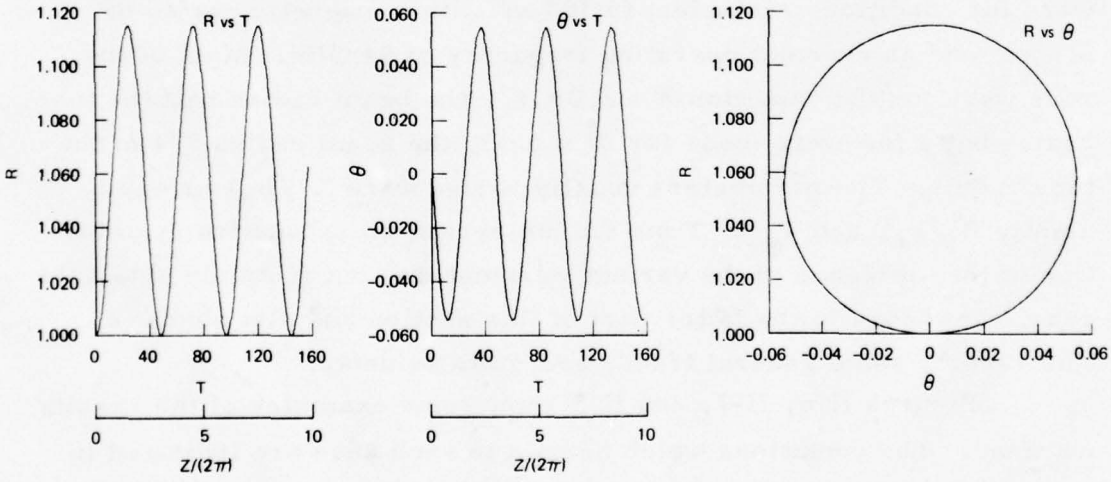


Figure II-5. Proof runs for program 2 DC relativistic electron equations of motion - cyclotron circles, V_{Θ_e} = - 0.0075.

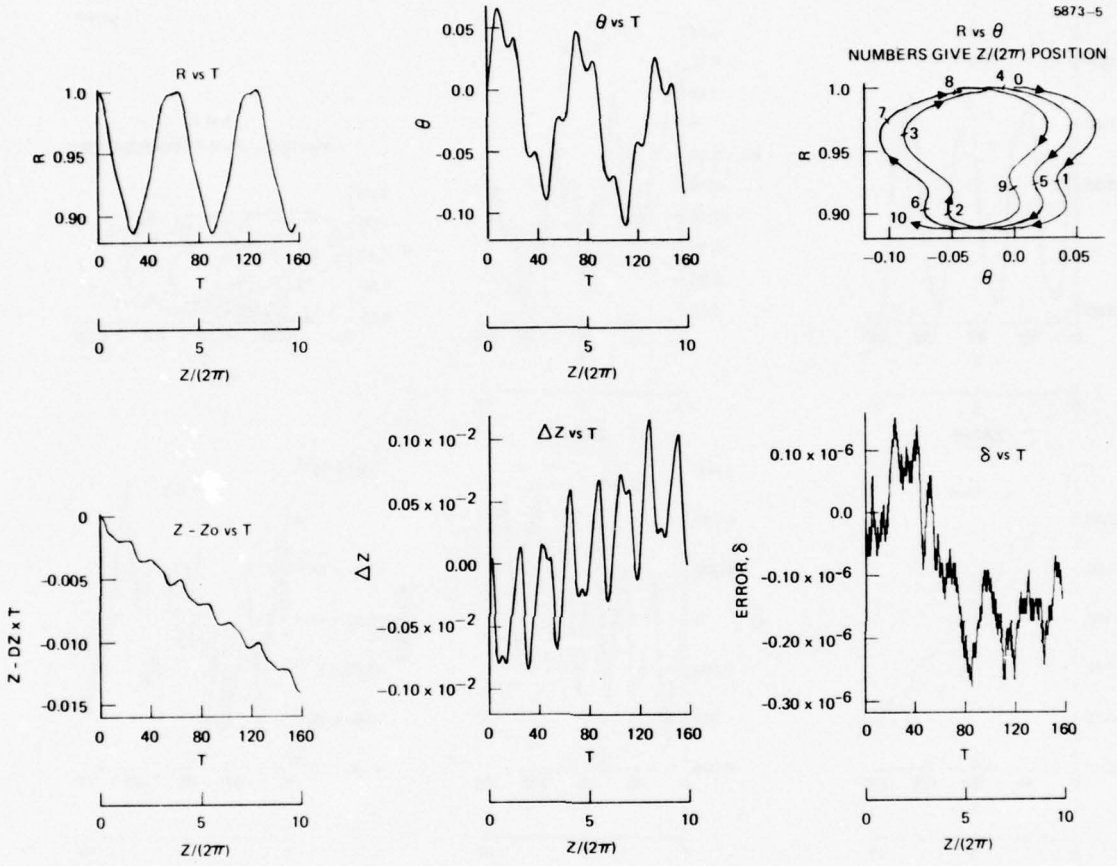


Figure II-6.
Computer solutions for DC only equations of motion for Ubitron conditions: B_1/B_0 = 0.1, B_0 = 5000 gauss V = 300 Kv, $V_{\Theta e}/V_{Ze}$ = 0.018, V_{Re}/V_{Ze} = 0.0 (cathode beam compression ratio) = 0.91, R = 2.0, $Z_e = \pi/2$ magnetic period for synchrorons operation at 94 GHz = L ≈ 0.6 cm.

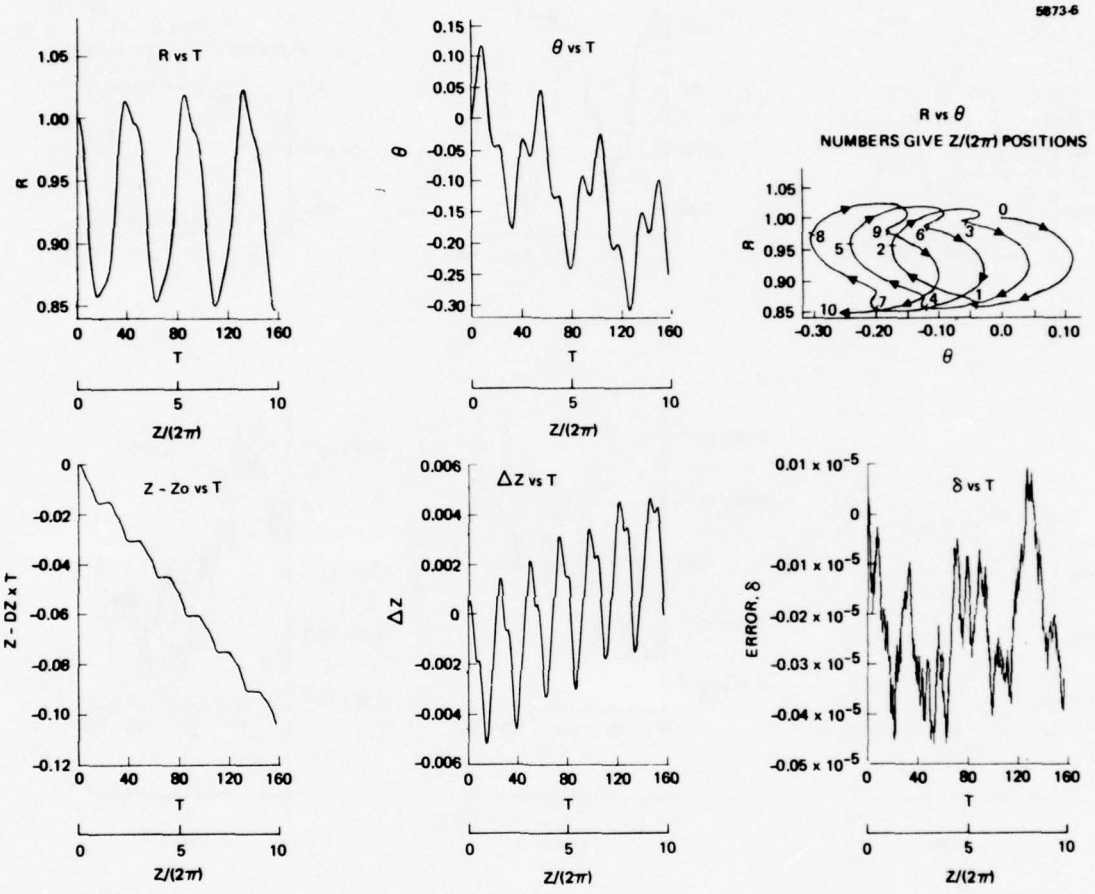


Figure II-7.
Computer solutions for DC only equations of motion for Ubitron conditions: B_1/B_0 = 0.1, B_0 = 7000 gauss V = 300 Kv, $V_{\theta e}/V_{Ze}$ = 0.027, V_{Re}/V_{Zc} = 0.0, (cathode beam compression ratio) = 0.89, R = 2.0, $Z_e = \pi/2$ magnetic period for synchrorons operation at 94 GHz = L ≈ 0.6 cm.

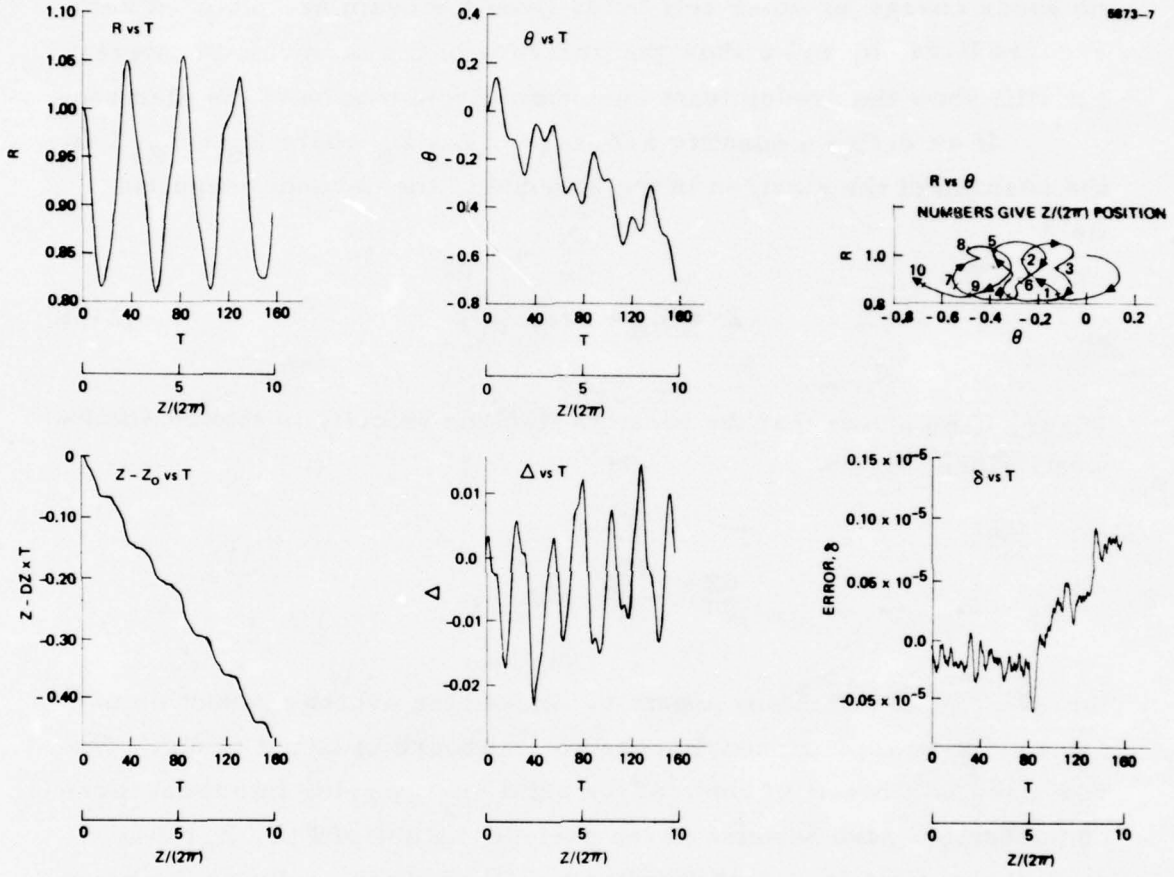


Figure II-8.
Computer solutions for DC only equations of motion for Ubitron conditions: B_1/B_0 = 0.1, B_0 = 7000 gauss, V = 300 Kv, $V_{\Theta e}/V_{Ze}$ = 0.04, V_{Re}/V_{Ze} = 0, (cathode beam compression ratio) = 0.89, R = 1.33, $Z_e = \pi/2$ magnetic period for synchrorons operation at 94 HGz = L ≈ 0.6 cm.

motion. Figure II-6 shows the electron motion for the case where B_1/B_0, the magnitude of the dominant magnetic harmonic, is 0.1, about half the maximum value currently considered practical for an average axial field of 5000 gauss. Considerable distortion of the cyclotron circle is evident in the R vs Θ plot of (Figure II-6) as well as the procession in Θ of this distorted circle. It should be recalled that no space charge or other self fields from the beam are included here. Figures II-6a, b, and c show the presence of the harmonic of interest but still show the predominant cyclotron circle motion of the electrons.

If we define a quantity $F(Z, Z_0) = Z - Z_0$ where $Z_0 = V_{Ze}T$ is the position of the electron in the absence of the periodic magnetic field

$$Z = Z_0 + F(Z, Z_0) \tag{2-96}$$

Figure II-6d shows that the average electron velocity is slowed somewhat, since

$$\frac{dZ}{dT} < \frac{dZ_0}{dT} = V_{Ze},$$

the average dF/dT being negative. Indeed the average reduction in axial velocity appears nearly constant, although in fact it is not. The reduction is a result of some of the axial energy going into transverse components. Also because of the periodic nature of $F(Z, Z_0)$ it is evident that time invariant standing waves of charge exist on the beam, since electrons leaving the entrance plane will slow down and speed up as a result of the periodic magnetic field. It is also evident that, based on the values shown for $F(Z, Z_0)$ for the conditions of Figure II-6, the average velocity change and the charge standing wave effects are relatively small. This has been true of the range of parameter

values so far investigated and seems to pertain generally. Incidentally, since $Z - Z_0$ vs T is so small Z vs T is not shown, since it is a straight line in any sensible scale. It should be noted again that these results are for the case of no rf power present.

Another plot of interest regarding Z motion is shown in Figure II-6e where DELTZ is defined as

$$\text{DELTZ} = Z - Z_{end} \frac{T}{T_{end}} \tag{2-97}$$

where Z_{end} and T_{end} are the normalized true position and elapsed time at the end of an integration run. DELTZ is an indication of the deviation of the electron velocity as a function of time or distance from some average velocity for a given total distance or time as evident from

$$\frac{d(\text{DELTZ})}{dT} = V_Z - \frac{Z_{end}}{T_{end}} = V_Z - V_{Zav(0\text{-end})}$$

It will be noticed that all the computer plots are shown as functions of T but a Z scale is also shown. In view of the remarks in connection with $Z - Z_0$ above, the graphs versus either variable appear negligibly different. However, in considering Ubitron performance details this difference must be considered. For example in Figure II-6d $Z - Z_0 \simeq -0.014$ at the end of 10 periods, or the electron is displaced only 0.2% of a period; on the other hand as seen from Figures II-7e and II-8e, for the conditions there $Z - Z_0$ is about 7 to 35 times this value respectively. In these cases, and particularly the latter, this deviation would be significant. Since Z is available from a data storage file as a result of the computer integration, the plotting subroutine could easily be altered to plot the variables versus Z rather than T.

Figure II-6f refers to the error δ as defined in eq. (2-51), where in the related discussion it was noted that in the absence of the beam self fields or other electric fields δ should be zero. As seen in Figure II-6e values of less than 10^{-6} are encountered during the entire run. Since the baseline value of E(0) in this and the other cases shown is close to 0.16, it seems clear that a rather accurate definition of the electron motion has been achieved.

Figure II-7 shows a similar set of graphs where the axial magnetic field has been increased to 7000 gauss, B_a/B_0 has been almost doubled so that B_1/B_0 is nearly 0.19, the initial θ directed velocity has been increased by 50%, but the other parameters remained substantially the same. Some examination indicates that the basic motion of the electrons has changed even more than for the case shown in Figure II-6. Because of the scale choice of the plotting routine this is not immediately obvious from the R and Θ plots but the value of $F(Z, Z_0) = Z - Z_0$ at the end of the run in Figure II-7d (-0.105) compared to that in Figure 2-6d (-0.014) shows the change in the former resulting from the parameter changes.

Finally, Figure II-8 is for all parameters identical to those in Figure II-7 except for a change in the entrance radius of the beam. In Figure II-7 $\mathcal{R} = r_a/r_b = 2.0$, whereas in Figure II-8, $\mathcal{R} = r_a/r_b = 1.33$. In the latter case the closer position of the beam to the wall with substantially larger value of the dominant magnetic field harmonic (and other harmonics as well) causes quite discernible differences in the electron motion as compared to those shown in Figure II-7. Again as a measure of the change the end value of $F(Z, Z_0) = Z - Z_0$ in Figure II-8d (-0.475) should be compared with that in Figure II-7d (-0.105).

4. Ubitron Type Fields - DC plus Constant RF Drive

As the present study program came to a close this computer code had been substantially debugged and was available for final proof runs and use. Unfortunately time did not permit obtaining results even to the extent available from the dc only code. However some early

tests had indicated that for P_z values in the range of 100 to 1000 watts for the TE_{01} mode, a dc voltage of 300 Kv, and with the other parameters in the range already used in the dc-only runs, the electron motion as determined from the direct R and Ⓗ plots was not substantially altered. In one case examined the energy difference measure δ as defined in eq. (2-51) showed an increasing amplitude envelope with increasing Z as might be expected. A better measure of the increasing kinetic energy imparted by the rf mode might be γ which is also available from the computer run; indeed perhaps even better might be $V_{Ⓗc}^2$ since it is only this velocity and resultant charge/current component which interacts with the E_θ component of the TE_{01} mode wave.

In any case, it is recommended that in any future work, the quantities which should be displayed are the differences between the dc-only and the dc-plus-rf parameters. These would be available from runs of the available codes and are the quantities of interest. Indeed these are the polarization parameters noted in the prior discussion. Further, such a separation would permit easy observation of the bunching action as well as other items of interest in Ubitron performance.

E. Equivalence Theory – Hybrid Small Signal Approach

1. Concept and Prior Small Signal Theory

Even with a complete small-signal theory which would come from the solution of the closed-loop system of the circuit and electronic equations as discussed in paragraph B. of this section, it would be convenient and useful as a check to have an alternative approach. Since the electron dc motion plays an important role in any useful solution and since we now have from the computer code means for accurate prediction of such motion, the question naturally arises whether this tool could be used in combination with the available planar sheet beam small-signal theory of the Ubitron[2] to achieve useful performance estimates. Even with adeqate analytic solutions to the dc motion which now appear available or possible, it would be

convenient to use these in a similar hybrid manner, in addition to the considerably more complex and difficult wave solution on the assumption that this latter can be achieved and put in useful form.

The following discussion develops what we call an equivalence theory via a hybrid small-signal approach. It combines the results from the available dc relativistic motion computer code to determine those major parameters in the previous small-signal planar sheet beam theory which would be affected by nonplanar motion. Thus it accounts for both the cylindrical nature of the Ubitron model of current interest as well as for the true radial motion of the electrons. Such hybrid or equivalence approaches are of course not uncommon in traveling-wave tube theory, and elsewhere. However, some possible novelty may attach to the development here because of the manner of extracting the parameters of interest via the use of some of the methods of generalized harmonic analysis, particularly the use of the autocorrelation function. Although used in a simple way here, it seems quite possible that these tools will prove quite useful in future work in determining Ubitron amplifier performance particularly as regards nonlinear or large signal operation and also as regarding noise performance and spectral output.

As a major determinant of performance and of interest here in the notation of Reference 2:

$$C_u^3 = \frac{K' \Lambda^2}{16 R_o} \tag{2-98a}$$

with

$$K' = \frac{E_y^2}{2\beta_e^2 P} \tag{2-98b}$$

$$= \frac{\dot{y}_o}{v_o} \tag{2-98c}$$

$$R_o = \frac{V_o}{I_o} \tag{2-98d}$$

Figure II-9 illustrates the concept of equivalence to be used. Some consideration shows that the cylindrical planar equivalence is

$$x \rightarrow r, \quad y \rightarrow r\theta, \quad z \rightarrow z \tag{2-99a}$$

and

$$v_x \rightarrow v_r, \quad v_y \rightarrow v_\theta, \quad v_z \rightarrow v_z . \tag{2-99b}$$

This concept of equivalence has been noted briefly in paragraph C.1 and, indeed, for a large radius beam and with motion in the x direction allowed, the equivalence between a planar model and a cylindrical model would be quite close. In the planar model of reference 2, x and v_x were taken as zero. The mode of interest in the planar model has E_y as the only rf electric field component and the mode of interest in the cylindrical model, the TE_{01} mode, has E_θ as the only rf electric field component. Further, in eq. (2-98), $\beta_e = \omega/v_o$ where ω is the radian frequency, v_o is the dc axial velocity (assumed equal to the entrance axial velocity), $\dot{y}_o$ is the maximum amplitude of the directed velocity resulting from the action of the transverse magnetic field, V_o and I_o are the dc beam voltage and current respectively, and P is the power carried in the mode of interest with maximum amplitude E_y. It is assumed in the planar model that the sheet beam maintains its position at the maximum of the E_y field.

If we rewrite eq. (2-98a) in the notation of this report using the planar-to-cylindrical equivalence of eq. (2-99) and the definitions above we find

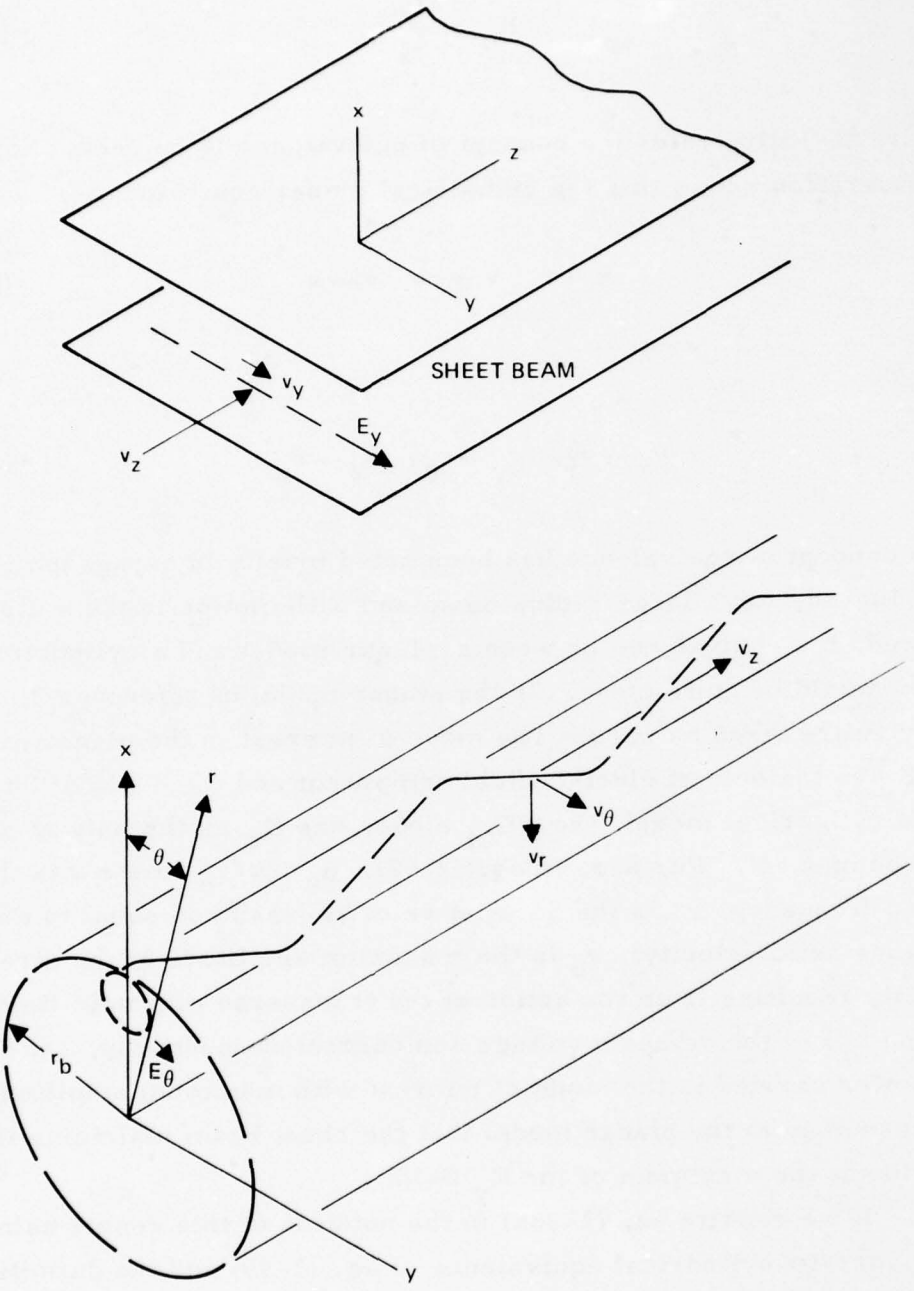


Figure II-9. Equivalence between planar sheet beam and hollow cylindrical beam.

$$C_u^3 = \frac{1}{16} \frac{E_\theta^2}{2\frac{\omega^2}{v_{ze}^2} P_z} \frac{v_{\theta 1}^2}{v_{ze}^2} \frac{I_o}{V_o} = \frac{1}{16} \frac{1}{2\omega^2 P_z V_o} \left(E_\theta^2 v_{\theta 1}^2 I_o\right) \tag{2-100}$$

In eq. (2-100) $v_{\theta 1}$ is defined as the amplitude of the θ directed velocity corresponding to $\dot{y}_o$ in the planar model. The subscript is attached since it is only this harmonic of the θ directed velocity which has the periodicity of the transverse magnetic field which results in the interaction of present interest at or near the synchronous voltage. The point here is that because of the complicated motion of the electrons it can be anticipated that the total velocity will contain harmonics of this periodicity and possibly others, as well as some other nonperiodic components. Further, since E_θ varies with radius the electrons will be acted on by this radially varying field. Also, because of the radially varying position of the electrons the value of I_o to use in eq. (2-100) will be affected. In this sense C_u^3 will vary with axial position, and to estimate tube performance we need to know the effective or weighted value of $E_\theta^2 v_{\theta 1}^2 I_o$. Thus we wish to determine the value of

$$C_u^3 = \frac{1}{16} \frac{1}{2\omega^2 P_z V_o} \left(E^2 v_{\theta 1}^2 I_o\right)_{eff} \tag{2-101}$$

where the factor

$$\frac{1}{16} \frac{1}{2\omega^2 P_z V_o}$$

is essentially invariant to electron motion and the factor $(E_\theta^2 v_{\theta 1}^2 I_o)_{eff}$ is a function of that motion. Additionally there is a correction to be made when the operating voltages are in the relativistic range. This correction is described below.

2. Relativistic Corrections to the Small-Signal Gain Theory of Ubitrons

Because of our interest in high-voltage designs, it has been necessary to make relativistic corrections to the small-signal theory previously given in the G.E. work by Bacon, Enderby, and Phillips.[2] The detailed derivation of these corrections is given in Appendix B and summarized here for convenience.

The small-signal derivation begins with the relativistically correct force equation which was previously given in equation (2-12). By using this equation we have shown that the existing G.E. small-signal analysis work can remain in essentially the same form with only the addition of relativistic correction factors which are functions of γ.

$$\gamma = \left[1 - \left(\frac{v_o}{c}\right)^2\right]^{-1/2} \simeq 1 + \frac{V_o(kV)}{511}$$

Then, using the previous arguments which relate the cylindrical to the planar geometry, we have arrived at a relativistically correct small-signal theory for cylindrical Ubitrons.

Table II-1 gives a summary of these relativistic correction factors along with the corresponding TWT and classical Ubitron parameters from the G.E. work. The definitions of the variables are given in Table II-2.

When all of the relativistic factors shown in Table II-1 are combined in the evaluation of the small-signal gain parameter C_u, we get the following result.

$$C_u^3(\text{relativistic}) = C_u^3(\text{classical}) \times \left[\frac{2}{\gamma^3 (\gamma + 1)}\right] \qquad (2\text{-}102)$$

Table II-1. Comparison of Small Signal Parameters for TWT, Classical Ubitron and Relativistic Ubitron (cylindrical geometry)

TWT	Classical Ubitron	Relativistic Ubitron
$C^3 = \frac{K}{4R_o}$	$C_u^3 = \frac{K' \Lambda^2}{16 R_o}$	$C_u^3 = \frac{K' \Lambda^2}{16 R_o} \left(\frac{2}{\gamma(\gamma + 1)}\right)$
	$K' = \frac{E_\theta^2}{2\beta_e^2 P}$	$K' = \frac{E_\theta^2}{2\beta_e^2 P}$
	$b' = b + \frac{4c^2}{\Lambda^2}\left(\frac{\beta_e}{\beta_o - \beta_e}\right)$	$b' = b + \frac{4C_u^2\gamma^2}{\Lambda^2}\left(\frac{\beta_e}{\beta_o - \beta_e}\right)$
	$\Lambda = \frac{\eta B_{rl}}{\beta_m v_o}$	$\Lambda = \frac{\eta B_{rl}}{\beta_m v_o}\left(\frac{1}{\gamma}\right)$
		$v_o = c\left(\frac{\sqrt{\gamma^2 - 1}}{\gamma}\right)$
		$\beta_e = \frac{v}{c}\left(\frac{\gamma}{\sqrt{\gamma^2 - 1}}\right)$

Table II-2. Definition of Small Signal Analysis Variables in Table I

C = Pierce small signal gain parameter for the TWT

C_u = equivalent small signal gain parameter for the Ubitron

K = TWT interaction impedance

K' = Ubitron interaction impedance

b = Pierce velocity parameter for TWT

b' = equivalent Ubitron velocity parameter

Λ = Ubitron undulation parameter (equals the ratio of the peak transverse velocity to the longitudinal velocity)

R_o = beam impedance = V_o/I_o

E_θ = peak electric field at the beam for the TE_{01} circular waveguide mode

P = rf power

$\beta_e = \omega/v_o$

β_o = circuit propagation constant

$\beta_m = 2\pi/L$ where L is the magnetic period

γ = relativistic factor

$\eta = \left| e/m_o \right|$

B_{rl} = peak radial component of the magnetic field harmonic at the beam radius

v_o = dc beam velocity

c = velocity of light

The relativistic factor on the rhs of (2-102) is plotted as a function of voltage in Appendix B. This plot shows that the relativistically correct gain parameter is one-half the classically predicted value when the design voltage is 400 kV. The relativistic correction is therefore very important for operating voltages above 100 kV.

By comparing equation (2-101) to the equation for C_u in Table II-1, we see that the proper relativistic correction to equation (2-101) is to multiply by the factor

$$\left[\frac{2}{\gamma(\gamma+1)}\right] .$$

The remaining relativistic correction to the peak transverse dc velocity $v_{\theta 1}$ is accounted for through the dc beam analysis. Thus the beginning point for the derivation of the small-signal equivalence theory is

$$C_u^3 = \frac{1}{16}\,\frac{1}{2\omega^2 P_z V_o}\left[\frac{2}{\gamma(\gamma+1)}\right]\left(E_\theta^2 v_{\theta 1}^2 I_o\right)_{eff} \qquad (2\text{-}103)$$

where a value for $(E_\theta^2 v_{\theta 1}^2 I_o)_{eff}$ is to be determined from the dc motion of the beam.

3. Derivation of Equivalence Beam Factor

Consider a function of z which can be expressed as a sum of several fourier series with different and unrelated periods. Thus

$$f(Z) = a_0 + \sum_{n=1}^{\infty} a_n \sin(nZ - \theta_n) + \sum_{n=1}^{\infty} b_n \sin(np_1 Z - \phi_n)$$

$$+ \sum_{n=1}^{\infty} c_n \sin(np_2 Z - \beta_n) + \cdots \qquad (2\text{-}104)$$

where $Z = (2\pi/L)\, z$, $p_1, p_2, \cdots p_m, \cdots$ are incommensurate numbers such that $p_m/p_n \neq$ integer, and θ_n, ϕ_n, β_n, etc. are appropriate phases.

We assume each fourier series is convergent in the usual sense, with well-behaved coefficients. From generalized harmonic analysis or by carrying out the operation we find

$$\frac{1}{Z}\int_0^Z f(Z)\, f(Z+Z')\, dZ = a_o^2 + \frac{a_1^2}{2}\cos Z' + \frac{a_2^2}{2}\cos Z' + \cdots \frac{a_n^2}{2}\cos nZ' + \cdots + \frac{\text{Remainder}}{Z} \tag{2-105}$$

If now we allow $Z \to \infty$ and then integrate further as follows we find

$$\int_0^{2\pi}\left[\lim_{Z\to\infty}\int_0^Z f(Z)\, f(Z+Z')\, dZ\right]\cos nZ'\, dZ' = \begin{cases} \pi/2\; a_n^2 & n \neq 0 \\ 2\pi\; a_o^2 & n = 0 \end{cases} \tag{2-106}$$

The above is the usual autocorrelation function approach to obtain the mean square values of the amplitudes of the harmonics of a periodic function.[32] As a practical matter, and as we shall see shortly, Z in in eq. (2-106) need not be large for good convergence to result. In eq. (2-104) for generality an additional nonperiodic function of Z of the appropriate form should be added to f(Z) but this would represent a noise term which in the present model has not been included.

As evident from Figure II-3 and the associated remarks there, in the ideal case of a very thin beam and in the absence of space charge the envelope of the beam will be modulated slightly from its constant entrance value. If we assume that r(z), $[\delta r(z)]$, $\rho(z)$ and dz/dt are the radius, thickness, charge density, and axial velocity respectively of the electrons, the axial current is given by

$$I_z \simeq 2\pi\, r(z)\, \delta r(z)\, \rho(z)\, \frac{dz}{dt} \,. \tag{2-107}$$

We write "$\simeq$" since for exactness we would need to integrate over the true values of the variables as a function of both r and z which can only come from a self-consistent solution of the equations of motion. At the entrance plane from eq. (2-107)

$$I_o \simeq 2\pi r_n\, [\delta r(0)]\, \rho_e\, v_{ze} \tag{2-108}$$

With this and eq. (2-107)

$$\frac{I_z}{I_o} \simeq \frac{r(z)}{r_n}\, \frac{\delta r(z)\, \rho(z)}{[\delta r]_e \rho_e}\, \frac{dz/dt}{v_{ze}} \tag{2-109}$$

On the basis of an assumed thin beam where the z positions of the electrons, their radial positions, and their velocities differ only slightly (since the initial entrance radial positions differ only slightly) we assume $[\delta r(z)]\, \rho(z) = [\delta r]_e \rho_e$ and $dz/dt / v_{ze} \simeq 1$ to obtain

$$I_z \simeq I_o\, \frac{r(z)}{r_b} = I_o R \tag{2-110}$$

where we recall the normalizing parameters of eqs. (2-19). We now assume that v_θ is given by eq. (2-104) where $a_o = v_{\theta o}$, $a_1 = v_{\theta 1}$, etc.

and the b_n and c_n correspond to velocity amplitudes of other harmonics which may be present. In addition the TE_{01} mode is given by eq. (2-74) and I_z by eq. (2-110). Then using the autocorrelation integral to filter out the weighted component of interest (n = 1), we have

$$(E_\theta^2 v_{\theta 1}^2 I_o)_{eff} =$$

$$\frac{4}{L}\int_0^L \left[\lim_{z\to\infty} \frac{1}{z}\int_0^z E_\theta E_\theta^* v_\theta(z) v_\theta(z+z')\, I_o\, \frac{r(z)}{r_b}\, dz\right] \cos\frac{2\pi}{L}\, z'dz' \tag{2-111a}$$

Substituting from eq. (2-74)

$$(E_\theta^2 v_{\theta 1}^2 I_o)_{eff} =$$

$$\frac{4}{L}\, D^2 I_o \int_0^L \left[\lim_{z\to\infty} \frac{1}{z}\int_0^z J_1^2(k_c r) v_\theta(z) v_\theta(z+z')\, \frac{r(z)}{r_b}\, dz\right] \cos\frac{2\pi}{L}\, z'dz' \tag{2-111b}$$

The 4/L factor is a normalizing factor which appears because of the integration intervals. Also, it should be recalled and emphasized that r in $J_1(k_c r)$ is a function of z.

We now show that eq. (2-111b) reduces to the expected values for a few easily understood limiting cases. First consider that the radial variation in the electrons' position is ngeligible, i.e., $r = r_b$ = constant. We would have

$$(E_\theta^2 v_{\theta 1}^2 I_o)_{\substack{\text{eff} \\ r=r_b}} =$$

$$\frac{4}{L} D^2 I_o J_1^2(k_c r_b) \int_0^L \left[\lim_{z\to\infty} \frac{1}{z} \int_0^z v_\theta(z) v_\theta(z+z')\, dz \right] \cos \frac{2\pi}{L} z' dz' \tag{2-112}$$

With the results of eqs. (2-105) and (2-106) we find

$$(E_\theta^2 v_{\theta 1}^2 I_o)_{\substack{\text{eff} \\ r=r_b}} = D^2 I_o J_1^2(k_c r_b)\, v_{\theta 1}^2 \tag{2-113}$$

which is precisely what one would expect for this condition.

On the other hand consider the case where only the dominant harmonic of the velocity is present, i.e., $v_\theta = v_{\theta 1} \sin(2\pi/L\, z - \theta_1)$ but the electron's radial position is variable. For the moment assume the effect of the beam's radial motion on the dc current is negligible, i.e., in eq. (2-111b) take $r(z)/r_b \simeq 1$. In this case we have

$$(E_\theta^2 v_{\theta 1}^2 I_o)_{\text{eff}} \simeq$$

r variable, $v_{\theta 1}$ only

$$\frac{4}{L} D^2 I_o v_{\theta 1}^2 \int_0^L \left[\lim_{z\to\infty} \frac{1}{z} \int_0^z J_1^2(k_c r) \sin\left[\frac{2\pi}{L} z - \theta_1\right] \sin\left[\frac{2\pi}{L}(z+z') - \theta_1\right] dz \right] \cdot \cos \frac{2\pi}{L} z' dz' \tag{2-114a}$$

$$\simeq D^2 I_o v_{\theta 1}^2 \left[\lim_{z\to\infty} \frac{1}{z} \int_0^z J_1^2(k_c r)\, dz \right] \tag{2-114b}$$

The term in the bracket is proportional to the rms value of the E_θ field which one would anticipate as the correct factor from the original definition of C_u^3 in eq. (2-101) and for this case. Finally, consider the somewhat hypothetical case where the rf electric field is constant over the radial region in which the beam moves and where only the dominant harmonic of the velocity is present. In this case we have from eq. (2-111a)

$$(E_\theta^2 v_{\theta 1}^2 I_o)_{eff} \simeq \frac{4}{L} \left| E_\theta \right|^2 v_{\theta 1}^2 I_o \int_0^L \left[\lim_{z \to \infty} \frac{1}{z} \int_0^z \frac{r(z)}{r_b} \sin\left(\frac{2\pi}{L} z \right.\right.$$

E_θ constant
$v_{\theta 1}$ only

$$\left.\left. - \theta_1 \right) \sin \left[\frac{2\pi}{L} (z + z') - \theta_1 \right] dz \right] \cos \frac{2\pi}{L} z' dz' \qquad (2\text{-}115a)$$

$$\simeq \left| E_\theta \right|^2 v_{\theta 1}^2 I_o \left[\lim_{z \to \infty} \frac{1}{z} \int_0^z \frac{r(z)}{r_b} dz \right] \qquad (2\text{-}115b)$$

where the term in the braces is now the average radius of the beam, the position where an equivalent constant radius beam would be expected. The expression for $(E_\theta^2 v_{\theta o}^2 I_o)_{eff}$ equals the expected value for each of the special cases and is therefore believed to be in the proper form for using in the planar small signal theory as an equivalence factor for obtaining results for a cylindrical model.

In view of the form of eqs. (2-105) and (2-106) some consideration was given to using $J_1[k_c r(z)]\ J_1[k_c r(z + z')]$ in the integrand of eq. (2-112) rather than $J_1^2[k_c r(z)]$. Although the former may be formally more correct, it was argued that since we are correlating on the natural θ periodicity of fundamental period L whereas r has a much larger natural periodicity (it will also have an L periodicity which would be accounted for) the latter is adequate and simpler both

computationally and analytically. Further using the expression for $J_1(x + y)$[33] we examined the influence of using the

$$J_1[k_c r(z)]\ J_1[k_c r(z + z')]$$

form as opposed to the $J_1^2[k_c r(z)]$ form for deviations in r/r_b of ±10% and ±20%. Although those deviations were taken around the peak of the J_1 function where the effect would be minimized, the difference in the resulting value of $(E_\theta^2 v_{\theta 1}^2 I_o)_{eff}$ was 1% and 6% respectively. In view of this and the relatively small impact on C_u values in eq. (2-103) the $J_1^2[k_c r(z)]$ form was retained, although this matter should be reviewed in the future.

Of possibly more importance in the equivalence factor are the assumptions regarding the beams' charge density and ultimate shape and the resulting influence on $(I_o)_{eff}$. Other assumptions regarding the electron beam, for example parallel electron paths, constant charge density, and nominal beam thicknesses, led to integration of the J_1^2 function and the appearance of the factor r^2/r_b^2 in the integrand in eq. (2-112). Still other assumptions led to just the r^2/r_b^2 factor. In view of the tentative nature of these assumptions, pending more information about the true distribution in the beam, it was deemed appropriate to leave the $(E_\theta^2 v_{\theta 1}^2 I_o)_{eff}$ factor in its present form in eq. (2-111b), again since an estimate of the influence of the different assumptions indicated no very major impact on C in eq. (2-101).

It is useful to put eq. (2-111b) in normalized form. With use of the normalization parameters of eq. (2-19) we find after substitution also using eq. (2-78),

$$(E_\theta^2 v_{\theta 1}^2 I_o)_{eff} = \omega^2 P_z I_o \frac{4}{\pi^2} \frac{1}{\mathscr{R}^2} \left(\frac{\mu_0}{\epsilon_0}\right)^{1/2} \frac{1}{\left|J_o(k_c r_a)\right|^2} \frac{1}{\sqrt{1 - \left(\frac{\lambda_o}{\lambda_{oc}}\right)^2}} B_{FNm} \tag{2-116}$$

where

$$B_{FNm} = \int_0^{2\pi} \left[\lim_{Z\to\infty} \frac{1}{Z} \int_0^{Z} R(Z)\, J_1^2 \left[\frac{3.832}{\mathscr{R}} R(Z) \right] V_{\circledR}(Z) V_{\circledR}(Z + Z')\, dZ \right] \cos Z'\, dZ' \qquad (2\text{-}117)$$

Thus we have as an final expression on substitution in eq. (2-103)

$$C_u^3 = \frac{1}{16} \left[\frac{2}{\gamma(\gamma+1)} \right] \frac{I_o}{V_o} \frac{1}{\mathscr{R}^2} \left[\frac{2}{\pi^2} \left(\frac{\mu_o}{\epsilon_o} \right)^{1/2} \frac{1}{\left| J_o(k_c r_a) \right|^2} \right] \frac{1}{\sqrt{1 - \left(\frac{\lambda_o}{\lambda_{oc}} \right)^2}} B_{Fnm} \qquad (2\text{-}118)$$

The factor in the bracket [ ] in eq. (2-116) has the value 470 ohms. B_{FNm} as defined in eq. (2-115) is one of the computer codes mentioned in Appendix A. Based on previous remarks, *at present the code allows* the option of choosing m in the $R^m(z)$ multiplying factor (not in the bessel function) in the integrand of eq. (2-117) with m = 1 shown there the usual and present choice. Also, although not a current option but easily included by using cos nZ' in place of cos Z' the weighted $(E_\theta^2 v_{\theta n}^2 I_o)_{eff}$ for other velocity harmonics is determinable although for the n = o case (generally of little interest) the normalization is different. It is taken in eq. (2-118) that the values in eq. (2-120) of R, ⊛, Z etc. used to obtain B_{FNm} for eq. (2-118) are relativistically correct, i.e. are solutions of the relativistic equations of motion. Based on the relationship between the nonrelativistic and relativistic equations and the resulting velocities (particularly the values of v_θ since in the absence of space change

$$v_{\theta_{rel}} = \frac{v_{\theta\ non\ rel}}{\gamma}$$

one can write,

$$B_{FNm}(\text{rel}) = \frac{1}{\gamma^2} B_{FNm}(\text{non rel}) \qquad (2\text{-}119)$$

Actually this is also an approximation, since the influence of the relativistic electron orbits and the weighting factors are somewhat more complex than eq. (2-119) would suggest.

4. Proof Test, Computer Results, Optimization

Figure II-10 shows a result of a simple test of the code for computing B_{FNm} from eq. (2-117). A test V_{θ} of the form and with the conditions shown was used as input. The extremely rapid convergence to the theoretically expected value is evident.

Two other runs of interest are shown in Figures II-11 and II-12. Figure II-11 was obtained using the equation of motion solution whose results are shown in Figure II-7; Figure II-12 was obtained from the solution of Figure II-8. It can be seen that in these cases quite good convergence is evident within nine periods. Indeed adequate estimates of final values of B_{FNm}, i.e., better than 5%, can most likely be made for runs of half that length. One significant point is the substantial increase in B_{FNm}. Some increase in the beam factor had been anticipated from moving the beam to where its diameter is 3/4 the tube diameter as opposed to the where it is 1/2 the diameter, since the dominant magnetic field harmonic is much larger there. Opposed to this is the E_{θ} field weighting factor which is decreasing as the beam radius increases from the half-tube diameter.

As an approximate estimate of the influence of the entrance beam diameter consider the following. From theory presented in part F of this Section and elsewhere, [2] it can be shown that if the diameter of the cyclotron circle orbits are small the normalized first harmonic relativistic velocity is given by

$$v_{\theta 1} = \frac{\gamma_c}{\gamma_e} \frac{1}{R_b} \frac{B_1}{B_0} I_1(R_b) \sin(Z - \theta_1) \qquad (2\text{-}120)$$

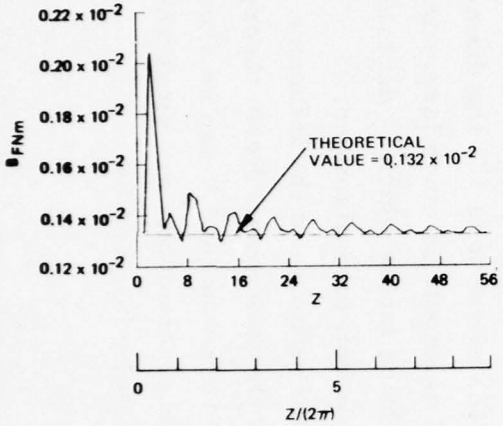


Figure 10.
Proof run for B_{FNm}.

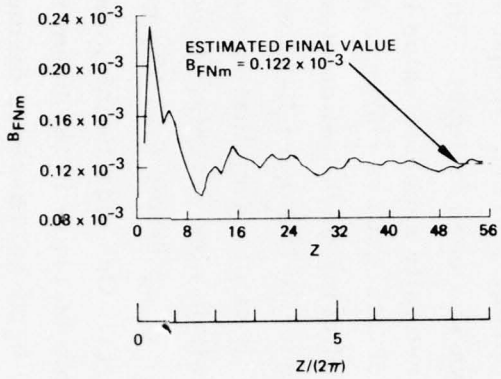


Figure 11.
B_{FNm} from run of Figure II-7.

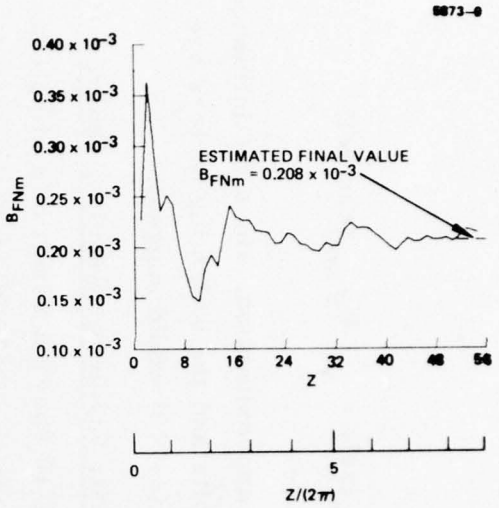
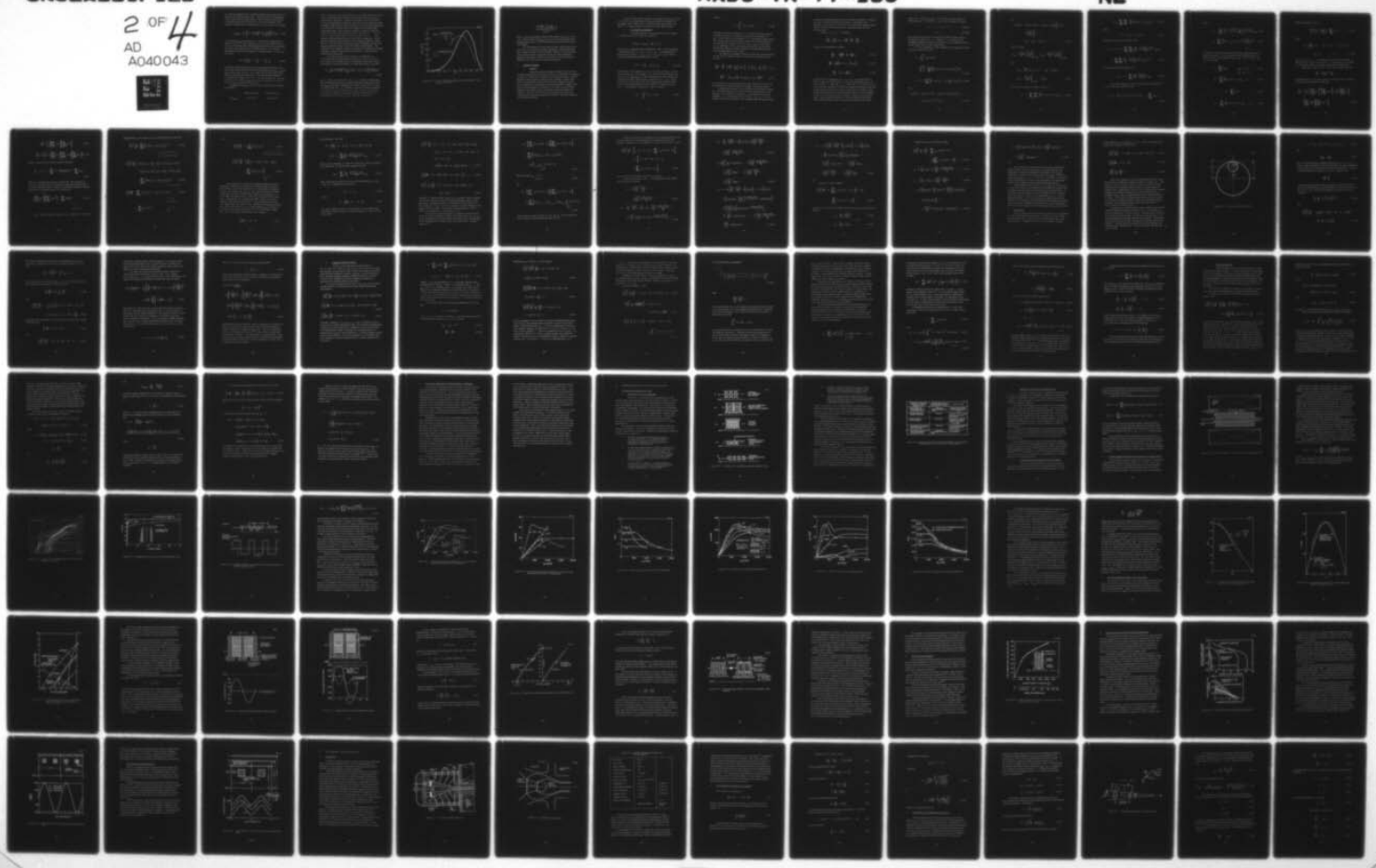


Figure 12.
B_{FNm} from run of Figure II-8.

AD-A040 043 HUGHES RESEARCH LABS MALIBU CALIF F/G 9/5
MILLIMETER WAVE UBITRON DEVELOPMENT PHASE I.(U)
APR 77 J M BAIRD, S SENSIPER, K AMBOSS F30602-76-C-0215
UNCLASSIFIED RADC-TR-77-133 NL

2 OF 4
AD
A040043

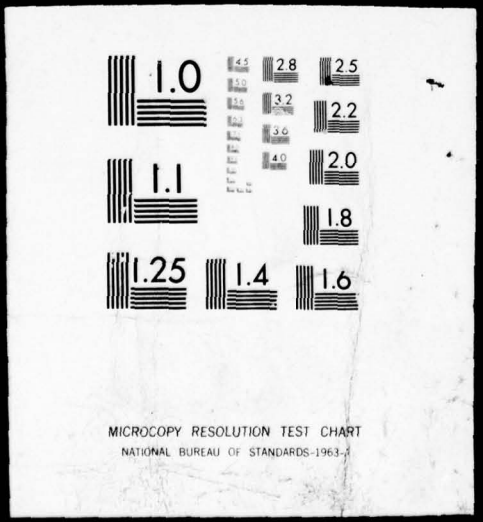


SIFIED

2 OF 4

AD

A040043



γ_e in the denominator is the relativistic factor which in the absence of space charge is the entrance value. Note that R_b in the denominator comes solely from the normalization. The R_b in the bessel function essentially comes from the first term in the representation of the periodic magnetic field. Insertion of eq. (2-120) in eq. (2-117) yields

$$B_{FNm0} = \frac{\pi}{2} \frac{\gamma_c^2}{\gamma_e^2} \bar{R} \; J_1^2 \left(\frac{3.832}{\mathscr{R}} \bar{R} \right) \frac{1}{R_b^2} \left(\frac{B_1}{B_0} \right)^2 I_1^2(R_b) \qquad (2\text{-}121)$$

We call this B_{FNm0} to identify it as a zeroth order approximation. Also we use $\bar{R}$ as a representation of some average radius to use in J_1^2 since to this order the radial position of the electron is nonvarying. The mean radius appears as a reasonable choice. If we use the unperturbed cyclotron orbits again as an approximation we have from eq. (2-93)

$$\bar{R} = \frac{r_b - r_c}{r_b} = 1 - \frac{r_c}{r_b} = 1 - \frac{\gamma_e}{\gamma_c} V_{\theta e} \qquad (2\text{-}122)$$

It should be noted that this value from the unperturbed orbits is very close (within about 1%) to the $\bar{R}$ values (estimated from $(R_{max} + R_{min})/2 \simeq \bar{R}$) in Figures II-7 and II-8, even though in these latter cases R_{max} and R_{min} are both somewhat larger. The unperturbed conditions determining $\bar{R}$ for Figures II-4, II-7, and II-8 are identical The other parameters for evaluating B_{FNm0} are given in Figures II-7 and II-8 where B_1/B_0 is obtained from eq. (2-36).

Evaluation of B_{FNm0} from eq. (2-119) for these cases yields the following

	Figure II-7 Case	Figure II-8 Case
B_{FNm0}	0.121×10^{-3}	0.134×10^{-3}

For the Figure II-7 case the agreement is very good indeed, and we now believe somewhat coincidental, whereas for the Figure II-8 case the agreement is rather poor. Indeed for the latter case we now believe, on the assumption that no untoward error has occurred, that the larger magnitude fundamental periodic field closer to the wall has substantially overcome the E field decrease and resulted in more fundamental component energy. Some evidence for this is evident on comparing Figure II-7d with Figure II-8d where in the latter case it can be seen that the electron's axial velocity and energy have been significantly reduced, with consequent increase in the other components. Thus it appears that aside from possible beam interception problems, moving the beam from the halfway to the three quarters position leads to more improvement than simple zeroth order theory would suggest. Substantially more computer results or completion of the theory permitting evaluation of larger radius perturbation effects is required before drawing final conclusions.

It is not the beam factor which is of significance in the overall Ubitron performance but rather C_u^3. From eq. (2-118), if we assume fixed voltage and current operation and merely consider the influence of the beam position in a fixed-radius tube we see that

$$C_u^3 \sim \frac{1}{\mathscr{R}^2}\,\bar{R}\,J_1^2\left(\frac{3.832}{\mathscr{R}}\,\bar{R}\right)\frac{1}{R_b^2}\,I_1^2(R_b) \approx J_1^2\left(3.832\,\frac{r_b}{r_a}\right) I_1^2\left(\frac{2\pi}{L}\,r_b\right) \tag{2-123}$$

In eq. (2-121) we have taken $\bar{R} = \bar{r}/r_b \simeq 1$ as a further simplification. This simplification alters the location of the peak in the curves for C^3 and B_{FNm0} somewhat, putting them at a higher value for $\bar{r} < r_b$ and at a lower value for $\bar{r} > r_b$. With the values for the parameters used in Figures II-7 and II-8, Figure II-13 shows a plot of the rhs of eq eq. (2-123). From this zeroth-order theory it appears that C_u^3 is maximized for $0.75 \geq r_b/r_a \geq 0.65$. Also note the plot for

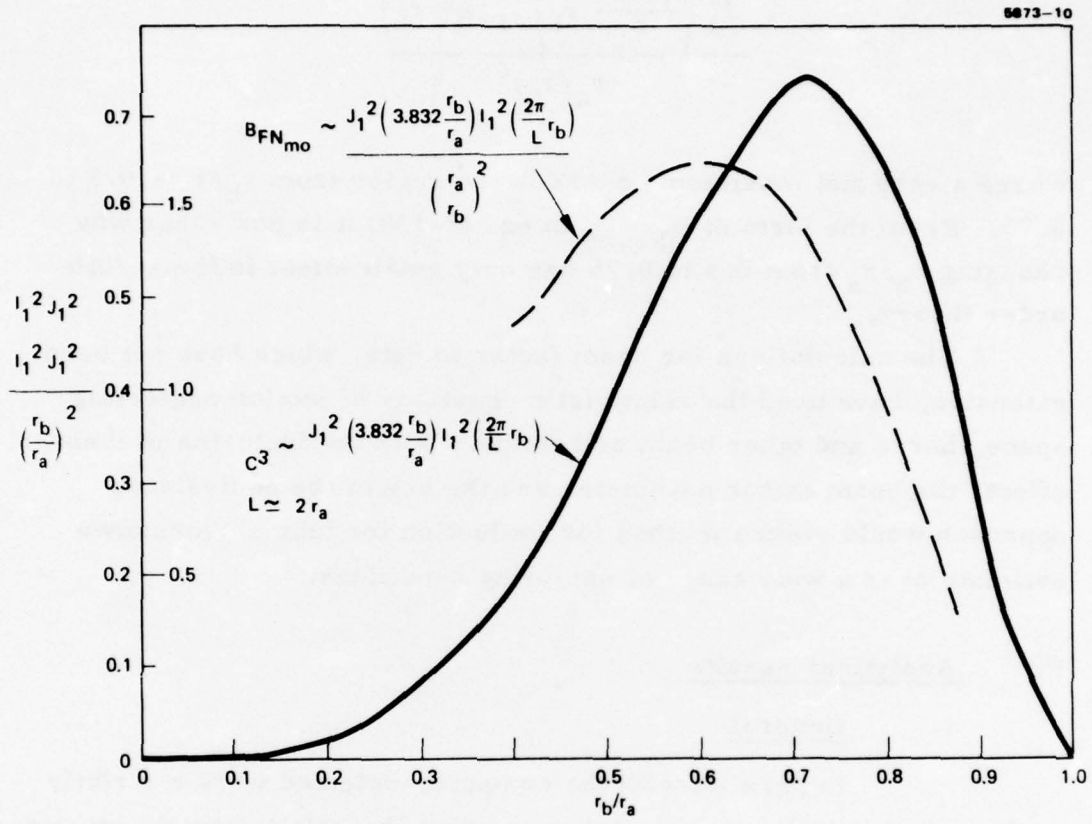


Figure II-13. Factors relating to optimizing zeroth-order C^3 and B_{FNmo} for Ubitron.

$$\frac{J_1^2\left(\frac{3.832}{r_a}\, r_b\right) I_1^2\left(\frac{2\pi}{L}\, r_b\right)}{(r_a/r_b)^2}$$

where a very flat maximum occurs in the region from $r_b/r_a \simeq 0.5$ to 0.75. From the form of B_{FNm0} in eq. (2-119) it is now clear why changing r_b/r_a from 0.5 to 0.75 has only small effect in the zeroth-order theory.

The calculations for beam factor to date, which have not been extensive, have used the relativistic equations of motion neglecting space charge and other beam self fields. With the inclusion of these effects the beam factor parameter and the use of the equivalence approach would yield a method for evaluation for tube performance estimate over a wide range of operating conditions.

F. Analytical Results

1. General

In parallel with the computer-oriented work a strictly analytical approach was undertaken to solve the relativistic dc equations of motion as a basis for an improved rf small-signal theory. Chronologically in this program an earlier effort resulted in approximate linearized differential equations which could be integrated exactly. These exhibited at least qualitative agreement with the computer solutions and fair quantitative agreement. The intent was to use these solutions as the initial step in an iterative process to improve the solutions. However, their form was cumbersome and it became evident that an improved approach was possible. The latter approach is described first below.

In some respects these analyses are similar to the one in a very recent reference in which quite general procedures for finding first and higher order solutions for a relativistic space charge beam are shown.[34] A related analysis in Section IV is also quite relevant.

2. Development of Equations

From the integrated un-normalized form for θ motion as shown in eq. (2-55) we have for reference

$$\gamma_2 r_2 v_{\theta 2} - \gamma_1 r_1 v_{\theta 1} = \frac{\eta}{2\pi} (\psi_2 - \psi_1)$$

where we have integrated between positions 1 and 2. If here position 2 is along the beam for $z > 0$ ($\gamma_2 = \gamma$, r_2 r, $v_{\theta 2} = v_c$) and position 1 is at the entrance point $z = 0$, ($\gamma_1 = \gamma_e$, $r_1 = r_b$, $v_{\theta 1} = v_{\theta e}$) we obtain using the normalization identities of eq. (2-19)

$$\gamma R V_\Theta - \gamma_e V_{\Theta_e} = \frac{\gamma_c}{2} (\Psi - \Psi_e) \qquad (2\text{-}124)$$

The definition of the quantities in eq. (2-124) are as before: γ is the general relativistic γ at any point, γ_e is its value at the entrance plane (eq. 2-64, 66) V_Θ and $V_{\Theta e}$ are the normalized Θ directed velocities at any point and at the entrance plane, respectively, $\gamma_c = \omega_c/\omega = \eta B_o/\omega$, and Ψ and Ψ_e are the normalized total integrated flux enclosed by the electron circumferential trajectory of radius r (R normalized) and r_b (R = 1 normalized), respectively. Thus, as before

$$\Psi_e = 2 \int_0^1 F_1(Z = 0)\, R dR \qquad (2\text{-}62)$$

and now

$$\Psi = 2 \int_0^R F_1(R, Z)\, R dR \qquad (2\text{-}125)$$

From the discussion in Section C.3.d in connection with the entrance conditions, it will be recalled that except for the assumption of $E_\theta = 0$ and the thin beam assumption (i.e., the equations apply strictly in an average sense or they must be integrated or summed over the beam thickness), equation (2-124) is exact. Also, as noted there, we are neglecting for the moment the emission thermal velocities and this will affect the entrance velocities and beam radius to some extent as they appear in eq. (2-124).

The other two equations of interest in the form most useful here are the R and Z equations, eqs (2-47) and (2-49) repeated here for reference

$$\frac{dV_R}{dT} = \frac{V_\theta^2}{R} - \frac{1}{\gamma}\frac{A_1}{R}\left[1 - \left(\frac{L}{\lambda_o}\right)^2 R_b^2 V_R^2\right] - \frac{\gamma_c}{\gamma}\left[V_\theta F_1 - \frac{A_2}{R_b}\frac{V_Z}{R}\right] \qquad (2\text{-}47)$$

$$\frac{dV_Z}{dT} = -\frac{\gamma_c}{\gamma} R_b V_R \frac{A_2}{R} + \frac{\gamma_c}{\gamma} R_b V_\theta F_2 + A_3 \frac{1}{\gamma}\frac{V_R V_Z}{R} \qquad (2\text{-}49)$$

As is evident we have circumvented the first integration of eq. (2-48) through the use of Busch's Theorem with $E_\theta = 0$ to obtain (2-124).

Although the inclusion of the self field terms with space charge etc. may not preclude the use of the procedure shown below, in the analysis so far available we assume as a start that these terms are negligible, i.e., low perveance and so take $A_1 = A_2 = A_3 = 0$. As a possible next step the solutions of the resulting equations could be used

as input to find the self field terms for an iterative approach. Probably, as a better start to the iterative procedure, if iteration is still required, the use of eqs. (2-47) and (2-49) as they stand with the simply derived self field terms would be best, assuming useful solutions could be found.

Taking $A_1 = A_2 = A_3 = 0$ and using

$$\frac{dV_R}{dT} = \frac{d^2R}{dT^2}, \quad V_\Theta = R\frac{d\Theta}{dT}, \quad \frac{dV_Z}{dT} = \frac{d^2Z}{dT^2}$$

we have as the equations to consider

$$\frac{d^2R}{dT^2} = R\left(\frac{d\Theta}{dT}\right)^2 - \frac{\gamma_c}{\gamma} R\frac{d\Theta}{dT} F_1 \tag{2-126}$$

$$\frac{d\Theta}{dT} = \frac{1}{R^2}\left[\frac{\gamma_c}{2\gamma}(\Psi - \Psi_e) + \frac{\gamma_e}{\gamma} V_{\Theta e}\right] \tag{2-127}$$

$$\frac{d^2Z}{dT^2} = \frac{\gamma_c}{\gamma} R_b R\frac{d\Theta}{dT} F_2 \tag{2-128}$$

Actually with the assumption of $A_1 = A_2 = A_3 = 0$, equivalent to no space charge and related forces, γ remains invariant and equal to its entrance value γ_e. Also with $\gamma = \gamma_e = 1$ then eqs. (2-3) to (2-5) are the non-relativistic equations of motion which apply to the Ubitron geometry of interest here (again in the absence of the beam self fields). From related experience and the general physical form we look for solutions in which R varies not too much from unity. Indeed, as will be noted later, a better approach might be to look for solutions which differ only a little from the cyclotron circles that result when no periodic

fields exist. In any case, since we expect the electrons to have R solutions near R = 1 for which r = r_b we make a change of variable

$$R = 1 + \mu = 1 + (R - 1) \tag{2-129a}$$

$$\mu = R - 1 \tag{2-129b}$$

The procedure will now be to expand the variables and the various parameters in power of μ, i.e., around R = 1. As will be seen, although the algebraic details are tedious they are straightforward and merely require some careful bookkeeping.

We must first define several expansions and related parameters. From eq. (2-125) and (2-35a)

$$\Psi = 2 \int_0^R F_1(R, Z)\, R dR$$

$$= 2 \int_0^R \left\{ 1 + \sum_m \frac{B_m}{B_o} \cos\left[m(Z - Z_e)\right] I_o(mR_b R) \right\} R dR \tag{2-130a}$$

$$\Psi = R^2 + 2 \sum_m \frac{B_m}{B_o} \cos\left[m(Z - Z_e)\right] \frac{R}{mR_b} I_1(mR_b R) \tag{2-130b}$$

Since

$$I_o(mR_b R) = I_o(mR_b + \mu m R_b) = I_o(mR_b) + \mu m R_n I_1(mR_b) + \cdots$$

$$= G_{om} + \mu G_{1m} + \mu^2 G_{2m} + \cdots \tag{2-131}$$

and

$$I_1(mR_bR) = I_1(mR_b + \mu mR_b) = I_1(mR_b) + \mu mR_b \left[I_o(mR_b - \frac{I_1(mR_b)}{mR_b} \right] + \cdots$$

$$= H_{om} + \mu H_{1m} + \mu^2 H_{2m} + \cdots \qquad (2\text{-}132)$$

where we define

$$G_{nm} \equiv \frac{(mR_b)^n}{n!} \frac{d^n I_o(z)}{dz^n}\Bigg]_{z=mR_b}, \quad H_{nm} = \frac{(mR_b)^n}{n!} \frac{d^n I_1(z)}{dz^n}\Bigg]_{z=mR_b}$$

and

$$G_{nm} = \frac{mR_b}{n} H_{n-1,m} \quad n \neq 0, \qquad G_{om} = I_o(mR_b),$$

$$H_{om} = \frac{dG_{om}(z)}{d^2 z}\Bigg]_{z=mR_b} = I_1(mR_b) \qquad (2\text{-}133)$$

we have from the above with Eqs. (2-35a, b)

$$F_1 = 1 + \sum_{n=0}^{\infty} \sum_{m}^{\infty} \frac{B_m}{B_o} \cos m(Z - Z_e)\, G_{nm}\, \mu^n \qquad (2\text{-}134)$$

$$F_2 = \sum_{n=0}^{\infty} \sum_{m}^{\infty} \frac{B_m}{B_o} \sin m(Z - Z_e) H_{nm} \mu^n \qquad (2\text{-}135)$$

using

$$R^2 = (1 + \mu)^2 = 1 + 2\mu + \mu^2 \qquad (2\text{-}136)$$

and Eq. (2-6a) we have from Eq. (2-7b)

$$\Psi = 1 + 2\mu + \mu^2 + 2 \sum_{n=0}^{\infty} \sum_{m=1}^{\infty} \frac{B_m}{B_o} \frac{\cos[m(Z - Z_e)]}{mR_b} H_{nm} \mu^n$$

$$+ 2 \sum_{n=0}^{\infty} \sum_{m=1}^{\infty} \frac{B_m}{B_o} \frac{\cos m(Z - Z_e)}{mR_b} H_{nm} \mu^{n+1} \qquad (2\text{-}137)$$

We also find from this and Eq. (2-62)

$$\Psi_e = 1 + 2 \sum_{m=1}^{\infty} \frac{B_m}{B_o} \frac{\cos m Z_e}{mR_n} H_{om} \qquad (2\text{-}138)$$

As evident from Eq. (2-127) we shall need an expression for $\Psi - \Psi_e$. With some algebra we find

$$\Psi - \Psi_e = 2P_o + 2\mu(1 + P_1) + \mu^2[1 + 2P_2] + 2 \sum_{n=3}^{\infty} P_n \mu^n \qquad (2\text{-}139)$$

where

$$P_o = \sum_{m=1} \frac{B_m}{B_o} \frac{\cos\left[m(Z - Z_e) - \cos m Z_e\right]}{mR_b} H_{om} \quad (2\text{-}140)$$

$$P_n = \sum_{m=1} \frac{B_m}{B_o} (H_{n-1,m} + H_{n,m}) \frac{\cos m(Z - Z_e)}{mR_b} \quad (2\text{-}141)$$

$$n \geq 1$$

It will prove convenient to express some of the double sums above in another way since we wish to separate out the various powers of μ. Thus from the related equations above, eqs. (2-134), (2-135), and (2-139), we write

$$F_1 = \sum_{n=0}^{\infty} \mathscr{P}_{\underline{n}} \mu^n \qquad \mathscr{P}_{\underline{o}} = 1 + \mathscr{P}_o \qquad (2\text{-}142)$$

$$\mathscr{P}_{\underline{n}} = \mathscr{P}_n, \; n \geq 1$$

$$\mathscr{P}_n = \sum_{m=1}^{\infty} \frac{B_m}{B_o} \cos m(Z - Z_e) G_{nm} \quad n \geq 0 \qquad (2\text{-}143)$$

$$F_2 = \sum_{n=0}^{\infty} \mathscr{S}_n \mu^n \qquad (2\text{-}144)$$

$$\mathscr{S}_n = \sum_{m=1}^{\infty} \frac{B_m}{B_o} \sin m(Z - Z_e) H_{nm} \quad n \geq 0 \qquad (2\text{-}145)$$

Another expression of use is

$$\left[\frac{\Psi - \Psi_e}{2} + \frac{V_{\circledR e}}{\gamma_c/\gamma_e}\right] = \sum_{i=0}^{\infty} P_i' \mu^i \qquad (2\text{-}146)$$

where

$$P_o' = \frac{V_{\circledR e}}{\gamma_c/\gamma_e} + P_o \ , \quad P_1' = 1 + P_1 \ , \quad P_2' = \frac{1}{2} + P_2$$

$$P_n' = P_n \qquad n \geq 3 \qquad (2\text{-}147)$$

where P_o, P_1, P_2, ... are defined in eqs. (2-140) and (2-141). In this case in eq. (2-127) we will take $\gamma = \gamma_e$ and retain γ_e as reminder we are dealing with the relativistic but non space-charge case.

From eqs. (2-126), (2-127), and (2-128) we now write since

$$\frac{dR}{dT} = \frac{d(1+\mu)}{dT} = \frac{d\mu}{dT} \ ,$$

substituting from eq. (2-127) into eqs. (2-126) and (2-128), and using the above series expansion expressions

$$\frac{d^2\mu}{dT^2} = \left(\frac{\gamma_c}{\gamma_e}\right)^2 \left[\sum_{i=0}^{\infty} P_i' \mu^i\right]^2 \left[\sum_{r=0}^{\infty} {}_3B_r \mu^r\right] - \left(\frac{\gamma_c}{\gamma_e}\right)^2 \left[\sum_{i=0}^{\infty} P_i' \mu^i\right] \cdot$$

$$\left[\sum_{n=0}^{\infty} \underline{\mathscr{P}}_n \mu^n\right]\left[\sum_{r=0}^{\infty} {}_1B_r \mu^r\right] \qquad (2\text{-}148)$$

$$\frac{d\Theta}{dT} = \left(\frac{\gamma_c}{\gamma_e}\right)\left[\sum_{i=0}^{\infty} P_i' \mu^i\right]\left[\sum_{r=0}^{\infty} {}_2B_r \mu^r\right] \tag{2-149}$$

$$\frac{d^2Z}{dT^2} = \left(\frac{\gamma_c}{\gamma_e}\right)^2 R_b\left[\sum_{i=0}^{\infty} P_i' \mu^i\right]\left[\sum_{n=0}^{\infty} \mathscr{L}_n \mu^n\right]\left[\sum_{r=0}^{\infty} {}_1B_r \mu^r\right] \tag{2-150}$$

In Eq. (2-148) to (2-150) we have used the expansion

$$\frac{1}{R^n} = (1+\mu)^{-n} = \sum_{r=0}^{\infty} (-1)^r \frac{(n+r-1)!}{(n-1)!\, r!} \mu^r = \sum_{r=0}^{\infty} {}_nB_r \mu^r \tag{2-151}$$

where ${}_nB_r$ designates the binomial coefficients. The equations are now in the form desired but of course the coefficients of the powers of μ must be obtained. This is readily accomplished through the following algorithm for multiplying series of the form here:

$$\left(\sum_{n=0}^{\infty} A_n \mu^n\right)\left(\sum_{m=0}^{\infty} B_m \mu^m\right) = \sum_{n=0}^{\infty} (A_i B_j)\mu^n \tag{2-152a}$$

$$i + j = n$$

$$i \geq 0,\ j \geq 0$$

$$= A_oB_o + (A_oB_1 + A_1B_o)\,\mu + (A_oB_2 + A_1B_1 + A_2B_o)\,\mu^2 + \cdots \tag{2-152b}$$

Although they can be written in more compressed form we then have

$$\left(\frac{\gamma_e}{\gamma_c}\right)^2 \frac{d^2\mu}{dT^2} = \sum_{m=0}^{\infty} \left[(P_i P_j)_3 B_r - (\underline{\mathscr{P}}_i P'_j)_1 B_r \right] \mu^m \qquad (2\text{-}153a)$$

$$i + j = n,\ i \geq 0,\ j \geq 0$$

$$n + r = m,\ n \geq 0,\ r \geq 0$$

$$\left(\frac{\gamma_e}{\gamma_c}\right)^2 \frac{d^2\mu}{dT^2} = \left\{ P'_o P'_o {}_3B_o - \underline{\mathscr{P}}_o P'_o {}_1B_o \right\} + \left\{ P'_o P'_o {}_3B_1 + (P'_o P'_1 + P'_1 P'_o)\ {}_3B_o - \mathscr{P}_o P'_o {}_1B_1 - (\underline{\mathscr{P}}_o P'_1 + \mathscr{P}_1 P'_o)\ {}_1B_o \right\} \mu$$

$$+ \sum_{m=2}^{\infty} \left[(P'_i P'_j)\ {}_3B_r - (\underline{P}_i P'_j)\ {}_1B_r \right] \mu^m \qquad (2\text{-}153b)$$

$$i + j = n, \text{ etc.}$$

$$\left(\frac{\gamma_e}{\gamma_c}\right)\frac{d\Theta}{dT} = \sum_{m=0}^{\infty} (P'_i\ {}_2B_r)\ \mu^m = P'_o\ {}_2B_1 + P'_1\ {}_2B_o)\ \mu \qquad (2\text{-}154)$$

$$i + r = m$$

$$i \geq 0,\ r \geq 0$$

$$+ \sum_{m=2}^{\infty} (P'_i\ {}_2B_r)\ \mu^m \qquad i + r = m$$

$$\text{etc.}$$

and

$$\left(\frac{\gamma_e}{\gamma_c}\right)^2 \frac{d^2Z}{dT^2} = R_b \sum_{m=0} (\mathscr{L}_i P_j')\ {}_1B_r\ \mu^m \qquad (2\text{-}155a)$$

$$i + j = n,\ n + r = m$$
$$i \geq 0,\ j \geq 0,\ n \geq 0, r \geq 0$$

$$\left(\frac{\gamma_e}{\gamma_c}\right)^2 \frac{d^2Z}{dT^2} = R_b \left\{ \mathscr{L}_o P_o' + (-\mathscr{L}_o P_o' + \mathscr{L}_o P_1' + \mathscr{L}_1 P_o')\mu \right.$$

$$\left. + \sum_{m=2}^{\infty} (\mathscr{L}_i P_j')\ {}_1B_r\ \mu^m \right\} \qquad (2\text{-}155b)$$

$$i + j = n,$$
$$\text{etc.}$$

We now have the dc relativistic nonspace-charge differential equations of motion to first order in the deviation from the entrance beam radius, μ, and can readily derive the coefficients of the higher orders. The values of P_n, $\mathscr{P}_n$, $\mathscr{L}_n$, etc. could be entered to find the coefficients explicitly in terms of the magnetic field parameter. If this is done as evident from eq. (2-147) $V_{\Theta e}$ will come into the equations. Although this is not undesirable since it puts into view the influence of the entrance Θ velocity, a more convenient form seems more appropriate which puts in view a possibly more significant parameter. This comes from eq. (2-61) which expresses $V_{\Theta e}$ in terms of the entrance flux and the parameter C, there related to the cathode flux. If we now use this, repeated here for reference

$$\frac{V_{\Theta e}}{\gamma_c/\gamma_e} = \frac{1}{2}(\Psi_e - C) \qquad (2\text{-}61)$$

then from Eq. (2-147) with

$$P_o' = \frac{V_{\oplus e}}{\gamma_c/\gamma_e} + P_o = \frac{1}{2}(\Psi_e - C) + P_o = \frac{1}{2}\Psi_e + P_o - \frac{1}{2}C$$

$$= \frac{1}{2}(1 - C) + \sum_{m=1}^{\infty} \frac{B_m}{B_o} \frac{\cos[m(Z - Z_e)]}{mR_b} H_{om} \qquad (2\text{-}156)$$

where we have used Eqs. (2-138) and (2-140) for Ψ_e and P_o to express P_o' in this form. We finally define another series as

$$\mathscr{M}_n = \sum_{m=1}^{\infty} \frac{B_m}{B_o} \frac{\cos[m(Z - Z_e)]}{mR_b} H_{nm} \qquad (2\text{-}157)$$

where generally only $\mathscr{M}_o$ may be of use here but note that $P_n = \mathscr{M}_{n-1} + \mathscr{M}_n$, $n \geq 1$. With this if we now place

$$\frac{1}{2}(1 - C) = \Delta \qquad (2\text{-}158)$$

we have

$$P_o' = \frac{V_{\oplus e}}{\gamma_c/\gamma_e} + P_o = \Delta + \mathscr{M}_o \qquad (2\text{-}159)$$

For reasons which will become clear shortly, we now write out the equations of motion to order μ as follows from Eqs. (2-153b), (2-154), and (2-155b)

$$\left(\frac{\gamma_e}{\gamma_c}\right)^2 \frac{d^2\mu}{dT^2} = \left\{ -(1-\Delta)\Delta - \mathcal{M}_o - \Delta(\mathcal{P}_o - 2\mathcal{M}_o) + \mathcal{M}_o^2 - \mathcal{P}_o\mathcal{M}_o \right\}$$

$$+ \mu \left\{ -(1-\Delta)(1-3\Delta) - \Delta + 3\mathcal{M}_o(1-2\Delta) - \mathcal{P}_o(1-\Delta) \right.$$

$$- P_1(1-2\Delta) - \Delta\mathcal{P}_1$$

$$\left. + \mathcal{M}_o\left[2P_1 + \mathcal{P}_o - \mathcal{P}_1 - 3\mathcal{M}_o\right] - \mathcal{P}_o P_1 \right\} + \cdots \quad (2\text{-}160)$$

$$\left(\frac{\gamma_e}{\gamma_c}\right)\frac{d\Theta}{dT} = \left\{ \Delta + \mathcal{M}_o \right\} + \mu \left\{ (1-2\Delta) - 2\mathcal{M}_o + P_1 \right\} + \cdots \quad (2\text{-}161)$$

$$\left(\frac{\gamma_e}{\gamma_c}\right)^2 \frac{1}{R_b}\frac{d^2Z}{dT^2} = \left\{ (\Delta + \mathcal{M}_o)\mathcal{L}_o \right\} + \mu \left\{ (\Delta + \mathcal{M}_o)(\mathcal{L}_1 - \mathcal{L}_o) \right.$$

$$\left. + \mathcal{L}_o(1 + P_1) \right\} + \cdots \quad (2\text{-}162)$$

It should be emphasized that except for the non-space-charge condition and entrance plane parameters averaging assumption made as noted previously, no approximations or truncations have been made so far. The coefficients of the μ terms are complete, and the coefficients of the higher order are readily, if somewhat tediously obtained. Also it should be recalled that μ is a function of Z or T.

The next step in this procedure is to find the coefficients of μ^m in terms of the given specific magnetic field parameters, B_o, B_1, etc. Some examination of the form of these shows that we need an algorithm for the multiplication of Fourier series in various forms. The two required are

$$\alpha\beta = \left\{ \sum_{m=1}^{\infty} a_m \cos m(Z - Z_e) \right\} \left\{ \sum_{m=1}^{\infty} \beta_m \cos m(Z - Z_e) \right\}$$

$$= \sum_{m=0}^{\infty} \left\{ \frac{1}{2} (a_i\beta_j)_{i+j=m} + \frac{1}{4} (2 - \delta_{om}) \left[(a_i\beta_j + a_j\beta_i) \right]_{i-j=m} \right\} \cos m(Z - Z_e)$$

$$i \geq 1$$
$$j \geq 1 \qquad (2\text{-}163)$$

where as usual $\delta_{om} = 1 \quad m = 0$

$$= 0 \quad m \neq 0 \qquad (2\text{-}164)$$

and

$$\alpha\beta = \left\{ \sum_{m=1}^{\infty} a_m \sin m(Z - Z_e) \right\} \left\{ \sum_{m=1}^{\infty} \beta_m \cos m(Z - Z_e) \right\}$$

$$= \frac{1}{2} \sum_{m=1}^{\infty} \left[(a_i\beta_j)_{i-j=m} - (a_j\beta_i)_{i-j=m} + (a_i\beta_j)_{i+j=m} \right] \sin m(Z - Z_e)$$

$$i \geq 1$$
$$j \geq 1$$

(2-165)

With the above and the definitions of $\mathcal{M}_n$, $\mathcal{P}_n$, P_n, $\mathcal{L}_n$ the coefficients can be readily if somewhat tediously determined.

These are shown below including terms to what are believed to be the most significant order although this will depend on some of the boundary conditions as will be explained. Thus we have from eq. (2-160)

$$\left(\frac{\gamma_e}{\gamma_c}\right)^2 \frac{d^2\mu}{dT^2} = \left\{ [-\Delta(1-\Delta) + a_0] + \sum_{m=1}^{\infty} a_m \cos m(Z - Z_e) \right\}$$

$$+ \mu \left\{ [-(1-\Delta)(1-3\Delta) - \Delta] + b_0 \right.$$

$$\left. + \sum_{m=1}^{\infty} b_m \cos m(Z - Z_e) \right\} + \ldots \qquad (2\text{-}166)$$

and we show only the expansion to order μ as before.

In eq. (2-166) we have with $+ \cdots$ meaning that only the leading term in a series is shown:

$$a_0 = \frac{1}{2}\left(\frac{B_1}{B_0}\right)^2 \frac{I_1^2(R_b)}{R_b^2} + \ldots.$$

$$- \frac{1}{2}\left(\frac{B_1}{B_0}\right)^2 \frac{I_0(R_b)\, I_1(R_b)}{R_b} + \cdots \qquad (2\text{-}167a)$$

$$a_1 = -\frac{B_1}{B_0} \frac{I_1(R_b)}{R_b} - \Delta \frac{B_1}{B_0} I_2(R_b) + \frac{B_1 B_2}{B_0^2} \frac{I_1(R_b) I_1(2R_b)}{2R_b^2} + \cdots$$

$$- \frac{1}{2} \frac{B_1 B_2}{B_0^2} \frac{1}{R_b} \left[I_0(2R_b)\, I_1(R_b) + \frac{I_0(R_b)\, I_1(2R_b)}{2} \right] + \cdots \qquad (2\text{-}167b)$$

$$a_2 = -\frac{B_2}{B_0}\ \frac{I_1(2R_b)}{2R_b} - \Delta\ \frac{B_2}{B_0}\ I_2(2R_b) + \frac{1}{2}\left(\frac{B_1}{B_0}\right)^2\ \frac{I_1^2(R_b)}{R_b^2} + \cdots$$

$$-\frac{1}{2}\left(\frac{B_1}{B_0}\right)^2\ \frac{I_0(R_b)\ I_1(R_b)}{R_b} + \cdots \qquad (2\text{-}167c)$$

$$b_0 = \left(\frac{B_1}{B_0}\right)^2\ \frac{1}{R_b}\ I_1(R_n)I_0(R_b) + \cdots + \frac{1}{2}\left(\frac{B_1}{B_0}\right)^2\ \frac{I_0(R_b)I_1(R_b)}{R_b} + \cdots$$

$$-\frac{1}{2}\left(\frac{B_1}{B_0}\right)^2\ I_1^2(R_b) + \cdots - \frac{3}{2}\left(\frac{B_1}{B_0}\right)^2\ \frac{I_1^2(R_b)}{R_b^2} + \cdots$$

$$-\frac{1}{2}\left(\frac{B_1}{B_0}\right)^2\ I_0^2(R_b) + \cdots \qquad (2\text{-}167d)$$

$$b_1 = (1 - 2\Delta)\left[\frac{3B_1}{B_0}\ \frac{I_1(R_b)}{R_b} - \frac{B_1}{B_0}\ I_0(R_b)\right] - (1 - \Delta)\ \frac{B_1}{B_0}\ I_0(R_b)$$

$$-\Delta\ \frac{B_1}{B_0}\ R_b I_1(R_b) + \frac{B_1 B_2}{R_b B_0^2}\ \left[\frac{I_1(2R_b)I_0(R_b)}{2} + I_1(R_b)I_0(2R_b)\right] + \cdots$$

$$+\frac{1}{2}\left(\frac{B_1 B_2}{B_0^2}\right)\ \frac{1}{R_b}\left[I_0(2R_b)I_1(R_b) + \frac{I_0(R_b)I_1(2R_b)}{2}\right] + \cdots$$

$$-\frac{5}{4}\ \frac{B_1 B_2}{B_0^2}\ [I_1(R_b)I_1(2R_b)] + \cdots - \frac{3}{2}\ \frac{B_1 B_2}{B_0^2}\ \frac{I_1(R_b)I_1(2R_b)}{R_b^2} + \cdots$$

$$-\frac{B_1 B_2}{B_0^2}\ I_0(R_b)I_0(2R_b) + \cdots \qquad (2\text{-}167e)$$

$$b_2 = (1 - 2\Delta)\left[\frac{3B_2}{B_0}\ \frac{I_1(2R_b)}{2R_b} - \frac{B_2}{B_0}\ I_0(2R_b)\right] - (1 - \Delta)\frac{B_2}{B_0} I_0(2R_b)$$

$$-\Delta\ \frac{2B_2}{B_0}\ R_b I_1(2R_b) + \left(\frac{B_1}{B_0}\right)^2\ \frac{1}{R_b}\ I_1(R_b) I_0(R_b) + \cdots$$

$$+\frac{1}{2}\left(\frac{B_1}{B_0}\right)^2 I_0(R_b)\, I_1(R_b) + \cdots - \frac{1}{2}\left(\frac{B_1}{B_0}\right)^2 I_1^2(R_b) + \cdots$$

$$-\frac{3}{2}\left(\frac{B_1}{B_0}\right)^2\ \frac{I_1^2(R_b)}{R_b^2} + \cdots - \frac{1}{2}\left(\frac{B_1}{B_0}\right)^2 I_0^2(R_b) \qquad (2\text{-}167f)$$

etc.

From eq. (2-161) we obtain

$$\left(\frac{\gamma_e}{\gamma_c}\right)\ \frac{d\Theta}{dT} = \Delta + \sum_{m=1}^{\infty} c_m \cos m(Z - Z_e) + \mu\left\{(1 - 2\Delta)\right.$$

$$\left. + \sum_{m=1}^{\infty} d_m \cos m(Z - Z_e)\right\} + \cdots \qquad (2\text{-}168)$$

where the coefficients are complete as shown below and are quite simple. We have

$$c_m = \frac{B_m}{B_0}\ \frac{I_1(mR_b)}{mR_b} \qquad (2\text{-}169a)$$

$$m \geq 1$$

$$d_m = \frac{B_m}{B_0}\ I_2(mR_b) \qquad (2\text{-}169b)$$

Finally from eq. (2-162) there results

$$\left(\frac{\gamma_e}{\gamma_c}\right)^2 \frac{1}{R_b} \frac{d^2Z}{dT^2} = \sum_{m=1}^{\infty} e_m \sin m(Z - Z_e)$$

$$+ \mu\left\{\sum_{m=1}^{\infty} f_m \sin m(Z - Z_e)\right\} + \cdots \quad (2\text{-}170)$$

$$e_1 = \Delta \frac{B_1}{B_0} I_1(R_b) + \frac{1}{4} \frac{B_1 B_2}{B_0^2} \frac{I_1(R_b)\, I_2(2R_b)}{R_b} + \cdots \quad (2\text{-}171a)$$

$$e_2 = \Delta \frac{B_2}{B_0} I_1(2R_b) + \frac{1}{2} \left(\frac{B_1}{B_0}\right)^2 \frac{I_1^2(R_b)}{R_b} + \cdots \quad (2\text{-}171b)$$

$$f_1 = \Delta \frac{B_1}{B_0} R_b I_2(R_b) + \frac{B_1}{B_0} I_1(R_b) + \frac{1}{2} \frac{B_1 B_2}{B_0^2} \Big[2I_2(2R_b) I_1(R_b)$$

$$- \frac{1}{2} I_2(R_b) I_1(2R_b) \Big] + \cdots$$

$$+ \frac{1}{2} \frac{B_1 B_2}{B_0^2} \left[I_1(2R_b) I_0(R_b) - I_1(R_b) I_0(2R_b) \right] + \cdots \quad (2\text{-}171c)$$

$$f_2 = \Delta \frac{B_2}{B_0} 2R_b I_2(2R_b) + \frac{B_2}{B_0} I_1(2R_b) + \frac{1}{2}\left(\frac{B_1}{B_0}\right)^2 I_1(R_b)I_2(R_b) + \cdots$$

$$+ \frac{1}{2}\left(\frac{B_1}{B_0}\right)^2 I_1(R_b)I_0(R_b) + \cdots \qquad (2\text{-}171d)$$

etc.

As is evident even to this order the resulting equations are rather involved. Some simplification is possible based on some reasonable assumptions regarding the amplitudes of the B_m/B_0 coefficients. Indeed for the idealized case noted in eq. (2-36) even values of B_m/B_0, $m = 2, 4, \cdots$ are zero. As evident from examination of the expressions for the series coefficients, this assumption reduces the complexity of their representation significantly.

Since the higher order terms, i.e., B_3/B_0, etc. will also be of very small value, it will probably be quite sufficient in many cases to consider only the influence of the B_1/B_0 and $(B_1/B_0)^2$ terms. In a practical case B_2/B_0 will not be zero although it will be small as noted in Section III. However as R_b approaches R_a, i.e., for $\mathscr{R}$ approaching unity, or for the beam diameter approaching the tube diameter, it would appear that the higher-order magnetic field components will begin to contribute significantly to the series coefficients which will in turn influence the characteristics of the electron motion.

3. Check Test

Because of the involved procedures used to derive the equations of motion in the form just presented, it would be useful as a check to demonstrate that in a special case of interest they reduce to the expected form. Consider the case where no periodic magnetic

field is imposed, i.e., $B_m/B_0 = 0$, $m \geq 1$. In this case to the order shown eqs. (2-160) to (2-162) become

$$\left(\frac{\gamma_e}{\gamma_c}\right)^2 \frac{d^2\mu}{dT^2} = -(1-\Delta)\Delta + \mu\left[-(1-\Delta)(1-3\Delta) - \Delta\right] + \cdots \quad (2\text{-}172)$$

$$\left(\frac{\gamma_e}{\gamma_c}\right) \frac{d\textcircled{H}}{dT} = \Delta + \mu(1-2\Delta) + \cdots \quad (2\text{-}173)$$

$$\left(\frac{\gamma_e}{\gamma_c}\right)^2 \frac{1}{R_b} \frac{d^2Z}{dT^2} = 0 \quad (2\text{-}174)$$

This case is identical to the one already noted in some detail with regard to testing the computer program in Section D.2. The electrons execute cyclotron circles as they move down the tube with parameters determined by the entrance velocities and axial magnetic field. Equations (2-172) to (2-174) must have these solutions although even with the coefficients of several more orders of μ exhibited, which could be readily obtained, these would be difficult to recognize. We therefore shall prove the point in an inverse manner, i.e., assume the required motion, derive the resulting differential equations, and demonstrate that at least to the order shown in eqs. (2-172) to (2-174) they agree.

Obviously eq. (2-174) yields the expected solution since for the required boundary conditions its solution is $Z = V_{ze}T$, where V_{ze} is the usual normalized z directed velocity. Consider Figure II-14 with the definitions explained there. We take the case of positive z and directed velocities so that the electrons circle inward. The alternate case where the electrons enter with positive z directed velocity and negative θ velocity and circle outward is merely an alternate case and need not be considered here. From the triangle with sides $(r_b - r_c)$, and r we write

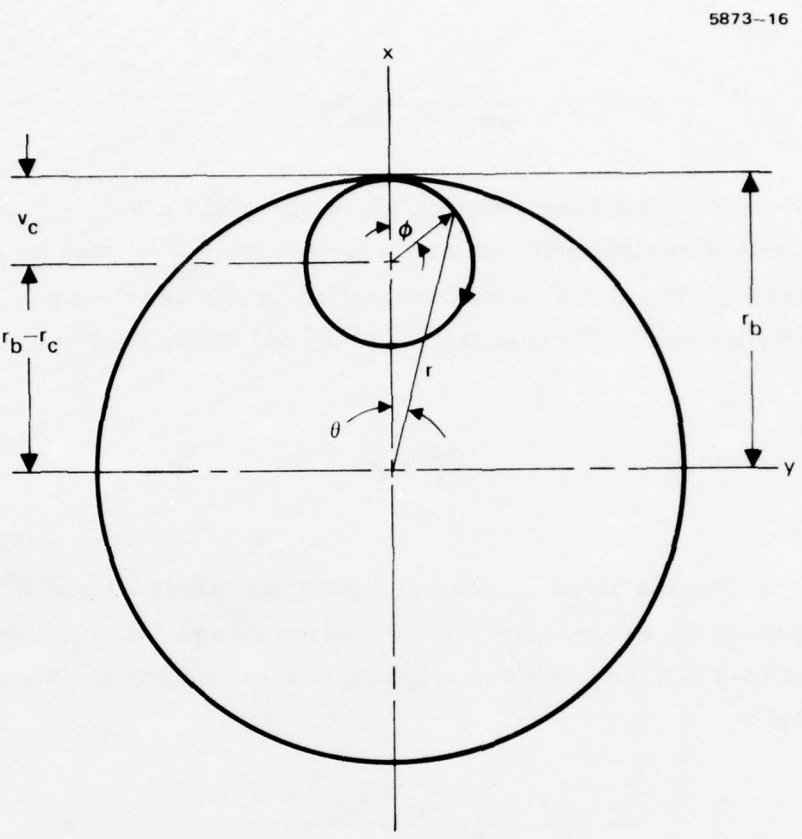


Figure II-14. End view of cyclotron circles.

$$r^2 = (r_b - r_c)^2 + r_c^2 + 2(r_b - r_c)\, r_c \cos\phi \qquad (2\text{-}175)$$

and

$$\frac{r}{\sin\phi} = \frac{r_c}{\sin\theta} \qquad (2\text{-}176)$$

We now take the electrons rotating about the point $x = r_b - r_c$, $y = 0$ with a constant relativistic cyclotron frequency ω_c/γ_e with γ_e dependent on the entrance θ and z directed velocities in the usual way. The term γ in the discussion in Section D.2 is γ_e here. Thus we have

$$\frac{d\phi}{dt} = \frac{\omega_c}{\gamma_e} \qquad (2\text{-}177)$$

Without showing the steps in detail, equations for $d\theta/dt$ and d^2r/dt^2 can be derived by successive differentiation of eqs. (2-175) and (2-176), the use of (2-177), and various trigonometric identities. We find eventually

$$\frac{\gamma_e}{\omega_c}\ \frac{d\theta}{dt} = \frac{1}{2} - \frac{(r_b - r_c)^2 - r_c^2}{2r^2} \qquad (2\text{-}178)$$

and

$$\left(\frac{\gamma_e}{\omega_c}\right)^2 \frac{d^2r}{dt^2} = -\frac{1}{4r^3}\left\{(r^2 - r_c^2)(3r^2 - r_c^2) - (r_b - r_c)^2\left[4r^2 + (r_c^2 - r_b^2) + 2r_b r_c\right]\right\} \qquad (2\text{-}179)$$

Now with the substitution of the usual normalization factors as per eq. (2-19), and with eq. (2-129), and recalling from eqs. (2-92, 93) that

$$\frac{r_{c-}}{r_b} = \frac{r_c(\text{here})}{r_b} = \frac{\gamma_e}{\gamma_c} V_{\Theta e} = \Delta$$

from eqs. (2-61) and (2-158) since $\Psi_e = 1$, eq. (2-62), here we find as the normalized forms of eqs. (2-178) and (2-179)

$$\frac{\gamma_e}{\gamma_c} \frac{d\Theta}{dT} = \frac{1}{2} - \frac{1}{2} \frac{1 - 2\Delta}{(1 + \mu)^2} \tag{2-180}$$

and

$$\left(\frac{\gamma_e}{\gamma_c}\right)^2 \frac{d^2\mu}{dT^2} = - \frac{1}{4(1 + \mu)^3} \left\{ [3(1 + \mu)^2 - \Delta^2] [(1 + \mu)^2 - \Delta^2] \right.$$

$$\left. - (1 - \Delta)^2 [4(1 + \mu)^2 - (1 - \Delta^2) + 2\Delta] \right\} \tag{2-181}$$

Expansion of the rhs of eqs. (2-180) and (2-181) in powers of μ results in the following

$$\frac{\gamma_e}{\gamma_c} \frac{d\Theta}{dT} = \Delta + \mu(1 - 2\Delta) + \cdots \tag{2-182}$$

and

$$\left(\frac{\gamma_e}{\gamma_c}\right)^2 \frac{d^2\mu}{dT^2} = - \Delta(1 - \Delta) + \mu(3\Delta - 3\Delta^2 - 1) + \cdots \tag{2-183}$$

which agree exactly with the reduced equations in (2-172) and (2-173) from the somewhat longer route. Aside from some confidence this yields in the form of the more complete equations, these results also suggest a means for starting their solution.

One other check point of interest which leads to other data results from direct examination of eq. (2-168). If we multiply eq. (2-168) by $R = 1 + \mu$, retain terms to order μ only, unnormalize and express the dominant first harmonic related term only we obtain:

$$v_{\theta}\,(\text{1st harmonic related}) = \frac{1}{\gamma_e}\left\{\frac{\eta B_1}{\frac{2\pi}{L}}\, I_1\left(\frac{2\pi}{L}\, r_b\right) + (r - r_b)\eta B_1\left[\frac{I_1\left(\frac{2\pi}{L}\, r_b\right)}{\frac{2\pi}{L}\, r_b} + I_2\left(\frac{2\pi}{L}\, r_b\right)\right]\right\} \cos\left[\frac{2\pi}{L}\,(z - z_e)\right] \qquad (2\text{-}184)$$

The first term on the rhs of eq. (2-184) is the usual planar transverse velocity, relativistically corrected here by $1/\gamma_e$, used elsewhere in this report and also noted by Phillips.[2] The second term thus consists of the first-order correction resulting from cylindrical geometry. Note it contains a varying term r. As a first step one might substitute the value for r from a simple unperturbed cyclotron orbit. A simple expression for r is evident from Figures II-3, II-14, and eqs. (2-95), and (2-175) as

$$r \simeq r_b - r_c + r_c \cos\left(\frac{2\pi}{L_c}\, z_o\right) \qquad (2\text{-}185)$$

where L_c is the relativistic cyclotron period expressed

$$L_c = \frac{\gamma_e}{\gamma_c} V_{Ze} L \tag{2-186}$$

with z_o the unperturbed electron position. Equation (2-185) turns out to be correct to order $(r_c/r_b)^2$. If this is inserted in (2-184) there results after some manipulation

$$\gamma_e v_\theta \text{ (1st harmonic related)} =$$

$$\eta B_1 \left\{ \frac{I_1\left(\frac{2\pi}{L} r_b\right)}{\frac{2\pi}{L}} - r_c \left[\frac{I_1\left(\frac{2\pi}{L} r_b\right)}{\frac{2\pi}{L} r_b} + I_2\left(\frac{2\pi}{L} r_b\right) \right] \right\} \cos\left[\frac{2\pi}{L}(z - z_e)\right]$$

$$+ \frac{r_c \eta B_1}{2} \left[\frac{I_1\left(\frac{2\pi}{L} r_b\right)}{\frac{2\pi}{L} r_b} + I_2\left(\frac{2\pi}{L} r_b\right) \right] \left\{ \cos\frac{2\pi}{L}\left[(z - z_e) + \frac{L}{L_c} z_o\right] \right.$$

$$\left. + \cos\frac{2\pi}{L}\left[(z - z_e) - \frac{L}{L_c} z_o\right] \right\} \tag{2-187}$$

Thus what was the first harmonic velocity component now contains not only the first harmonic component but also the cyclotron frequency shifted "side bands" or doppler components. This well-known point made in several of the references[5, 12] is also noted in another part of this report, Section IV. The substitution of an approximate r value made above or an improved expression is a possible starting point for obtaining solutions to the entire set of the equations of motion. This is discussed in the next section.

4. Suggested Solution Methods

The form of the equations of motion shown in eqs. (2-153b, 154, 155b) or in eqs. (2-166, 168, 170) to order μ had been obtained only towards the close of the current program and little effort towards solving them could be expended. However from their form, from the computer solutions available at the time, as well as from earlier analytical work some possible procedures and approaches are possible and these are noted.

For ease of viewing we write eqs. (2-166, 168, 170) as follows retaining only the first harmonic terms and making some obvious abbreviations:

$$\left(\frac{\gamma_e}{\gamma_c}\right)^2 \frac{d^2\mu}{dT^2} = a_0' + a_1 \cos(Z - Z_e) + \mu \left[b_0' + b_1 \cos(Z - Z_e)\right] \quad (2\text{-}188)$$

$$\left(\frac{\gamma_e}{\gamma_c}\right) \frac{d\Theta}{dT} = \Delta + c_1 \cos(Z - Z_e) + \mu \left[(1 - 2\Delta) + d_1 \cos(Z - Z_e)\right] \quad (2\text{-}189)$$

$$\left(\frac{\gamma_e}{\gamma_c}\right)^2 \frac{1}{R_b} \frac{d^2Z}{dT^2} = e_1 \sin (Z - Z_e) + \mu\, f_1 \sin (Z - Z_e) \quad (2\text{-}190)$$

Note that as defined a_0', a_1, b_0', b_1, e_1, and f_1 all contain Δ with Δ a function of the initial θ directed velocity. Even with this simplification a difficulty remains in that all the equations are given as derivatives of the independent variable T whereas the "forcing functions" or inhomogeneous terms are all functions of Z. From the physical characteristics of the problem, other related problems, the available computer solutions, and early analytical work, we expect solutions for Z of the form

$$Z = \sum_{n=1}^{\infty} z_n Z_0^n + \sum_{m=1}^{\infty} \epsilon_m \left[\sin m (Z - Z_e) + \sin m Z_e \right]$$

$$= z_1 Z_0 + \cdots + \epsilon_1 \left[\sin (Z - Z_e) + \sin Z_e \right] + \cdots \qquad (2\text{-}191)$$

with $Z_0 = V_{Ze} T$ the unperturbed (i.e., no periodic magnetic field) position of the electrons. Further, one anticipates that $z_1 \simeq 1$, with $z_n \ll 1$ for $n \geq 2$, and that all the ϵ's are quite small. The sense of this form of a suggested solution is evident from eq. (2-96) and the related discussion regarding Figures II-6d, -7d, and 8d. Clearly the z_m and ϵ_m in eq. (2-191) will be functions of the physical parameters of the system including the initial conditions, i.e., entrance velocities and their ratios.

If we assume that as an adequate approximation to Z we can take

$$Z \simeq z_1 Z_0 \simeq \frac{1}{A} Z_0,$$

(i.e., $z_n = 0$, $n \geq 2$) where we choose $z_1 = 1/A$ for reasons related to earlier analytical work and $\epsilon_m \simeq 0$, $m \geq 1$ we have

$$Z_0 = V_{Ze} T = A Z \qquad (2\text{-}192a)$$

$$\frac{dZ}{dT} = \frac{V_{Ze}}{A} \qquad (2\text{-}192b)$$

With this in eq. (2-188) to (2-190) we obtain

$$\left(\frac{\gamma_e}{\gamma_c}\right)^2 \left(\frac{V_{Ze}}{A}\right)^2 \frac{d^2\mu}{dZ^2} \simeq a_0' + a_1 \cos (Z - Z_e)$$

$$+ \mu \left[b_0' + b_1 \cos (Z - Z_e) \right] \cdots \tag{2-193}$$

$$\left(\frac{\gamma_e}{\gamma_c}\right)\left(\frac{V_{Ze}}{A}\right) \frac{d\Theta}{dZ} \simeq \Delta + c_1 \cos (Z - Z_e) + \mu \left[(1 - 2\Delta) \right.$$

$$\left. + d_1 \cos (Z - Z_e) \right] + \cdots \tag{2-194}$$

$$\left(\frac{\gamma_e}{\gamma_c}\right)^2\left(\frac{V_{Ze}}{A}\right)^2 \frac{1}{R_b} \frac{d^2Z}{dZ^2} \simeq 0 \simeq e_1 \sin (Z - Z_e)$$

$$+ \mu f_1 \sin (Z - Z_e) + \cdots \tag{2-195}$$

The last equation (2-195) is considered as only an indication of the order of the error in this approximation and yields no useful or valid information. Examination shows eq. (2-193) to be substantially in the form of the Mathieu equation, or if the Fourier series are continued, in the form of Hill's equation.[13] However an additional term $a_1 \cos (Z - Z_e)$, actually the first term of a series, appears and this may modify the solution. Equation (2-194) is not integrable without a solution or assumed solution for μ. If one takes $\mu \approx 0$ here as an approximation, (i.e.,

$r \simeq r_b$, $R = 1$) then it can be integrated in a trivial manner. Or, more correctly, as noted before in relation to eqs. (2-184) to (2-187) if the unperturbed μ solution in the form of the first term of a Fourier series is chosen integration of eqs. (2-193) to (2-195) results. From this one is led to the following possible route for solution.

Consider eq. (2-190) where it will be recalled that e_1 and f_1 are functions of Δ, B_m/B_0, $I_m(R_b)$ or essentially fixed or determinable by design or choice but are not variables, whereas, of course, μ is a function of Z, T, or Z_o.

Then there follows in order:

$$\left(\frac{\gamma_e}{\gamma_c}\right)^2 \frac{1}{R_b} \frac{d^2Z}{dT^2} = e_1 \sin (Z - Z_e) + \mu f_1 \sin (Z - Z_e) \qquad (2\text{-}190)$$

$$\left(\frac{\gamma_e}{\gamma_c}\right)^2 \frac{1}{R_b} \frac{1}{2} \frac{d}{dT}\left[\left(\frac{dZ}{dT}\right)^2\right] = \left[e_1 \sin (Z - Z_e)\right.$$

$$\left. + \mu f_1 \sin (Z - Z_e)\right] \frac{dZ}{dT} \qquad (2\text{-}196)$$

$$\frac{1}{2}\left(\frac{\gamma_e}{\gamma_c}\right)^2 \frac{1}{R_b} \left[V_Z^2 - V_{Z_e}^2\right] = e_1 \left[\cos Z_e - \cos (Z - Z_e)\right]$$

$$+ f_1 \int_0^Z \mu (Z) \sin (Z - Z_e)\, dZ$$

(2-197)

or finally with some manipulation

$$V_{Ze}T = Z_0$$

$$= \int_0^Z \frac{dZ}{\left\{ 1 + \frac{2R_b}{V_{Ze}^2}\left(\frac{\gamma_c}{\gamma_e}\right)^2 \left[e_1[\cos Z_e - \cos (Z - Z_e)] + f_1 \int_0^Z \mu(Z) \sin (Z - Z_e)\, dZ \right] \right\}^{1/2}} \tag{2-198}$$

With

$$\frac{2R_b}{V_{2e}^2}\left(\frac{\gamma_c}{\gamma_e}\right)^2 [\cdots]$$

in the denominator of eq. (2-198) quite small compared to unity, which it is most generally, it can be expanded and only the first or possibly first two terms retained. One is still left with the need to assume or find $\mu(Z)$ to determine

$$\int_0^Z \mu(Z) \sin(Z - Z_e)\, dZ \ .$$

If an unperturbed $\mu(Z)$ is assumed $V_{Ze}T$ can be found and the remaining equations integrated. Although the bookkeeping appears somewhat tedious with the available algorithms it appears manageable. To the order of approximation described one could just evaluate A in eq. (2-192) and proceed with the assumptions made in connection with

eqs. (2-193) to (2-195). Indeed with A available and with the same μ assumption then used in eqs. (2-193) and (2-194), the set is complete and integration can be accomplished. With this first order μ solution available, we call the assumed $\mu(Z)$ the zeroth order solution, the procedure can be iterated with anticipated improved results. It would appear that even the next order in μ might be handled in this manner, although the effort might be substantial.

Since the set of equations eqs. (2-188) to (2-190) have inhomogeneous periodic terms which come from the imposed periodic magnetic field and since indeed the unperturbed electron cyclotron circle orbits are also exactly periodic, at least in the absence of space charge, one might expect that the eventual solution might be expressible as a combination of such periodic forms. Assumed solutions of this form, for example eq. (2-191), and the imposition of the orthogonality conditions on the terms, i.e., the equating of terms of the same periodicity may lead to tractable and useful solutions.

As a last point in this section and as an indication of the possible form for assumed μ solutions we note that the unperturbed cyclotron orbits can be expressed as fourier series. Consider Figure II-10 eq. (2-178). It is clear on examination that $d\Theta/dT$ and Θ are periodic functions of ϕ. Substitution of eq. (2-175) into (2-178) and the use of standard expansion and fourier coefficients forms leads with some effort to the following:

$$\theta = -\sum_{m=1}^{\infty} \frac{(-1)^m}{m} \left(\frac{r_c}{r_b}\right)^m \frac{1}{\left(1 - \frac{r_c}{r_b}\right)^m} \sin m\phi \qquad (2\text{-}199)$$

In obtaining (2-199) we have assumed $r_c/r_b = 1/2$ and used eq. (2-177) to integrate $d\theta/dt$ assuming $\theta = 0$ for $\phi = 0$. If (2-199) is put in normalized form recalling that it describes the unperturbec cyclotron orbits with the use of the relationships of eq. (2-95) for the rotation period and eqs. (2-61), (2-93), and (2-158) relating the orbit radii we obtain:

$$\Theta = - \sum_{m=1}^{\infty} \frac{(-1)^m}{m} (\Delta)^m \frac{1}{(1-\Delta)^m} \sin m\left(\frac{\gamma_c}{\gamma_e} \frac{Z_0}{V_{Ze}}\right) \qquad (2\text{-}200)$$

Although (2-200) was derived for orbits with $r < r_b$ (but $r_c < r_b/2$) it appears that it applies to those for $r > r_b$ if the proper sign is taken for $V_{\Theta e}$ in the definition of Δ. It was taken that the constant axial magnetic field is in the positive z direction. An expansion for the case where $r_c > r_b$ (the electron orbits enclose the origin) is also possible. It would contain a constantly increasing as well as periodic terms. However this case is of no interest to us here.

Of substantial interest is the expansion for r or one of its equivalents. In this case starting with eq. (2-175) we obtain via the usual route

$$r = \sum_{m=0}^{\infty} r_m \cos m\phi \qquad (2\text{-}201)$$

with

$$r_m = 2(2 - \delta_{0m}) \frac{r_b}{\pi} \int_0^{\pi/2} [1 - k^2 \sin^2 \beta]^{1/2} \cos 2m\beta \, d\beta \qquad (2\text{-}202)$$

$$= (2 - \delta_{0m}) r_b \frac{(-1)^m t^m}{1+t} \frac{\Gamma\left(m - \frac{1}{2}\right)}{\Gamma\left(-\frac{1}{2}\right)\Gamma(m+1)} {}_2F_1\left(-\frac{1}{2}, m - \frac{1}{2}; m+1; t^2\right)$$

$$m \geq 0 \qquad (2\text{-}203)^{35}$$

In eq. (2-203) ${}_2F_1$ is the usual hypergeometric function and

$$k^2 = \frac{4r_c(r_b - r_c)}{r_b^2} = 4\Delta(1 - \Delta) = \frac{4t}{(1 + t)^2} \tag{2-204}$$

and

$$t = \frac{1 - \sqrt{1 - k^2}}{1 + \sqrt{1 - k^2}} = \frac{\Delta}{1 - \Delta} \tag{2-205}$$

The r_m are related to elliptic functions and

$$r_0 = r_b \frac{1}{1 + t}\ {}_2F_1\left(-\frac{1}{2}, \frac{1}{2}; 1; k^2\right)(1 + t) = \frac{2}{\pi}\ r_b\ E \tag{2-206}$$

$$r_1 = \frac{4}{\pi}\ r_b\left[\frac{2}{3k^2}(E - K) + \frac{1}{3}(2K - E)\right] \tag{2-207}$$

$\ddots$

etc. or

$$r_m = r_b\ \frac{(-1)^{m+1}}{m}\ \frac{t^m}{1 + t}\ {}_2F_1\left(-\frac{1}{2}, m - \frac{1}{2}; m + 1; t^2\right) \tag{2-208}$$

$$m \geq 1$$

where the higher order r_m can be found in terms of the K and E, the complete elliptic integrals of the first and second kind, via the available recurrence forms.[35, 36] Again although the above development was obtained for $r < r_b$ and $r_c < r_b/2$, as evident from the form of (2-175) and the resulting integrals, if k^2 changes sign, (with $r > r_b$) or the cyclotron circles outside of r_b) the results still apply and the functional forms are proper when used appropriately.

If equation (2-201) is now put in normalized form we have as in eq. (2-200)

$$R = \sum_{m=0}^{\infty} \frac{r_m}{r_b} \cos m \left(\frac{\gamma_c}{\gamma_e} \frac{Z_0}{V_{Ze}} \right) \tag{2-209}$$

where the r_m/r_b are obtained from the above. The r_m/r_b coefficients are not so easily expressed as the coefficients in ⊛ but to the order shown from eq. (2-206) and (2-207) or directly by expansion and integration from eq. (2-202) one finds

$$\frac{r_0}{r_b} = 1 - \frac{r_c}{r_b} + \frac{1}{4} \left(\frac{r_c}{r_b} \right)^2 + \cdots \simeq 1 - \Delta \tag{2-210}$$

$$\frac{r_1}{r_b} = \frac{r_c}{r_b} - 2 \left(\frac{r_c}{r_b} \right)^3 + \cdots \simeq \Delta \tag{2-211}$$

if one retains only the linear terms. It is evident that even for Δ's of the order of 0.2 these are rather fair approximations and for Δ of the order of 0.1 they are quite good indeed. With these in eq. (2-209) we have showing only the first harmonic

$$\mu = R - 1 \simeq - \Delta + \Delta \cos \left(\frac{\gamma_c}{\gamma_e} \frac{Z_0}{V_{Ze}} \right) . \tag{2-212}$$

As seems evident from the above using this value in eq. (2-198) or in eqs. (2-193) and (2-194) would be a good start in obtaining solutions of adequate accuracy for use in further small signal analysis.

5. Early Development

If the somewhat extreme initial approximation is made in the above development that $\mu \simeq 0$ a start can be made in integrating the Z and Ⓗ equations. The results of these operations when inserted in the μ or R equation then yields a first order solution which when iterated through the set should yield improved and converging results. It was this approach which was first tried before the alternative, and we believe improved, procedure shown in the previous section was developed.

Because these results are indicative of what might be expected from the improved procedure they are reported in the following.

Consider eq. (2-170) where using the definitions previously given we find

$$\left(\frac{\gamma_e}{\gamma_c}\right)^2 \frac{1}{R_b}\frac{d^2Z}{dT^2} = \left\{\frac{V_{Ⓗe}}{\gamma_c/\gamma_e} + \frac{B_1}{B_0}\frac{I_1(R_b)}{R_b}\left[\cos(Z - Z_e) - \cos Z_e\right]\right\}\left\{\frac{B_1}{B_0} I_1(R_b) \sin(Z - Z_e)\right\} \qquad (2\text{-}213)$$

In the early development $V_{Ⓗe}$ rather than Δ was retained and we follow that procedure here. They are of course related through eq. (2-159). Also it is assumed in eq. (2-213) that the only harmonic field of significance is B_1/B_0. Indeed if the idealized field of eq. (2-159) is assumed, $B_n/B_0 = 0$, $n = 2, 4, \cdots$, and the higher order odd harmonics will be small. But again the caution regarding the situation for R_b approaching R_a must be recalled. In addition a term of order B_1/B_0 from $\mathcal{M}_o \mathcal{L}_o$ in eq. (2-162) has been included which might not be considered directly from eq. (2-170) alone to the order and for the harmonic terms otherwise retained. This is believed consistent since terms of order $(B_1/B_0)^2$ will be comparable in size to $V_{Ⓗe}/\gamma_c/\gamma_e$. If

both sides of eq. (2-213) are multiplied by dZ/dT and integrated, we obtain a form like

$$V_Z^2 = V_{Ze}^2 \left[1 - (B_1' f_1 + B_2' f_2)\right] \tag{2-214}$$

where

$$f_1(Z) = \cos Z_e \left[\cos Z_e - \cos (Z - Z_e)\right]$$

$$- \frac{1}{4} \left[\cos 2 Z_e - \cos 2 (Z - Z_e)\right] \tag{2-215}$$

and

$$f_2(Z) = \cos Z_e - \cos (Z - Z_e) \tag{2-216}$$

B_1' and B_2' are determinable functions of $V_{\Theta e}/\gamma_c/\gamma_e$, B_1/B_0, etc.

From eq. (2-214) there results then on further integration

$$V_{Ze} T = Z_0 = \int_0^Z \frac{dZ}{\left[1 - (B_1' f_1 + B_2' f_2)\right]^{1/2}} \tag{2-217}$$

where $V_{Ze} T = Z_0$ is the position of the electron in the absence of a periodic magnetic field. Equation (2-217) is an inverse relationship reminiscent of elliptic functions. Indeed if $(B_1' f_1 + B_2' f_2)$ is written in exponential form from the trigonometric functions via $\ell \equiv e^{jZ}$ and $\ell_e \equiv e^{jZe}$ it can be demonstrated that the term in the braces in the denominator of eq. (2-217) can be written as a quartic in ℓ and can be expressed as an integrable elliptic function form.[37] Unfortunately this requires the roots of the quartic which are probably not easily or at all expressible in explicit form. For special cases and

with some reasonable approximations, eq. (2-217) can be easily integrated in terms of the elliptic function of the first kind. This leads to easily calculable expressions showing the modification of the electrons z position as a function of the $V_{\circledast e}$ and B_1/B_0 parameter. As an alternative approach it should be noted that $(B_1' f_1 + B_2' f_2)$ is expressible as a fourier series with period L (recall $Z = (2\pi/L)z$) so that Z_0 is similarly expressible. We have so far been unable to easily evaluate the coefficients in this series except for some of the early terms, the coefficients themselves being infinite series. This approach would be highly advantageous and is considered worthy of further pursuit.

As an alternative since $(B_1' f_1 + B_2' f_2) < 1$ with the obvious expansion in eq. (2-218) and integration we obtain

$$V_{Ze} T = Z_0 = Z\,(1 + K_0) + K_1 \left[\sin (Z - Z_e) + \sin Z_e\right]$$

$$+ K_2 \left[\sin 2\,(Z - Z_e) + \sin 2\, Z_e\right] + \ldots \quad . \qquad (2\text{-}218)$$

where

$$K_0 = \frac{1}{2}\mathcal{A}_{\theta 1}^2 - \mathcal{A}_{\theta 1}\mathcal{R}_{V\circledast Z} \cos Z_e + \frac{1}{4}\mathcal{A}_{\theta 1}^2 \cos 2\, Z_e \qquad (2\text{-}219)$$

$$K_1 = -\mathcal{A}_{\theta 1}\,(\mathcal{A}_{\theta 1} \cos Z_e - \mathcal{R}_{V\circledast Z}) \qquad (2\text{-}220)$$

$$K_2 = \frac{\mathcal{A}_1^2}{8} \qquad (2\text{-}221)$$

and

$$\mathcal{A}_{\theta 1} = \frac{\gamma_c}{\gamma_e}\,\frac{B_1}{B_0}\,\frac{I_1(R_b)}{V_{Ze}} \qquad (2\text{-}222)$$

and

$$\mathscr{R}_{V\circledast Z} = \frac{v_{\theta e}}{v_{\theta z}} = \frac{R_b V_{\circledast e}}{V_{Ze}} \qquad (2\text{-}69)$$

the latter equation repeated here for reminder. Typically $\mathscr{A}_{\theta 1}$ is a number in the range 0.05 to 0.1. If now we assume that Z is expressible as

$$Z = \frac{Z_0}{A} + \delta \qquad (2\text{-}223)$$

where $A = 1 + K_0$ and δ small, substitute in eq. (2-218) expand in an obvious way retaining terms of δ^2 only and solve we find eventually that

$$Z - Z_0 \simeq -\frac{K_0 Z_0}{1 + K_0} + \delta = \frac{1 - A}{A} Z_0$$

$$- \frac{\left\{K_1\left[\sin (Z_0' - Z_e) + \sin Z_e\right] + K_2\left[\sin 2 (Z_0' - Z_e) + \sin 2 Z_e\right]\right\}}{A}$$

(2-224)

where

$$Z_0' = \frac{Z_0}{A}$$

Comparison with the computer plots in Figs. 2-5d, 6d, 7d shows that indeed the general properties of those curves are demonstrated by eq. (2-224). Numerical comparison was also fair becoming better as B_1/B_0 approached zero, i.e., as μ approached zero, as would be expected.

In a similar way to the above one writes from eq. (2-168)

$$\frac{\gamma_e}{\gamma_c}\frac{d\Theta}{dT} = \frac{V_{\Theta e}}{\gamma_c/\gamma_e} + \frac{B_1}{B_0}\frac{I_1(R_b)}{R_b}\left[\cos(Z - Z_e) - \cos Z_e\right] \qquad (2\text{-}225)$$

with dZ/dT from (2-218) retaining only the first term in the expansion of

$$\left[1 - (B_1' f_1 + B_2' f_2)\right]^{1/2}$$

we find after integration with the initial Θ, $\Theta_e = 0$,

$$\begin{aligned} R_n\Theta = -Z\Big[&\mathcal{A}_{\theta 1}(1 + \mathcal{R}^2_{V\Theta Z})\cos Z_e - \mathcal{R}_{V\Theta Z} \\ &- \mathcal{R}_{V\Theta Z}\mathcal{A}^2_{\theta 1}\left(1 + \cos Z_e + \tfrac{3}{4}\cos 2Z_e\right)\Big] \\ &+ \mathcal{A}_{\theta 1}\left[\sin(Z - Z_e) + \sin Z_e\right]\Big[1 + \tfrac{9}{8}\mathcal{A}^2_{\theta 1} + \mathcal{R}^2_{V\Theta Z} \\ &- 3\mathcal{A}_{\theta 1}\mathcal{R}_{V\Theta Z}\cos Z_e + \tfrac{3}{4}\mathcal{A}^2_{\theta 1}\cos 2Z_e\Big] + \cdots \end{aligned} \qquad (2\text{-}226)$$

where only the first harmonic term is shown and terms of order $\mathcal{A}^3_{\theta 1}$ are dropped. Indeed even some of the terms shown are probably not of significant order. Within the limitations of the approximation of $\mu \simeq 0$ the general properties of this solution agreed with the computer solution becoming better as B_1/B_0 approached zero.

Finally, from eq. (2-166) the equation for $d^2\mu/dT^2$ can be written and integrated in a manner similar to the above using dZ/dT, finding first $d\mu/dT$ and then μ. It became evident at this point that retaining the harmonic terms in dZ/dT, in this procedure at least, leads to very cumbersome equations of possibly limited utility. The solution for R, i.e., $1 + \mu$ took the form where only the first harmonic term is shown

$$R = 1 + \frac{C_0}{R_b V_{Zc}^2}\left\{C_1\left[\cos(Z - Z_e) - \cos Z_e\right] + C_2 Z + C_3 Z^2\right\}$$

$$+ \frac{\mathscr{A}_{\theta 1}^2}{R_b V_{Ze}^2}\left\{C_4\left[\cos(Z - Z_e) - \cos Z_e\right]\right.$$

$$+ C_5\left[\sin(Z - Z_e) + \sin Z_e\right]$$

$$\left. + C_6 Z \sin(Z - Z_e)\right\} \qquad (2\text{-}227)$$

C_n, $n \geq 0$, are various constants which are functions of the initial conditions, the magnetic field component B_1/B_0 and $I_1(R_b)/R_b$. The appearance of the secular terms Z and Z^2 in this form of the solution indicated the possible limited range of its utility.[38,39] Further, the emergence of the more complete approach of the just previous section persuaded us to pursue these earlier methods no further.

G. Review and Conclusion of Electron Beam – rf Analysis

Starting with the general equations of motion we have derived the specific equations applicable to the relativistic regime for the cylindrical form of the Ubitron. The non-rf equations were put in exact form for the no-space-charge or negligible perveance case and in approximate form for the substantial perveance situation. The initial emphasis on the non-rf equations was to obtain a firm and sufficiently accurate basis for proceeding with the dc-plus-rf performance analysis. In the relativistic non-space-charge case with cylindrical geometry, the dc equations were obtained in the form of exact expansions to any order. Explicit expressions for the coefficients of the first order terms were obtained and means for obtaining those of any order were shown.

Although time did not permit full analytical solution of these exact equations of motion for even the first order, it was shown that they correspond to known forms and possible means for solution were indicated. The significance of the cyclotron circles in the solution procedure was noted. In this regard it was noted briefly that expansion around the center of the cyclotron circles rather than the entrance beam radius might be more appropriate. This would probably lead to more rapidly converging series, and other analytic benefits might accrue. Also, although not emphasized in the text, it became evident that care must be exercised in keeping higher order terms in the expansions if adequate solutions useful over a wide range of values of parameters are to be achieved. An earlier analytic effort was described, in which explicit expressions for the parameters of motion were obtained and fair agreement with computer solutions was indicated.

Computer codes were developed in parallel with the analysis effort using the same cylindrical relativistic equations as in the analysis. These included codes for a dc field only, and for a dc field plus constant rf drive. These codes were checked against several known asymptotic solutions and found to be correct. Further, a code

for extracting a relativistic beam factor from the equations of motion via an autocorrelation procedure was developed and checked. This beam factor is useful in what we called the equivalence theory. This latter hybrid approach is suggested as a simple but useful alternative to a complete dc-plus-rf multidimensional small-signal theory. Since it combines the effects of the multidimensional relativistic dc motion of the beam with the dc-plus-rf planar small-signal theory previously developed, it offers a simple and probably adequate means for at least initial design. This is especially true now that we have modified the small-signal theory to include relativistic corrections.

One factor not considered in detail except indirectly is the beam stability and transmission problem. As evident the equations and analysis considered here are related to prior work on long-beam traveling-wave tubes. However, the Ubitron is somewhat unique perhaps in that its practical performance is dependent on the periodic characteristics of the beam as well as on the beam stability and transmission properties. Thus in its design the constraints are somewhat more confining and sophisticated since for optimum performance a multiple set of conditions must be met. From another point of view an adequate, even small, signal theory, much less a large signal theory, not only must consider the multidimensional perturbations resulting from the rf motion of the electrons, but also must start from an adequate and accurate description of the dc motion. It was this latter point of view which influenced the direction of the analysis reported here.

III. PERIODIC MAGNETIC FIELD STRUCTURES STUDY

A. Introduction and Summary of Task

1. Overview of Work Accomplished

This task is considered to be an important part of the overall Ubitron design program for the following two reasons. (1) Prior work has emphasized that Ubitron gain varies directly with the amplitude of the magnetic field undulations. This effect is very important at millimeter wavelengths. (2) The prior work was performed between 10 and 15 years ago before rare-earth cobalt magnetic materials became available and before the development of sophisticated computer codes which can analyze saturated magnetic field structures. The fact that new materials and analysis techniques are now available to help increase the magnetic field undulations is ample motivation to undertake this task.

Five techniques for generating a periodic magnetic field were studied and compared. These five techniques are illustrated in Figure III-1 and described as follows. Numbers in parentheses correspond to detail views of Figure III-1.

(1) Periodic soft magnetic pole pieces immersed in a solenoidal field. The gap/period ratio and the shape of the pole pieces can be varied to optimize the amplitude of the first harmonic of the magnetic field at the axis.

(2) Periodic permanent magnets. (PPM) In Figure III-1(2) we show the technique for using the third harmonic of what is known as a "double" PPM assembly. An alternative is to use the fundamental component of a PPM stack if the magnets are not too thin. Experience has shown that thin samarium-cobalt ($SmCo_5$) magnets are difficult to work with because they tend to break up.

(3) Periodic electro-magnets. In this technique tiny, iron-clad dc coils are used to produce a periodically varying magnetic field. Power dissipation is a dominant consideration for this scheme.

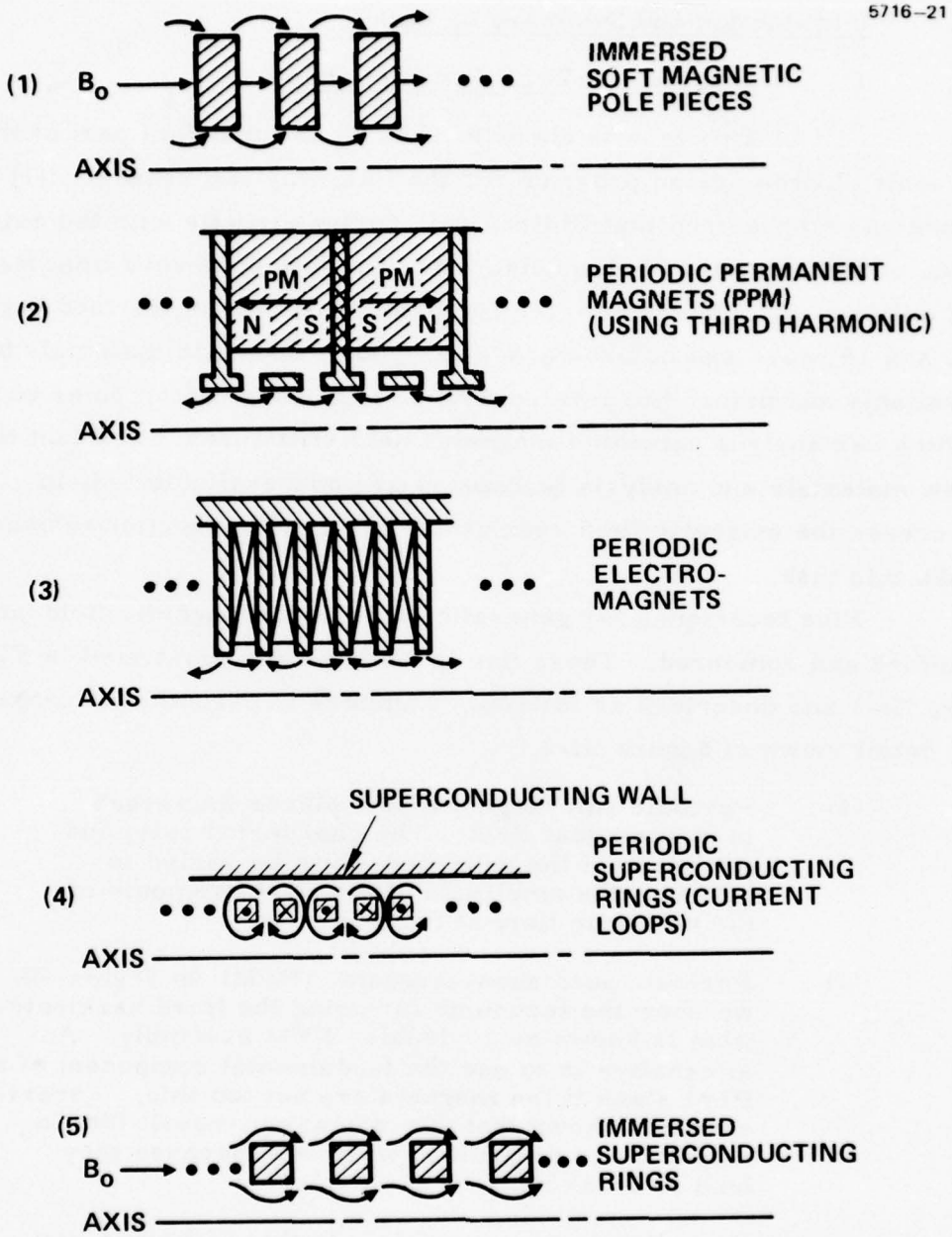


Figure III-1. Techniques for producing a periodic magnetic field.

(4) Periodic superconducting current loops. In this technique a ring-bar structure or a bifilar helix structure is used to produce alternating current loops and the desired periodic magnetic field.

(5) Periodic superconducting rings immersed in a solonoidal magnetic field. In this structure the expulsion of the magnetic flux from the superconducting material is used to produce a periodic disturbance in a solonoidal magnetic field.

These five structures were analyzed during this study program to determine the maximum fields which can be obtained and the limiting factors. In all cases the best present-day materials were assumed and the designs were pushed to their limits. The results of this work are presented in this section.

The five techniques listed above are compared in Figure III-2 for one particular application. In this case, each of the five techniques was used to design the periodic magnetic field for a 94-GHz, 300-kV Ubitron. In this tube design the rf circuit i.d. and the magnetic period are approximately equal. Note that the largest magnetic field harmonic was obtained using the superconducting ring structure and operating close to the critical current density for Niobium-Tin. This gave about 2000 gauss peak. The next best structure was the immersed soft magnetic pole pieces (#1) which produced about 1250 gauss peak in a solonoidal field of 7000 gauss. The remaining structures gave considerably weaker magnetic fields.

The overall conclusion of this study task is that superconducting ring structures, though very complex to implement, are the most effective for producing strong undulating magnetic fields. The next best choice is periodic magnetic pole pieces immersed in a solenoidal field. Of the two techniques, immersed periodic magnetic pole pieces are by far the easiest to implement from an engineering point of view. A third technique, periodic permanent magnet structures, would be used only where weight and prime power are the major considerations.

5716-23R1

TECHNIQUE FOR PRODUCING PERIODICALLY VARYING MAGNETIC FIELD	MAXIMUM AMPLITUDE OF DESIRED HARMONIC ON AXIS (FOR DIAMETER ≃ PERIOD)	LIMITING FACTORS
1. PERIOD MAGNETIC STRUCTURES IMMERSED IN SOLENOIDAL FIELD	~ 1250 GAUSS (7000 GAUSS SOLENOIDAL FIELD)	MAGNETIC SATURATION (7000 GAUSS SOLENOIDAL FIELD)
2. PERIODIC PERMANENT-MAGNET STRUCTURES	~700 GAUSS	COERSIVE FORCE OF $SmCo_5$ MAGNETS, AND MAGNETIC SATURATION
3. SMALL PERIODIC ELECTRO-MAGNETS	~800 GAUSS	MAGNETIC SATURATION AND DISSIPATED POWER DENSITY (P_{DISS} (MAX) ~ 1 kW/ PERIOD)
4. SUPERCONDUCTING CURRENT CARRYING RINGS (OR BIFILAR HELIX) STRUCTURE	~2000 GAUSS	SELF QUENCHING CURRENT DENSITY (FOR NIOBIUM-TIN COMPOUND)
5. SUPERCONDUCTING PERIODIC STRUCTURE IMMERSED IN SOLENOIDAL FIELD	~ 300 GAUSS (10,000 GAUSS SOLENOIDAL FIELD)	SMALL MAGNETIC DISTURBANCE

Figure III-2. Application of the five periodic magnetic field techniques to the design of a 94 GHz, 360 kV Ubitron device.

2. Magnetic Circuit Analysis Computer Code

The key tool used to analyze magnetic structures during this study is a magnetic circuit analysis computer code developed by E. Munro at Cambridge University.[40] This computer code uses the technique of "finite elements" as opposed to the more commonly used "difference equation" approach.

The finite element approach is a relatively recent development in computer codes for magnetic circuit analysis. The accuracy of the program has been checked quite extensively by Munro. He has made numerous comparisons between the axial magnetic field output from his computer code and theoretical and measured values. He concludes that the accuracy is within 1% for non-saturated magnetic circuits and within 5% for saturated circuits. In his calculations he used a 25 x 50 grid pattern, adjusted to provide several grid lines per smallest magnet feature.

For our work on this program we have checked the accuracy of the axial field for two simple cases for which analytical solutions exist: an air-filled current loop and an iron-clad, nonsaturated magnetic solenoid. In each case the axial field was within 1% of the theoretical values.

Some claims have been made in the literature that computer codes based on the finite element approach give superior performance in their running time, ease of matching the grid mesh to the problem, and programming simplicity.[41, 42] Others seem to disagree or are undecided.[43, 44] The important point for the purposes of this study is that the accuracy of the technique is not questioned and is entirely adequate for our design purposes.

3. Axial and Off-Axis Magnetic Field Descriptions

As noted in paragraph 2 above, one of the outputs of the magnetic analysis computer code is the tabulated values of the magnetic field on the axis of the structure being analyzed. In order

to use this computed field for beam and rf analysis, it is necessary to relate this axial field to the off-axis field in the region of the hollow electron beam used in the device.

In Appendix C the following general equations are derived.

$$B_z(r, z) = B_o + \sum_{n=1}^{\infty} I_0(\gamma_n r)[B_{cn} \cos(\gamma_n z) + B_{sn} \sin(\gamma_n z)] \quad (3\text{-}1)$$

$$B_r(r, z) = -\sum_{n=1}^{\infty} I_1(\gamma_n r)[B_{cn} \sin(\gamma_n z) - B_{sn} \cos(\gamma_n z)] \quad (3\text{-}2)$$

In these equations the axial and radial magnetic fields (B_z and B_r) are given in terms of B_o (the average constant axial magnetic field), B_{cn} and B_{sn}, (the peak amplitudes of the nth harmonic for the cosine and sine terms respectively), and γ_n ($\gamma_n = 2\pi/L$, L = magnetic period length).

The analytical procedure used during this study has been to execute the Munro computer code for the selected magnetic structure and then to perform a numerical fourier analysis on the axial magnetic field obtained. This procedure gives the values of B_o, B_{cn}, and B_{sn} for the first few field harmonics. (usually $n \lesssim 5$). The above equations then provide a complete description of the magnetic field in the volume of interest.

B. Periodic Magnetic Structures Immersed in a Solenoidal Field

In this section we give the results of our analysis on the periodic magnetic field structure shown in Figure III-3. Here, a set of ring-shaped magnetic and non-magnetic pole pieces are stacked together alternately to produce a long cylinder through which the rf circuit and electron beam are placed. This whole structure is then placed in

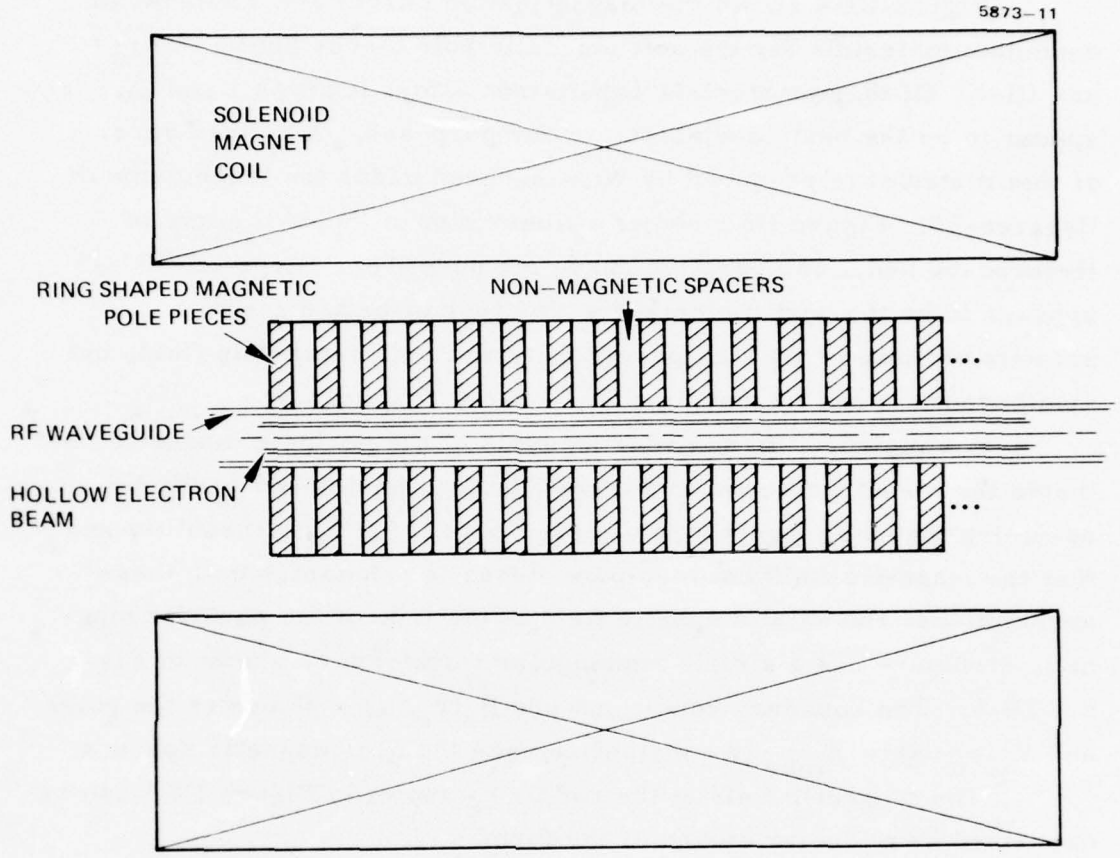


Figure III-3. Periodic magnetic structure immersed in solenoidal field.

a solenoid having a uniform axial magnetic field. The alternating magnetic and non-magnetic rings produce the desired periodic disturbance of the field in the vicinity of the electron beam.

Figure III-4 shows the magnetization curves for a number of candidate materials for the soft magnetic pole pieces shown in Figure III-3. Of these materials cobalt-iron alloys (Curves 1 and 2) appear to be the best candidates for our purposes. A refined version of this material is produced by Westinghouse under the trade name of Hyperco-50. Figure III-5 shows a linear plot of the B-H curve of Hyperco-50 and a comparative curve for pure iron. Hyperco-50 appears to be the best material for this type of periodic structure, not only because of its high permittivity and high saturation field, but also because it can be machined and brazed readily.

A simplified, first-order analysis of the periodic magnetic field inside the structure shown in Figure III-3 can be derived easily by assuming that the magnetic pole pieces have infinite permeability and that the magnetic field between pole pieces is constant. With these assumptions, the axial magnetic field at the i.d. of the periodic magnetic structure has a simple rectangular waveform as shown in Figure III-6. The boundary conditions are $B_z(r_c, z) = 0$ across the poles and $B_z(r_c, z) = B_{max}$ (a constant) across the non-magnetic spacers.

The magnetic field at the radius r_c shown in Figure III-6 can be described by a fourier series of the form

$$B_z(r_c, z) = B_{ave} + \sum_{n=1}^{\infty} 2\, B_{ave} \left[\frac{\sin\left(\frac{n\pi G}{L}\right)}{\left(\frac{n\pi G}{L}\right)} \right] \cos\left(\frac{n\, 2\pi\, z}{L}\right)$$

where $B_{ave} = B_{max}\, G/L$. When this series is compared with equation (3-1) we find that in terms of the peak field existing at the pole pieces the axial magnetic field can be approximated by

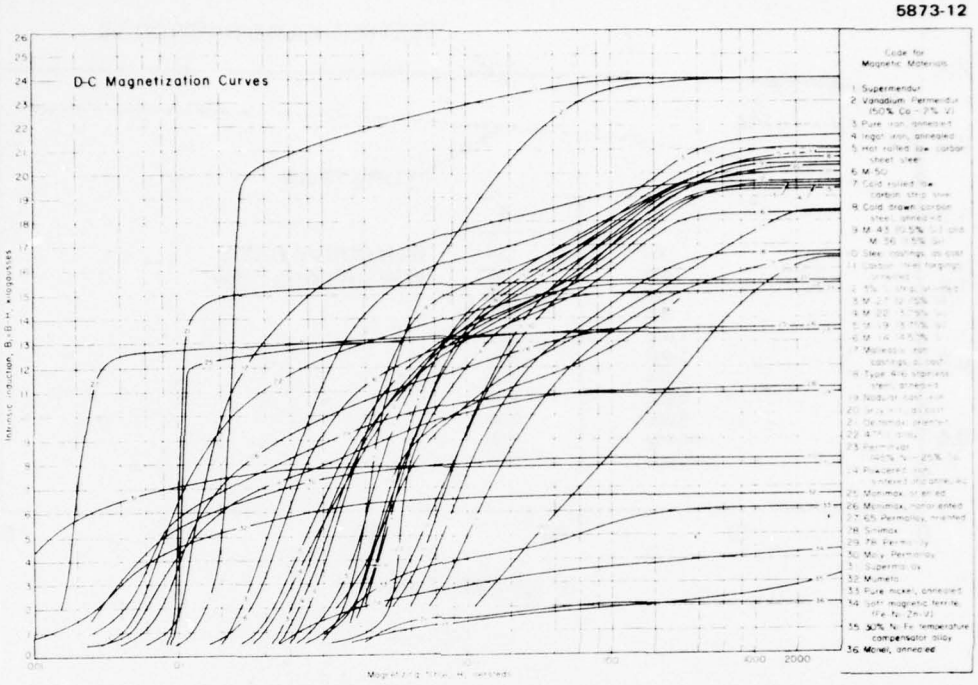
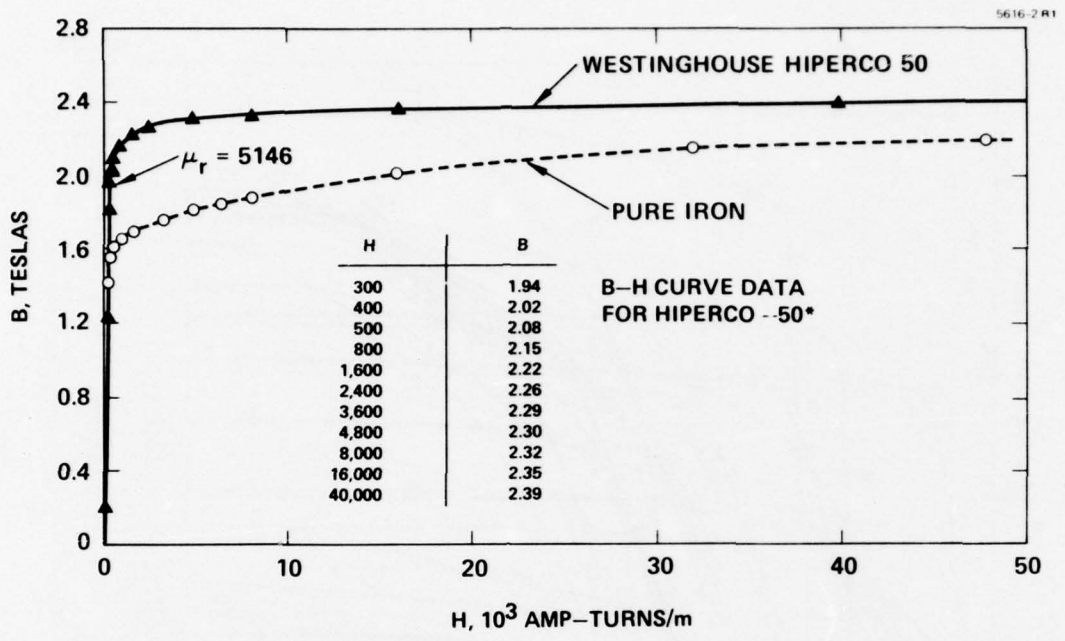


Figure III-4. Direct-current magnetization curves for various magnetic materials.



H	B
300	1.94
400	2.02
500	2.08
800	2.15
1,600	2.22
2,400	2.26
3,600	2.29
4,800	2.30
8,000	2.32
16,000	2.35
40,000	2.39

Figure III-5. Comparison of B-H curves for iron and Hiperco-50.

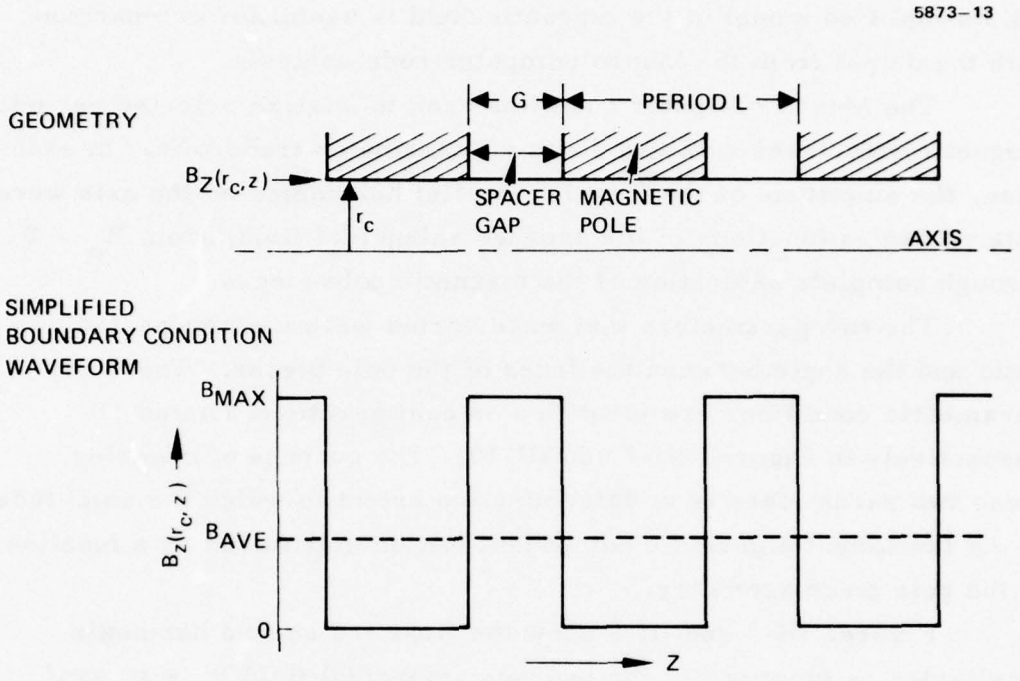


Figure III-6. Simplified boundary conditions for first order analysis of periodic magnetic field.

$$B_z(r, z) \cong \left(B_{max} \frac{G}{L}\right) + \sum_{n=1}^{\infty} \left[\frac{2\, B_{max} \sin\left(\frac{n\pi G}{L}\right)}{n\pi\, I_o(\gamma_n r_c)}\right] I_o(\gamma_n r) \cos(\gamma_n z) \tag{3-3}$$

This simplified model of the magnetic field is useful for comparison with the output from the Munro computer code analysis.

The Munro computer code was used to analyze selected periodic magnetic structures with two different parameter trade-offs. In each case, the amplitude of the first few spatial harmonics on the axis were determined as functions of the average solenoidal field, from $B_o = 0$ through complete saturation of the magnetic pole pieces.

The two parameters that were varied were the gap/period ratio and the angle between the faces of the pole pieces. These two parametric conditions are identified as configurations 1A and 1B respectively in Figures III-7 and 1B-10. The purpose of choosing these two parameters is to determine the extent to which the amplitude of the fundamental periodic component can be maximized as a function of the pole piece geometry.

Figures III-7 and III-8 show the first and second harmonic amplitudes as functions of the average solenoidal field B_o with gap/period ratio as a parameter. Note that the peak field occurs near $G/L = 1/2$ as predicted by equation (3-3) if B_{max} is held constant at B_{sat} (the value at which the pole pieces saturate). Note also that the curves remain nearly flat after saturation occurs.

For some cases of beam focusing it may be desirable to select the ratio of B_1/B_o independently. Figure III-9 shows the range of possible values of B_1/B_o that may be obtained by changing the gap/period ratio and/or operating into the saturation region.

Figures III-10, III-11, and III-12 show the first and second harmonic amplitudes and the B_1/B_o ratio for the case where the angle between the pole faces is varied as a parameter. For these curves, the mean gap-to-period ratio was held constant at 1/3. This configuration, designated as configuration 1B, is illustrated in Figure III-10.

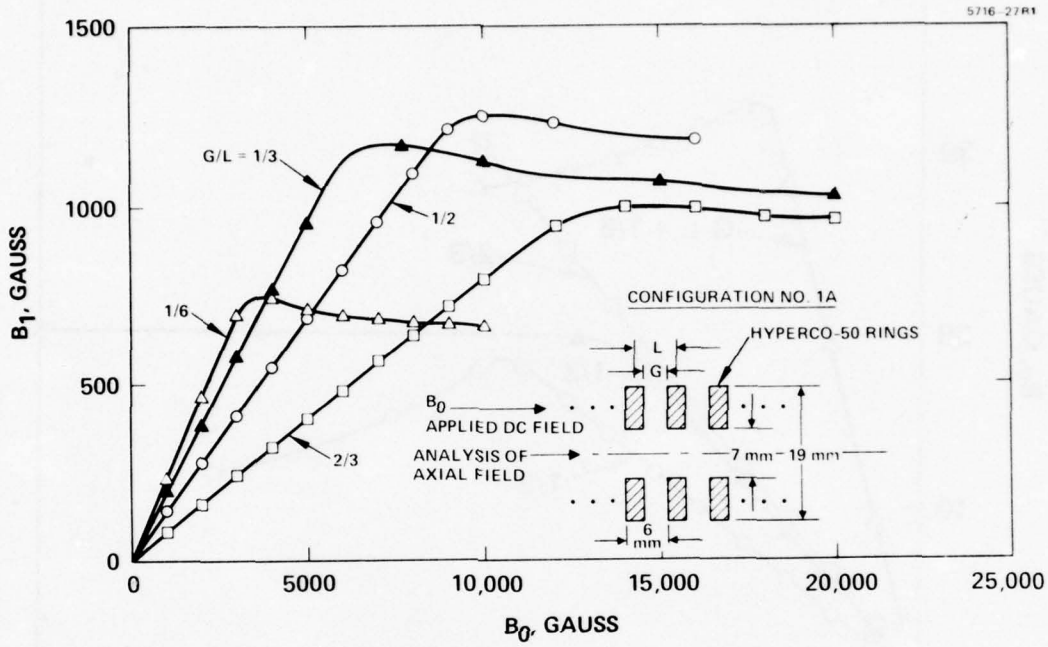


Figure III-7. Plot of first harmonic amplitude B_1 versus average solenoidal field B_o with G/L parameter.

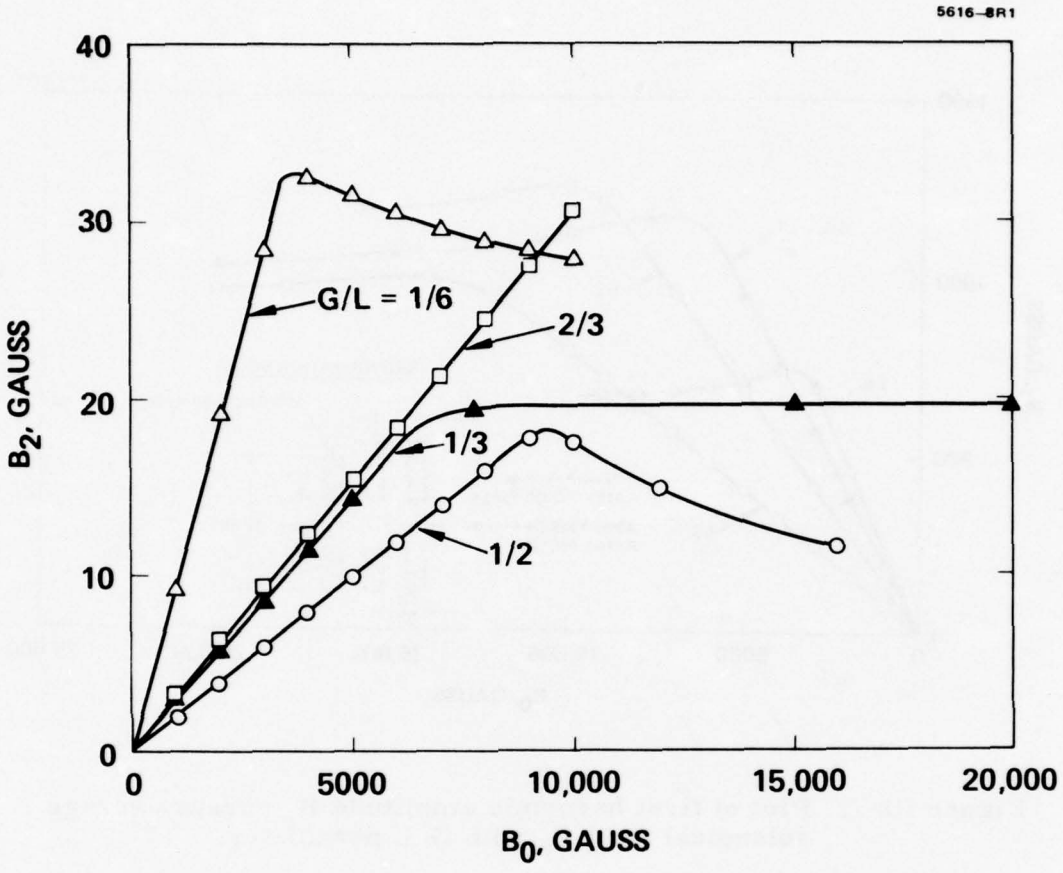


Figure III-8. Plot of second harmonic amplitude B_2 versus average solenoidal field B_o with G/L parameter.

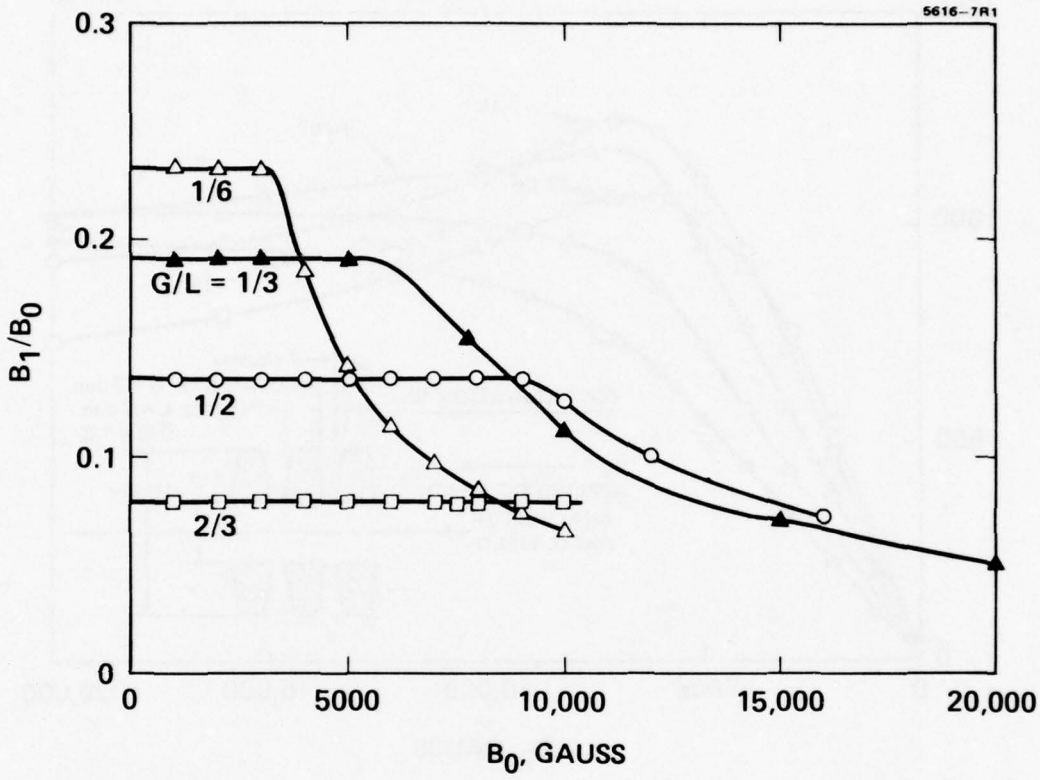


Figure III-9. Plot of B_1/B_0 versus B_0 with G/L parameter.

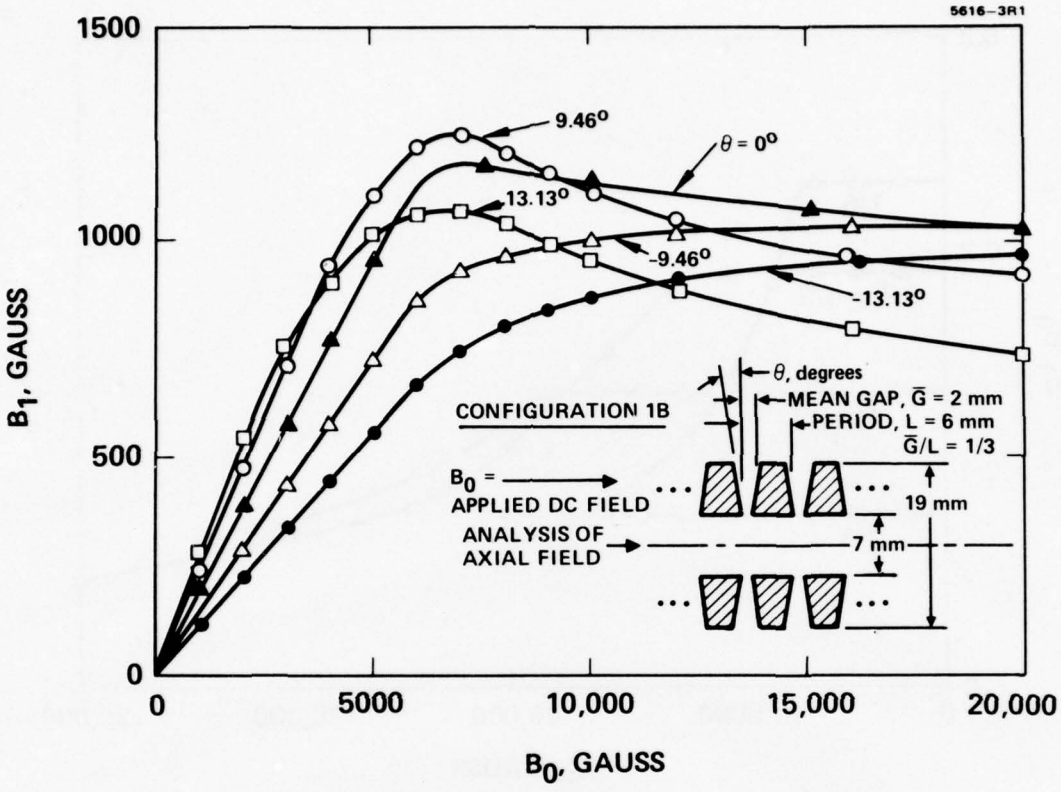


Figure III-10. Plots of B_1 versus B_0 for parameter θ.

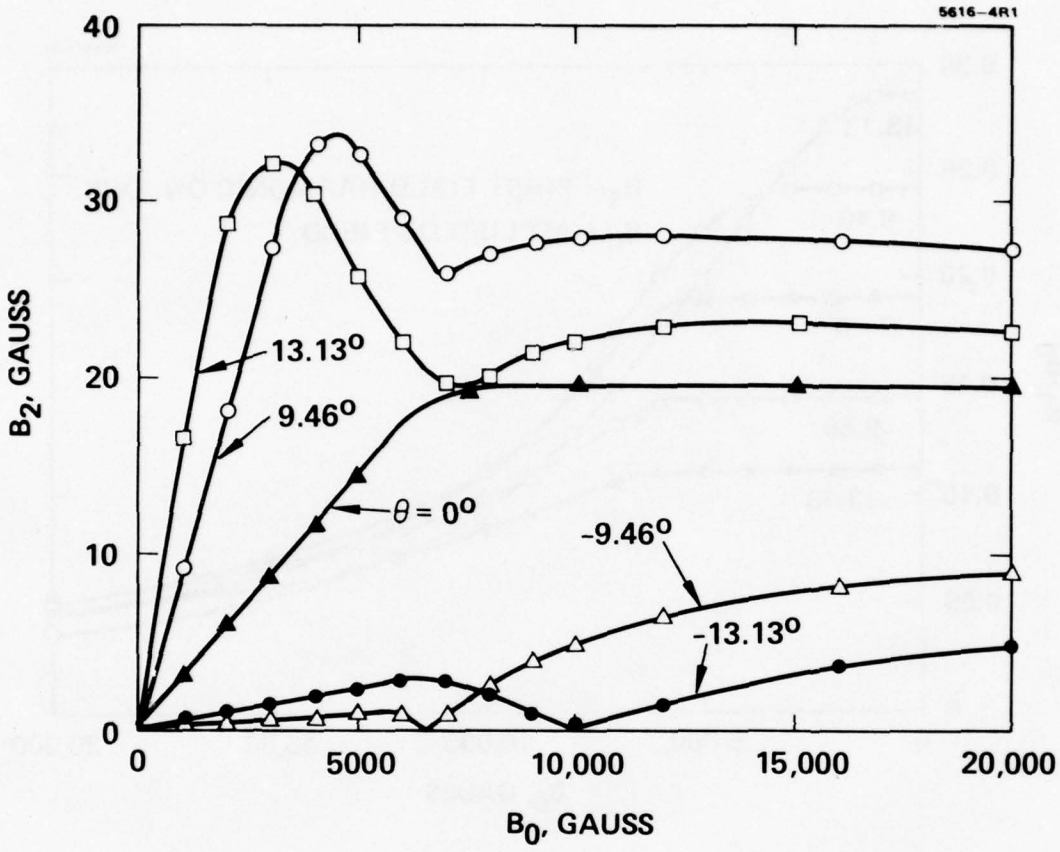


Figure III-11. Plots of B_2 versus B_0 for parameter θ.

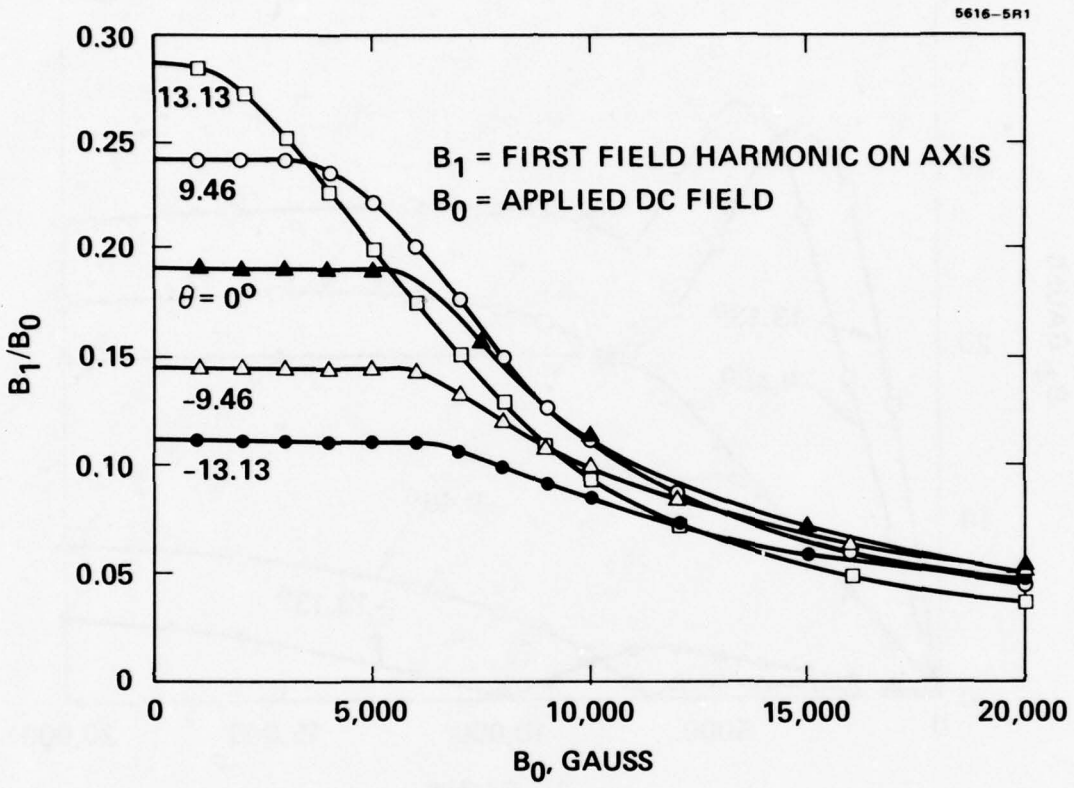


Figure III-12. Plots of B_1/B_0 versus B_0 for parameter θ.

In comparing the peak values of B_1 taken from Figures III-7 and III-10, it will be noted that they are about the same at $B_1 \cong 1250$ gauss. In Figure III-10 the peak occurs for $\theta \cong 10$ degrees. Using the geometry shown with a mean gap-to-period ratio of 1/3, this angle corresponds to an i.d. gap/period ratio of 1/2. Thus, the peak B_1 in Figure III-10 occurs at the same value of i.d. gap/period ratio as the peak in Figure III-7. This should not be surprising based on equation 3-3 and the manner in which it was derived; i.e., matching the i.d. of the circuit as an ideal magnetic boundary. From the results of Figure III-10 we would therefore anticipate that the peak value of B_1 always occurs near the point where the gap/period ratio at the i.d. of the structure is about 1/2, and that it would always have about the same amplitude.

The important thing to note for design purposes is that the average value of magnetic field required to produce maximum B_1 is substantially reduced through tapering of the pole piece faces. From Figure III-7 we see that it required 10,000 gauss to produce the maximum harmonic field, whereas by using the 10-degree taper shown in Figure III-10, this same harmonic amplitude is achieved using only 7000 gauss. The tapered pole pieces thus act as a means for concentrating the magnetic field and reducing the requirements of the solenoid without significant loss in usable harmonic field. The main trade-off in using this technique appears to be in the width of the B_1 curve peak as a function of B_o. Reduction in the peak amplitude of B_1 is small and of secondary concern.

It is informative to compare the results from the Munro computer code with the first order analytical results obtained from equation 3-3. Note in Figure III-9 that prior to saturation the values of B_1/B_o are constant as functions of B_o but vary as a function of G/L. If we identify $B_o = B_{ave} = B_{max}(G/L)$ in equation (3-3), we get for B_1/B_o

$$\frac{B_1}{B_o} = \frac{2}{I_o\left(\frac{2\pi r_c}{L}\right)} \frac{\sin\left(\frac{\pi G}{L}\right)}{\left(\frac{\pi G}{L}\right)} \qquad (3\text{-}4)$$

Plotting this function of G/L together with the nonsaturated values taken from Figure III-9 gives the result shown in Figure III-13. Considering the assumptions used in obtaining equation (3-3), the agreement is quite good — certainly good enough for first-order design trade-off work.

The peak values of B_1 (which occur in the saturation region) may be estimated from equation (3-3) by determining an effective maximum value for B_{max} (called B_{sat}) based on the maximum values of B_1 obtained from the Munro computer code. This has been done as shown in Figure III-14 by plotting the peak values of B_1 taken from Figure III-7 as a function of G/L and then finding a value of B_{max} in equation (3-3) which most closely matches the resulting curve. Note that the effective value of B_{sat} for this case is 17000 Gauss. Note also that there is an effective phase shift between the results from equation (3-3) and the Munro computer code. For first-order design trade-off work, this phase shift is inconsequential because it simply means that a final design would require a slight adjustment in the G/L ratio. The important thing to consider is that an effective value of $B_{max} = B_{sat} = 17000$ gauss has been identified in equation (3-3), which can give reasonably accurate results for determining the maximum obtainable value of B_1.

C. Periodic Permanent Magnet (PPM) Structures

Since about 1970 there has been a rapid development and marketing of new samarium cobalt ($SmCo_5$) permanent magnets which are significantly more powerful and magnetically harder than any previously available materials. Figure III-15 shows the demagnitization curves for a number of magnetic materials compared to that of $SmCo_5$.

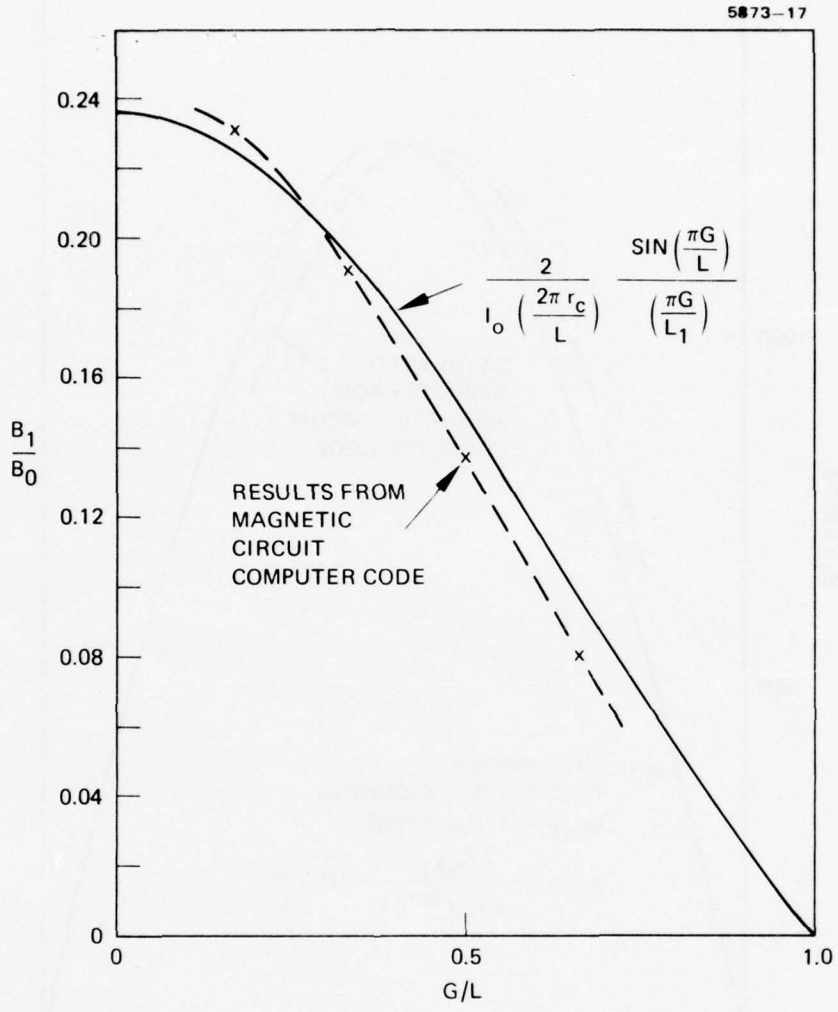


Figure III-13. Non saturated values of B_1/B_0 versus gap/period ratio (for configuration 1A).

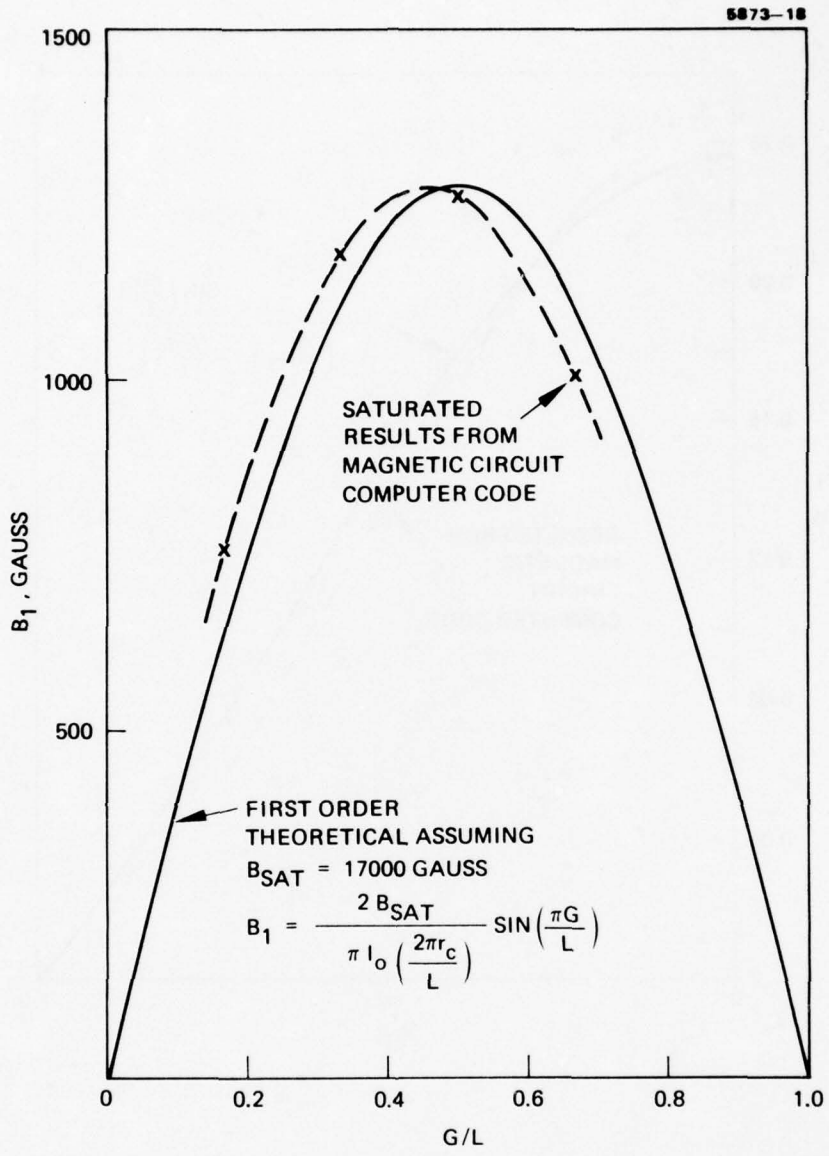


Figure III-14. Saturated peak values of B_1 versus gap/period ratio (for configuration 1A).

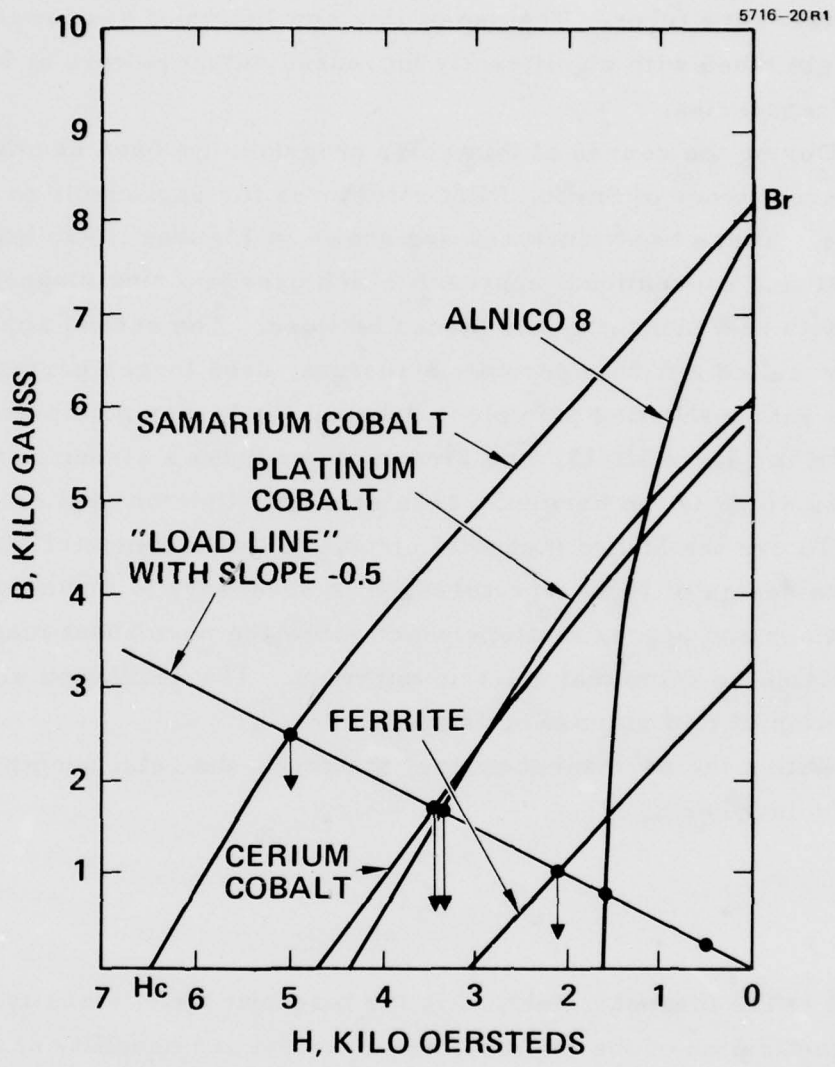


Figure III-15. Demagnetization curves for common high coercive PM materials compared to samarium cobalt.

Samarium cobalt magnets have been assimilated rapidly into the designs of PPM beam focusing structures for microwave and millimeter-wave tubes. The use of this new material has provided lightweight tubes with significantly increased output powers and at higher frequencies.

During the course of this study program, we have examined two different types of $SmCo_5$ PPM structures for application to Ubitrons. These two structures are shown in Figures III-16 and III-17. The first is a conventional approach which uses two ring magnets per period with soft magnetic pole pieces between. The second approach, normally called a double periodic structure, uses longer permanent magnets with a shunting pole piece between the larger pole pieces. As shown in Figure III-17, this structure produces a strong third harmonic which is the harmonic of interest for Ubitron applications.

To use the Munro magnetic circuit analysis computer code to aid in the design of PPM structures, it is necessary to make some assumptions and approximations which allow the permanent magnets to be simulated by azimuthal electric currents. The derivation and justification of this simulation is given here.

Within the permanent magnet material, the relationship between the fields is given by

$$\vec{B} = \mu_o (\vec{H} + \vec{M}) \qquad (3\text{-}5)$$

where $\vec{B}$ is the magnetic field, $\vec{H}$ is the magnetic field intensity, $\vec{M}$ is the magnetization of the material and μ_o is the permeability of free space. Since the permanent magnets shown in Figures III-16 and III-17 are uniformly magnetized in the $\hat{z}$ direction and since the $\vec{B}$ and $\vec{H}$ fields are also essentially uniform and $\hat{z}$ directed due to the soft magnetic pole pieces, we can make the assumption that all of the fields ($\vec{B}$, $\vec{H}$, and $\vec{M}$) within the permanent magnets are uniform and have the same direction. This approximation is fairly good when the permanent magnets are thin, as shown in Figures III-16 and III-17, and the pole pieces are not saturated.

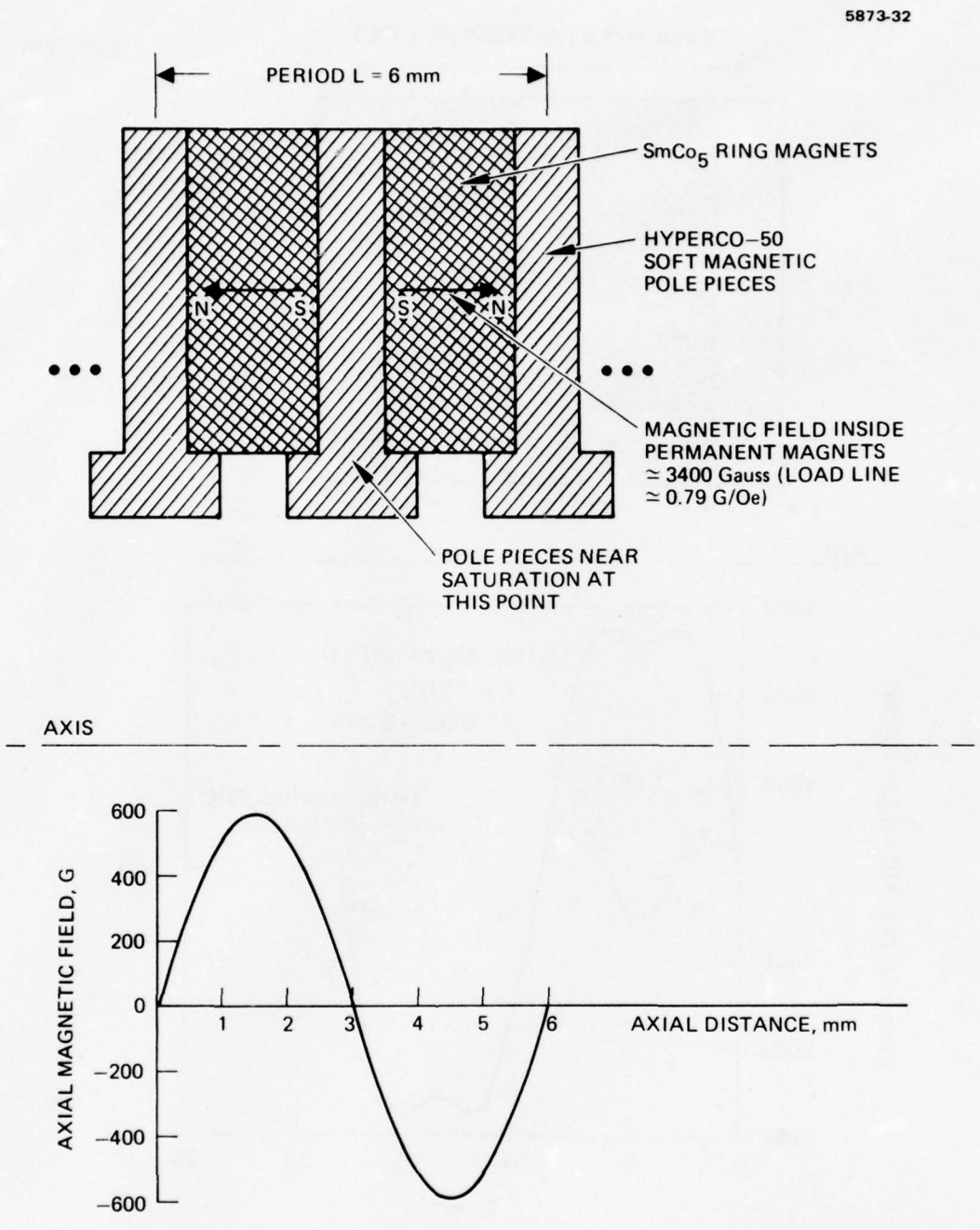


Figure III-16. Periodic permanent magnet (PPM) structure.

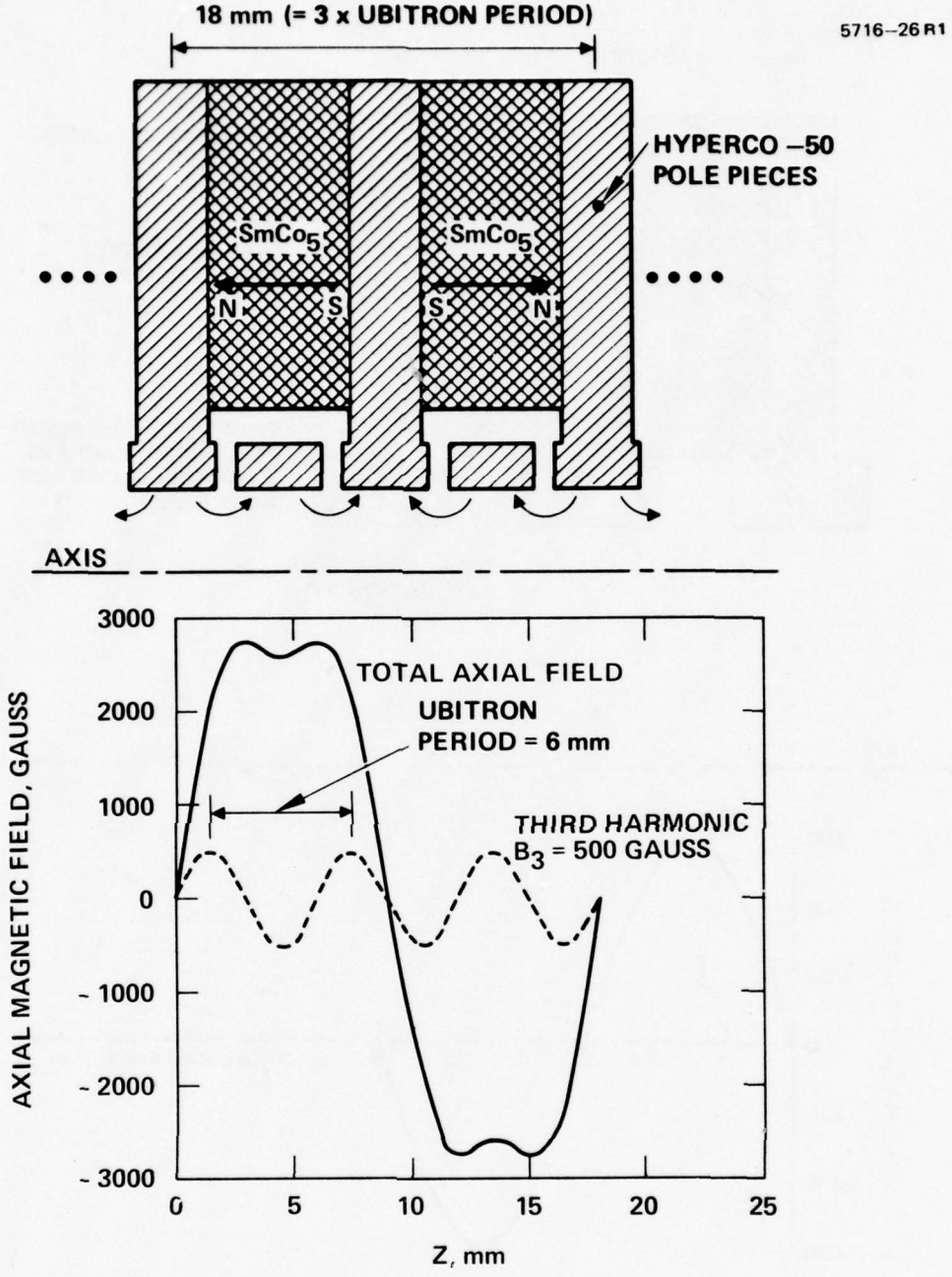


Figure III-17. Doubly periodic permanent magnet structure.

We now choose to re-define $\vec{B}$ in terms of the $SmCo_5$ demagnetization curve shown in Figure III-18. Let μ be the slope of a line running from $-H_c$ to any given working point (B_1, H_1) on the curve as illustrated in Figure III-18. Then, in terms of μ, B is given by

$$B = (\mu)(H + H_c) \tag{3-6}$$

where μ is a function of the working point on the curve. Thus, when $H = 0$, the value of B is

$$B = \mu_c H_c \equiv B_r \text{ (residual magnetic field)}$$

and when $H = -H_c$, B is zero as required. Note that the function μ in equation (3-6) is the nonlinear permeability for a new B-H curve obtained by shifting the actual curve by an amount H_c (see Figure III-18).

Solving equation (3-6) for H and substituting this value into the macroscopic Maxwell equation $\nabla \times \vec{H} = 0$, we get the following equation:

$$\nabla \times \frac{\vec{B}}{\mu} = \nabla \times \vec{H}_c \tag{3-7}$$

Based on equation (3-7) the boundary condition at the surface of the permanent magnet is

$$\hat{n} \times \left(\frac{\vec{B}_2}{\mu_2} - \frac{\vec{B}_1}{\mu_1} \right) = -\hat{n} \times \vec{H}_{c_1} \tag{3-8}$$

where $\hat{n}$ is an outward directed unit vector normal to the surface of the magnet and the subscripts 1 and 2 refer to quantities inside and outside of the magnet respectively.

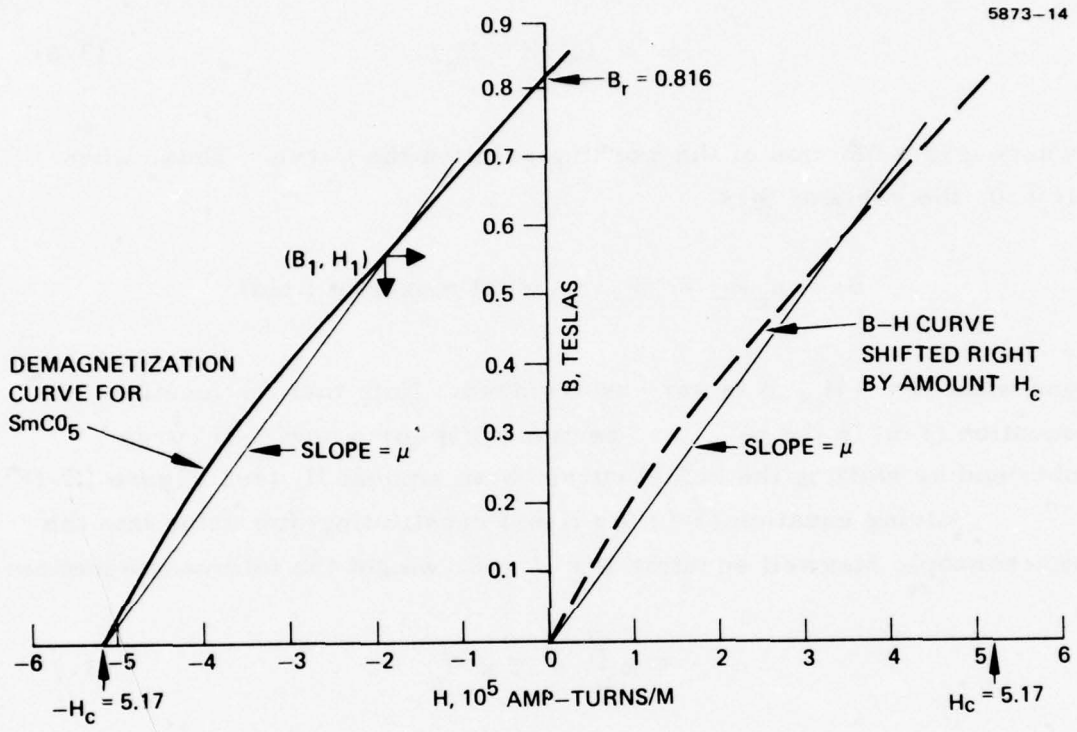


Figure III-18. Samarium cobalt demagnetization curve and shifted curve.

If we now compare equation (3-8) to the equivalent equation obtained for a problem involving soft magnetic materials; i.e.,

$$\hat{n} \times \left(\frac{\vec{B}_2}{\mu_2} - \frac{\vec{B}_1}{\mu_1} \right) = \vec{J}_s$$

we see that the PPM problem is equivalent to one in which there are surface currents on the permanent magnet of value

$$\vec{J}_s = -\hat{n} \times \vec{H}_c$$

and where the permanent magnet volume is replaced by a soft magnetic material of nonlinear permeability μ. The permeability in this case is treated as a function of the magnetic field B, as it is in the Munro computer code.

The net result of this equivalency is shown in Figure III-19. A thin layer of current on the inner and outer surfaces of the magnets are the equivalent magnetization of the permanent magnets and the volume of the magnets is treated as a soft magnetic material of permeability μ. In terms of the current layer thickness "t," the current density within the layer is

$$|J| = \left| \frac{J_s}{t} \right| = \left| \frac{H_c}{t} \right| \qquad (3\text{-}9)$$

The correctness of the above equivalence theory has been checked using the computer code to solve the asymptotic case of a short-circuited magnet (i.e., a permanent magnet which is completely encased in a high-permeability, non-saturating material). The result was $B = B_r$ throughout the volume of the permanent magnet as required. Also, other PPM structures analyzed by the computer code gave reasonable results which are approximated by those of simple magnetic-circuit theory for non-saturating structures. The equivalence theory is

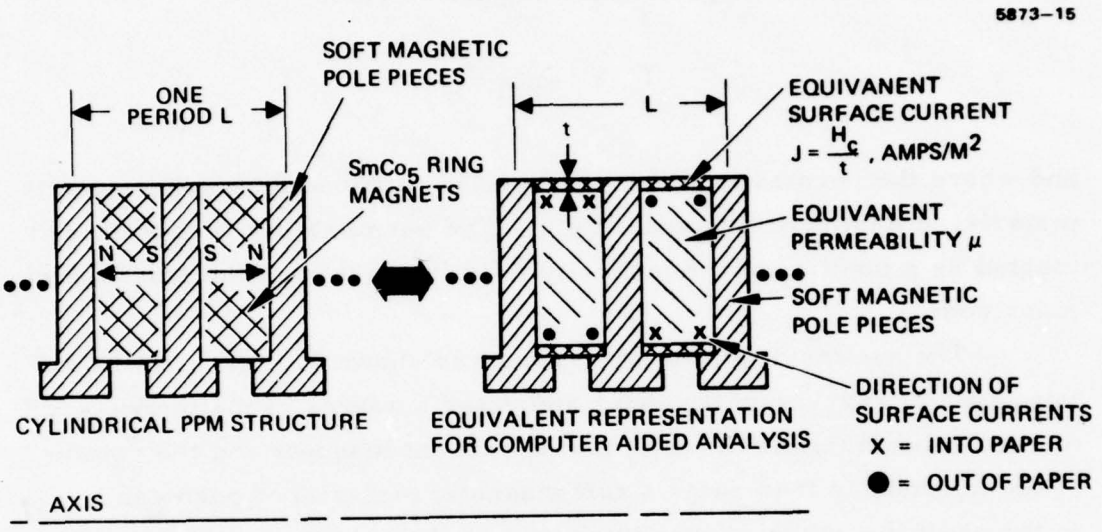


Figure III-19. PPM equivalent magnetic structure for computer aided analysis.

therefore believed to be correct. In most cases it was also observed that the calculated magnetic field within the permanent magnets was essentially uniform as required by the initial assumptions for magnetic circuit equivalency. Where saturation begins to occur, this is no longer true, and the equivalency begins to break down.

The advantage of using the Munro computer code for PPM analysis is that a better approximation of the fringing fields is obtained, which results in better accuracy in calculating the axial magnetic field amplitudes.

The results of a computer-aided design trade-off of PPM structures for use in a 300-kV Ubitron amplifier at 94 GHz are shown in Figures III-16 and III-17. The final design cross-sectional drawings of the structures are also shown. These designs were arrived at through the process of adjusting the PPM structure dimensions and analyzing the result until (1) the maximum flux density in the pole pieces (which occurs approximately at the i.d. of the magnets) was below saturation limit, and (2) the average B/H within the magnets was about -0.5 (i.e., a magnet load line of 1/2 in gaussian units) both of these criteria are common practice for good PPM design.

As shown in the figures the simple PPM structure gave the best results with about 600 Gauss peak fundamental harmonic compared to 500 gauss peak third harmonic in the double PPM structure. We believe that the upper limit which can be achieved by pushing the design limits past the normal design criteria is approximately 700 gauss peak using the simple PPM structure. This is the value used for the comparative results shown in Figure III-16.

One of the problems associated with $SmCo_5$ ring magnets is that, because of their high energy and brittleness, they are difficult to work with when the thickness dimensions become small. Experience at Hughes has shown that magnets as thin as 0.050 inches must be processed and handled with considerable care. A consensus of opinion from magnet vendors seems to be that magnets as thin as 0.030 inches could be fabricated and used in PPM structures as long as the (o.d./thickness) ratio did not exceed about 10.

The magnets in the simple PPM structure shown in Figure III-16 are easily within the constraints described above. If, however, there was a need to lower the operating voltage of a 94 GHz amplifier to the vicinity of 100 kV, the result would be magnet thickness on the order of 0.015 to 0.020 inches, which may not be possible. In this case, it would be necessary to use a double PPM structure like the one shown in Figure III-17. The effects of the double PPM magnetic field shape on beam focusing and rf interaction were not studied during this program.

D. Periodic Electromagnets

We anticipated at the beginning of this portion of the study that periodic electromagnets for Ubitron applications would not be comparative with other techniques because of the added power dissipation very close to the rf circuit. For the sake of completeness, however, some quantitative results were obtained.

Figure III-20 shows the results of computer-aided analysis on a periodic electromagnet structure applicable to a 94-GHz, 300-kV Ubitron. The electric windings in this structure are very small but are consistent with what is being done in the field of miniaturized magnetic lenses for electron microscope work.[45]

Note from the figure that the soft magnetic material encasing the coils saturates quickly as the current density is increased. This limits severely the maximum field which is attainable. After saturation of the pole pieces, the dissipated power per winding increases rapidly with very little net gain in the magnetic field amplitude.

A peak axial magnetic field of 800 gauss requires a power dissipation of approximately 1 kW per period. For the design shown in Figure III-20 this represents an outer surface heat flow of about 200 W/cm^2. Much larger heat flows are possible (2000 W/cm^2 SOA) but 200 W/cm^2 is sufficiently large that any further increase could only be justified on the basis of a detailed thermal analysis. It must also be remembered that rf circuit cooling is superimposed on the problem of cooling the magnetic structure.

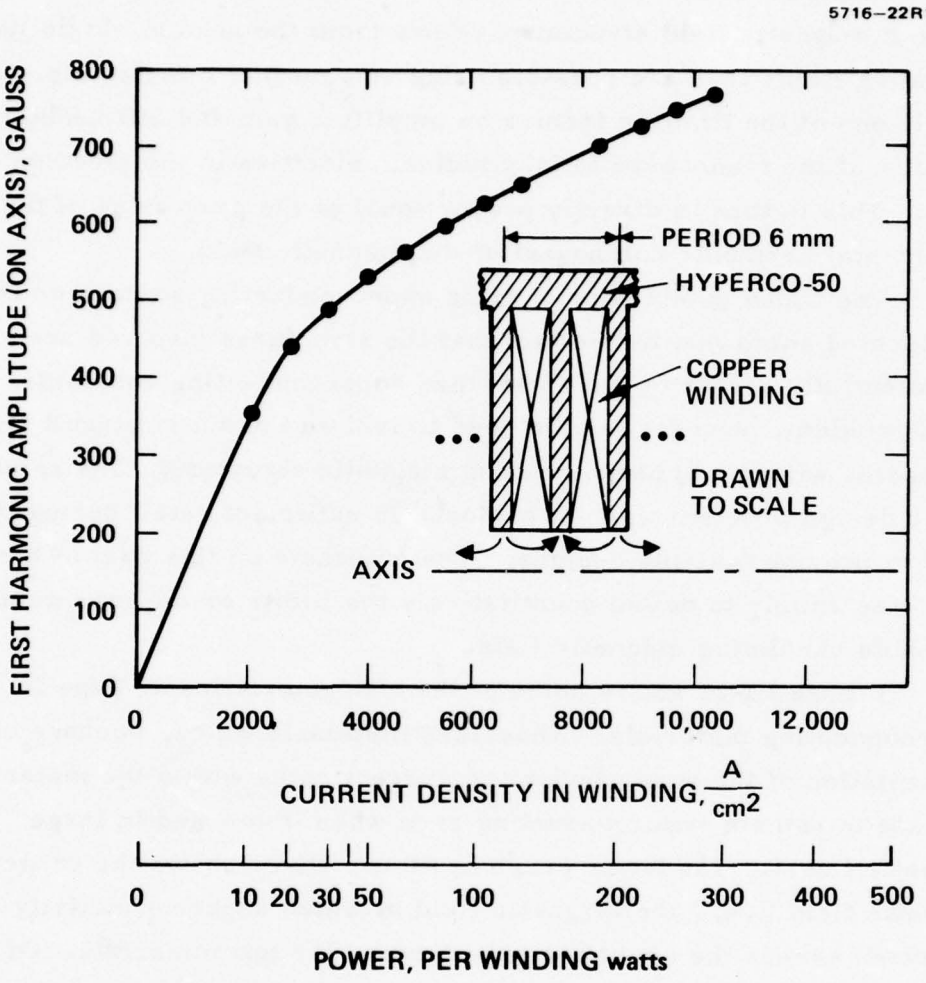


Figure III-20. Axial magnetic field versus dissipated power using periodic electromagnets.

E. Superconducting Current-Carrying Ring Structure

The motivation for determining the capabilities of superconducting periodic magnetic field structures comes from the need to obtain larger undulating fields than are possible using soft magnetic materials. At 94 GHz one of the limiting factors on amplifier gain and efficiency is the ratio of the transverse to longitudinal velocities in the electron beam. This in turn is directly proportional to the peak value of the fundamental harmonic component of the magnetic field.

The added complexity of using superconducting structures is ameliorated somewhat by the fact that the structures involved are small and potentially easier to work with than superconducting solenoids. An added problem, however, is the need to isolate the hot rf circuit from the closely adjacent superconducting magnetic structure. The solution to this design problem was not explored in sufficient detail during this study to provide feasible designs. The emphasis on this part of the study was simply to define quantitatively the limits on the maximum attainable undulating magnetic field.

Figure III-21 shows some of the characteristics of Type II superconducting materials. These are materials which, because of filamentation of the superconducting current paths within the material, are able to remain superconducting even when immersed in large magnetic fields. The lower graph in Figure III-21 shows the critical magnetic field (i.e., the magnetic field at which superconductivity is quenched) versus the operating temperature for two materials. Of the two materials, niobium tin compounds have been used extensively in superconducting solenoids. Using powder metallurgy and sintering processes, niobium-tin can be fabricated into almost any desired shape.

The upper graph in Figure III-21 shows the critical current density versus applied magnetic field. As with the critical magnetic field, the critical current density is the current density at which superconductivity in the material is quenched. This curve shows that

5716–19

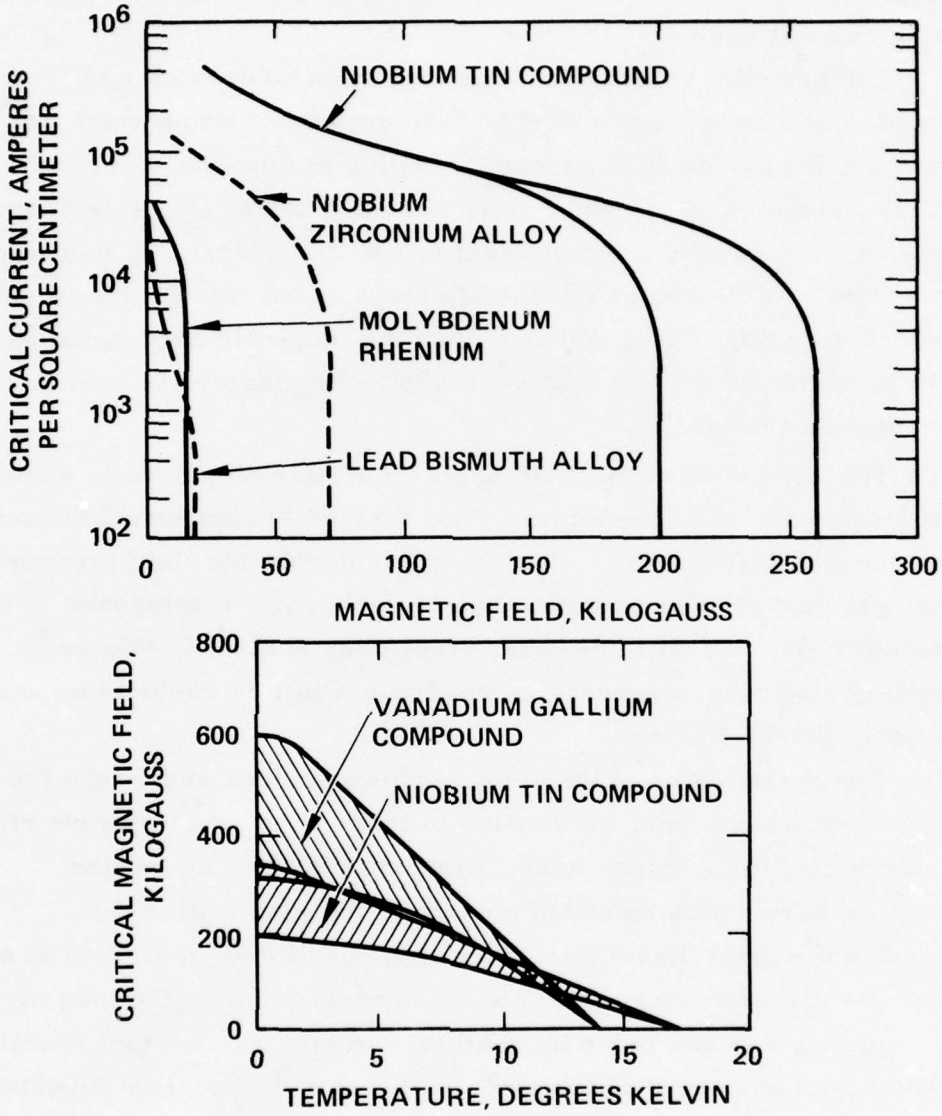


Figure III-21. Characteristics of superconducting materials.

for niobium tin operating in magnetic fields of a few kilogauss the maximum current density is between 10^5 and 10^6 A/cm^2. For the purposes of this study we have used a value of 6×10^5 A/cm^2 as the limiting current density.

The periodic superconducting ring structure which was analyzed is shown in Figure III-22. The superconducting rings are spaced two per period with current traveling in opposite directions. The cross sections of the rings were assumed to be square as shown and the current density was set equal to 6×10^5 A/cm^2. A wall was placed outside of the super conducting rings which was also assumed to be superconducting. This wall confines the magnetic field to the axial region by virtue of the fact that superconducting materials tend to exclude magnetic fields.

The net result of the field analysis on this structure is shown in the lower portion of the figure. The desired fundamental harmonic is very nearly 2000 gauss. This is nearly double the field produced by the next best structure; viz, magnetic pole pieces immersed in a solenoidal field. As with the other structures analyzed, this superconducting ring structure was designed to operate in conjunction with a 94-GHz, 300-kV Ubitron.

The construction of the superconducting rings could take the form of a ring-bar structure similar to those used in microwave rf slow-wave circuits. In our case, alternate rings would be tied together by bars which extended outside of the ring radius and traveled in the axial direction. Each ring would then be broken at one point on its circumference to allow the current to enter the loop by one connecting bar and leave by another. In this way current traveling one way would excite all of the rings with one of the current directions and current traveling back would excite all of the remaining rings.

The structure described above is equivalent to a bifilar helix in which the current traveling in the two windings is going in opposite directions. The spiraling periodic magnetic field created by a

5716–24

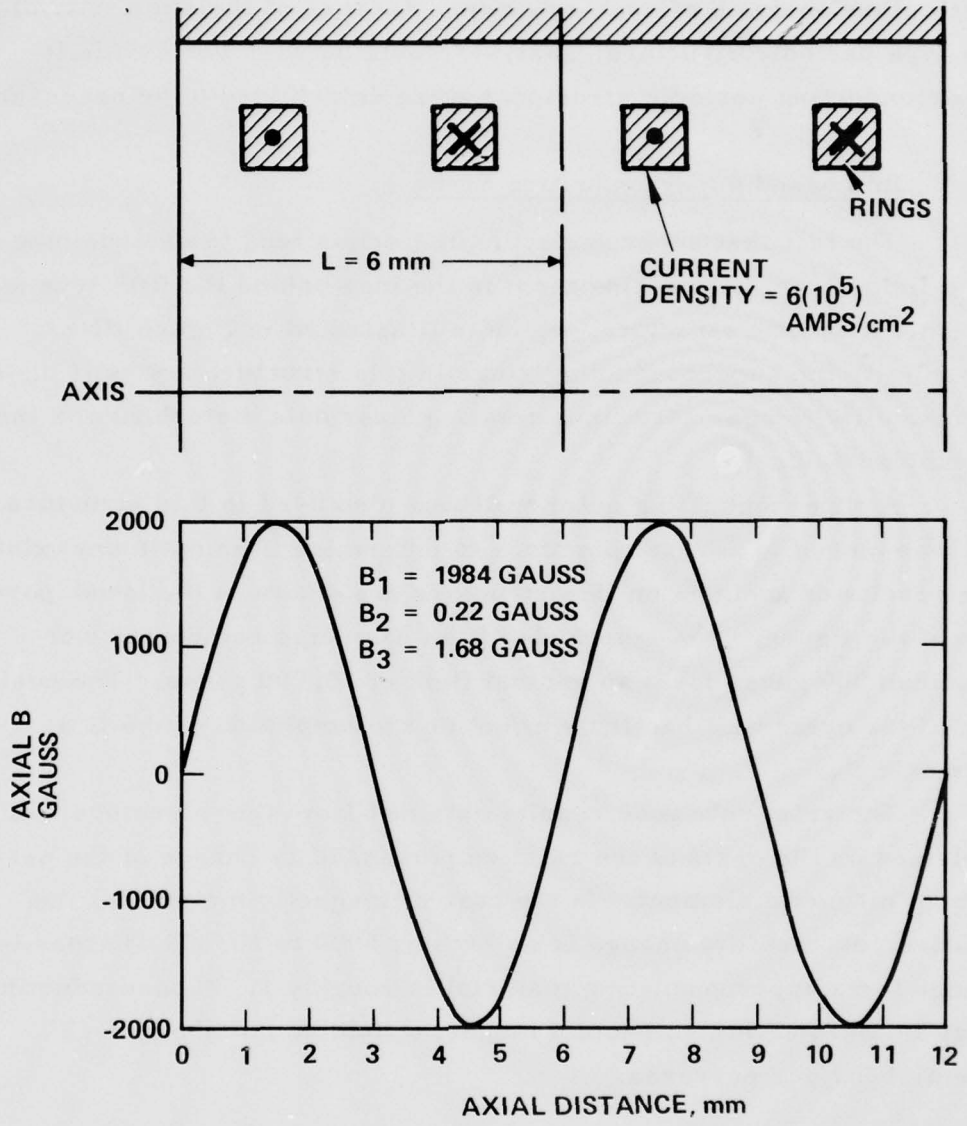


Figure III-22. Axial magnetic field using periodic superconducting rings.

bifilar-wound superconductor would probably provide a suitable field for Ubitron operation, but at present no tools have been developed which allow analysis of such a device. Because of the simplicity of this type periodic structure, analysis would be well worthwhile if superconducting periodic structures were determined to be necessary.

F. Immersed Superconducting Rings

The fact that superconducting materials tend to exclude magnetic fields from penetrating them is the idea behind the fifth type of periodic magnetic structure, which is illustrated in Figure III-23. Essentially the superconducting rings in this structure act as if their permeability is near zero, thus creating a periodic disturbance in the solenoidal field.

A superconducting outer wall was also used in this structure and was moved to several positions to determine if an optimum existed. The results of analysis on this structure are shown in the lower portion of the figure. The amplitude of the harmonic component was less than 300 gauss for a solenoidal field of 10,000 gauss. The position of the outer wall had little effect on the amplitude of the first harmonic B_1.

The relatively poor results obtained from this structure can be explained on the basis of the relative permeability change of the perturbing magnetic element. In the case of magnetic materials, the relative permeability change is as high as 5000 to 10,000 whereas the change for a superconducting material is roughly 1. Superconducting rings immersed in a solenoidal magnetic field do not show much potential for our purposes.

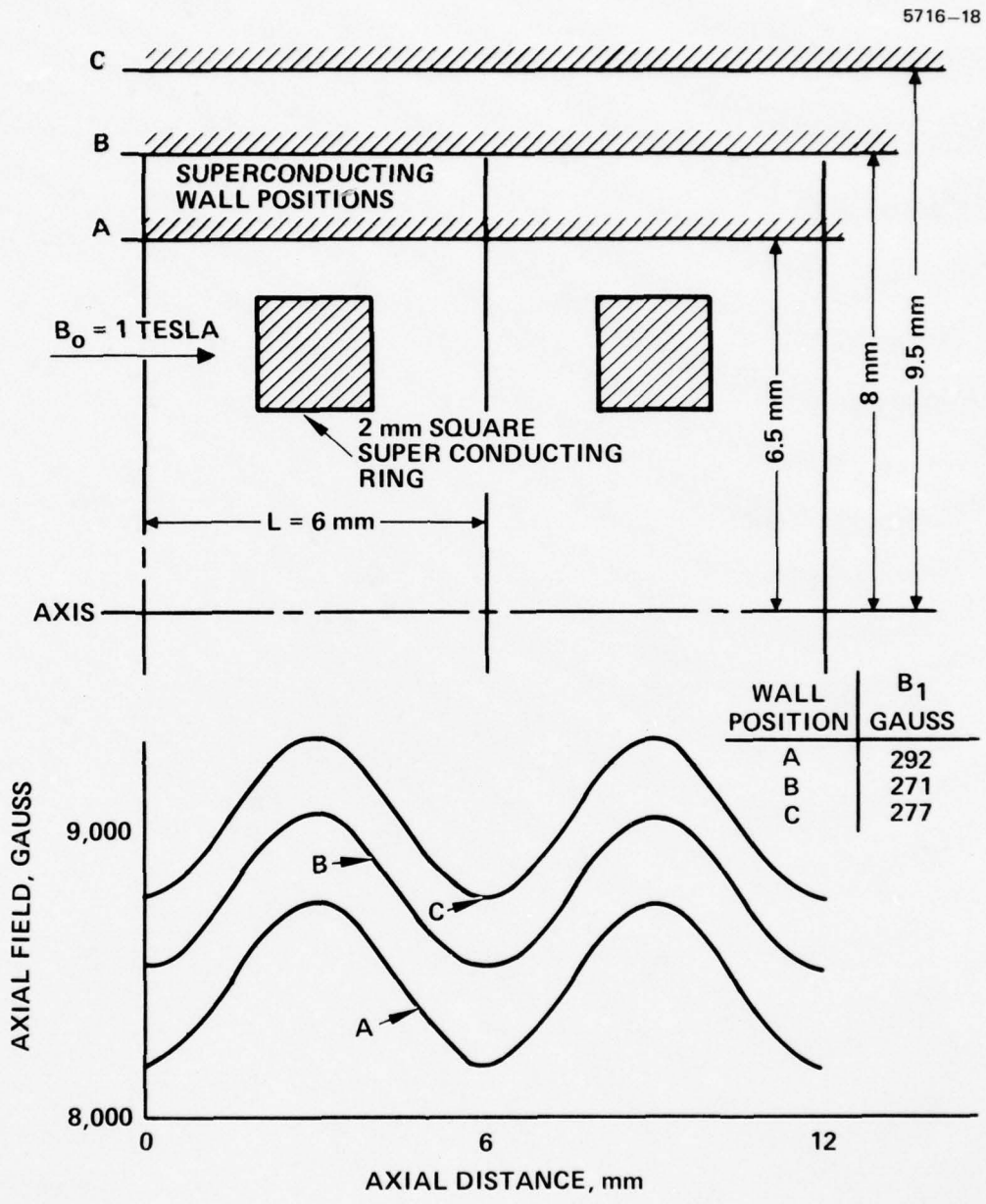


Figure III-23. Axial magnetic field using immersed superconducting rings.

IV. THE DESIGN OF THE ELECTRON GUN

A. Introduction

The Ubitron concept requires a hollow electron beam traveling down a circular waveguide with its sense of rotation periodically changed by a static magnetic field which varies periodically about a constant value with distance along the waveguide.

A baseline design of a 50-kW Ubitron amplifier was originally made in which the electron beam was defined. The parameters of this design are listed in Table IV-1 and are retained in the present study with some exceptions which resulted from the newly acquired knowledge of the magnetic field configuration. Inspection of the table shows the beam to be relativistic but to carry only a small amount of space charge which is neglected in the analysis. Furthermore, it is evident that the cathode must be considerably larger in area than the cross-sectional area of the beam in the interaction region even in the limiting case of a solid 0.30 cm diameter beam. A solid beam with this diameter would have a current density of 60 A/cm^2. Since cathodes do not operate reliably at emission densities greater than about 3 A/cm^2 the minimum area compression of the beam is 20:1 for the solid beam and larger for annular beams.

Two types of electron gun have been considered to generate the beam for the Ubitron; the convergent hollow beam gun shown in Figure IV-1 and the magnetron injection gun shown in Figure IV-2. Unfortunately the time available has not been adequate to make a comparative study of the merits of the two guns. Because the current Russian work on fast-wave devices has shown a preference for magnetron injection guns for generation of annular beams, we have chosen to investigate the magnetron injection gun in the time available.

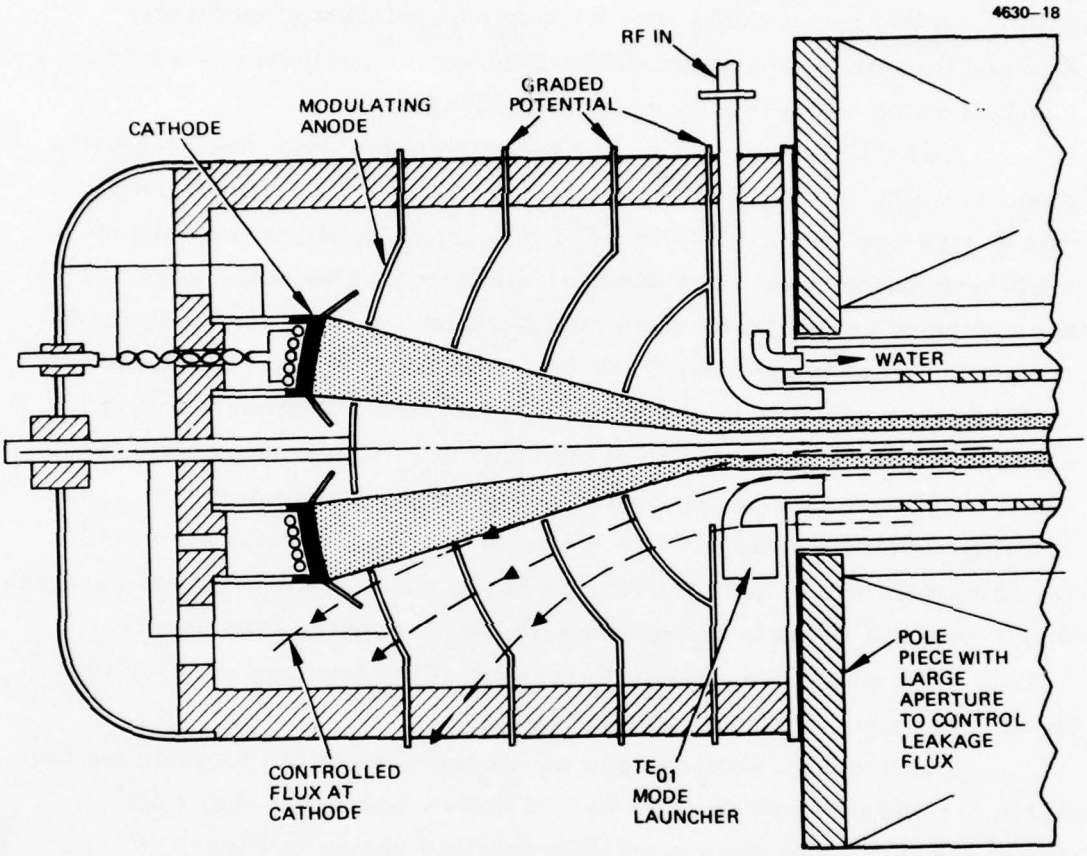


Figure IV-1. Convergent hollow beam gun.

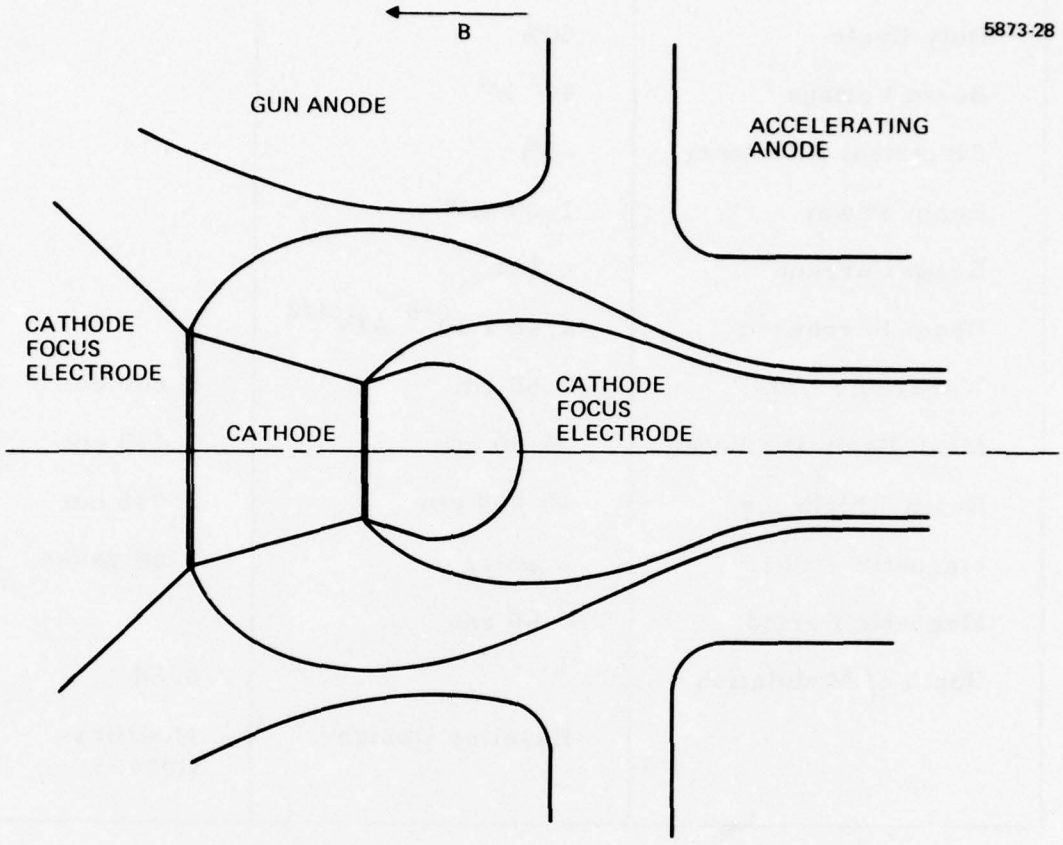


Figure IV-2. Magnetron injection gun.

Table IV-1. Baseline Operating Parameters of 50 kW Ubitron

RF Power	50 kW	
Duty Cycle	50%	
Beam Voltage	300 kV	
Electrical Efficiency	~4%	
Beam Power	1.25 MW	
Beam Current	4.2 A	
Beam Perveance	2.42×10^{-8} A/V$^{3/2}$	
Waveguide I. D.	0.60 cm	0.600 cm
Mean Beam Diameter	~0.30 cm	0.470 cm
Beam Thickness	~0.004 cm	0.045 cm
Magnetic Field	~ gauss	7500 gauss
Magnetic Period	0.60 cm	
Depth of Modulation		0.18
	Baseline Design	Modifications

Because the electron gun parameters of Table IV-1 were under constant review as a consequence of the development of the rf theory, we chose to investigate the general relationships of the gun design parameters of the magnetron injection gun to the parameters of the electron beam in the interaction region, in preference to concentrating on a specific gun design.

In paragraph B. we review the relativistic Lorentz force equation and in paragraph C. we discuss the motion of the electrons in the region of the magnetron injection gun, using a simplified gun geometry.

This part of the report parallels the work of Tsimring.[46] Paragraph D. is devoted to a discussion of the invariants of the motion which are used to relate the parameters of the electron gun to the boundary conditions on the dc beam at the beginning of the rf interaction region. In paragraph E. we develop the relativistic paraxial ray equation which is used to describe the motion in the region of uniform magnetic field and also in the region where the field undulates, for small amplitudes of undulation. The simple analytic expressions for the electron motion could be useful in the further development of small-signal theory. A sample calculation of a suitable magnetron injection gun using the theory developed is presented in paragraph F.

B. The Relativistic Lorentz Force Equation

The Lorentz force equation is

$$\frac{d}{dt}[m_o\gamma\vec{v}] = -e[\vec{E} + \vec{v}\times\vec{B}] \tag{4-1}$$

where m_o is the rest mass of the electron, e its charge, and $\vec{v}$ its velocity. $\vec{E}$ and $\vec{B}$ are the electric and magnetic field, and the relativistic γ is

$$\gamma = \frac{1}{\sqrt{1 - \vec{v}\cdot\vec{v}/c^2}} \tag{4-2}$$

In the following we briefly summarize the expansion of equation (4-1) previously given in Section II, and derive relativistic potential equations useful in beam analysis.

Equation (4-1) is, with $\eta = e/m_o$

$$\gamma \frac{d\vec{v}}{dt} + \vec{v} \frac{d\gamma}{dt} = -\eta \left[\vec{E} + \vec{v}x\vec{B}\right] \tag{4-3}$$

Scalar multiplication by $\vec{v}$ gives

$$\vec{v} \cdot \frac{d\vec{v}}{dt} + \vec{v} \cdot \vec{v} \frac{d\gamma}{dt} = -\eta \vec{v} \cdot \vec{E} \tag{4-4}$$

Using the definition of

$$\vec{v}.\vec{v} = c^2 \left[1 - \frac{1}{\gamma^2}\right] \tag{4-5}$$

$$\vec{v} \cdot \frac{d\vec{v}}{dt} = -\frac{c^2}{\gamma^3} \frac{d\gamma}{dt} \tag{4-6}$$

Hence after substitution into (4-4)

$$m_o c^2 \frac{d\gamma}{dt} = -e \vec{v}.\vec{E} \tag{4-7}$$

The right-hand side is the work done on the electron. If T is the kinetic energy of the electron, then

$$T = m_o c^2 (\gamma - 1) \quad m_o c^2 \left(1 + \frac{1}{2} v^2/c^2 - \cdots - 1\right) \tag{4-8}$$

and (4-7) becomes

$$\frac{d}{dt}(T) = -e \vec{v}.\vec{E} \tag{4-9}$$

Integration of (4-9) gives

$$m_o c^2 (\gamma - 1) = e\Phi$$

and hence

$$\frac{v}{c} = \sqrt{\frac{2e\Phi}{m_o c^2}} \frac{\left[1 + \frac{1}{2}\frac{e\Phi}{m_o c^2}\right]^{1/2}}{\left[1 + \frac{e\Phi}{m_o c^2}\right]} \qquad (4\text{-}10a)$$

or

$$\frac{v}{c} = \sqrt{\frac{2\Phi}{511.0}} \frac{\left[1 + \frac{\Phi}{1022.0}\right]^{1/2}}{\left[1 + \frac{\Phi}{511.0}\right]} \qquad (4\text{-}10b)$$

where Φ is measured in kilovolts.

C. The Motion in the Magnetron Injection Gun

A typical magnetron injection gun is shown in the previous Figure IV-2. In such a gun the extraction of the electrons depends on the presence of a magnetic field at the cathode. Unfortunately, this magnetic field plays a considerable role in determining the subsequent electron motion and therefore restricts the options available to the designer of the electron gun. Specifically, the energy in rotation in the magnetic field imparted to the electrons in the gun is related to the energy in the magnetic field downstream by the "transverse

adiabatic invariant" and by the need to conserve angular momentum. To determine these quantities we consider a simple model of the electron gun in which a conical cathode with a narrow cone angle is surrounded by a concentric cylinder as shown in Figure IV-3. A uniform axial magnetic field B_c exists in this region. Electrons leave the cathode with initial velocity components $v_{\xi T}$, $v_{\eta T}$, $v_{\nu T}$ measured in a Cartesian coordinate system (ξ, η, ν) located on the cathode. In the cylindrical coordinate system (r, θ, z) of the gun the initial velocity components are

$$v_{\theta T} = v_{\xi T} \tag{4-11a}$$

$$v_{rT} = v_{\eta T} \cos \delta - v_{\nu T} \sin \delta \tag{4-11b}$$

$$v_{zT} = v_{\eta T} \sin \delta + v_{\nu T} \cos \delta \tag{4-11c}$$

The electric field E between the cathode and the anode is approximately described by the space charge free electric field between concentric cylinders. This field is

$$E = - \frac{\Phi_A}{r} \frac{1}{\log (r_a/r_c)} \tag{4-12}$$

The average value $\overline{E}$ of this field is

$$\overline{E} = \frac{-2\Phi_A}{(r_a + r_c)} \frac{1}{\log (r_a/r_c)} \tag{4-13}$$

and will be used to calculate the electron trajectories in the gun.

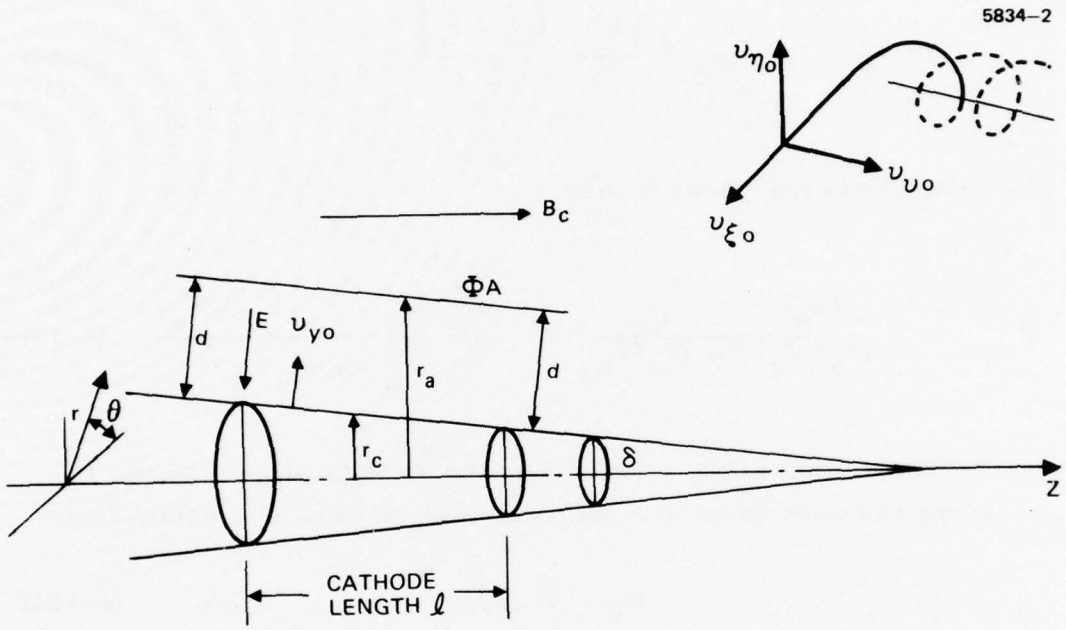


Figure IV-3. Coordinate system used in analysis of gun.

The magnetic field B_c in the cathode region must be strong enough to prevent the electrons from being accelerated into the anode. The critical mangetic field which just prevents this is related to the anode voltage by the magnetron "cut-off" condition which is given by (4-2)

$$\Phi_A \leq \frac{\eta B_c^2}{8} \frac{\left(r_a^2 - r_c^2\right)^2}{r_a^2} \tag{4-14}$$

The critical average field is then

$$\overline{E}_{crit.} = -\frac{2\Phi_A}{(r_a + r_c)} \frac{1}{\log (r_a/r_c)} = -\frac{\eta B_c^2}{4} \frac{\left(r_a^2 - r_c^2\right)(r_a - r_c)}{r_a^2 \log (r_a/r_c)} \tag{4-15}$$

The motion of the electrons in the vicinity of the cathode is therefore assumed to be in a uniform electric field with components

$$E_r = \overline{E} \cos \delta \tag{4-16a}$$

$$E_\theta = 0 \tag{4-16b}$$

$$E_z = \overline{E} \sin \delta \tag{4-16c}$$

In order to simplify the analysis, Cartesian coordinates are used to approximately describe the motion in the vicinity of the cathode with $E_y = E_r$. The non-relativistic Lorentz force equation is used since the electrons travel slowly in the gun region. The components of this equation are

$$\frac{dv_x}{dt} = -\eta v_y B_z \tag{4-17a}$$

$$\frac{dv_y}{dt} = -\eta [E_y - v_x B_c] \tag{4-17b}$$

$$\frac{dv_z}{dt} = -\eta E_z \tag{4-17c}$$

A transformation is made to a coordinate system moving with velocity $\vec{E} \times \vec{B}/B^2$, i.e.

$$v_x = v'_x + E_y/B_c \tag{4-18a}$$

$$v_y = v'_y \tag{4-18b}$$

$$v_z = v'_z \tag{4-18c}$$

On making this substitution, and using

$$\omega_{cc} = \eta B_c \tag{4-19}$$

the equations of motion are,

$$\frac{dv'_z}{dt} = -\omega_{cc} v'_y \tag{4-20a}$$

$$\frac{dv'_y}{dt} = \omega_{cc} v'_x \tag{4-20b}$$

$$\frac{dv'_z}{dt} = -\eta E_z \tag{4-20c}$$

AD-A040 043 HUGHES RESEARCH LABS MALIBU CALIF F/G 9/5
MILLIMETER WAVE UBITRON DEVELOPMENT PHASE I.(U)
APR 77 J M BAIRD, S SENSIPER, K AMBOSS F30602-76-C-0215
UNCLASSIFIED RADC-TR-77-133 NL

3 OF 4
AD
A040043



SIFIED

3 OF 4

AD

A040043



Since the axial velocity component does not appear in the equations for the transverse motion and vice versa, these two motions may be discussed separately. The axial field serves merely to extract the electrons from the magnetron injection gun.

Since the axial velocity component does not appear in the equations for the transverse motion and vice versa, these two motions may be discussed separately. The axial field serves merely to extract the electrons from the magnetron injection gun.

The solutions to the transverse equations are:

$$v_x' = A_x \cos \omega_{cc} t + B_x \sin \omega_{cc} t \qquad (4\text{-}21a)$$

$$v_y' = A_y \cos \omega_{cc} t + B_y \sin \omega_{cc} t \qquad (4\text{-}21b)$$

At time $t = 0$, $v_x' = v_{\theta T} = v_{\xi T}$ and hence $v_x' = (v_{\theta T} - E_y/B_c)$. Also $dv_x'/dt = -\omega_{cc} v_{yT} = -\omega_{cc} v_{rT}$. Hence for the x motion

$$v_x' = (v_{\theta T} - E_y/B_c) \cos \omega_{cc} t - v_{rT} \sin \omega_{cc} t \qquad (4\text{-}22a)$$

Similarly for the y motion

$$v_y' = v_{rT} \cos \omega_{cc} t + (v_{\theta T} - E_y/B_c) \sin \omega_{cc} t \qquad (4\text{-}22b)$$

The transverse component of the electron velocity relative to the coordinate system moving with velocity E_y/B_c in the x direction is

$$v_{\perp c} = \sqrt{v_x'^2 + v_y'^2} = \sqrt{(v_{\theta T} - E_y/B_c)^2 + v_{rT}^2} \qquad (4\text{-}23)$$

Integration of v_x' and v_y' gives the equation of the electron trajectory

$$x' = \frac{1}{\omega_{cc}} \left[(v_{\theta T} - E_y/B_c) \sin \omega_{cc} t - v_{r_T} (1 - \cos \omega_{cc} t) \right] \quad (4\text{-}24a)$$

$$y' = \frac{1}{\omega_{cc}} \left[(v_{\theta T} - E_y/B_c)(1 - \cos \omega_{cc} t) + v_{r_T} \sin \omega_{cc} t \right] \quad (4\text{-}24b)$$

Elimination of the time variable shows the equation of the trajectory to be a circle

$$\left[x' + \frac{r_{ro}}{\omega_{cc}} \right]^2 + \left[y' - \frac{(v_{\theta T} - E_c/B_c)}{\omega_{cc}} \right]^2 = \frac{v_{\perp c}^2}{\omega_{cc}^2} \quad (4\text{-}25)$$

with radius

$$a_c = v_{\perp c}/\omega_{cc} . \quad (4\text{-}26)$$

Integration of the z equation gives

$$z = -\frac{1}{2} \eta \bar{E} \sin \delta \, t^2 + v_{zT} t \quad (4\text{-}27)$$

This equation may be rewritten as

$$z = -\frac{1}{2} \frac{E_y \tan \delta}{B_c \omega_{cc}} \omega_{cc}^2 t^2 + \frac{v_{zT}}{\omega_{cc}} \omega_{cc} t \quad (4\text{-}28)$$

Figure IV-4 is used to calculate the maximum potential energy in the gun. This is reached when the electron has completed a half period i.e., when

$$\omega_{cc} t = \pi . \quad (4\text{-}29)$$

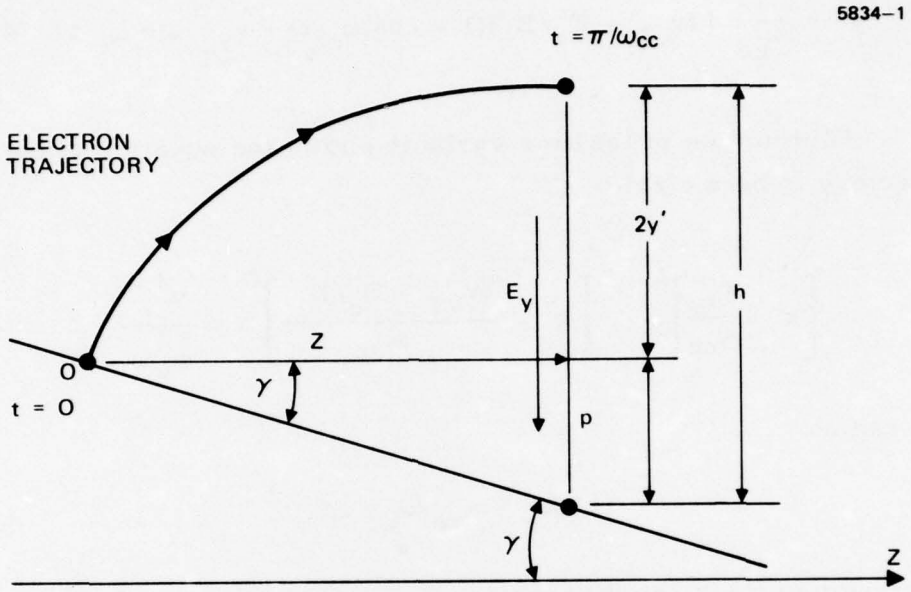


Figure IV-4. Projection of electron trajectory in θ = 0 plane.

The displacement of the electron gun from the cathode is then $h = 2y' + p$. We find that

$$h = \frac{2}{\omega_{cc}} \frac{E_y}{B_c} \left[1 + \frac{\pi^2}{4} \tan^2 \delta \right] - \frac{v_{zT}}{\omega_{cc}} \pi . \qquad (4\text{-}30)$$

The potential Φ_m at a distance from the cathode is then

$$\Phi_m = E_y h \qquad (4\text{-}31)$$

$$\eta \Phi_m = \frac{2\bar{E} \cos^2 \delta}{B_c^2} \left[1 + \frac{\pi^2}{4} \tan^2 \delta \right] - \frac{\bar{E}}{B_c} \cos \delta \, v_{zT} \, \pi . \qquad (4\text{-}32)$$

D. Boundary Conditions for the DC Beam — The Adiabatic Invariant

It can be shown for slow variations of the magnetic field B in time and in space, that the magnetic moment μ of a charged particle remains nearly constant. This property is used to relate the beam parameters in the gun to the boundary conditions imposed on the beam in the interaction region.

The relativistically correct magnetic moment μ is defined by[47]

$$\mu = \frac{1}{2} \frac{p_\perp^2}{m_o B} \qquad (4\text{-}34)$$

where $p_\perp$ is the electron momentum perpendicular to B and is

$$p_\perp = m_o \gamma v = \frac{m_o v_\perp}{\sqrt{1 - v^2/c^2}}$$

In the region of the electron gun μ is

$$\mu = \frac{1}{2} \frac{m_o}{B_c} v_{\perp c}^2 = \frac{1}{2} \frac{m_o}{B_c} \left[v_{rT}^2 + (v_{\theta T} - E_y/B_c)^2 \right] . \quad (4\text{-}35)$$

Using the value of the critical field $\bar{E}_{crt}$ to replace E_y/B_c we find that

$$\frac{E_y}{B_c} = - \frac{\eta B_c}{4} \frac{(r_a - r_c)(1 - r_c^2/r_a^2)}{\cos \delta \log (r_a/r_c)} . \quad (4\text{-}36)$$

The electron motion in the rf interaction region is in an undulating magnetic field of the form

$$B_z = B_o + B_1 \sin \frac{2\pi}{L} (z - z_o) . \quad (4\text{-}37)$$

The boundary conditions for motion in this field are applied at $z = z_o$ the beginning of the undulating region. The form of the magnetic field is indicated in Figure IV-5; it consists of a region of uniform field B_c of low value in the gun, a gradually increasing region in which the beam is compressed and accelerated to relativistic speeds and a region of undulating field in which the rf interaction takes place.

The constancy of the magnetic moment μ allows us to calculate the transverse momentum at $z = z_o$ and hence the radius of gyration. Using eq. (4-35)

$$\frac{1}{2} \frac{m_o}{B_c} v_{\perp c}^2 = \frac{1}{2} \frac{m_o}{B_o} \gamma^2 v^2 . \quad (4\text{-}38)$$

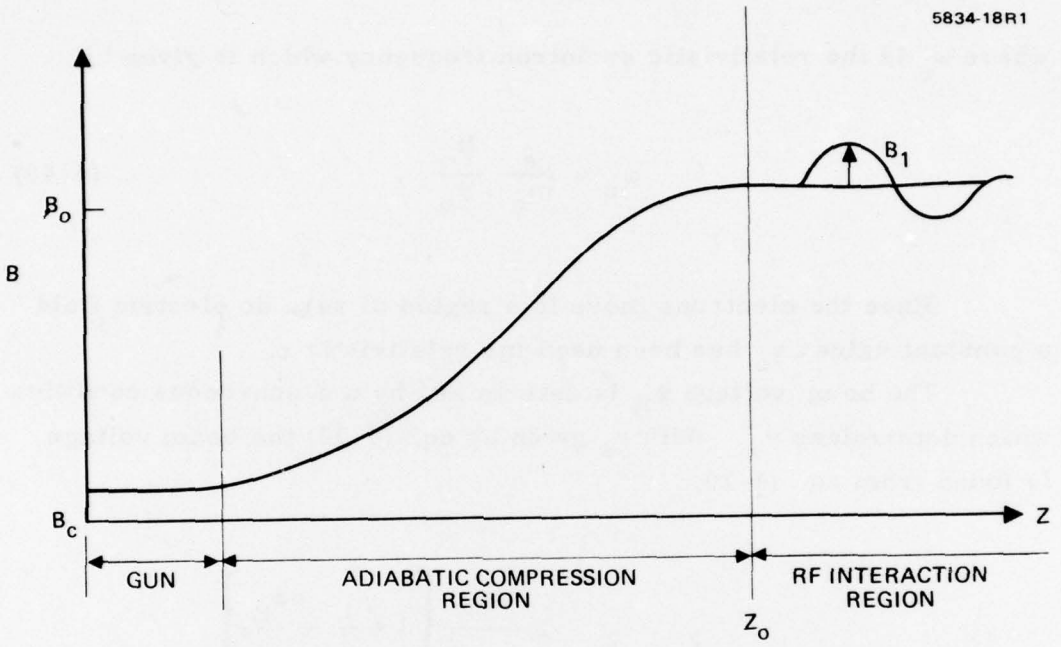


Figure IV-5. The form of the magnetic field in the Ubitron.

The radius of gyration a_o corresponding to the transverse velotocy $v_\perp$ is

$$a_o = v_\perp / \omega_c \tag{4-39}$$

where ω_c is the relativistic cyclotron frequency which is given by

$$\omega_c = \frac{e}{m_o} \frac{B_o}{\gamma_o} \quad . \tag{4-40}$$

Since the electrons move in a region of zero dc electric field a constant value γ_o has been used for relativistic γ.

The beam voltage Φ_B is determined by a synchronous condition which determines v_z. With $v_\perp$ given by eq. (4-38) the beam voltage is found from eq. (4-10)

$$\frac{v^2}{c^2} = \frac{v_z^2}{c^2} + \frac{v_\perp^2}{c^2} = \frac{2 \dfrac{e\Phi_B}{m_o c^2} \left[1 + \dfrac{1}{2} \dfrac{e\Phi_B}{m_o c^2} \right]}{\left[1 + \left(\dfrac{e\Phi_B}{m_o c^2} \right)^2 \right]} \quad . \tag{4-41}$$

E. The Paraxial DC Electron Motion in the RF Interaction Region

Prior to entering the rf interaction region, the electron beam has been accelerated to a relativistic voltage. However, in the rf guide there is no applied dc electric field and hence $\gamma = \gamma_o$, a constant. The Lorentz force equation now has components

$$\ddot{x} + \eta \frac{B_z}{\gamma_o} \dot{y} - \eta \frac{B_y}{\gamma_o} \dot{z} = 0 \tag{4-42a}$$

$$\ddot{y} - \eta \frac{B_z}{\gamma_o} \dot{x} + \eta \frac{B_x}{\gamma_o} \dot{z} = 0 \qquad (4\text{-}42b)$$

Since the magnetic field is not constant, transverse components of the magnetic field appear.

An exact solution of the Lorentz force equation is presented in Section II of this report; here we wish to develop an understanding of the parameters affecting the electron motion and present a first-order theory in which only terms linear in the x, y coordinates are retained.

Using $\vec{\nabla} \cdot \vec{B} = 0$ and the existence of rotational symmetry, we find that

$$\frac{\partial B_x}{\partial x} = \frac{\partial B_y}{\partial y} = -\frac{1}{2} \frac{\partial B_z}{\partial z} \qquad (4\text{-}43)$$

and

$$B_x = -\frac{\partial B_z}{\partial x} x, \qquad B_y = \frac{1}{2} \frac{\partial B_z}{\partial x} y \qquad (4\text{-}44)$$

Hence equation (4-42) becomes

$$\ddot{x} + \frac{\eta}{\gamma_o} B_z \dot{y} + \frac{\eta}{2} \frac{B_z}{\gamma_o} y = 0 \qquad (4\text{-}45a)$$

$$\ddot{y} + \eta \frac{B_z}{\gamma_o} \dot{x} \frac{\eta}{2} \frac{B_z}{\gamma_o} x = 0 \qquad (4\text{-}45b)$$

where we have used

$$\frac{dB_z}{dt} = \frac{\partial B_z}{\partial z} \quad z \tag{4-46}$$

It is convenient to describe the motion by a complex coordinate u which relates to Cartesian and cylindrical coordinates by

$$u = x + iy = re^{i\theta} . \tag{4-47}$$

Equation (4-45) becomes

$$\ddot{u} - 2i\omega_\ell \dot{u} - i\dot{\omega}_\ell u = 0 . \tag{4-48}$$

where

$$\omega_\ell = \frac{\eta B_z}{2\gamma_o} \tag{4-49}$$

is the relativistic Lamor radian frequency. A transformation to a rotating coordinate frame, which rotates about the z axis at the Larmor frequency, is made. This transformation

$$u = u\, e^{i \int_o^t \omega_\ell dt} \tag{4-50}$$

eliminates the imaginary terms in eq. (4-48) and results in the equation

$$\ddot{u}_\ell + \omega_\ell^2 u_\ell = 0 . \tag{4-51}$$

Equation (4-51) contains a real and an imaginary part, each of which is equal to zero. Differentiation of

$$u_\ell = re^{i(\theta - \int \omega_\ell dt)} \tag{4-52}$$

and substitution into eq. (4-51) gives the real part as

$$\ddot{r} - r(\dot{\theta} - \omega_\ell)^2 + \omega_\ell^2 r = 0 \tag{4-53}$$

and the complex part as

$$\frac{1}{r} \frac{d}{dt} (r^2 (\theta - \omega_\ell)) = 0 . \tag{4-54}$$

Equation (4-54) describes the conservation of angular momentum in the Larmor frame. Integration of eq. (4-54) gives

$$r^2(\dot{\theta} - \omega_\ell) = \text{const.} = r_o^2(\dot{\theta}_o - \omega_{\ell o}) = r_c^2(\dot{\theta}_c - \omega_{\ell c}) . \tag{4-55}$$

In this equation the subscript o denoted the values in a plane at $t = t_o$ and the subscript c refers to values at the cathode. The quantity $r_c \dot{\theta}_c = v_{\theta T}$, the θ component of the thermal velocity at the cathode defined in equation (4-11a). Substitution for $(\dot{\theta} - \omega_\ell)$ from eq. (4-55) into eq. (4-53) gives

$$\ddot{r} + \omega_\ell^2 \left[1 - \frac{r_c^4}{r^4} \frac{(\dot{\theta}_c - \omega_{\ell c})^2}{\omega_\ell^2} \right] r = 0 . \tag{4-56}$$

1. A Motion in a Uniform Magnetic Field

The dc motion of the electrons in the waveguide is in a uniform axial magnetic field B_o with a superimposed periodically varying component. Although the amplitude of the periodic field can reach 58% of B_o at the beam radius the undulating field is treated as a first-order perturbation in order to gain insight into the electron motion.

Equation (4-51) with ω_ℓ - const gives a simple harmonic variation for u_ℓ;

$$u = ae^{i\omega_\ell t} + be^{-i\omega_\ell t} \tag{4-57}$$

where a and b are in general complex constants. A transformation to the laboratory frame gives

$$re^{i\theta} = ae^{2i\omega_\ell t} + b \tag{4-58}$$

Equation (4-58) is the equation of a circle of radius $|a|$ which is traced out at the cyclotron frequency $\omega_c = 2\omega_\ell$. The circle is displaced a distance $|b|$ from the coordinate axis. In a uniform field $|b|$ is arbitrary since there is no axis of symmetry. However, an axis of symmetry is required when a beam from an axially symmetric cathode is to be described.

In the case of the magnetron injection gun the radius of gyration has the value determined by the constancy of the magnetic moment μ and is given by equation (4-39). Hence

$$a = a_0 e^{i\epsilon} \tag{4-59}$$

where ϵ is a phase angle.

Differentiation of (4-57) gives

$$\dot{u}_\ell = [\dot{r} + ir(\dot{\theta} - \omega_\ell)]\, e^{i(\theta-\chi)} = i\omega_\ell \left[a_0 e^{i(\omega_\ell t+\varepsilon)} - b_0 e^{-i(\omega_\ell t-\sigma)} \right] \quad (4\text{-}60)$$

where we have written

$$b = b_0 e^{i\sigma} \quad (4\text{-}61)$$

The boundary condition is evaluated at $z = z_0$ (c. f. equation (4-37)) at the beginning of the uniform field which coincides in this analysis with time $t = 0$. Equation (4-60) is then

$$[\dot{r}_0 + ir_0(\dot{\theta}_0 - \omega_\ell)]\, e^{i\theta_0} = i\omega [\, a_0 e^{i\varepsilon} - b_0 e^{i} \,] \quad (4\text{-}62)$$

In a rotationally symmetric system the θ origin is arbitrary and hence we set θ_0 equal to zero. Hence

$$\dot{r}_0 = -\omega_\ell\, a_0 \sin\varepsilon + \omega_\ell b_0 \sin \quad (4\text{-}63)$$

The radial velocity component has two contributions, from the rotation of the electron about the guiding center and from the radial velocity of the guiding center itself. The task of the electron gun design is to produce an annular beam of constant radius and hence the guiding center must be at a constant radius. Hence $\sigma = 0$. The remaining contribution to r_0 is set equal to zero by inspecting the beam at a different axial location when it has its furthest position from the axis as shown by location Q in Figure IV-6 since all of the electron velocity is then in the azimuthal direction. Then

$$r_0(\dot{\theta}_0 - \omega_\ell) = \omega_\ell (a_0 - b_0) \quad (4\text{-}64)$$

5834-19

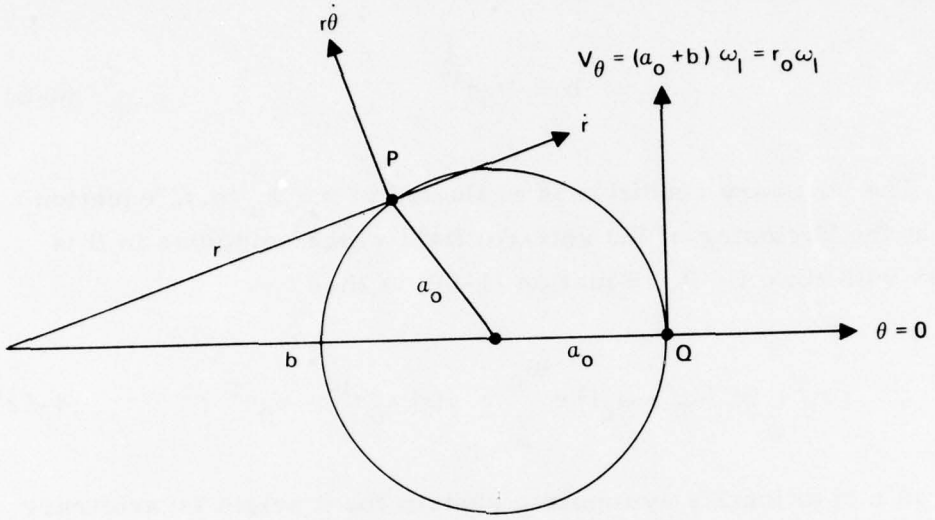


Figure IV-6. Velocity components of the beam in the magnetic field.

Conservation of angular momentum equation (4-55) is used to eliminate $(\dot{\theta} - \omega_\ell)$. Also we note that $r_0 = a_0 + b_0$. Thus

$$r_c^2(\dot{\theta}_c - \omega_{cc}) = (a_0 + b_0(a_0 - b_0)\,\omega_\ell \tag{4-65}$$

Hence b_0 is

$$b_0 = a_0 \left(1 + \frac{r_c^2}{a_0^2}\,\frac{\omega_{\ell c}}{\omega_\ell} - \frac{r_c^2\,\dot{\theta}_c}{a_0^2\,\omega_\ell}\right)^{1/2} \tag{4-66}$$

It is seen from equation (4-66) and also from equation (4-39) that conditions at the cathode have a considerable influence on both the position of the guiding center b_0 and on the radius of gyration a_0.

2. The Effect of a Perturbing Undulating Magnetic Field

We assumed in equation (4-37) that the axial magnetic field B_z has the form

$$B_z = B_0 + B_1 \sin \frac{2\pi}{L}\, z \tag{4-37}$$

where B_0 is the uniform magnetic field value and L the undulation period. Since we are using time as the independent variable equation (4-37) is rewritten:

$$B_z = B_0 + B_1 \sin \Omega_m t \tag{4-67}$$

where

$$\Omega_m = \frac{2\pi}{L} \dot{z}_0 \tag{4-68}$$

and where $\dot{z}_0$ is the axial velocity of the beam which we assume to remain constant for small values of B_1. The form of ω_ℓ is now

$$\omega_\ell = \frac{\eta B_0}{2\gamma_0}\left[1 + \frac{B_1}{B_0} \sin \Omega_m t\right]$$

$$= \omega_{\ell 0}\left(1 + \frac{B_1}{B_0} \sin \Omega_m t\right). \tag{4-69}$$

We now separate the variable u into an unperturbed part u_0 and a perturbed part u_1 where $u_1 \ll u_0$; equation (4-37) is rewritten using (69) with $B_1 \ll B_0$ as follows:

$$\ddot{u}_0 - 2i\omega_{\ell 0}\dot{u}_0 - i\dot{\omega}_{\ell 0}u_0 = 0 \tag{4-70}$$

$$\ddot{u}_1 - 2i\omega_{\ell 0}\dot{u}_1 - i\dot{\omega}_{\ell 0}u_1 = i\frac{B_1}{B_0}\left[2\omega_{\ell 0}\dot{u}_0 \sin \Omega_m t + \dot{\omega}_{\ell 0}u_0 \sin \Omega_m t\right.$$

$$\left. + \Omega_m \omega_{\ell 0} u_0 \cos \Omega_m t\right] \tag{4-71}$$

where only linear perturbation terms have been retained. Making the transformation to the Larmor frame

$$u_0 = u_{\ell 0} e^{i\int \omega_{\ell 0} dt} \tag{4-72}$$

$$u_1 = u_{\ell 1} e^{i\int \omega_{\ell 0} dt} \tag{4-73}$$

gives first of all the unperturbed equation

$$\ddot{u}_{\ell 0} + \omega_{\ell 0}^2 u_{\ell 0} = 0 \tag{4-22a}$$

and the perturbed equation

$$\ddot{u}_{\ell 1} + \omega_{\ell 0}^2 u_{\ell 1} = i \frac{B_1}{B_0} \left\{ 2\omega_{\ell 0}(\dot{u}_{\ell 0} + i u_{\ell 0}\omega_{\ell 0}) \sin \Omega_m t \right.$$

$$\left. + \dot{\omega}_{\ell 0} u_{\ell 0} \sin \Omega_m t + \Omega_m \omega_{\ell 0} u_{\ell 0} \cos \Omega_m t \right\} \tag{4-74}$$

We specialize to the case of a uniform magnetic field for which $\dot{\omega}_{\ell 0} = 0$. Using

$$u_{\ell 0} = a_0 e^{i\omega_{\ell 0} t} + b_0 e^{-i\omega_{\ell 0} t} \tag{4-57a}$$

$$\dot{u}_{\ell 0} = i\omega_{\ell 0}\left(a_0 e^{i\omega_{\ell 0} t} - b_0 e^{-i\omega_{\ell 0} t}\right) \tag{4-75}$$

we obtain for equation (4-71)

$$\ddot{u}_{\ell 1} + \omega_{\ell 0}^2 u_{\ell 1} = R \tag{4-76}$$

where the residue R is given by

$$R = i\omega_{\ell 0} \frac{B_1}{B_0} \left\{ a_0 e^{i\omega_{\ell 0} t} \left[\left(\frac{\Omega}{2} m + 2\omega_{\ell 0} \right) e^{i\Omega m t} \right.\right.$$

$$\left. + \left(\frac{\Omega}{2} m - 2\omega_{\ell 0} \right) e^{-i\Omega m t} \right] + \frac{b_0}{2} e^{-i\omega_{\ell 0} t} \left[\Omega_m e^{i\Omega m t} \right.$$

$$\left.\left. + \Omega_m e^{-i\Omega m t} \right] \right\} \tag{4-77}$$

The solution of (47) is

$$u_{\ell 1} = a_1 e^{i\omega_{\ell 0} t} + b_1 e^{-i\omega_{\ell 0} t} + \frac{1}{W} \left[e^{i\omega_{\ell 0} t} \int e^{-i\omega_{\ell 0} t} R \, dt \right.$$

$$\left. - e^{-i\omega_{\ell 0} t} \int e^{i\omega_{\ell 0} t} R \, dt \right] \tag{4-78}$$

The function W is the Wronskian determinant of the two solutions $g = e^{i\omega_{\ell 0} t}$, $h = e^{-i\omega_{\ell 0} t}$ which satisfy the homogeneous part of equation (4-45). W is given by

$$W = \begin{vmatrix} g & h \\ \dot{g} & \dot{h} \end{vmatrix} = -2i\omega_{\ell 0} \tag{4-79}$$

After considerable mathematical manipulation the particular integral can be reduced to

$$\text{P.I.} = -2\frac{B_1}{B_0}\frac{\omega_{\ell 0}}{\Omega_m}\frac{1}{\left(\Omega_m^2 - \omega_{c0}^2\right)}\left[a_0 e^{i\omega_{\ell 0}t}\left(\Omega_m\omega_{\ell 0}\sin\Omega_m t - i\left(\frac{\Omega_m^2}{2} - \omega_{c0}^2\right)\cos\Omega_m t\right)\right.$$

$$\left. + b_0 e^{-i\omega_{\ell 0}t}\left(\Omega_m\omega_{\ell 0}\sin\Omega_m t - i\frac{\Omega_m^2}{2}\cos\Omega_m t\right)\right] \quad (4\text{-}80)$$

where ω_{c0} is the unperturbed cyclotron frequency; $\omega_{c0} = 2\omega_{\ell 0}$.

Recombination of the variables u_0 and u_1 leads to the following solution of the combined ray equations (4-41) and (4-46)

$$re^{i\theta} = a_0\left[\left(1 - 2\frac{B_1}{B_0}\frac{\omega_{\ell 0}^2}{\left(\Omega_m^2 - \omega_{c0}^2\right)}\sin\Omega_m t\right)\right.$$

$$\left. + i\,2\frac{B_1}{B_0}\frac{\left(\Omega_m^2/2 - \omega_{c0}^2\right)}{\left(\Omega_m^2 - \omega_{c0}^2\right)}\frac{\omega_{\ell 0}}{\Omega_m}(1 - \cos\Omega_m t)\right] e^{i\omega_{c0}t}$$

$$+ b_0\left[\left(1 - 2\frac{B_1}{B_0}\frac{\omega_{\ell 0}^2}{\left(\Omega_m^2 - \omega_{c0}^2\right)}\sin\Omega_m t\right)\right.$$

$$\left. + i\frac{B_1}{B_0}\frac{\omega_{\ell 0}\Omega_m}{\left(\Omega_m^2 - \omega_{c0}^2\right)}(1 - \cos\Omega_m t)\right]. \quad (4\text{-}81)$$

In this equation the boundary condition that the perturbation vanish at $t = 0$ has been obtained by evaluation of the constants a_1 and b_1. The constants a_0 and b_0 are given equations (4-39) and (4-66). Inspection of equation (4-81) shows that the electron now describes a perturbed circle at the cyclotron frequency; moreover, the center of the circle also changes position. Unless Ω_m is a multiple of $\omega_{\ell 0}$ the figure will not trace out the same path. When $\Omega_m = \omega_{c0}$ equation (4-81) predicts an instability which can be calculated from the residue R, equation (4-77). In this case terms linear in t are obtained showing that the beam radius increases with distance.

Figure IV-7 shows the perturbed radius of gyration for the case of $b_0 = 9.5\ a_0$ and $\Omega_m = 3.0\ \omega_c$.

3. The Parameters of the Beam-Design of a Gun

A cursory examination of the problem of maximizing the interaction of the annular electron beam with the θ directed component of the rf electric field in the waveguide leads to the conclusion that the thin annular beam must be placed in the region of maximum electric field at a radius of $0.5\ r_a$, where r_a is the radius of the waveguide. Computer studies of the electron motion using the exact relativistic ray equation show, however, that the interaction is maximized for a radius of $0.78\ r_a$. The efficiency of the interaction is decreased by the finite width of the annulus; however, a width Δr_b of less than $0.15\ r_a$ produces an acceptable reduction in efficiency. Hence the subsequent calculations are for a beam of width $0.15\ r_a$ and mean radius $0.78\ r_a$.

The current density in the beam is $63.5\ A/cm^2$ and hence, using $3\ A/cm^2$ as the maximum permitted value for the cathode loading, we find that a beam area compression A_c of 21.2 is required.

The cathode current density distribution depends on the method of operation of the gun. For space-charge-limited operation it depends on the form of the magnetic field as Dryden has shown.[49] For a uniform axial magnetic field the space-charge-limited emission varies linearly with $\bar{r}$ the distance measured from the apex of the cathode cone as indicated in Figure IV-8.

5873-31

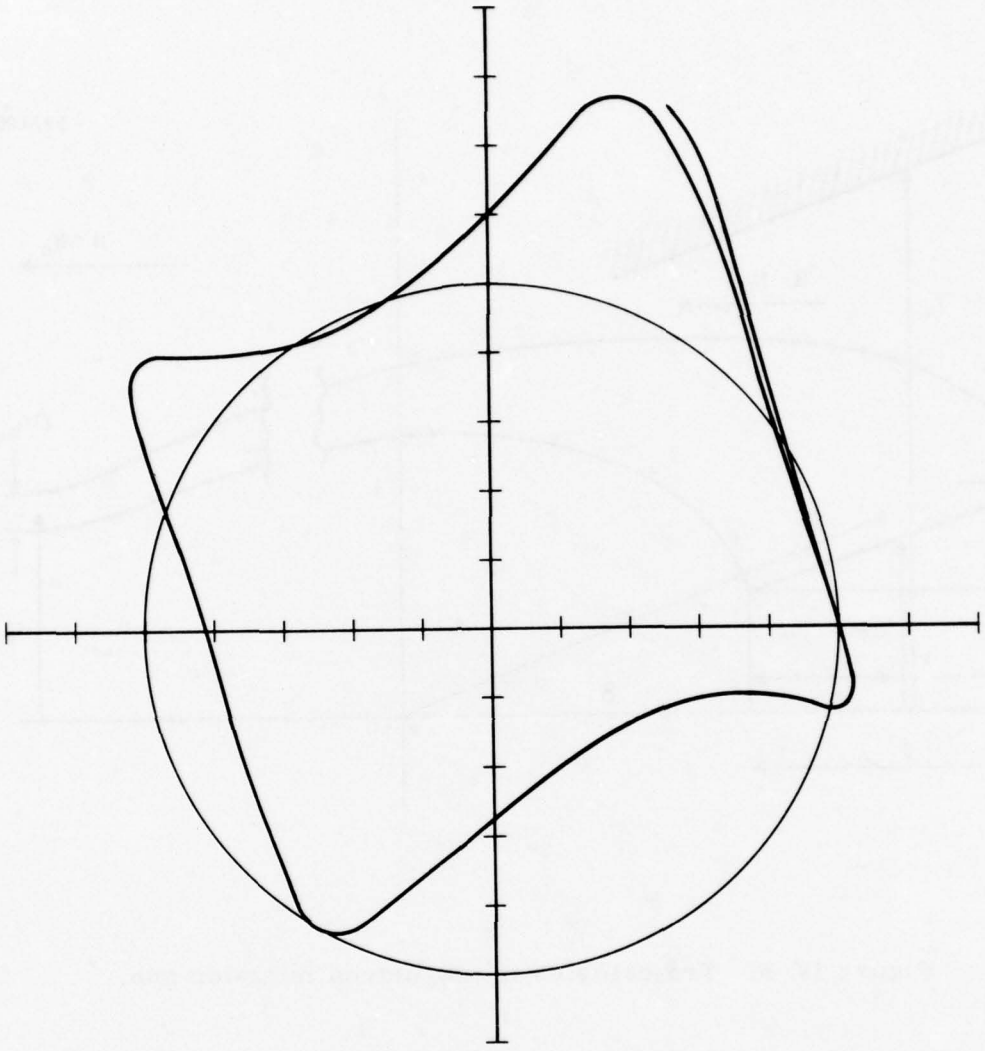


Figure IV-7. Perturbed trajectory in the undulating field: $B_1/B_0 = 0.18, B_0 = 9.50\ a_0, \Omega_m = 3.0\ \omega_c$.

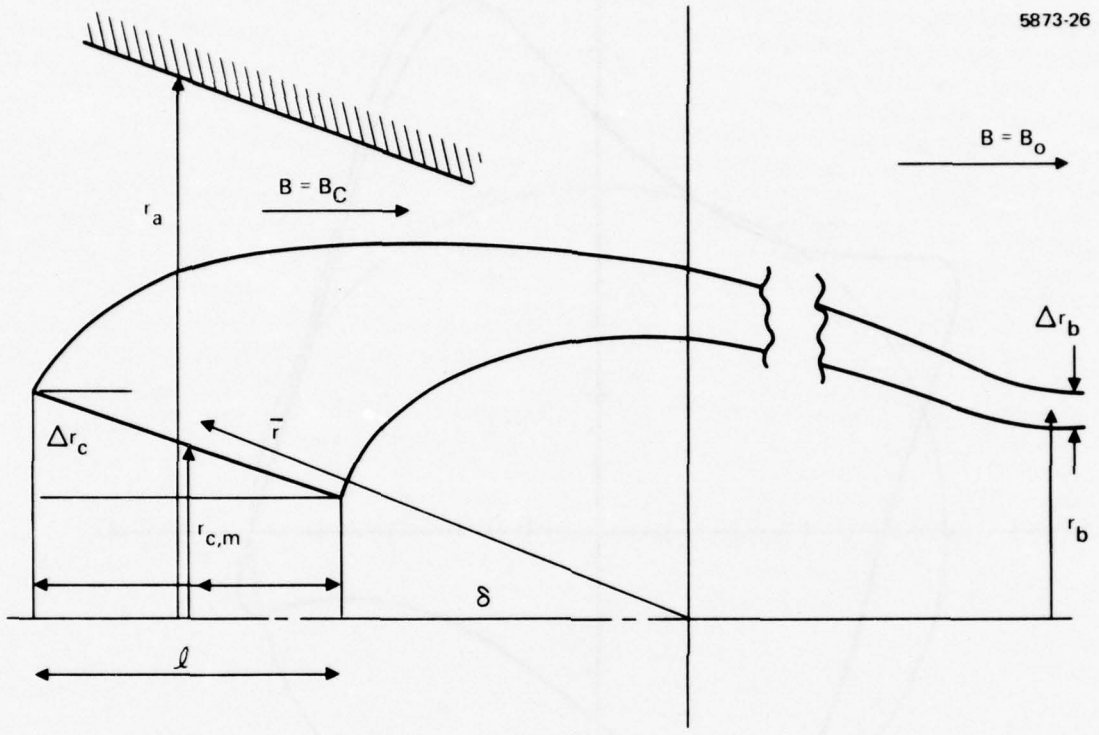


Figure IV-8. Trajectories in magnetron injection gun.

Table IV-2. Beam Parameters

Waveguide radius r_a	0.30 cm
mean beam radius r_b	0.234 cm
beam width Δr_b	0.045 cm
beam current I_A	4.20 A
current density j_b	63.50 A/cm^2
cathode loading j_c	3.0 A/cm^2
beam area compression A_c	21.2

The assumption underlying all of the theoretical analyses of space-charge-limited magnetron injection guns is that of laminar flow.[49, 50] Under this assumption, which makes such problems mathematically tractable, the electrons cannot have intersecting trajectories and hence a flow in which electrons spiral about a guiding center is not admissible. In practice beam-probing experiments show that the electrons move for the most part like individual particles in a field which obeys Poisson's equation instead of Laplace's equation. The actual flow is therefore much more closely related to the space-charge free flow than the laminar flow. The modeling of such flows can only be carried out in an iterative manner using a high-speed digital computer for a specific geometry. In this study we primarily wish to obtain an understanding of the magnitude of various gun parameters and hence we use the space-charge-free theory developed above.

The gun design does not include the electrodes required to accelerate the beam to the potential of the interaction region since the accelerating field must be designed in conjunction with the magnetic field to produce a flow in which the guiding center of the electrons is parallel to the beam axis at the beginning of the uniform field region.

The area compression A_c can be obtained in a number of ways; the mean cathode radius $r_{c,m}$ may be made large and the height l of the frustrum of the cone of cathode material may be made very short, or vice versa. The effect of a high frustrum is shown in Figure IV-9; trajectories from the top and bottom of the frustrum tend to spread out so that it becomes difficult to compress the beam. A short but large-diameter cathode avoids this effect but such a beam suffers from the effects of a large degree of radial compression. A compromise solution might be to shrink the beam uniformly by making

$$\frac{r_{cm}}{r_b} = \frac{\ell}{\Delta r_b} = \sqrt{A_c} = 4.6$$

This results in a cathode of mean radius $r_{c,m}$ 1.10 cm and length = 0.207 cm. We now are faced with a choice of anode radius $r_{a,m}$ which is to some extent arbitrary. We choose a convenient value of 1.70 cm. We note that the maximum value of the radius of gyration a_c is then 0.30 cm under cut-off conditions. Table IV-3 shows E_y/B_c and Φ_A calculated from equations (4-15) and (4-14) respectively for these gun parameters.

Using equations (4-22) and (4-26) one obtains the following approximate value for a_c, when thermal velocity effects are neglected

$$a_c \simeq \frac{1}{\eta} \frac{E_y}{B_c^2}$$

Using equations (4-38) and (4-39) and (4-40) one finds that

$$a_0 = a_c \sqrt{B_c/B_0}$$

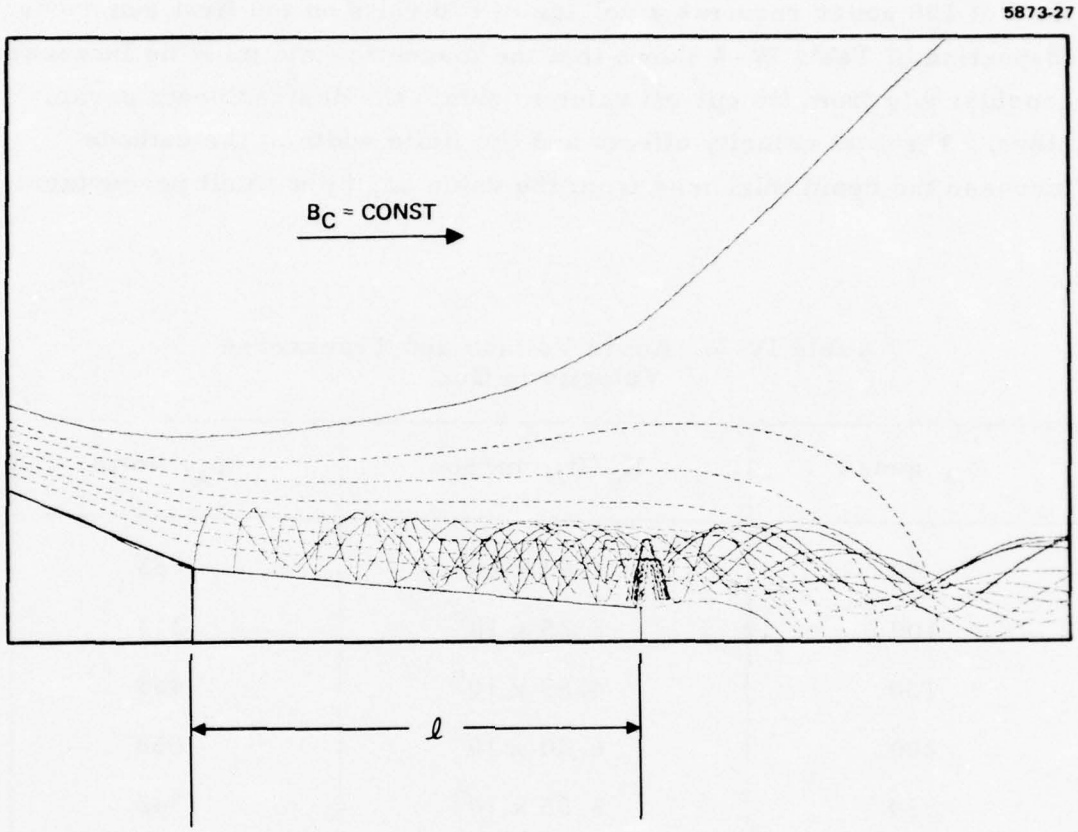


Figure IV-9. Computed trajectory in magnetron injection gun with large ratio of $\ell/r_{c,m}$.

Table IV-4 gives the variation with B_c of a_c, a_0 and b_0 (calculated from equation (4-66)) for the above gun design for a magnetic field of B_0 = 7500 gauss in the interaction region. Choosing a cut-off field of 200 gauss requires a voltage of 858 volts on the first gun anode. Inspection of Table IV-4 shows that the magnetic field must be increased considerably from its cut-off value to obtain the desired beam parameters. Thermal velocity effects and the finite width of the cathode increase the beam thickness from the value $2a_0$ by a small percentage.

Table IV-3. Anode Voltage and Transverse Velocity in Gun

B_c, gauss	E_y/B_c, m/sec	Φ_A, volts
50	1.62×10^6	53
100	3.25×10^6	214
150	4.87×10^6	483
200	6.50×10^6	858
250	6.98×10^6	1342
300	9.75×10^6	1932
500	1.62×10^7	5366
750	2.43×10^7	12076
1000	3.25×10^7	21467
$r_{c,m}$ = 1.10 cm		
$r_{a,m}$ = 1.70 cm		

Table IV-4. Radius of Gyration a and Guiding Center Displacement b_0 for B_0 = 7500 gauss as a function of B_c

B_c, gauss	a_c cm (in gun)	a_0 cm	b_0 cm
200	0.184	0.030	0.167
250	0.147	0.027	0.202
300	0.123	0.024	0.220
350	0.105	0.023	0.235
400	0.092	0.021	0.254

V. PRELIMINARY UBITRON DESIGN AND CONFIGURATION

In this section we present a summary of the basic Ubitron design considerations using small-signal theory, and show the effects of including radial-electron-motion averaging via the use of the beam factor described in Section II. We have used this theory to provide a set of curves showing small-signal design parameters and electronic performance as functions of voltage. Finally we have applied these design equations to determine the basic dimensions and electronic performance of a 94-GHz, 50-kW Ubitron amplifier operating at 300 kV. We have also included a first-order design description of the overall amplifier package including voltage standoff requirements, cooling, and collector depression.

At the beginning of this program we believed from the previous work that the best procedure to improve gain and efficiency was to increase the undulation parameter. We believed this could be done most effectively by increasing the period-to-diameter ratio of the circuit so that the undulating field would penetrate more strongly into the electron-beam region. As a result of this initial bias, most of the work on the program has been aimed at a design in the vicinity of 300 kV. In retrospect we see that even though the undulation parameter does indeed increase with increasing voltage as expected, other factors in the small-signal gain expressions, especially relativistic effects, turn out to be overriding. It now appears that a lower design voltage would be more desirable for improved gain and efficiency.

Even though the dc beam, magnetic circuit, and gun analysis work on this program was primarily aimed at a 300 kV Ubitron design, the principles and tools of analysis developed are entirely applicable to lower voltage designs. In this section we provide small-signal design trade-offs as a function of voltage which we believe to be as accurate as possible without further experimental data. The only thing lacking for lower voltage designs is a detailed analysis of the effects of the dc beam radial variations. Based on the analysis

at 300 kV we do not anticipate a large degradation in gain and efficiency due to this factor. Future analysis of the beam factor for lower voltage design will be comparatively easy to accomplish using the tools developed during this study program.

A. Relativistic Small-Signal Design Equations

The basic design criteria which specifies the relationship between frequency, magnetic period, voltage, and rf waveguide diameter comes from the requirement of phase synchronism between the -1 beam harmonic wave and the rf wave. This is illustrated in Figure V-1 in the form of an "ω-β diagram." Because of our desire to maintain maximum bandwidth we have chosen to design such that the beam harmonic is just tangential to the TE_{01} waveguide mode, thus optimizing the frequency over which the two waves stay in synchronism.

The fundamental phase relationship is obtained from the figure as

$$\beta_e = \beta_m + \beta_{01} \tag{5-1}$$

where

$$\beta_e = \frac{\omega}{v_o} = \text{beam propagation constant}$$

$$\beta_m = \frac{2\pi}{L} = 2\pi/\text{magnetic period}$$

and

$$\beta_{01} = \sqrt{k^2 - \gamma_{10}^2} = TE_{01} \text{ circular waveguide mode propagation constant}$$

Equation (5-1) can be easily solved for k by recognizing that

$$\beta_e = \frac{\omega}{c}\frac{c}{v_o} = k\frac{\gamma}{\sqrt{\gamma^2 - 1}} \tag{5-1a}$$

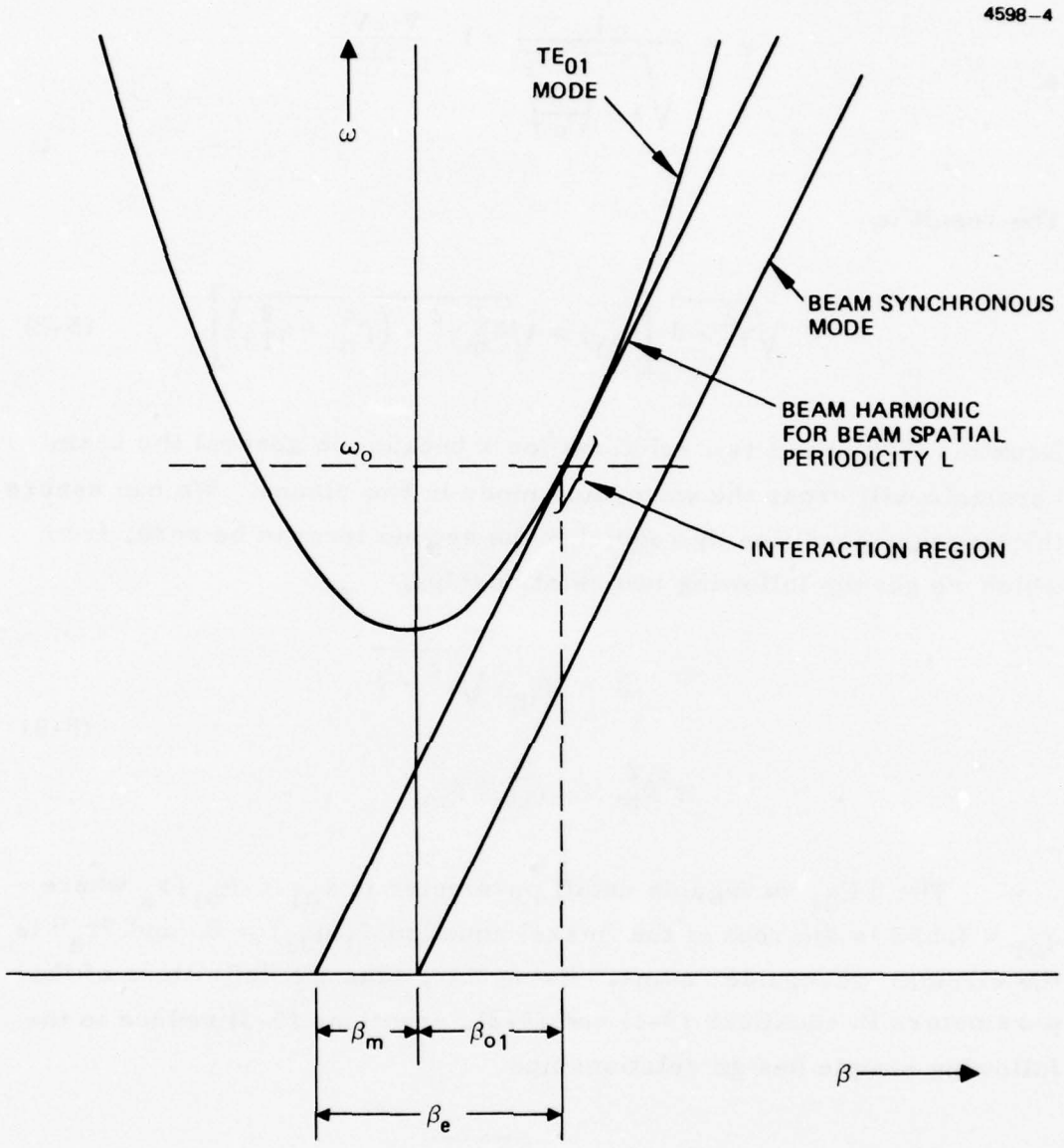


Figure V-1. Dispersion diagram for wideband TE_{01} circular waveguide Ubitron.

where γ is the relativistic parameter

$$\gamma = \frac{1}{\sqrt{1 - \left(\frac{v_o}{c}\right)^2}} \simeq 1 - \frac{V(kV)}{511}$$

The result is

$$k = \sqrt{\gamma^2 - 1}\left[\beta_m\gamma \pm \sqrt{\beta_m^2\gamma^2 - \left(\beta_m^2 + \gamma_{10}^2\right)}\right] \qquad (5\text{-}2)$$

Equation (5-2) gives two solutions for k because in general the beam harmonic will cross the waveguide mode in two places. We can assure the tangency condition by requiring the second term to be zero, from which we get the following two relationships.

$$k = \beta_m\gamma\sqrt{\gamma^2 - 1}$$

$$\gamma^2\beta_m^2 = \gamma_{10}^2 + \beta_m^2 \qquad (5\text{-}3)$$

The TE_{01} waveguide cutoff parameter is $\gamma_{01} = q_{01}/r_a$ where $q_{01} \simeq 3.832$ is the root of the Bessel equation $J_1(q_{01}) = 0$, and "r_a" is the circular waveguide radius. Using this, plus the definitions of the parameters in equations (5-1) and (5-2), equations (5-3) reduce to the following simple design relationships.

$$L = \gamma\sqrt{\gamma^2 - 1}\,\lambda_o$$

$$r_a = \frac{2\pi}{q_{10}}\gamma\lambda_o \qquad (5\text{-}4)$$

These are plotted in Figure V-2 as a function of voltage for λ_o = 3.19 mm (94 GHz).

Note in the above derivations that full use has been made of the relativistically correct beam velocity. Equations (5-4) are therefore correct for any voltage. Note also that magnetic period equals circuit diameter at a voltage near 300 kV. This was the initial choice for design during this program.

1. Small-Signal Gain and Efficiency

In the Ubitron the transverse motion in the electron beam interacts with the θ-directed E field of the TE_{01} waveguide mode and the undulating magnetic field to produce axial beam bunching similar to that which occurs in TWT's. In fact, a small-signal analysis of the Ubitron previously carried out by G. E.[2] and extended during this program to include relativistic effects (see Appendix B) shows that the design equations can be cast into the familiar Pierce form for the TWT.

$$G = A + B\, C_u\, N_e \tag{5-5}$$

where

G = gain in dB

A, B = constants

$$C_u = \text{gain parameter} = \left[\frac{K'\, \Lambda^2\, I_o}{16\, V_o}\right]^{1/3} \left(\frac{2}{\gamma(\gamma+1)}\right)^{1/3} \tag{5-6}$$

N_e = circuit length in electronics wavelengths.

I_o = beam current

V_o = beam voltage.

γ = relativistic correction factor

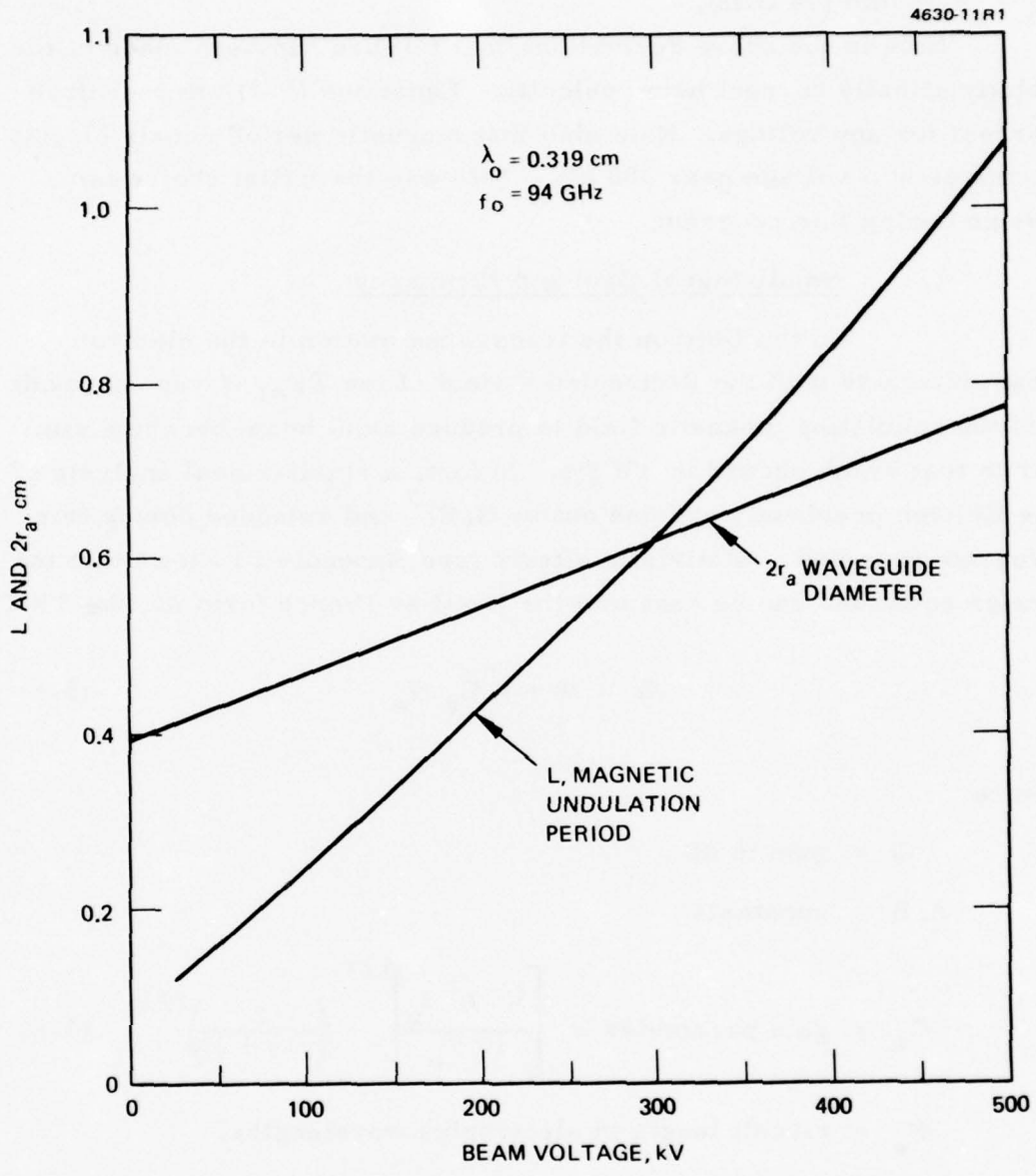


Figure V-2. Guide diameter $2r_a$ and magnetic undulation period L as a function of beam voltage.

The interaction impedance is given by

$$K' = \frac{E_\theta^2}{2\beta_e^2 P} \quad , \tag{5-7}$$

where E_θ is the peak electric field at the radius of the hollow beam, β_e is the beam propagation constant, and P is the circuit power. The remaining parameter Λ is called the "undulation parameter" and is defined as the ratio of the peak transverse velocity v_θ to the dc axial velocity v_o.

$$\Lambda = \frac{v_\theta}{v_o} \tag{5-8}$$

In terms of circuit parameters Λ is defined as

$$\Lambda = \frac{\eta B_{rb}}{\gamma v_o \beta_m} \tag{5-9}$$

where

$\eta = \left|\frac{e}{m}\right|$ = electron charge to mass ratio

B_{rb} = peak radial magnetic field harmonic with period L (evaluated at the beam radius; i.e., $B_{rb} \equiv B_r(r_b, z)\big|_{peak}$. See eq. 11 in Appendix C).

Note in equations (5-7), (5-8) and (5-9) above that variables appropriate to the cylindrical Ubitron have been substituted for the planar variables used in the derivation in Appendix B. Specifically, E_θ has been substituted for E_y, v_θ for $v_{transverse}$, and B_{rb} for B_1 (the amplitude of the B_x magnetic field).

The justification for these substitutions and the derivation of a small-signal equivalence beam factor which takes into account the variations in the beam radius was given in section II-E. This beam factor allows correction of the small-signal gain due to variations in the dc beam radius.

In TWT design work it is often found that for a particular class of amplifiers, the overall efficiency is roughly proportional to the small-signal gain parameter. This proportionality constant or "efficiency parameter" usually is found to be a value between 2 and 3. For lower-frequency tubes in the microwave region with low-voltage and high-perveance beams, this factor tends to be close to 2. In the millimeter-wave region, however, where beam voltages must be increased and beam perveance is low, the factor usually approaches 3.

In the previous G. E. work, a Ubitron design in the microwave frequency region was reported to have an efficiency parameter of about 2. If the same trends hold for the Ubitron which are true for TWT, then we would expect that the millimeter-wave Ubitron being considered here will have an efficiency factor on the order of 2.5 to 3.

If we define B_η to be the efficiency parameter, then the mathematical expression for efficiency is

$$\eta_e = B_\eta C_u \tag{5-10}$$

where η_e is the fractional electronic efficiency, and C_u is the Ubitron small-signal gain parameter.

From the design trade-off point of view, it is necessary to make some assumption similar to equation (5-10) in order to relate gain and efficiency to the overall tube design parameters. For example, the efficiency given by equation (5-10) can be used to eliminate the beam current in the small-signal gain parameter by the following expression.

$$\frac{1}{R_o} = \frac{I_o}{V_o} = \frac{I_o V_o}{V_o^2} = \frac{P}{\eta_e V_o^2} = \frac{P}{B_\eta C_u V_o^2} \qquad (5\text{-}11)$$

The variable P is the rf power of the Ubitron. If this is substituted into equations (5-6) and the result is solved for C_u, we get

$$C_u = \left[\left(\frac{K' \Lambda^2 P}{16 B_\eta V_o^2}\right)\left(\frac{2}{\gamma(\gamma+1)}\right)\right]^{1/4} \qquad (5\text{-}12)$$

If all of the factors entering into equation (5-12) are examined in detail for dependence on voltage, frequency, and power, we get the following expressions.

$$K' = \frac{\sqrt{\frac{\mu_o}{\epsilon_o}}\, J_1^2\left(\frac{q_{01}\, r_b}{r_a}\right)}{\sqrt{1 - \left(\frac{q_{01}}{k r_a}\right)^2}\, \pi \beta_e^2 r_a^2 J_o^2(q_{01})} \qquad (5\text{-}13)$$

$$\Lambda = \frac{\eta B_{sat} L \sin\left(\frac{\pi G}{L}\right) I_1\left(\frac{2\pi r_b}{L}\right)}{\gamma \pi^2 v_o I_o\left(\frac{2\pi r_c}{L}\right)} \qquad (5\text{-}14)$$

where

$\sqrt{\frac{\mu}{\epsilon}}$ = impedance of Free Space (~377 Ω)

$q_{01} \cong 3.832$ (first Root of $J_1(q_{01}) = 0$)

$$k = \frac{\omega}{c} \qquad (5\text{-}15)$$

$\beta_e = \frac{\omega}{v_o}$

r_a = waveguide radius

r_b = beam radius

r_c = inside radius of periodic magnetic structure.

L = period of magnetic structure.

$\eta = \left|\frac{e}{m_o}\right|$

B_{sat} = effective saturation magnetic field which gives maximum harmonic amplitude. (= 17,000 Gauss as per Section III)

G/L = gap to period ratio of magnetic structure.

J_o, J_1, I_o, I_1 = Bessel functions.

$$\gamma = \frac{1}{\sqrt{1 - \left(\frac{v_o}{c}\right)^2}} \simeq 1 + \frac{\eta}{c^2} V_o \simeq 1 + \frac{V_o(kV)}{511} \qquad (5\text{-}15)$$

The additional factors in eq. (5-12) are

P = rf power

V_o = beam voltage

B_η = efficiency parameter (eq. 5-10)

In equations (5-13) and (5-14) r_b/r_a and r_c/r_a are usually fixed at some specified ratio and therefore, because r_a/L is independent of frequency, the Bessel function arguments in these equations also have no frequency dependence. Using equations (5-1a) and (5-4) it is also easy to show that kr_a and $\beta_e r_a$ are also functions of voltage only, with no frequency

dependence. If we now choose G/L = 0.5 to maximize Λ, it becomes evident that the only remaining variable with any frequency dependence is $L = \left(\gamma\sqrt{\gamma^2 - 1}\right) c/f$ in equation (5-14).

The net result of the above analysis of factors which affect the gain parameter C_u is as follows.

$$C_u \sim \left(\frac{P^{1/4}}{f^{1/2}\,\beta_\eta^{1/4}}\right) \times h\left(\frac{r_b}{r_a},\ \frac{r_c}{r_a},\ V_o\right) \tag{5-16}$$

The gain increases as $(\text{power})^{1/4}$ due to decreasing beam impedance, decreases as $(\text{frequency})^{-1/2}$ due to decreasing period, and is a relatively complex function h of beam voltage, r_b/r_a, and r_c/r_a. As will be shown later in this section, the function h decreases with increasing voltage.

The beam factor derived in Section II provides a correction to the small-signal gain which accounts for the variations of the beam radius along the beam. This correction is required because the small-signal assumptions entering into the derivation of the gain parameter in Appendix B include the assumption that electron motion occurs only in the E-plane of the waveguide. For cylindrical geometry this corresponds to motion only in the (θ, z) directions. As shown in Section II, however, the dc electron motion in a cylindrical Ubitron will have significant radial motion due mainly to the cyclotron orbit. This radial variation will cause some reduction in the overall gain parameter given by equation (5-6).

The beam factor is derived in Section II and is given there by equations (2-116) through (2-118). The latter equation is rewritten here in terms of the gain parameter C_u and the basic design quantities. It is

$$C_u^3 = \frac{1}{8\pi^2 R_o}\left(\frac{\sqrt{\frac{\mu}{\epsilon}}}{\sqrt{1 - \left(\frac{q_{01}}{ka}\right)^2}}\right)\left(\frac{\left(\frac{r_b}{r_a}\right)^2}{J_o^2(q_{01})}\right)\left(\frac{2}{\gamma(\gamma+1)}\right) B_{FNm} \tag{5-17}$$

where all of the parameters have been previously defined (equations (5-15)) except B_{FN_m} which is the beam factor. This factor is calculated from the computer-generated dc electron paths using equation (2-117).

If we compare C_u from equation (5-17) to C_u given in equation (5-6), we see that B_{FNm} in equation (5-17) replaces the quantity

$$\frac{\pi}{2}\left(\frac{J_1^2\left(\frac{q_{01} r_b}{r_a}\right)\Lambda^2}{\beta_e^2 r_b^2}\right) \tag{5-21}$$

in equation (5-6). This quantity contains all of the factors in C_u which vary with beam radius, r_b. Thus the effect of the beam factor can be described in terms of an effective beam radius $\bar{r}_b$ given by the equation

$$\frac{\pi}{2}\left(\frac{J_1^2\left(\frac{q_{01} \bar{r}_b}{r_a}\right)\Lambda^2(\bar{r}_b)}{\beta_e^2 \bar{r}_b^2}\right) = B_{FNm} \tag{5-18}$$

where $\Lambda(\bar{r}_b)$ is obtained from equation (5-14) by replacing r_b by $\bar{r}_b$. Solving equation (5-18) for $\bar{r}_b$ gives an effective beam radius which, when used in the Pierce small-signal theory, gives gain and efficiency values corrected for the effects of large radial variations in the dc beam.

The curve shape of the function on the LHS of equation (5-18) has been given previously in Figure II-3. From this figure we note that multiple solutions may exist for $\bar{r}_b$ in equation (5-18). It is necessary, therefore, to select the value which falls near the mean of the maximum and minimum dc beam radii. This is then the "effective beam radius."

B. RF Modes and Attenuation in Circular Waveguide

Because the basic Ubitron circuit being considered on this program consists of a cylindrical waveguide, we present here a summary of the basic properties of this type of fast-wave circuit.

Wave propagation in a circular waveguide is governed by the dispersion relation

$$\beta_{mn} = \sqrt{k^2 - \gamma_{mn}^2} \tag{5-19}$$

where β_{mn} is the propagation constant for the (m, n)th mode, k is the propagation constant of free space ($= \omega/c$), and γ_{mn} is a constant given by

$$\gamma_{mn} = \begin{cases} \dfrac{q_{mn}}{r_a}, & \text{for T.E. modes} \\ \dfrac{p_{mn}}{r_a}, & \text{for T.M. modes} \end{cases}$$

The constants q_{mn} and p_{mn} are respectively the nth roots of the Bessel function equations

$$\frac{dJ_m(x)}{dx} = 0$$

$$Jm(x) = 0 \tag{5-20}$$

and r_a is the waveguide radius. Waveguide cutoff ($\beta_{mn} = 0$ in equation (5-19)) occurs at the wavelength

$$\lambda_{cmn} = \begin{cases} \dfrac{2\pi\, r_a}{q_{mn}} , & \text{for T.E. modes} \\ \dfrac{2\pi\, r_a}{p_{mn}} , & \text{for T.M. modes} \end{cases} \qquad (5\text{-}21)$$

Figure V-3 gives a plot of the number of modes which can exist in a cylindrical waveguide as a function of r_a/λ. The beginning of propagation for each mode is represented by a heavy dot at the value of r_a/λ_c determined from equation (5-21).

Using the previous equation (5-4), we have also included an equivalent design voltage scale in Figure V-3. This voltage corresponds to a wideband design in which the -1 beam mode harmonic mode is made to be tangential to the waveguide TE_{01} circuit mode. (See Figure V-1.) Note that 6 modes exist for a 100-kV design, and 10 modes for a 300-kV design.

Of all the modes which can exist in the Ubitron, the one most likely to cause problems is the TM_{11} mode which has a dispersion characteristic identical to the TE_{01} mode. Thus the TM_{11} mode is in synchronism with the beam and can be expected to have some net interaction if azimuthal asymmetries exist in the beam-circuit system. No detailed analysis has been made of interactions with these spurious modes.

Figure V-4 is a plot of the waveguide attenuation which can be expected using a copper waveguide. This curve is plotted versus the same normalized radius and voltage scales as Figure V-3 to facilitate comparisons.

Figure V-4 is obtained from the following values for the attenuation constant α in nepers/meter.[29]

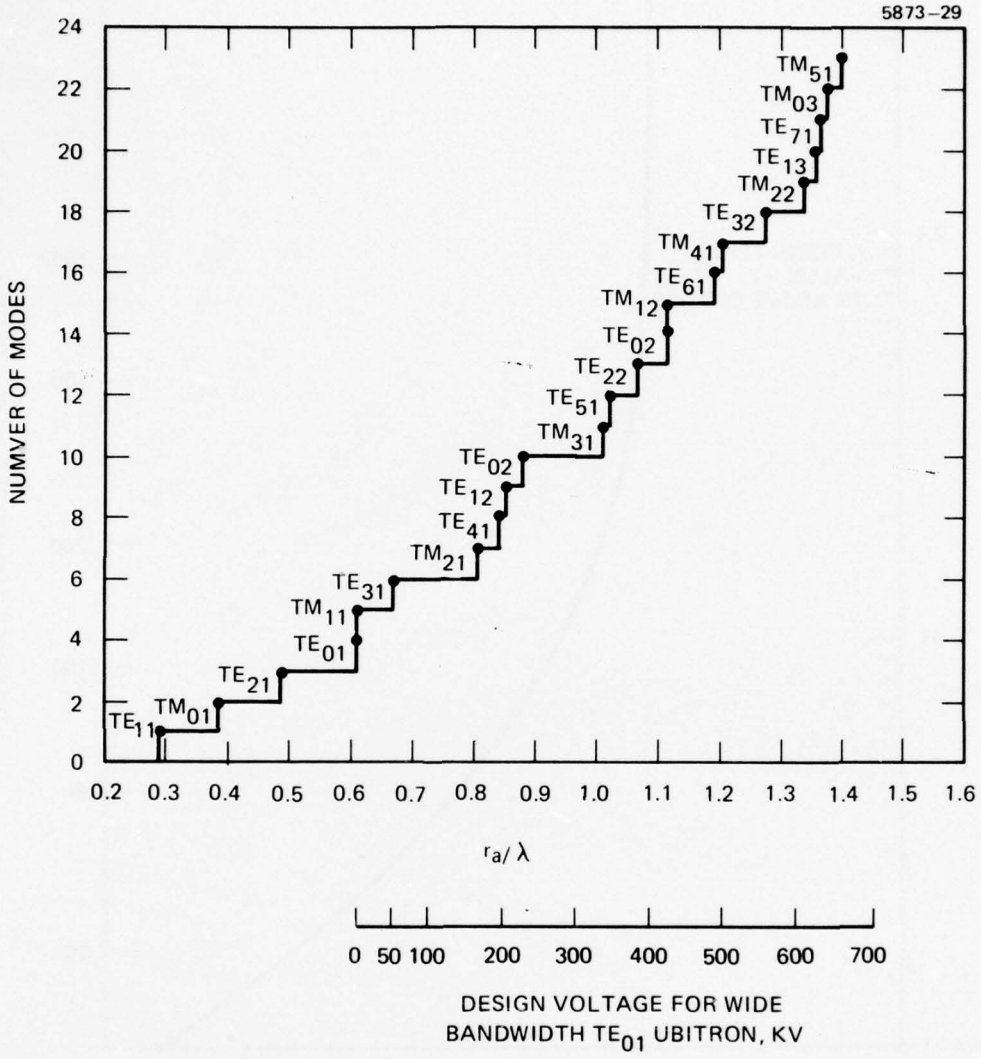


Figure V-3. Circular waveguide modes versus (radius/wavelength) ratio and design voltage.

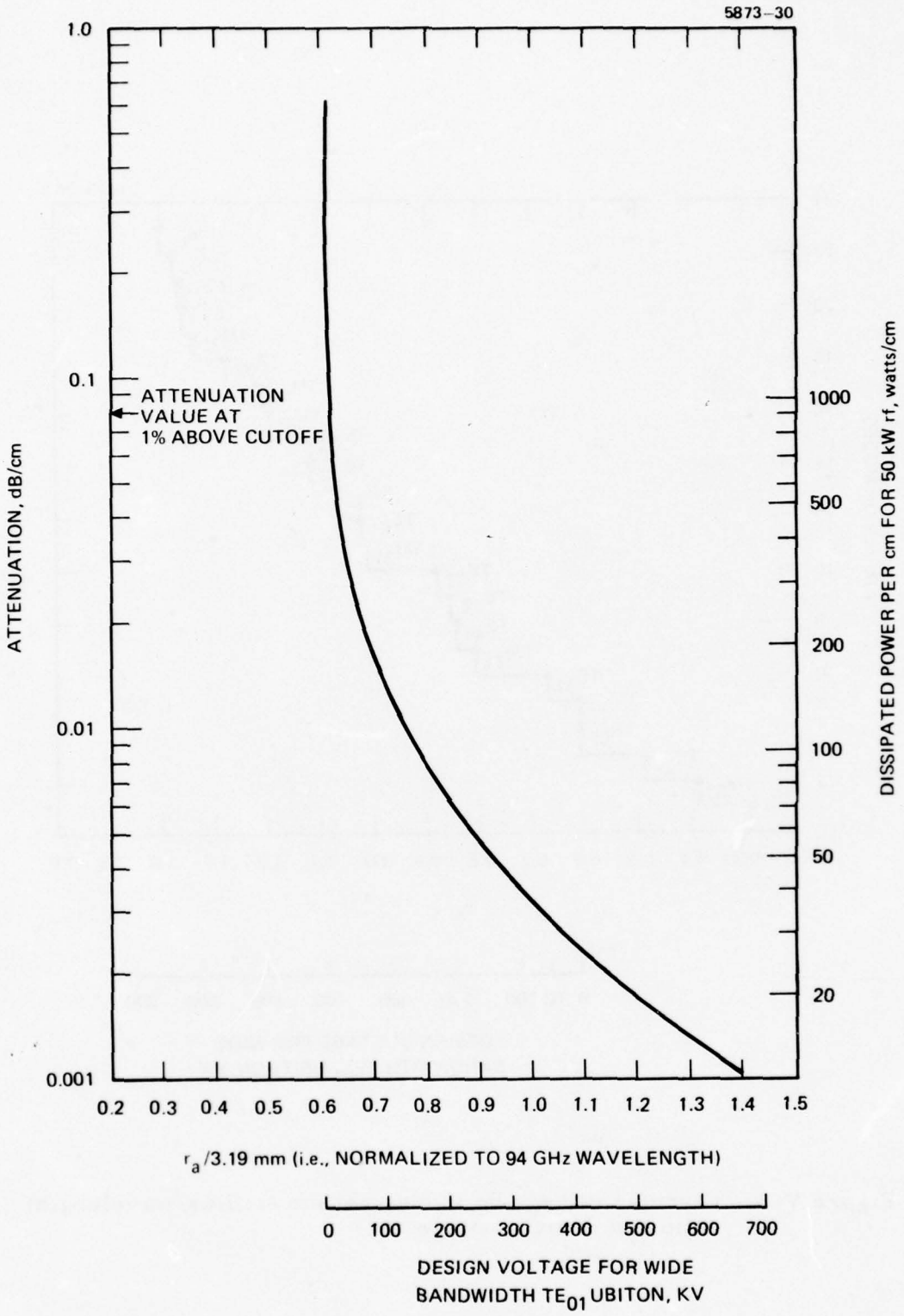


Figure V-4. Circular waveguide TE_{01} mode losses versus waveguide radius and design voltage at 94 GHz.

$$\alpha_{mn} = \begin{cases} \dfrac{R_s}{Z_o r_a}\left[\dfrac{m^2}{q_{mn}^2 - m^2} + \left(\dfrac{q_{mn}}{k r_a}\right)^2\right]\left(\dfrac{1}{\sqrt{1 - \left(\dfrac{q_{mn}}{ka}\right)^2}}\right) & \text{, for TE modes} \\ \dfrac{R_s}{Z_o r_a}\left[\dfrac{1}{\sqrt{1 - \left(\dfrac{p_{mn}}{ka}\right)^2}}\right] & \text{, for TM modes} \end{cases}$$

where

$$R_s = \frac{\pi Z_o}{\lambda}\sqrt{\frac{\omega \mu_o \sigma}{2}} = \text{surface resistance}$$

$$Z_o = \sqrt{\frac{\mu_o}{\epsilon_o}} = \text{impedance of free space}$$

σ = conductivity of waveguide material ($\cong 4\ (10^7)$ mhos/m for Copper)

Note in Figure V-4 that the attenuation has been plotted in dB/cm (= 8.686 α, α in nepers/cm) and that an additional scale is provided showing the power dissipated per cm due to 50 kW rf power. This plot clearly shows that rf power dissipation in a simple waveguide circuit will not be a problem for design voltages over 100 kV. In fact, because the 50 kW of power only exists within the last few centimeters of the circuit (before the waveguide can be expanded to decrease the losses) it appears to be feasible to work down to within 1% of waveguide cutoff. At this point the waveguide wall must dissipate a power density of ~740 watts/cm^2 which is feasible. In such a case, however, we would have to abandon the wideband design criteria previously discussed, and use a synchronous condition in which the -1 beam mode crossed the waveguide mode at 1% above the cutoff frequency.

C. Design Trade-offs Versus Voltage

We have used the small-signal design equations (5-6) through (5-15) to evaluate the gain and efficiency of wideband Ubitrons versus design voltage. Figures V-5 through V-9 give the results of this work. All of these designs must be considered preliminary in nature because very little experimental work exists upon which to base a good estimate of the efficiency parameter.

In Figure V-5 we have plotted the electronic efficiency η_e versus voltage for three different 94-GHz Ubitron designs. The efficiency parameter for these cases is assumed to be 3. The first curve, which applies to a 50-kW Ubitron, assumes a simple cylindrical waveguide circuit with the i.d. of the magnetic pole pieces equal to the waveguide diameter. This circuit could be constructed from a brazed stack of alternating magnetic and non-magnetic rings with a thin inner lining of high-conductivity copper. The design curve for this case shows electronic efficiency decreasing from about 2% at 100 kV to near 1% at 500 kV.

The second curve in Figure V-5 is based on the assumption of an enhanced waveguide circuit such as shown in Figure V-6. This waveguide has no periodicity in the z direction and therefore remains a true fast-wave circuit.

The purpose of this circuit design is to allow the magnetic pole pieces to extend inside of the effective waveguide wall and therefore enhance the magnetic field undulations at the location of the beam. This type circuit was proposed and tested in the previous G.E. work.[51] It was shown to be effective in enhancing the small-signal gain.

Even though this enhanced circuit configuration does not substantially alter the dispersion characteristics of the guide, it does have significantly-increased wall currents and the beam must be placed much closer to the waveguide wall. We would therefore anticipate substantially increased rf circuit losses and higher beam interception on the circuit. Since no further analysis of these phenomena

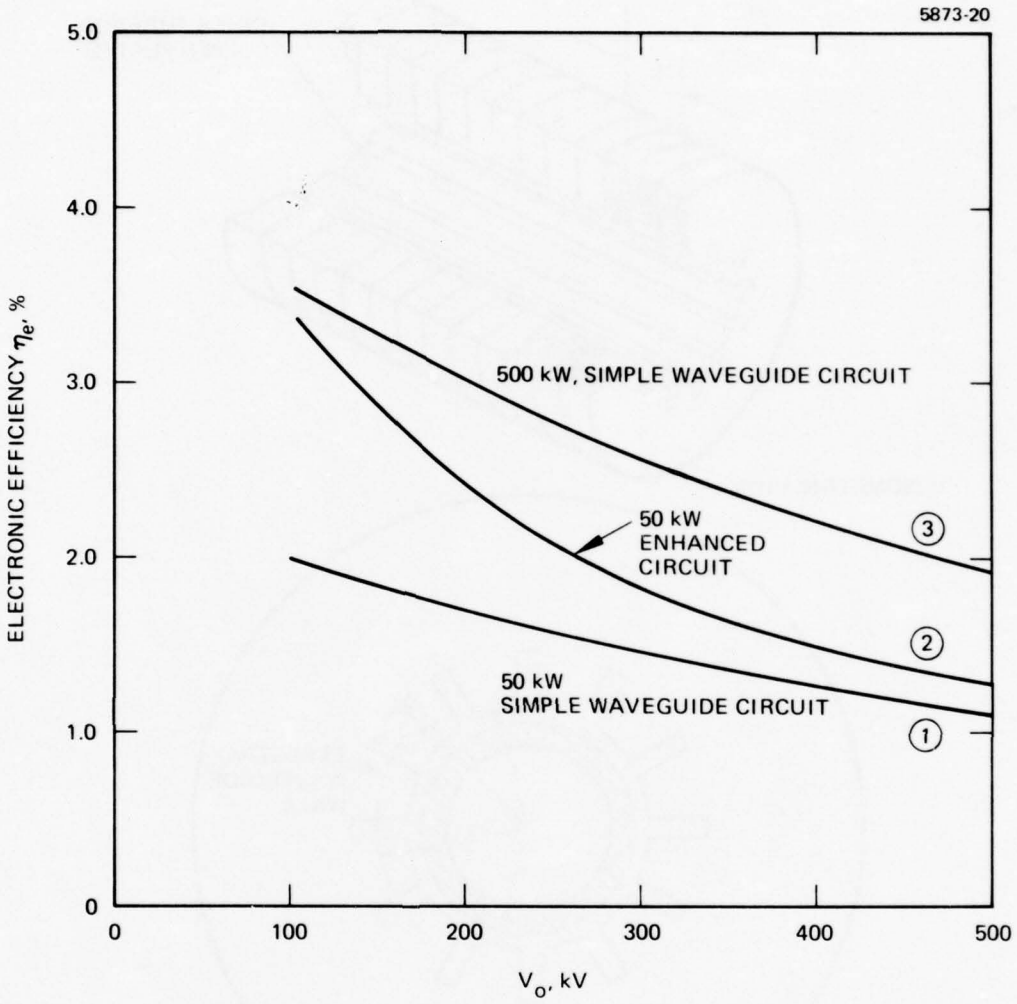
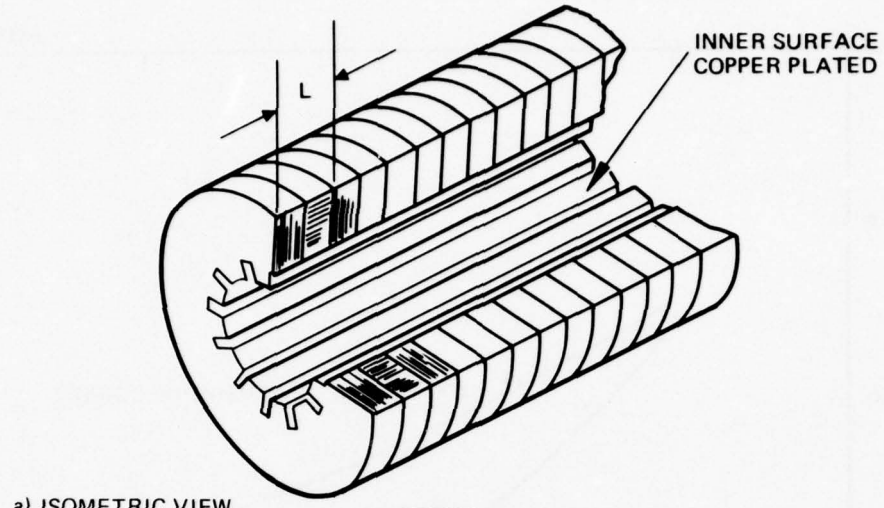
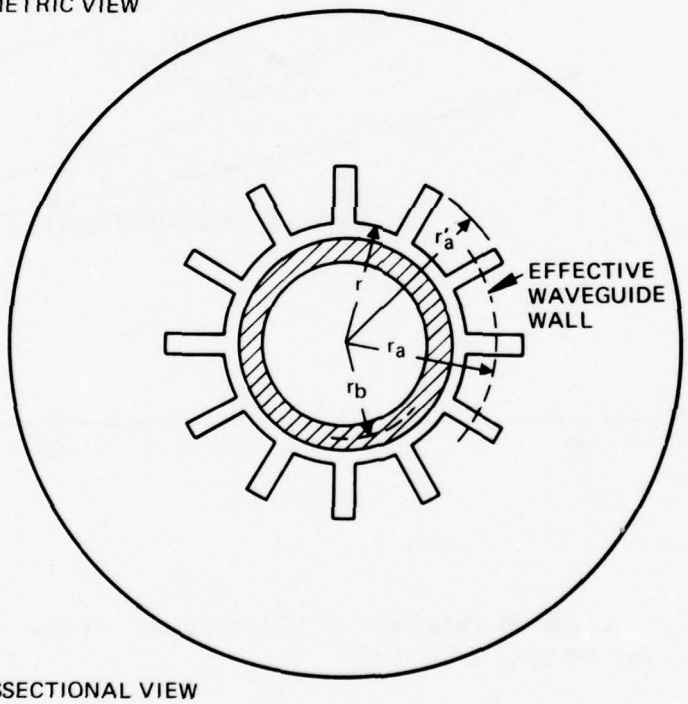


Figure V-5. Calculated relativistic efficiencies versus voltage for 94 GHz Ubitron.

5873-19



a) ISOMETRIC VIEW



b) CROSSECTIONAL VIEW

Figure V-6. Enhanced interaction circuit for Ubitron.

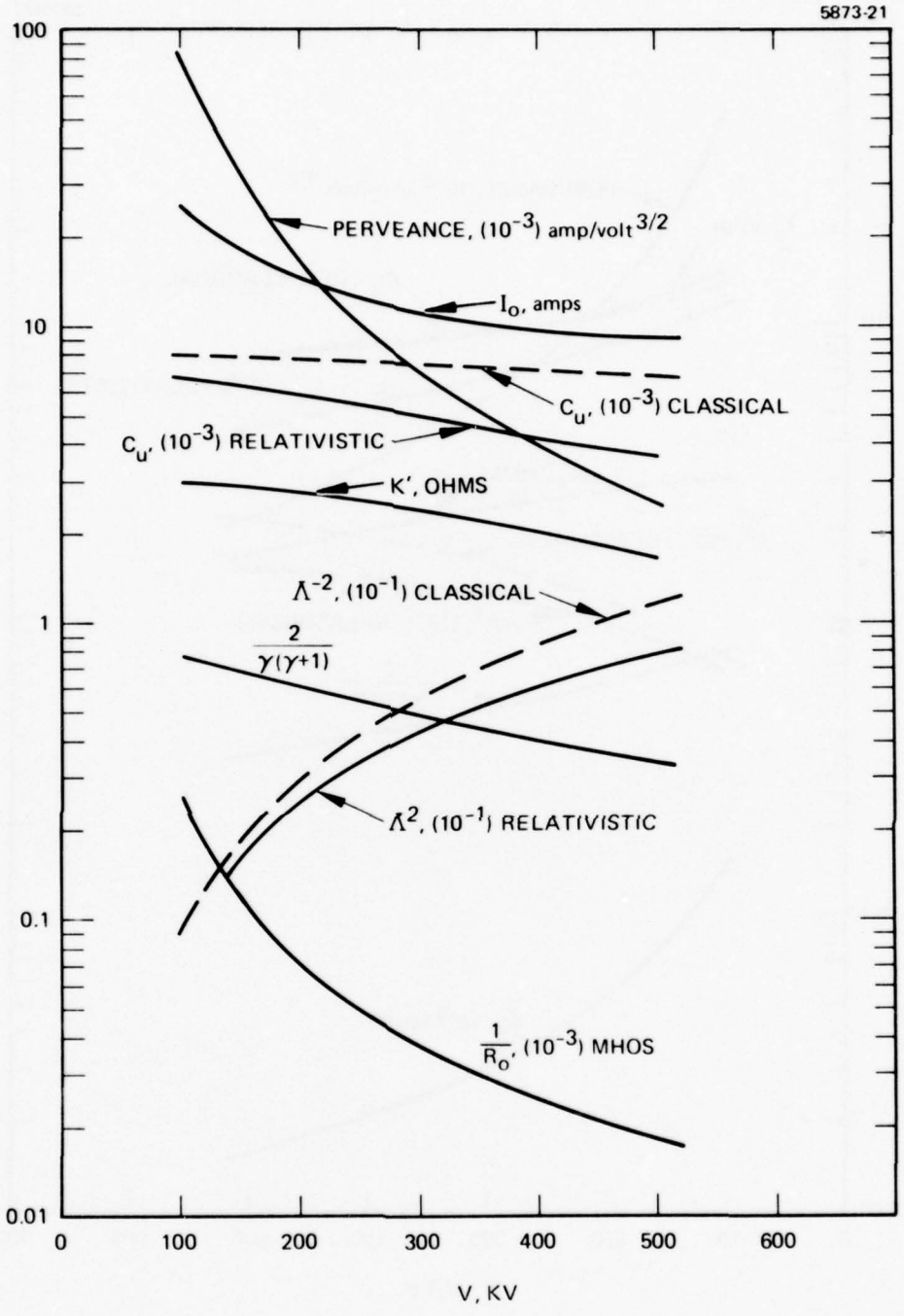


Figure V-7. Variation of Ubitron parameters versus voltage for case 1.

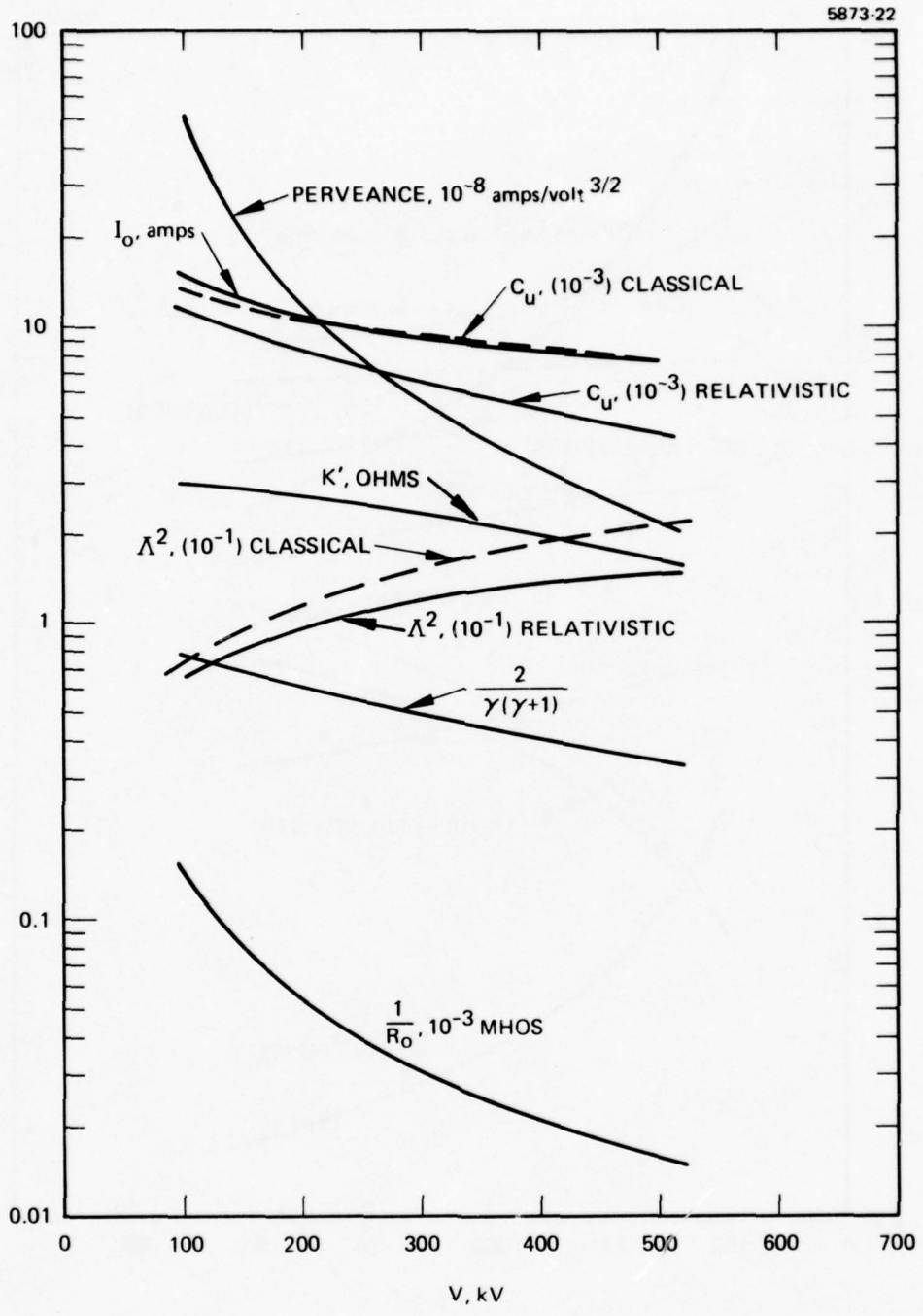


Figure V-8. Variation of Vbitron parameters versus voltage for case 2.

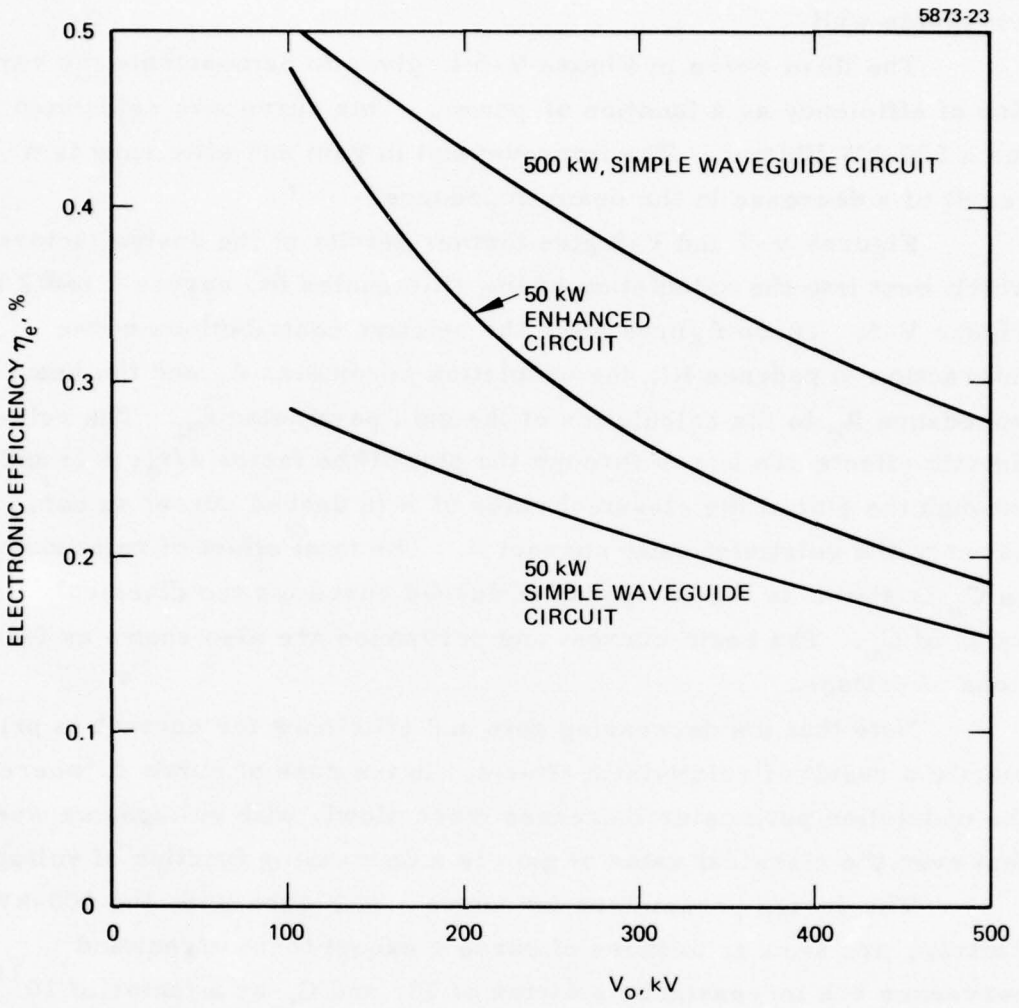


Figure V-9. Calculated relativistic efficiency versus voltage for 35-GHz Ubitron.

was carried out during this study we do not know the extent of the increased losses at this time. Curve 2 in Figure V-5 assumes the magnetic pole piece i.d. is 0.8 times the effective i.d. of the rf waveguide wall.

The third curve in Figure V-5 is given to demonstrate the variation of efficiency as a function of power. This curve was calculated for a 500-kW Ubitron. The improvement in gain and efficiency is a result of a decrease in the beam impedance.

Figures V-7 and V-8 give further details of the design factors which went into the calculation of the efficiencies for curves 1 and 2 in Figure V-5. These figures show the relative contributions of the interaction impedance K', the undulation parameter Λ, and the beam impedance R_o to the calculation of the gain parameter C_u. The relativistic effects are shown through the plot of the factor $2/\gamma(\gamma + 1)$ and through the plot of the classical value of Λ (a dashed curve) as compared to the relativistically correct Λ. The total effect of relativity on C_u is shown by the comparative dashed curve for the classical value of C_u. The beam current and perveance are also shown as functions of voltage.

Note that the decreasing gain and efficiency for curve 1 is primarily a result of relativistic effects. In the case of curve 2, where the undulation parameter increases more slowly with voltage, we see that even the classical value of gain is a decreasing function of voltage.

The design parameters for curve 3 in Figure V-5, the 500-kW Ubitron, are similar to those of curve 1 except that current and perveance are increased by a factor of 10, and C_u by a factor of $10^{1/4}$.

The change in efficiency as a function of frequency is illustrated by the curves in Figure V-9. These curves apply to the design of a 35-GHz Ubitron using the same parameters as in the 94-GHz case except for the frequency and the efficiency parameter. The efficiency parameter was reduced from 3 to 2.5 to reflect a best estimate based on comparable TWT experience. Note that the curves in Figure V-9 show an overall increase in electronic efficiency of about 1% due to this frequency change.

It should be noted again here that all of the preceding design trade-offs apply to the case of a wideband Ubitron in which the design criterion has been to make the -1 beam mode tangential to the rf circuit mode as shown in the previous Figure V-1. This design criteria provides wave synchronism over the widest possible frequency range.

The next logical step in furthering Ubitron trade-off studies would be to abandon this wideband design criteria and allow beam voltage and frequency to be independent of each other. When this is done, it will be possible to trade off voltage, magnetic period, and waveguide diameter to gain control over the amplifier bandwidth at a given operating frequency. In general, a reduction in bandwidth will be accompanied by an increase in electronic efficiency due to the ability to (1) operate closer to waveguide cutoff where interaction impedance increases and (2) keep the undulation parameter high by maintaining a sufficiently long magnetic period. Both of these design trends, however, tend to increase the voltage thus increasing the effects of relativity. A detailed trade-off study of these design conditions is needed to explore the extent to which efficiency can be enhanced. It is anticipated that electronic efficiencies as high as 4 to 6% may be possible for narrow-band Ubitrons operating within 1 to 2% of the cutoff frequency. For example, the G. E. work[51] predicts 4% efficiency in a 50-kW, 94-GHz Ubitron operating at 80 kV (2% above cutoff). With slightly higher voltage, we anticipate this efficiency could be increased still further.

D. 300-kV Design of a 94-GHz, 50-kW Ubitron

As mentioned in the beginning of this section, an early decision during this program to maintain the design voltage high enough to keep the magnetic period about equal to the waveguide diameter caused us to perform a large amount of work on beam analysis and magnetic circuit design which is applicable of a 300-kV Ubitron. Then, after completing the relativistic small-signal analysis which indicated that lower voltages would actually provide better efficiency, there was not sufficient

time to redo the beam and magnetic-circuit analysis for a lower voltage design. We therefore present here a preliminary design for a 300-kV Ubitron. Althoug it is lower in electronic efficiency than a lower-voltage Ubitron would be, we anticipate that this amplifier would have about 50% bandwidth. It may therefore be able to fill ECM applications which cannot be handled by other devices.

The dc analysis for a 300-kV electron beam was presented in Section II. In that analysis, an initial cyclotron motion was assumed which caused the beam radius to have maximum and minimum values of 0.75 r_a and 0.645 r_a respectively. This beam motion is believed to be compatible with what would be obtained from a magnetron injection gun designed for this device.

By computer analysis, the beam factor for this 300-kV electron beam was determined to be 2.2 (10^{-4}) as shown in Section II, Figure II-12. When this value is used in equation (5-17) with R_o given by equation (5-11), we get a value for the efficiency of 1.36%. To see the effects of the beam factor, this value should now be compared with the small-signal theory efficiency given by equations (5-10) through (5-15). In order to apply these equations, it is necessary to determine some acceptable value to use as the beam radius. A logical choice is to use the average value of the radius which is 0.6975 r_a. The result of this calculation is 1.46% efficiency.

From these calculations, we see that the net effect of the radial dc beam motion for this design was to reduce the gain and efficiency by about 7%. This is not a large factor but we believe that the effort expended during this program to obtain a quantitative result has been worthwhile. The results of this calculation tend to give new confidence in applying the small-signal design theory to Ubitrons even when there is a significant amount of radial motion in the beam. This was a previously un-answered question.

Using the gain and efficiency values calculated from the beam factor described above, a 300-kV Ubitron design will have the following design parameters.

f = 94 GHz frequency

P = 50 kW cw (rf power)

V_o = 300 kV (beam voltage)

I_o = 12.25 amps (beam current)

perveance = $7.46\ (10^{-8})$ amp/volt$^{3/2}$

Cu = $4.53\ (10^{-3})$ (small-signal gain parameter)

η_e = 1.36% (efficiency)

r_a = 3.09 mm (waveguide diameter)

$r_b = 0.7\ r_a$

$r_c = r_a$ (magnetic circuit inside radius)

L = 6.24 mm (magnetic period)

Circuit length = $\begin{cases} 22.9 \text{ cm (for 10 dB gain)} \\ 28.7 \text{ cm (for 15 dB gain)} \\ 34.5 \text{ cm (for 20 dB gain)} \end{cases}$

The magnetic circuit applicable to this Ubitron design is very close to that shown in Figure III-3. The period will be 6.24 mm with a total of 55 periods required for a 20 dB gain amplifier. With a taper on the magnetic pole piece faces as shown in Figure III-10, we can use a solenoidal magnetic field strength of about 7000 gauss as was described in Section III-B.

By making rc = 0.8 ra in the above design we can increase the efficiency to a value just under 2%. This would not change any of the other design parameters except beam current and perveance. Beam current for the enhanced circuit design would decrease to about 9 A.

The overall Ubitron envelope will look something like that shown in Figure V-10. In this envelope we have provided sufficient room in the gun region to stand off 300 kV, and sufficient room in the collector region to provide for a depressed collector.

Depressing the collector will be a requirement in this device if any kind of reasonably efficiency is to be achieved. The way to accomplish this has not been explored in detail, but Figure V-10 shows a first step in the approach to the problem. By breaking the output waveguide up into short rings or sections of waveguide separated by thin ceramic rings, we will be able to change the voltage on the waveguide wall in a stepwise fashion which can be tailored to produce the best overall collector depression. As long as the ceramic gaps between these waveguide sections or rings are small compared to a wavelength, the TE_{01} waveguide mode will be transmitted with very minor effects. This is because this mode is supported by azimuthal wall currents with no components in the z direction. Collector depression is an important area which should be investigated further.

It will be important in the above Ubitron design to make sure that none of the electron beam reaches the rf output window. This can be accomplished in a number of ways, the simplest being to provide sufficient length with a transverse magnetic field in front of the window.

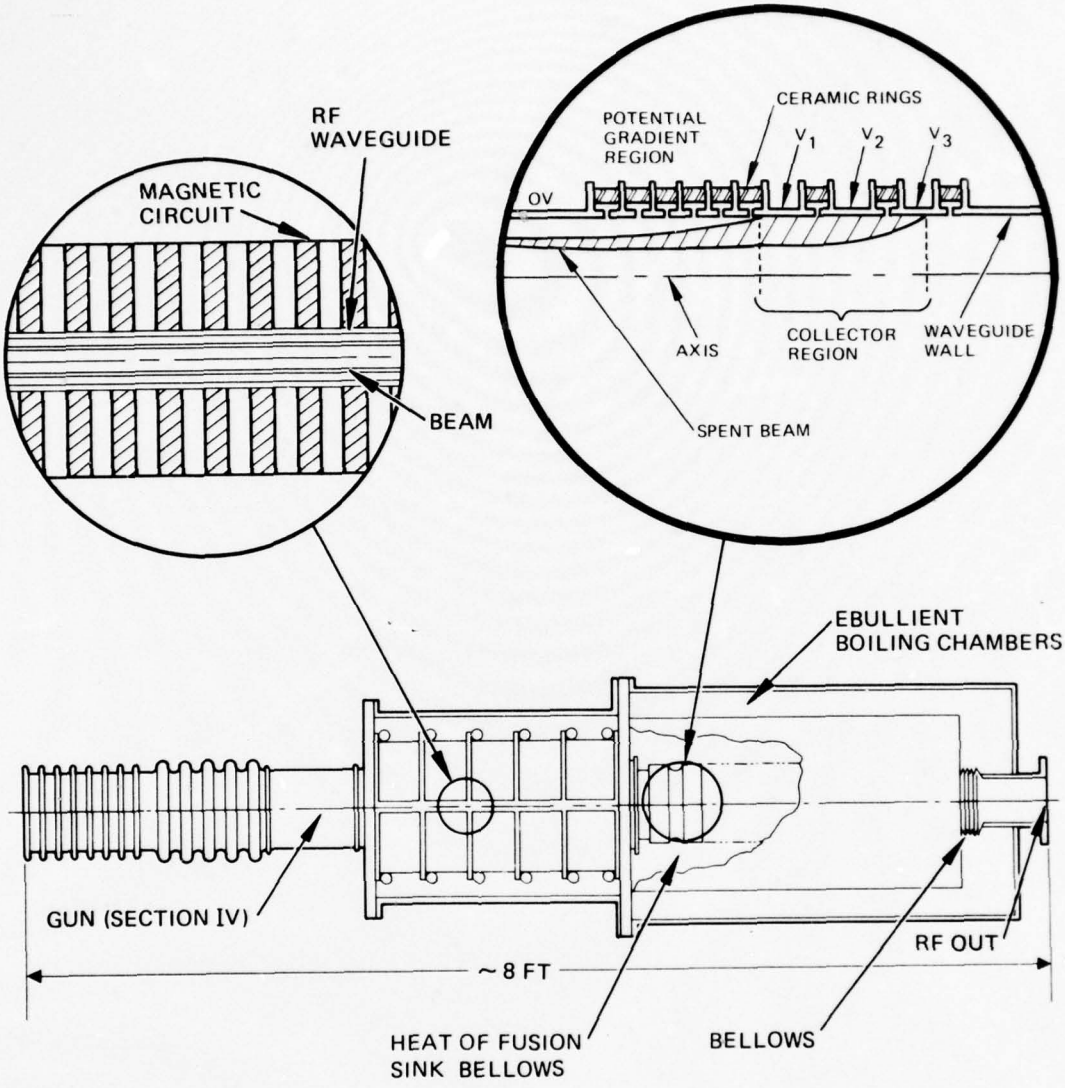


Figure V-10. Outline of high-power Ubitron amplifier.

VI. CONCLUSIONS AND RECOMMENDATIONS

During this nine-month study program we have been able to answer several important questions regarding Ubitron amplifier theory. Primarily, we have extended the previous planar small-signal theory to include (1) the effects of relativity and (2) the effects of large variations in the dc beam radius of cylindrical Ubitrons. We also have investigated new periodic magnetic circuits which can be applied to millimeter-wave Ubitrons and have investigated the design criteria required to develop hollow-beam guns for these amplifiers.

With respect to the feasibility of high-power millimeter-wave amplifiers, we restate the following conclusions given in Section I.

A. Conclusions

1. The development of a 94-GHz, 50-kW cw Ubitron amplifier appears to be feasible, using a 7000-G solenoid and a waveguide circuit with embedded periodic magnetic pole pieces.

2. Under the small-signal assumption that efficiency is proportional to the gain parameter, the following relationships occur.

$$\eta_e = B_\eta C_u \sim B_\eta^{3/4} P^{1/4} f^{-1/2} h$$

where η_e is the electronic efficiency; B_η is the assumed efficiency parameter; C_u is the Pierce type small-signal gain parameter for the Ubitron; P is the rf power; and f is the operating frequency. The factor hs is a relatively complex function of the voltage, the beam-to-waveguide diameter ratio, and the magnetic polepiece i.d.-to-waveguide diameter ratio. This function decreases with increasing voltage primarily due to the effects of relativity.

3. Using the small-signal assumptions described above, a 300-kV Ubitron design would have an inherent efficiency just under 2%. The estimated bandwidth would be on the order of 50% since f/f_{co} is 1.6 at 300 kV. At a lower design voltage of 100 kV, the efficiency would rise to between 3 and 4% but the bandwidth would decrease to about 10%. The lower efficiency at higher voltage is mainly due to relativistic effects contained in the factor h above.

4. There will be a slight degradation of gain and efficiency due to the radial variations which must exist in the undulating electron beam, but with proper design these effects are shown to be on the order of 10% or less in the rf small-signal regime.

5. Because of the low inherent efficiency of the Ubitron, it will be necessary to take advantage of every available means to both enhance the electronic efficiency and recover the energy in the spent beam through collector depression. Because the spent beam and the rf power exit the Ubitron at the same place, collector depression needs further feasibility study and demonstration.

B. Recommendations

As is true in any limited study program, we have been able to identify numerous areas of investigation which would enhance and expand upon the results of this reported work. In the remaining part of this section we present a list of recommendations which we believe to be the next logical steps in the development of high-power Ubitron amplifiers.

The order of these recommendations reflects our estimate of their relative importance.

1. We recommend that the small-signal voltage trade-off study given in this report be augmented to include the most general condition for mode synchronism. It is emphasized that the present study has been aimed at wideband Ubitrons in which the design criterion has been to maintain synchronism between the beam and the circuit wave over the widest possible frequency range. This occurs when the -1 beam mode on a disperson diagram is just tangential to the TE_{01} circular waveguide mode. This results in simple design relationships between the four primary variables of frequency, voltage, waveguide diameter, and magnetic period; but it also requires that only two of these variables can be independent. The general synchronism condition in which the beam and the circuit dispersion curves are allowed to cross, allows three of the variables to be independent, which provides one more degree of design freedom. It now appears that a region of design exists at moderately high voltage (100 to 200 kV) in which the efficiency can be

optimized at the expense of some bandwidth. This would be a desirable thing to do for most millimeter-wave applications. The maximum efficiency for any given bandwidth would be determined by varying the waveguide diameter and magnetic period with voltage as a parameter.

Although this will not be a large task in any future work, it is included here as a first recommendation because higher electronic efficiency is very important in this device and because the trade-off needs to be done for the sake of completeness prior to any further experimental work. Now that a relativistically correct small-signal theory is available, this extended trade-off study is a next logical step.

2. Collector depression to recover the power in the spent electron beam is, in most cases, essential to the practical application of high-power Ubitron amplifiers. Because of the fact that the spent electron beam and the rf output power occupy the same output port, it is most likely that an experimental high-power Ubitron will have to be built in order to study this important aspect of the device. We recommend that follow-on work include both theoretical and experimental evaluation of collector depression techniques.

3. We believe that any significant effort leading to the development of high-power Ubitron amplifiers requires that a large-signal computer code be acquired. Once a code is available, it can be used both to determine the basic Ubitron efficiency under relativistic design conditions, and to evaluate efficiency enhancement techniques such as circuit tapering, etc. It would also be an invaluable tool for analysis of collector depression techniques.

   Because the Ubitron gain mechanism involves a mixture of both longitudinal and transverse interactions, a large-signal computer code will have to be at least a 2-1/2 dimensional code (i.e., r, x, $\dot{r}$, $\dot{\theta}$, $\dot{z}$ dimensions) such as the code now used for plasma analysis studies. An example of such a code is CYLRAD, [14] which was developed by the Naval Research Laboratory. There is little doubt that any existing code would require adaptation before it could be used satisfactorily for Ubitron analysis. Such an adaptation, however, appears to be the most logical way to proceed and is recommended.

4. The final recommendation deals with the spurious modes which can exist in Ubitrons.

As shown in Section V, at least five modes or more exist in a circular waveguide Ubitron and more work needs to be done to identify how these modes might interact with the electron beam and circuit in this device. We recommend that a small signal analysis be carried out for each of these modes in terms of their rf field structures and various assumed beam and magnetic field asymmetries. Such an analysis would provide a starting point from which to analyze and understand any spurious outputs from experimental devices. It may also be possible to use the large-signal computer code recommended in item 3 to accomplish some of this analysis. This would require a full three-dimensional code, however, to account for asymmetries. Any spurious mode analysis must also include the effects of waveguide perturbations resulting from input couplers, etc.

REFERENCES

1. R. M. Phillips, "The Ubitron, a High Power Traveling Wave Tube Based on Periodic Beam Interaction in an Unloaded Waveguide," IRE ED-7, pp. 231-241, October 1960.

2. L. C. Bacon, E. E. Enderby, and R. M. Phillips, "V-Band Ubitron Amplifier Development," prepared by G. E. Company under Contract AF 33(616)-8356, April 1962.

3. W. M. Mannheimer and E. Ott, "Theory of Microwave Generation by Intense Relativistic Electron Beam in a Rippled Magnetic Field," Physics of Fluids, 17, 2, pp. 463-473, February 1974.

4. V. L. Granatstein, P. Sprangle, M. Herndon, R. K. Parker, and S. P. Schlesinger, "Microwave Amplification with an Intense Relativistic Electron Beam," J. of Appl. Physics, 46, 9, p. 3800-3805, September 1975.

5. P. Sprangle, "Excitation of Electromagnetic Waves from a Rotating Annular Relativistic E-Beam," NRL Memorandum Report 3209, Naval Research Laboratory, Washington, DC, January 1976.

6. S. I. Krementsov, M. D. Raizer, and A. V. Smorgonskii, "Ubitron Oscillators with a Relativistic Electron Beam," Pis'ma v. Zhurnal Tekhn. Fiziki, vol. 2, May 26, 1976, p. 453-457. Also available in English translation about 9 months after Russian publication.

7. M. I. Petelin and A. V. Smorgonskii, "Nonlinear Theory of the Ubitron, Iz. VUZ. Radiofiz. 16, 2, pp. 294-304 (English trans. pp. 219-226), February 1973.

8. A. V. Gaponov, M. I. Petelin, "High Frequency Instability of a Curved Beam of Electrons Moving in a Periodic Static Field," Radioteknika i Electronica, 9, 8, p. 1368 (English translation pp. 1128-1132), 1964.

9. A. V. Gaponov, M. I. Petlin, and V. K. Yulpatov, "The Induced Radiation of Excited Classical Oscillators and its Use in High Frequency Electronics," Iz. VUZ. Radiofiz. 10, 9-10, pp. 1414-1453 (English trans. pp. 794-813), 1967.

10. M. I. Petelin, "The Similarity Principle for High-Frequency Devices having Ultra Relativistic Electron Beams," Iz. VUZ. Radiofiz. 13, 10, pp. 1586-1588 (English trans. pp. 1229-1231) October 1970.

11. D. L. Bobroff, "Independent Space Variables for Small-Signal Electron Beam Analyses," IRE Trans. on Electron Devices, ED-5, 1, pp. 68-78, January 1956.

12. C. M. Durney, and C. C. Johnson, Electromechanical Waves on Rotating Electron Beams, Univ. of Utah Report ALTDR 64-229, Contract AF 33(657)-8677, September 1964.

13. F. M. Arscott, "Periodic Differential Equations, an Introduction to Matheiu, Lame, and Allied Functions," Pergamon Press, 1964.

14. J. P. Boris, "Relativistic Plasma Simulation-Optimization of a Hybrid Code," pp. 3-67, Proceedings of Fourth Conference on Numerical Simulation of Plasmas, Edited by J. P. Boris, and R. A. Shanny, Nov. 2, 3, 1970; Naval Research Laboratory, Wash. D.C., U.S. Govt. Printing Office Stock No. 085100059.

15. R. L. Schreiver and C. C. Johnson, "Rotating Beam Devices," Quarterly Report dated December 21, 1966, Technical Report MDL-Q19; Microwave Device and Physical Electronics Laboratory, University of Utah, Contracts NonR1288(05), AF33(615)3686, etc. pp. 1-33, pp. 33-53. This report is one of a series relating both practical and analytical problems related to transverse fast wave devices.

16. L. D. Landau and E. M. Lifshitz, "The Classical Theory of Fields," Pergamon Press, Addison Wesley Publishing Co. Revised Second Edition, 1962, p. 53.

17. A. Sommerfield, "Electrodynamics," Academic Press, 1952, p. 263.

18. P. G. Begmann, "Introduction to the Theory of Relativity" Dover Publications 1976 Edition, p. 103.

19. W. B. Herrrmannsfeldt, "Electron Trajectory Program" SLAC-166(A) UC-28, Stanford University, Contract No. AT (04-3) 515, September 1973, U. S. Atomic Energy Comm.

20. Ref. 16, p. 54.

21. Ref. 17, p. 264.

22. D. A. Dunn, "Models of Particles and Moving Media," Academic Press, 1971, p. 140-142.

23. G. R. Brewer, "Some Characteristics of a Cylindrical Electron Stream in Immersed Flow," IRE Trans. on Electron Devices, ED-4, 1957, pp. 134-140.

24. P. Diament, "Exact Self-Consistent Equilibria of Relativistic Electron Beams," Phys. Rev. Letters, 37, 3, pp. 168-171, 19 July 1976.

25. P. Diament, "Exact Annular Relativistic Electron Beam Equilibria," Bull. Am. Phys. Soc., 21, 693 (1976).

26. A. A. Kurayev, G. Ya Slepian, "Computation of the Effect of Forces Exerted by Space Charge in Axially Symmetrical, Gyro-Resonant Devices with Uniformly Mixed Cylindrical Electron Beams of Finite Thickness," Radio Eng. 8 Electron Physics (USA) Vol. 20, No. 1, p. 141-4 (Jan. 1975) (Trans. of Radiotekh. and Electron (USSR) Vol. 20, No. 1, p. 202-5 (Jan. 1975).

27. G. A. Nagy and M. Szilagyi, "Introduction to the Theory of Space Charge Optics," Halstead Press, John Wiley and Sons, 1974, p. 250.

28. W. J. Kleen, "Electronics of Microwave Tubes," Academic Press, 1958, p. 19.

29. S. Ramo, J. R. Whinnery, T. Van Duzer, "Fields and Waves in Communication Electronics," Wiley and Sons, 1965, p. 430.

30. H. K. Detweiler and J. E. Rowe, "Electron Dynamics and Energy Conversion in O-Type Linear Beam Devices, p. 47 in Advances in Microwaves, V. 6, Academic Press, 1971.

31. J. R. M. Vaughn and G. Good, "Users Manual for TWTVA Traveling Wave Tube Trajectory Computation Program" Litton Industries, Electron Tube Division, Contract No. N00123-76-C0424, NELC, San Diego, Cal. (also, but not available at the time of this report Report No. L-5933-2 on analysis underlying this reference.)

32. Y. W. Lee, "Statistical Theory of Communications," J. Wiley and Sons, 1960, Chapter 1 particularly.

33. W. Magnus, F. Oberhettinger, R. P. Soni, "Formulas and Theorems for the Special Functions of Mathematical Physics," Springer. Verlag. 1966, 3rd ed., p. 108.

34. G. Bosi, "First Order Treatment of Combined Effect of Space-Charge and External Fields on Plane-Symmetric Finite-Emittance Beams of Charged Particles," J. A. P., v. 47, No. 12, Dec. 1976, p. 5292-6.

35. Ref. 33, pp. 37-65.

36. S. Sensiper and R. Weglein, "Capacitance and Charge Coefficients for Parametric Diode Devices," P. I. R. E. pp. 1482-83, eq. (13) upper limit should be $\pi/2$.

37. P. F. Byrd and M. D. Friedman, "Handbook of Elliptic Integrals for Engineers and Physicists," Springla-Verlag, Berlin, Germany, 1971, p. 9, 12 (115.01, 125.01, 125.02).

38. M. E. Goldstein and W. H. Brown, "Advanced Methods for the Solution of Differential Equations," NASA SP-316, V. S. G. P. O. 3300-00478, Washington, D. C., 1973; p. 306-311.

39. H. T. Davis, "Introduction to Nonlinear Differential and Integral Equations," U. S. A. E. C.; U. S. G. P. O.; Washington, D. C.; pp. 300-303.

40. E. Munro, Dissertation, 1971, Cambridge.

41. E. Munro, "Computed-Aided Design of Electron Lenses by the Finite Element Method," Published in Image Processing and Computer-Aided Design in Electron Optics, Edited by P. W. Hawkes, Academic Press, N. Y., 1973, pp. 284-323.

42. N. A. Demerdash and T. W. Nehl, "Flexibility and Economics of Implementation of the Finite Element and Difference Techniques in Nonlinear Magnetic Fields of Power Devices," IEEE Trans., Vol. MAG-12, p. 1036, Nov. 1976.

43. J. S. Colonias, "Calculation of Magnetic Fields for Engineering Devices," IEEE Trans., Vol. MAG-12, p. 1030, Nov. 1976.

44. M. S. Sarma, "Magnetostatic Field Computation by Finite Element Formulation," IEEE Trans., Vol. MAG-12, p. 1050, Nov. 1976.

45. T. Mulvey, "Mini-Lenses and the SEM," Proceedings of the Seventh Annual Scanning Electron Microscope Symposium, IIT Research Institute, Chicago, Ill., Apr. 1974, Part I, p. 43.

46. Tsimring, Radiofizika 15, p. 1247 (1972).

47. J. R. Pierce, "Theory and Design of Electron Beams," Chapter 4.3 equ. 4.17, D. Van Nostrand (1954).

48. T. G. Northcotte, "The Adiabatic Motion of Charged Particles," Interscience Publishers, J. Wiley and Sons (1963) p. 27.

49. V. Dryden, J.A.P. 33, p. 3118 (1962).

50. W. E. Waters, "Magnetron Guns – an Exact Theoretical Treatment," Diamond Ordnance Fuze Labs. Report TR-843 (1960).

51. C. E. Enderby and R. M. Phillips, "V-Band Ubitron Amplifier Development," Tech. Documentary Report No. ASD-TDR-63-847, Jan. 1964, Prepared for AF Avioncis Lab, by G. E. TWT Product Section, Under Contract No. AF 33(616)-8356.

APPENDIX A

COMPUTER PROGRAM DESCRIPTION

Four computer programs were generated during the course of the Ubitron Project. The first two programs called PROG2 and PROG5 solve a set of second-order differential equations. The other two programs called RTHETA and CORREL use the output of PROG2 or PROG5 to plot the variable R versus (THETA) and correlation integration. These programs were developed using the USC PDP10 time-sharing system. A brief description of each follows.

PROG2 and PROG5

The two programs use the Clippenger-Dimsdale method to solve the differential equations. The mathematical discussion of the method is found in "Numerical Analysis" by Kunz. This method was compared with the Runge-Kutta method by making several runs using the same input data and same convergence criteria. The results were almost identical, differing only at the seventh or eighth digita. On the average the running time of the Clippenger-Dimsdale was half of that of Runge-Kutta method. Exact figures are not quoted because it is not possible to get constant run time for the same data, same method, on the time-sharing system. Execution time varies with the load average of the computer.

The Clippenger-Dimsdale method is coded as subroutine CLIPDI. The inputs, DELT, TO, TEND, EMAX, EMIN, E, PRNDEL in the main program are the parameters of subroutine CLIPDI. EMIN and EMAX are the lower and upper bounds of convergence criteria. DELT is the initial integration step size, a good starting value is 0.01. During the course of the integration the DELT is changed by the program depending on the accuracy obtained at each step. If the accuracy is better than EMIN it is doubled, if greater than EMAX it is halved. TO and TEND are the limits of integration. PRNDEL is a time

interval. When the accumulated DELT becomes equal to or greater than PRNDEL the print subroutine (PRNT) is called to save the values of the variables on output file. Special attention is due to PRNDEL, as it determines the size of the arrays T and Z. In the program T and Z are dimensioned 1000, it is determined as follows: dimension of T and Z > (TEND/TO)/PRNDEL.

At the start of execution the program writes the message "Name of Input File" on the TTY and waits for the user response. A file name of more than three and less than 11 characters should be typed in followed by a carriage return. This file contains the input data. As the execution resumes again, the program changes the fourth character of input file to Y by calling library subroutine KMOVE. This file, with the fourth character as Y, becomes the output file. The program continues now by reading the content of input file up to ICOMP. It then checks the value of flag ICOMP; if it is zero it continues to read SRA, L, and RA from the same file. If ICOMP is one then it computes SRA, L, and RA. From these inputs the program continues to compute other parameters and initial values of $d\theta/dT$ and dZ/dT. The computation of $d\theta/dT$ involves the Bessel function of first order. The accuracy desired is not an input but is fixed to 0.0001 in the program. If the Bessel function does not converge for this accuracy the message "BESSEL FUNCTION DID NOT CONVERGE" is printed on the TTY.

After the parameters are computed the program calls subroutine CLIPDI to do the integration. In CLIPDI at every step of integration the variable R is tested. If $R \geq$ SCRIPR or $R \leq 0$ an error message is printed on TTY and CLIPDI is exited. If this error occurs, it means that the electron trajectory has exceeded allowable bounds. Whenever accumulated DELT becomes equal to or greater than PRNDEL, subroutine PRNT is called to save the values of the variables on the output file. The integration terminates and CLIPDI is exited when T becomes equal to or greater than TEND.

Upon return from CLIPDI, in the main program the flag NTHSET is read from the input file. If NTHSET is greater than zero the program goes to the beginning to read a new set of data and repeat the process. If NTHSET is zero, subroutine PLOTPR is called to plot R, Z, θ, etc. versus T. The plots are put on file SPLT02. After plotting, the main program is exited and execution is terminated.

Inputs to Programs PROG2 or PROG5

There are eight read statements, all in the main program. They are discussed here in the same sequence as they appear in the program.

NAMEI	– NAMI is the name of the input file which contains all the input to the program. It is more than three and less than 11 characters.
DELT, TO, TEND, EMAX, EMIN, E, PRNDL	– These were described on previous page in the discussion of subroutine CLIPDI.
R	– Initial value of variable R
THETA	– Initial value of variable θ
ZO	– Initial value of variable Z
DR	– Initial value of DR/DT
FGHZ	– Nominal Frequency in Gigahertz
VKV	– Nominal Voltage in Kilovolts
C	– Gun Entrance Parameter
BABO	– Magnetic Field Modulation Parameter
ZSUBE	– Magnetic Field Entrance Phase
SCIPR	– Beam/Tube Ratio
BO	– Average Field – gauss

ICOMP	– If ICOMP = 1, then compute the values of SRA, L, and RA If ICOMP = 0, then Read values of SRA, L, and RA
SRA	– Tube radius
L	– Magnetic period
RA	– RA is a dimensionless number, the normalized tube radius
NTHSET	– NTHSET = 0 means no more cases to run NTHSET > 0 means there is another set of data to run.

SAMPLE INPUT

IDATE

DELT TO TEND EMAX EMIN E PRND L

R THETA ZO DR

FGHZ VKV C BABO ZSUBE SCRIPR BO

ICOMP

SRA L RA

NTHSET

COLUMN 1

Dec. 17, 1976

Δ0.01000Δ0.00000Δ157.080Δ0.00010Δ0.00001Δ0.00005Δ0.16000

Δ1.00000Δ0.00000Δ0.00000Δ0 00000

Δ94.0000Δ300.000Δ0.88500Δ0.74500Δ1.57079Δ2.33000Δ7000.00

0

0.003086 0.606238Δ3.10911

00

PROGRAMS CORREL AND RTHETA

These two programs are short and simple. They read the output file generated by PROG2 or PROG5. The file contains N values of the variables R, θ, Z, dR/dT, dθ/dT, dZ/dT. Program RTHETA fetches the variables R and θ and plots R versus . Program CORREL fetches all N values of R, Z, and dθ/dT and integrates the mathematical equation (2-114). The result of integration is saved on file TTYOUT. The result is also plotted and saved on file BFNM. The THETA limits of integration are 0 to 360 degrees in steps of 5 degrees. The Z limits of integration are 0 to 61 in steps of 60/61. In both cases the step size is fixed in the program and is not input. The output limit of Z is dependent on TEND. (Used in Subroutine CLIPDI of Program PROG2 or PROG5.) The upper limit 61 of Z mentioned above corresponds to TEND = 50 π.

BEST AVAILABLE COPY


```
C  ORBITRON STUDY PROGRAM #2 FOR SAM SENSIPER OCTOBER 18,1976
C  DC EQUATIONS, EXACT RELATIVISTIC, NO SPACE CHARGE
      DOUBLE PRECISION NAMEO,NAMEI
      DIMENSION FIOMRA(15), Y(6),T(1000),Z(1000),PARAM(70),IDATE(3)
      COMMON/LAB5/PARAM,IER,A1,GAM,LOVLAM,T,Z,NPOINT,DZ,ENERO,RSUBB2,
     !    FIOMRA,ZSUBE,RSUBB,EPS,GAMMAC,EREBW2,BABO,IDATE,RA,SCRIPR
      REAL LOVLAM,L,LAMBDA
      OPEN(UNIT=12,DEVICE='DSK',FILE='SAMY02.DAT')
      OPEN(UNIT=6,DEVICE='TTY')
      JJ=1
 5     WRITE(5,510)
510   FORMAT(1H ,' NAME OF INPUT FILE',$)
      IER=0
      READ(5,500) NAMEI
500   FORMAT(A10)
      NAMEO=NAMEI
      CALL RMOVE('Y',0,NAMEO,3,1)
      OPEN(UNIT=10,DEVICE='DSK',FILE=NAMEO)
      OPEN(UNIT=11,DEVICE='DSK',FILE=NAMEI)
      READ(11,400)IDATE(1),IDATE(2),IDATE(3)
      READ(11,100)DELT,TO,TEND,EMAX,EMIN,E,PRNDEL
     READ(11,100)R,THETA,ZO,DR
      READ(11,100)FGHZ,VKV,C,BABO,ZSUBE,SCRIPR,BO
      READ(11,4) ICOMP
4     FORMAT(I1)
      PI=3.1415926
      PI2=PI+PI
      GAMMAI=1.0+VKV/511.006
      IF(ICOMP .EQ. 1) GO TO 3
      READ(11,100) SRA,L,RA
      GO TO 2
3     SRA=GAMMAI*0.299792/(1.6398*FGHZ)
      L=1.6398*SRA*SQRT(GAMMAI*GAMMAI-1.0)
      RA=PI2*SRA/L
      WRITE(6,450) SRA,L,RA
2     RSUBB=RA/SCRIPR
      RSUBB2=RSUBB*RSUBB
      GAMMAC=0.279923E-2*BO/FGHZ
      LAMBDA=0.299792/FGHZ
      LOVLAM=L/LAMBDA
      CONS=4.0*BABO/(PI*RSUBB)
      WRITE(6,515)
515   FORMAT(1H ,'START NEW CASE')
      H=DELT
      X=TO
      EPS=1.0E-5
      NPOINT=0
      SUM=0.0
      FM=-1.0
      FI=1.0
      CONST=4.0*BABO/PI
      DO 10 J=1,12
      FM=FM+2.0
      ARG=FM*RA
      CALL BIO(ARG,RIO)
      ARG1=FM*RSUBB
      CALL BESJ(ARG1,1,RB1,0.0001,IER)
      IF(IER .GT. 0) GO TO 1000
      FIOMRA(J)=FI*CONST/(FM*RIO)
      SUM=SUM+FI*CONS*COS(FM*ZSUBE)*RB1/(FM*FM*RIO)
      FI=-FI
10     CONTINUE
      PHI=1.0+SUM+SUM
      DTHETA=GAMMAC*0.5*(PHI-C)/GAMMAI
      RVTHZ=RSUBB*DTHETA*L/(LAMBDA*SQRT(1.0-1.0/(GAMMAI*GAMMAI)))
      DZ=LAMBDA*SQRT(1.0-1.0/(GAMMAI*GAMMAI))/(L*SQRT(1.0+RVTHZ*RVTHZ)
     1)
      ENERO=RSUBB2*((DR*DR+R*R*DTHETA*DTHETA)+DZ*DZ
      WRITE(10,175)
```

BEST AVAILABLE COPY

```
C  <SAGHER>PROG2.FOR;57   TUE 21-DEC-76 11:51AM                    PAGE 1:1

175      FORMAT(1H ,'PROGRAM #2,DC EQ. EXACT RELATIVISTIC,NO SPACE CHARGE
     !')
         WRITE(10,180)(IDATE(M),M=1,3),R,THETA,Z0,DR,DTHETA,DZ,BAB0,
     !     GAMMAC,ZSUBE,FGHZ,VKV,C,SCRIPR,B0,SRA,L,RA
180      FORMAT(1H ,3A5/1H ,'R=',E15.8,'  THETA=',E15.8,'  Z=',E15.8/
     !           1H ,'  DR=',E15.8,'  DTHETA=',E15.8,'  DZ=',E15.8/
     !           1H ,'  BAB0=',E15.8,'  GAMMAC=',E15.8,'  ZSUBE=',E15.8/
     !           1H ,'  FGHZ=',E15.8,'  VKV=',E15.8,'  C=',E15.8/
     !            1H ,'  SCRIPR=',E15.8,'  B0=',E15.8,'  SRA=',E15.8/
     !           1H ,'  L=',E15.8,'  RA=',E15.8/)
         GAM=1.0/SQRT(1.0-LOVLAM*LOVLAM*(RSUBB2*(DR*DR+R*R*DTHETA*DTHETA
     !       )+DZ*DZ))
         CALL SCHARG
         A1=GAM*GAM*GAM*LOVLAM*LOVLAM
         PARAM(JJ)=BAB0
         PARAM(JJ+1)=GAMMAC
         PARAM(JJ+2)=ZSUBE
         PARAM(JJ+3)=RA
         PARAM(JJ+4)=LOVLAM
         PARAM(JJ+5)=GAM
         Y(1)=R
         Y(2)=THETA
         Y(3)=Z0
         Y(4)=DR
         Y(5)=DTHETA
         Y(6)=DZ
         CALL CLIPDT(H,X,6,Y,TEND,EMAX,EMIN,E,PRNDEL)
         K=0
         WRITE(12,150) K
         ZT=Z(NPOINT)/T(NPOINT)
         DO 15 K=1,NPOINT
15       Z(K)=Z(K)-T(K)*ZT
         WRITE(10,185) (Z(K),K=1,NPOINT)
185      FORMAT(1H ,'Z(T)-T(T)*Z(END)/T(END)'/(5E16.7))
         WRITE(12,150) NPOINT
         WRITE(12,300) (Z(K),K=1,NPOINT)
         NPOINT=0
C AT THIS POINT ONE SET OF INPUT DATA HAS BEEN READ, THE DIFFERENTIAL
C EQUATIONS SOLVED AND THE OUTPUT SAVED ON FILE, NOW READ NTHSET WHICH
C IS A 2 DIGIT INTEGER. IF NTHSET IS NONZERO, IT MEANS THERE IS ANOTHER
C SET OF INPUT DATA TO EXECUTE,GO TOSTATEMENT NUMBER 5 TO REPEAT PROCESS.
C IF NTHSET IS ZERO IT MEANS THERE IS NO MORE DATA, START PLOTTING.
         READ(11,250) NTHSET
         IF(NTHSET) 20,20,25
25        WRITE(12,150) NPOINT
         JJ=JJ+6
         GO TO 5
20       NPOINT=-1
         WRITE(12,150) NPOINT
         CLOSE(UNIT=12,DEVICE='DSK',FILE='SAMY02.DAT')
         CALL PLOTPR
         GO TO 1002
250      FORMAT(I2)
150      FORMAT(I4)
100      FORMAT(7F8.5)
300      FORMAT(9E15.8)
400      FORMAT(3A5)
450      FORMAT(1H ,'SMALL R SUB A=',E15.8,'  L=',E15.8,'  RA=',E15.8/)
1000     WRITE(6,1001)
1001     FORMAT(1H ,'BESSEL FUNCTION DID NOT CONVERGE')
1002     STOP
         END
```

BEST AVAILABLE COPY

```
C
C
      SUBROUTINE SCHARG
      COMMON/LABS/PARAM,IER,A1,GAM,LOVLAM,T,Z,NPOINT,DZ,ENERO,RSUBB2,
     !  FIOMRA,ZSUBE,RSUBB,EPS,GAMMAC,EREBW2,BABO,IDATE,RA,SCRIPR
      REAL LOVLAM
      DIMENSION IDATE(3),PARAM(70),T(1000),Z(1000),FIOMRA(15)
      EREBW2=0.0
      RETURN
      END

C  <SAGHER>PROG2.FOR;57    TUE 21-DEC-76 11:51AM                    PAGE 1:2

C
C
      SUBROUTINE PLOTPR
      DIMENSION X(1002),Y(1002),Q(6,1000),IYAXIS(7),LABEL(2),
     !    IGAMC(2),NAME(2),IDATE(3),IGAM(2),ILOVLM(2),PARAM(70),
     !    Z(1000),T(1000),FIOMRA(15),IBABO(2)
      REAL LOVLAM
      COMMON/LABS/PARAM,IER,A1,GAM,LOVLAM,T,Z,NPOINT,DZ,ENERO,RSUBB2,
     !   FIOMRA,ZSUBE,RSUBB,EPS,GAMMAC,EREBW2,BABO,IDATE,RA,SCRIPR
      DATA IXAXIS,IYAXIS/'T','R','THETA','Z','Z-DZ*','T','ERROR',
     !     'DELTZ'/
      DATA NAME/'PROGR','AM #2'/
      DATA IBABO,IRSUBA,IGAMC,IZSUBE/'BA/BO','=','RA=','GAMMA','C=',
     !     'ZE='/
      DATA IGAM,ILOVLM/'GAMMA','=','L/LAM','BDA='/
      DATA IBLANK/' '/
      OPEN(UNIT=12,DEVICE='DSK',FILE='SAMY02.DAT')
      JJ=1
8     I=0
      WRITE(6,150)
150   FORMAT(1H ,' PLOT NEW CASE')
      OPEN(UNIT=20,DEVICE='DSK',FILE='SPLT02.DAT')
      CALL PLOTE(30,20)
      BABO=PARAM(JJ)
      GAMMAC=PARAM(JJ+1)
      ZSUBE=PARAM(JJ+2)
      RA=PARAM(JJ+3)
      LOVLAM=PARAM(JJ+4)
      GAM=PARAM(JJ+5)
9     READ(12,120) NPOINT
      IF(NPOINT) 11,11,10
10    I=I+1
      IF(I .GT. 1000) GO TO 15
      READ(12,130)X(I),Q(1,I),Q(2,I),Q(3,I),A,B,C,Q(4,I),Q(5,I)
      GO TO 9
11    READ(12,120) NPOINT
      READ(12,130) (Q(6,K),K=1,NPOINT)
      DO 12 J=1,6
      LABEL(1)=IYAXIS(J)
      LABEL(2)=IBLANK
      IF(J.EQ.4) LABEL(2)=IYAXIS(5)
      IF(J .EQ. 5) LABEL(1)=IYAXIS(6)
      IF(J .EQ. 6) LABEL(1)=IYAXIS(7)
      DO 13 K=1,I
13    Y(K)=Q(J,K)
      CALL CPLOT1(1,X,7.0,IXAXIS,1,I,Y,6.0,LABEL,6)
      CALL PLOT(0.0,0.0,999)
      CALL SYMBOL(5.0,8.0,0.10,NAME,0.0,10)
      CALL SYMBOL(5.0,7.75,0.10,IDATE,0.0,12)
      CALL SYMBOL(5.0,7.50,0.10,IBABO,0.0,6)
      CALL NUMBER(6.2,7.50,0.10,BABO,0.0,5)
      CALL SYMBOL(5.0,7.25,0.10,IGAMC,0.0,7)
      CALL NUMBER(6.2,7.25,0.10,GAMMAC,0.0,5)
      CALL SYMBOL(5.0,7.00,0.10,IZSUBE,0.0,3)
```

```
      CALL NUMBER(6.2,7.00,0.10,ZSUBE,0.0,5)
      CALL SYMBOL(5.0,6.75,0.10,IRSUBA,0.0,3)
      CALL NUMBER(6.2,6.75,0.10,RA,0.0,5)
      CALL SYMBOL(5.0,6.50,0.10,ILOVLM,0.0,9)
      CALL NUMBER(6.4,6.50,0.10,LOVLAM,0.0,5)
      CALL SYMBOL(5.0,6.25,0.10,IGAM,0.0,6)
      CALL NUMBER(6.2,6.25,0.10,GAM,0.0,5)
      CALL PLOT(0.0,0.0,999)
      CALL PLOT(8.5,0.0,-3)
12    CONTINUE
      JJ=JJ+6
      READ(12,120) NPOINT
      IF(NPOINT .EQ. 0) GO TO 8
      GO TO 16
15    WRITE(6,140)

C  <SAGHER>PROG2.FOR;57   TUE 21-DEC-76 11:51AM                    PAGE 1:3

120   FORMAT(I4)
130   FORMAT(9E15.8)
140   FORMAT(1X,'MORE THAN 1000 POINTS')
16    STOP
      END
C
C
C SUBROUTINE CLIPDI PARAMETERS
C  H IS DEL T
C  X IS T(TIME)
C  NOEQ IS NUMBER OF EQUATIONS
C  Y IS AN ARRAY CONTAINING INITIAL VALUES OF VARIABLES
C  XMAX IS THE END VALUE OF T (CLIPDI IS EXITED WHEN T=TMAX)
C  EMAX IS UPPER BOUND OF CONVERGENCE CRITERION
C  EMIN IS LOWER BOUND OF CONVERGENCE CRITERION
C  E=(EMAX+EMIN)/2
C  PRNDEL IS USED JUST FOR THE PURPOSE OF DETERMINING WHEN TO CALL PRINT SUB
      SUBROUTINE CLIPDI(H,X,NOEQ,Y,XMAX,EMAX,EMIN,E,PRNDEL)
      DIMENSION IDATE(3),Y(6),DY(6),Y1(6),DY1(6),DY1C(6),HY(6),
     !     DHY(6),HYC(6),Y1C(6),FIOMRA(15),T(1000),Z(1000),PARAM(70)
      COMMON/LABS/PARAM,IER,A1,GAM,LOVLAM,T,Z,NPOINT,DZ,ENERO,RSUBB2,
     !   FIOMRA,ZSUBE,RSUBB,EPS,GAMMAC,EREBW2,RABO,IDATE,RA,SCRIPR
      INTEGER BOOL,BOOLH
      REAL LOVLAM
      CALL F(X,Y,DY)
10    DELTA=0.0
      IF(NPOINT .GE. 1000) GO TO 150
      CALL PRNT(X,H,NOEQ,Y,DY)
15    IF((Y(1).GE.SCRIPR) .OR. (Y(1).LE.0.0)) GO TO 110
      KOUNT=0
      BOOLH=0
      BOOL=0
      IF((X+H) .GT. XMAX) GO TO 100
20    DO 21 I=1,NOEQ
21    Y1(I)=DY(I)*H+Y(I)
      CALL F(X+H,Y1,DY1)
      DO 22 I=1,NOEQ
22    HY(I)=0.5*(Y(I)+Y1(I))+0.125*H*(DY(I)-DY1(I))
30    CALL F(X+0.5*H,HY,DHY)
      DO 31 I=1,NOEQ
31    Y1C(I)=((4.0*DHY(I)+DY(I)+DY1(I))*H)/6.0+Y(I)
      CALL F(H+X,Y1C,DY1C)
      IF(IER.GT.0) RETURN
      DO 32 I=1,NOEQ
```

BEST AVAILABLE COPY

BEST AVAILABLE COPY

```
32      HYC(I)=0.5*(Y(I)+Y1C(I))+0.125*H*(DY(I)-DY1C(I))
        DO 52 I=1,NOEQ
        CO=0.0
        IF((Y1C(I) .EQ. 0.0) .AND. (Y1(I) .NE. 0.0)) GO TO 70
        IF((Y1C(I) .NE. 0.0) .AND. (Y1(I) .EQ. 0.0)) CO=10.0
        IF((Y1C(I) .NE. 0.0) .AND. (Y1(I) .NE. 0.0)) CO=ABS((Y1C(I)-
     !       Y1(I))/Y1(I))
        IF(BOOL.EQ.1) GO TO 50
        IF(CO.LE.EMAX) GO TO 33
        BOOL=1
        H=0.5*H
        KOUNT=KOUNT+1
        IF(KOUNT.LE.10) GO TO 20
        WRITE(6,130)
        GO TO 140
33      IF(BOOL=.EQ.1) GO TO 50
        IF((I.NE.1).OR.((CO.GE.EMIN).OR.((H+H+X).GE.XMAX)) GO TO 40
        DO 34 J=2,NOEQ
        CO=0.0
        IF((Y1C(J) .EQ. 0.0) .AND. (Y1(J) .NE. 0.0)) GO TO 70
        IF((Y1C(J) .NE. 0.0) .AND. (Y1(J) .EQ. 0.0)) CO=10.0
        IF((Y1C(J) .NE. 0.0) .AND. (Y1(J) .NE. 0.0)) CO=ABS((Y1C(J)-
     !       Y1(J))/Y1(J))
        IF(CO .EQ. 0.0) GO TO 40
        IF(CO.LT.EMIN) GO TO 34
        GO TO 40


C  <SAGHER>PROG2.FOR;57    TUE 21-DEC-76 11:51AM                    PAGE 1:4

34      CONTINUE
        H=H+H
        GO TO 20
40      BOOL=1
50      IF(CO.LE.E) GO TO 52
        DO 51 J=1,NOEQ
        HY(J)=HYC(J)
        Y1(J)=Y1C(J)
        DY1(J)=DY1C(J)
51      CONTINUE
        GO TO 30
52      CONTINUE
        X=X+H
        DO 60 I=1,NOEQ
        Y(I)=Y1C(I)
60      DY(I)=DY1C(I)
        DELTA=DELTA+H
        IF(DELTA.LT.PRNDEL) GO TO 15
        GO TO 10
100     CONTINUE
        RETURN
110     WRITE(6,120)
120      FORMAT(1X,'H IS GREATER THAN SCRIPR OR LESS THAN 0')
130     FORMAT(1X,'HALVED H 10 TIMES, NO CONVERGENCE')
140     CONTINUE
        RETURN
150     WRITE(6,160)
160     FORMAT(1H ,'NUMBER OF POINTS EXCEEDED 1000'/
     !          1H ,'INCREASE DIMENSION OF T AND Z')
        RETURN
70      WRITE(6,170)
170      FORMAT(1H ,'PROGRAM CAN NOT CONVERGE,Y1C=0,Y1 NOT 0')
        RETURN
        END
```

BEST AVAILABLE COPY

```
C
C
C  MODIFIED BESSEL FUNCTION OF ORDER 0
C  X IS THE INPUT, RI0 IS THE OUTPUT
      SUBROUTINE BI0(X,RI0)
      RI0=ABS(X)
      IF(RI0-3.75)1,1,2
1     Z=X*X*7.111111E-2
      RI0=(((((4.5813E-3*Z+3.60768E-2)*Z+2.659732E-1)*Z+1.206749)*Z
     1   +3.089942)*Z+3.515623)*Z+1.0
      RETURN
2     Z=3.75/RI0
      RI0=EXP(RI0)/SQRT(RI0)*(((((((((3.92377E-3*Z-1.647633E-2)*Z
     1        +2.635537E-2)*Z-2.057706E-2)*Z+9.16281E-3)*Z-1.57565E-3)*Z
     #        +2.25319E-3)*Z+1.328592E-2)*Z+3.989423E-1)
      RETURN
      END
C
C
C  MODIFIED BESSEL FUNCTION OF ORDER 1
C  X AND ZI ARE INPUT, RI1 IS OUTPUT
C  X IS THE ARGUMENT
C  ZI IS THE OUTPUT OF MODIFIED BESSEL FUNCTION OF ORDER 0 FOR
C  THE SAME ARGUMENT X.
      SUBROUTINE BI1(X,ZI,RI1)
      Q1=0.5*X
      IF(ABS(X)-5.0E-4) 6,6,2
2     A0=1.0
      A1=0.0
      B0=0.0
      B1=1.0
      FI=2.0


C  <SAGHER>PROG2.FOR;57    TUE 21-DEC-76 11:51AM                    PAGE 1:5


3     FI=FI+2.0
      AN=FI/ABS(X)
      A=AN*A1+A0
      B=AN*B1+B0
      A0=A1
      B0=B1
      A1=A
      B1=B
      G0=G1
      G1=A/B
      IF(ABS((G1-G0)/G1)-1.0E-6) 4,4,3
4     IF(X) 5,6,6
5     G1=-G1
6     G1=X/(2.0+X*G1)
      RI1=G1*ZI
10    RETURN
      END
C
C
C   Z AND R ARE INPUT, F1 AND F2 ARE OUTPUT
C   F1 AND F2 ARE COMPUTED FROM A SUMMATION EQUATION WHICH HAS A
C   MODIFIED BESSEL FUNCTION. THE SUMMATION IS SUMMED UP TO 12 TERMS.
C   IF IT DOES NOT CONVERGE WITHIN 12 TERMS AN ERROR MESSAGE IS PRINTED.
C   THE SUMMATIO IS TERMINATED AT TERM 12 BECAUSE AT TERM 13 AND ON
C  THE MODIFIED BESSEL FUNCTION RESULTS IN UNDERFLOW. EPS IS THE
C   CONVERGENCE CRITERION SET TO 10E-5 IN MAIN PROGRAM,IF NO CONVERGENCE
C   THEN CHANGE EPS TO 10E-4.
      SUBROUTINE F1F2(ZEE,R,F1,F2)
      DIMENSION FIOMRA(15),IDATE(3),T(1000),Z(1000),PARAM(70)
      COMMON/LABS/PARAM,IER,A1,GAM,LOVLAM,T,Z,NPOINT,DZ,ENERO,RSUBR2,
     !    FIOMRA,ZSUBE,RSUBR,EPS,GAMMAC,ERERW2,RAR0,IDATE,RA,SCRIPR
```

BEST AVAILABLE COPY

```
      REAL LOVLAM
      I=0
      SUM1=0.0
      SUM2=0.0
      FM=-1.0
1     I=I+1
      IF(I .GE. 13) GO TO 2
      FM=FM+2.0
      ARG1=FM*(ZEE-ZSUBE)
      ARG2=FM*RSUBB*R
      CALL BI0(ARG2,RI0)
      CALL BI1(ARG2,RI0,RI1)
      TERMI0=FIOMRA(I)*COS(ARG1)*RI0
      TERMI1=FIOMRA(I)*SIN(ARG1)*RI1
      SUM1=SUM1+TERMI0
      SUM2=SUM2+TERMI1
      IF(I.EQ.1) GO TO 3
      IF(ABS(SUM1-S1) .GT. EPS) GO TO 3
      IF(ABS(SUM2-S2) .LE. EPS) GO TO 4
3     S1=SUM1
      S2=SUM2
      GO TO 1
4     F1=SUM1+1.0
      F2=SUM2
      RETURN
2     WRITE(6,100)
100   FORMAT(1X,'F1 OR F2 DID NOT CONVERGE WITHIN 12 TERMS')
      IER=1
      RETURN
      END
C
C
      SUBROUTINE F(IEE,Y,DY)
      DIMENSION IDATE(3),Y(6),DY(6),PARAM(70),Z(1000),T(1000),
     !    FIOMRA(15)
      COMMON/LABS/PARAM,IER,A1,GAM,LOVLAM,T,Z,NPOINT,DZ,ENERO,RSUBB2,

C  <SAGHER>PROG2.FOR;57    TUE 21-DEC-76 11:51AM                    PAGE 1:6

     !    FIOMRA,ZSUBE,RSUBB,EPS,GAMMAC,EREBW2,RABO,IDATE,RA,SCRIPR
      REAL LOVLAM
      IF(IER.GT.0)RETURN
      CALL F1F2(Y(3),Y(1),F1,F2)
      IF(IER.GT.0)RETURN
      DY(1)=Y(4)
      DY(2)=Y(5)
      DY(3)=Y(6)
      A2=Y(1)*Y(5)
      A8=Y(4)*Y(5)
      A3=GAMMAC*RSUBB*A2*F2
      A4=RSUBB**2*Y(4)
      A9=RSUBB**2*A2
      A6=A9*A8
      A7=GAM*A1*Y(6)*Y(6)
      A5=A9*Y(1)
      B1=-GAMMAC*(F2*Y(6)/RSUBB-F1*Y(4))
      B2=2.0*GAM*A8
      B3=GAM*Y(1)
      B13=A1*A2
      B14=B13*A4
      B15=B13*A6
      B16=B13*A5
```

BEST AVAILABLE COPY

```
      B14=A1*Y(6)*Y(6)/A7
      B7=B3+B6*(1.0-B14)
      B8=B1-B2-B5
      B9=B4*(1.0-B14)
      B10=B13*A3*Y(6)/A7-B5*B14
      B11=(B8-B10)/B7
      B12=B9/B7
      C1=-GAMMAC*A2*F1+EREBW2
      C2=GAM+A1*A4*Y(4)
      C6=A1*Y(4)
      C3=-B3*Y(5)*Y(5)+C6*A6
      C4=C6*A5
      C5=C6*Y(6)
      D1=A1*A5
      D2=C4*B11
      D3=A1*Y(6)
      D4=C5/A7
      DY(4)=(C1-C3-D2-D4*(A3-D3*A6-D1*Y(6)*B11))/
     !       (C2-C4*B12-D4*D3*A4+D4*D1*Y(6)*B12)
      DY(5)=B11-B12*DY(4)
      DY(6)=(A3-A1*(A4*DY(4)+A6+A5*DY(5))*Y(6))/A7
      GAM=1.0/SQRT(1.0-LOVLAM*LOVLAM*(RSUBB2*(DR*DR+R*R*DTHETA*DTHETA)
     !       +DZ*DZ))
      A1=GAM*GAM*GAM*LOVLAM*LOVLAM
      RETURN
      END
C
C
C  SUBROUTINE PRNT IS CALLED BY SUBROUTINE CLIPDI WHENEVER DELTA T BECOMES
C  GREATER OR EQUAL TO PRNDEL
C    X IS THE VALUE OF CURRENT T
C    H IS THE VALUE OF CURRENT DELTA T
C    NOEQ IS THE NUMBER OF EQUATIONS
C    Y IS AN ARRAY CONTAINING THE 6 VARIABLES
C    DY IS AN ARRAY CONTAINING THE DERIVATIVES OF THE 6 VARIABLES
      SUBROUTINE PRNT(X,H,NOEQ,Y,DY)
      DIMENSION T(1000), Z(1000),Y(1),DY(1),PARAM(70),IDATE(3),
     !   FIOMRA(15)
      COMMON/LABS/PARAM,IER,A1,GAM,LOVLAM,T,Z,NPOINT,DZ,ENER0,RSUBB2,
     !   FIOMRA,ZSUBE,RSUBB,EPS,GAMMAC,EREBW2,BARO,IDATE,RA,SCRIPR
      REAL LOVLAM
      ZMDZT=Y(3)-DZ*X
C  COMPUTE ENERGY
      ENER1=RSUBB2*(DY(1)*DY(1)+Y(1)*Y(1)*DY(2)*DY(2))+DY(3)*DY(3)
      ENER=(ENER1-ENER0)/ENER0
      NPOINT=NPOINT+1

C  <SAGHER>PROG2.FOR;57    TUE 21-DEC-76 11:51AM                    PAGE 1:7

C  NPOINT IS THE COUNT OF HOW MANY TIMES THE 6 VARIABLES R,THETA,ETC. ARE SAVED
      WRITE(12,50)NPOINT
50    FORMAT(I4)
      WRITE(12,60) X,(Y(I),I=1,NOEQ),ZMDZT,ENER
60    FORMAT(9E15.8)
      T(NPOINT)=X
      Z(NPOINT)=Y(3)
      WRITE(10,10)X,H,ZMDZT
10    FORMAT(3H X=,E14.8,' H=',E15.8,' Z-DZ*T=',E15.8)
      WRITE(10,20)
20    FORMAT(/9X,'I',10X,'Y',17X,'DY')
      DO 40 I=1,NOEQ
      WRITE(10,30)I,Y(I),DY(I)
30    FORMAT(I10,2E17.8)
40    CONTINUE
      RETURN
      END
```

BEST AVAILABLE COPY

```
C  <SAGHER>PROGS.FOR;21    TUE 21-DEC-76 10:54AM                    PAGE 1

C ORBITRON STUDY PROGRAM #5 FOR SAM SENSIPER NOVEMBER 24,1976
C DC EQUATIONS, EXACT RELATIVISTIC, PLUS CONSTANT AC DRIVE, NO SPACE CHARGE
      DOUBLE PRECISION NAMED,NAMEI
      DIMENSION FIOMRA(15), Y(6),T(1000),Z(1000),PARAM(110),IDATE(3)
      REAL LORA,LOL,LLG,LOVLAM,L,LAMBDA,LORA2
      COMMON/LABS/PARAM,IER,RC1,TC1,TC2,TC3,ZC1,RESC1,LLG,PSI,PZ,LOL,
     !   LORA,PI2,T,Z,NPOINT,DZ,ENERO,RSUBB2,FIOMRA,ZSURF,RSUBB,EPS,
     !   GAMMAC,EREST2,BABO,IDATE,RA,A1,GAM,LOVLAM,SCRIPR
      OPEN(UNIT=12,DEVICE='DSK',FILE='SAMY02.DAT')
      OPEN(UNIT=6,DEVICE='TTY')
      JJ=1
 5    WRITE(5,510)
510   FORMAT(1H ,' NAME OF INPUT FILE',$)
      IER=0
      READ(5,500) NAMEI
500   FORMAT(A10)
      NAMED=NAMEI
      CALL RMOVE('Y',0,NAMED,3,1)
      OPEN(UNIT=10,DEVICE='DSK',FILE=NAMED)
      OPEN(UNIT=11,DEVICE='DSK',FILE=NAMEI)
      READ(11,400)IDATE(1),IDATE(2),IDATE(3)
      READ(11,100)DELT,TO,TEND,EMAX,EMIN,E,PRNDEL
     READ(11,100)R,THETA,ZO,DR
      READ(11,100)FGHZ,VKV,C,BABO,ZSURF,SCRIPR,BO,PZ,PSI
      READ(11,4) ICOMP
4     FORMAT(I1)
      PI=3.1415926
      PI2=PI+PI
      GAMMAI=1.0+VKV/511.006
      IF(ICOMP .EQ. 1) GO TO 3
      READ(11,100) SRA,L,RA
      GO TO 2
3     SRA=GAMMAI*0.299792/(1.6398*FGHZ)
      L=1.6398*SRA*SQRT(GAMMAI*GAMMAI-1.0)
      RA=PI2*SRA/L
      WRITE(6,450) SRA,L,RA
2     RSUBB=RA/SCRIPR
      RSUBB2=RSUBB*RSUBB
      GAMMAC=0.279923E-2*BO/FGHZ
      LAMBDA=0.299792/FGHZ
      CONS=4.0*BABO/(PI*RSUBB)
      LORA=LAMBDA/RA
      LOL=LAMBDA/L
      LOVLAM=L/LAMBDA
      WRITE(6,515)
515   FORMAT(1H ,'START NEW CASE')
      H=DELT
      X=TO
      EPS=1.0E-5
      NPOINT=0
      SUM=0.0
      BAB=BA/RSUBB
      LORA2=LORA*LORA
      SQRTPZ=SQRT(PZ)
      C1=(1.0-LORA2/(1.64*1.64))**0.25
      C2=.0623*LORA2*SQRTPZ
      C3=1.64/(RSUBB*LORA)
      RC1=1.1E-4*C2/C1
      TC1=C1*C2*C3
      TC2=C2/C1
      TC3=C2*C3*LOL/C1
      C4=1.64*RSUBB/LORA
```

```
      ZC1=1.18E-4*C1*C2*C4
      BESC1=3.83/RAB
      LLG=SQRT(1.0-LORA2/(1.64*1.64))/LOL
      FM=-1.0
      FI=1.0
      CONST=4.0*BARO/PI
      DO 10 J=1,12
C   <SAGHER>PROG5.FOR;21    TUE 21-DEC-76 10:54AM                    PAGE 1:1

      FM=FM+2.0
      ARG=FM*RA
      CALL BIO(ARG,RIO)
      ARG=FM*RSUBB
      CALL BESJ(ARG,1,RB1,0.0001,IER)
      IF(IER .GT. 0) GO TO 1000
      FIOMRA(J)=FI*CONST/(FM*RIO)
      SUM=SUM+FI*CONS*COS(FM*ZSURE)*RB1/(FM*FM*RIO)
      FI=-FI
10      CONTINUE
      PHI=1.0+SUM+SUM
      DTHETA=GAMMAC*0.5*(PHI-C)/GAMMAI
      RVTHZ=RSUBB*DTHETA*L/(LAMBDA*SQRT(1.0-1.0/(GAMMAI*GAMMAI)))
      DZ=LAMBDA*SQRT(1.0-1.0/(GAMMAI*GAMMAI))/(L*SQRT(1.0+RVTHZ*RVTHZ)
     !)
      ENERO=RSUBB2*(DR*DR+R*R*DTHETA*DTHETA)+DZ*DZ
      WRITE(10,175)
175   FORMAT(1H ,'PROGRAM#5,DC EQ.')
      WRITE(10,180)(IDATE(M),M=1,3),R,THETA,ZO,DR,DTHETA,DZ,BARO,
     !   GAMMAC,ZSURE,FGHZ,VKV,C,SCRIPR,RO,SRA,L,RA
180   FORMAT(1H ,3A5/1H ,'R=',E15.8,'  THETA=',E15.8,'  Z=',E15.8/
     !   1H ,'  DR=',E15.8,'  DTHETA=',E15.8,'  DZ=',E15.8/
     !   1H ,'  BARO=',E15.8,'  GAMMAC=',E15.8,'  ZSURE=',E15.8/
     !   1H ,'  FGHZ=',E15.8,'  VKV=',E15.8,'  C=',E15.8/
     !   1H ,'  SCRIPR=',E15.8,'  RO=',E15.8,'  SRA=',E15.8/
     !   1H ,'  L=',E15.8,'  RA=',E15.8/)
      CALL SCHARG
      GAM=1.0/SQRT(1.0-LOVLAM*LOVLAM*(RSUBB2*(DR*DR+R*R*DTHETA*DTHETA
     !     )+DZ*DZ))
      A1=GAM*GAM*GAM*LOVLAM*LOVLAM
      PARAM(JJ)=BARO
      PARAM(JJ+1)=GAMMAC
      PARAM(JJ+2)=ZSURE
      PARAM(JJ+3)=RA
      PARAM(JJ+4)=LOVLAM
      PARAM(JJ+5)=GAM
      PARAM(JJ+6)=LORA
      PARAM(JJ+7)=LOL
      PARAM(JJ+8)=PZ
      PARAM(JJ+9)=PSI
      Y(1)=R
      Y(2)=THETA
      Y(3)=ZO
      Y(4)=DR
      Y(5)=DTHETA
      Y(6)=DZ
      CALL CLIPDI(H,X,6,Y,TEND,FMAX,FMIN,E,PRNDEL)
      K=0
      WRITE(12,150) K
      ZT=Z(NPOINT)/T(NPOINT)
      DO 15 K=1,NPOINT
15    Z(K)=Z(K)-T(K)*ZT
      WRITE(10,185) (Z(K),K=1,NPOINT)
```

BEST AVAILABLE COPY

BEST AVAILABLE COPY

```
185     FORMAT(1H ,'Z(I)-T(I)*Z(END)/T(END)'/(5E16.7))
        WRITE(12,150) NPOINT
        WRITE(12,300) (Z(K),K=1,NPOINT)
        NPOINT=0
C AT THIS POINT ONE SET OF INPUT DATA HAS BEEN READ,THE DIFFERENTIAL
C EQUATIONS SOLVED AND THE OUTPUT SAVED ON FILE. NOW READ NTHSET WHICH
C IS A 2 DIGIT INTEGER. IF NTHSET IS NONZERO IT MEANS THERE IS ANOTHER SET
C OF INPUT DATA TO EXECUTE,GO TO STATEMENT LABEL 5 TO REPEAT PROCESS.
C IF NTHSET IS ZERO IT MEANS THERE IS NO MORE DATA, START PLOTTING.
        READ(11,250) NTHSET
        IF(NTHSET) 20,20,25
25       WRITE(12,150) NPOINT
        JJ=JJ+10
        GO TO 5

C  <SAGHER>PROG5.FOR;21    TUE 21-DEC-76 10:54AM                PAGE 1:2

20      NPOINT=-1
        WRITE(12,150) NPOINT
        CLOSE(UNIT=12,DEVICE='DSK',FILE='SAMY02.DAT')
        CALL PLOTPR
        GO TO 1002
250     FORMAT(I2)
150     FORMAT(I4)
100     FORMAT(9E8.5)
300     FORMAT(9E15.8)
400     FORMAT(3A5)
450      FORMAT(1H ,'SMALL R SUB A=',E15.8,'  L=',E15.8,'  RA=',E15.8/)
1000    WRITE(6,1001)
1001    FORMAT(1H ,'BESSEL FUNCTION DID NOT CONVERGE')
1002    STOP
        END
C
C
        SUBROUTINE SCHARG
        COMMON/LABS/PARAM,IER,RC1,TC1,TC2,TC3,ZC1,RESC1,LLG,PSI,PZ,LOL,
     !    LORA,PI2,T,Z,NPOINT,DZ,ENERO,RSUBR2,FIOMRA,ZSUBE,RSUBB,EPS,
     !    GAMMAC,EREBW2,BABO,IDATE,RA,A1,GAM,LOVLAM,SCRIPR
        REAL LLG,LOL,LORA,LOVLAM
        DIMENSION IDATE(3),PARAM(110),FIOMRA(15),T(1000),Z(1000)
        EREBW2=0.0
        RETURN
        END
C
C
        SUBROUTINE PLOTPR
        DIMENSION PARAM(110),ILOL(2),ILORA(2),X(1002),Y(1002),Q(6,1000),
     !  IYAXIS(7),LABEL(2),IRABO(2),IGAMC(2),NAME(2),IDATE(3),T(1000),
     !  IGAM(2),ILOVLM(2),Z(1000),FIOMRA(15)
        REAL LLG,LOL,LORA,LOVLAM
        COMMON/LABS/PARAM,IER,RC1,TC1,TC2,TC3,ZC1,RESC1,LLG,PSI,PZ,LOL,
     !    LORA,PI2,T,Z,NPOINT,DZ,ENERO,RSUBR2,FIOMRA,ZSUBE,RSUBB,EPS,
     !    GAMMAC,EREBW2,BABO,IDATE,RA,A1,GAM,LOVLAM,SCRIPR
        DATA IPZ,ILOL,ILORA,IPSI/'PZ=','LAMBD','A/L=','LAMBD','A/RA=',
     !    'PSI='/
        DATA IXAXIS,IYAXIS/'T','R','THETA','Z','Z-DZ*','I','ERROR',
     !        'DELTZ'/
        DATA NAME/'PROGR','AM #5'/
        DATA IRABO,IRSUBA,IGAMC,IZSUBE/'RA/BO','=','RA=','GAMMA','C=',
     !        'ZE='/
        DATA IGAM,ILOVLM/'GAMMA','=','L/LAM','BDA='/
        DATA IBLANK/' '/
        OPEN(UNIT=12,DEVICE='DSK',FILE='SAMY02.DAT')
        JJ=1
```

```
8       I=0
        WRITE(6,150)
150     FORMAT(1H ,' PLOT NEW CASE')
        OPEN(UNIT=20,DEVICE='DSK',FILE='SPLT02.DAT')
        CALL PLOTF(30,20)
        RABO=PARAM(JJ)
        GAMMAC=PARAM(JJ+1)
        ZSUBE=PARAM(JJ+2)
        RA=PARAM(JJ+3)
        LOVLAM=PARAM(JJ+4)
        GAM=PARAM(JJ+5)
        LORA=PARAM(JJ+6)
        LOL=PARAM(JJ+7)
        PZ=PARAM(JJ+8)
        PSI=PARAM(JJ+9)
9       READ(12,120) NPOINT
        IF(NPOINT) 11,11,10
10      I=I+1
        IF(I .GT. 1000) GO TO 15
        READ(12,130)X(I),Q(1,I),Q(2,I),Q(3,I),A,B,C,Q(4,I),Q(5,I)
        GO TO 9

C  <SAGHER>PROGS.FOR;21    TUE 21-DEC-76 10:54AM                    PAGE 1:3

11      READ(12,120) NPOINT
        READ(12,130) (Q(6,K),K=1,NPOINT)
        DO 12 J=1,6
        LABEL(1)=IYAXIS(J)
        LABEL(2)=IBLANK
        IF(J.EQ.4) LABEL(2)=IYAXIS(5)
        IF(J .EQ. 5) LABEL(1)=IYAXIS(6)
        IF(J .EQ. 6) LABEL(1)=IYAXIS(7)
        DO 13 K=1,I
13      Y(K)=Q(J,K)
        CALL CPLOT1(1,X,7.0,IXAXIS,1,I,Y,6.0,LABEL,6)
        CALL PLOT(0.0,0.0,999)
        CALL SYMBOL(5.0,8.0,0.10,NAME,0.0,10)
        CALL SYMBOL(5.0,7.75,0.10,IDATE,0.0,12)
        CALL SYMBOL(5.0,7.50,0.10,IRABO,0.0,6)
        CALL NUMBER(6.2,7.50,0.10,RABO,0.0,5)
        CALL SYMBOL(5.0,7.25,0.10,IGAMC,0.0,7)
        CALL NUMBER(6.2,7.25,0.10,GAMMAC,0.0,5)
        CALL SYMBOL(5.0,7.00,0.10,IZSUBE,0.0,3)
        CALL NUMBER(6.2,7.00,0.10,ZSUBE,0.0,5)
        CALL SYMBOL(5.0,6.75,0.10,IRSUBA,0.0,3)
        CALL NUMBER(6.2,6.75,0.10,RA,0.0,5)
        CALL SYMBOL(5.0,6.50,0.10,ILOVLM,0.0,9)
        CALL NUMBER(6.4,6.50,0.10,LOVLAM,0.0,5)
        CALL SYMBOL(5.0,6.25,0.10,IGAM,0.0,6)
        CALL NUMBER(6.2,6.25,0.10,GAM,0.0,5)
        CALL SYMBOL(5.0,6.00,0.10,IPZ,0.0,3)
        CALL NUMBER(6.2,6.00,0.10,PZ,0.0,4)
        CALL SYMBOL(5.0,5.75,0.10,ILORA,0.0,10)
        CALL NUMBER(6.5,5.75,0.10,LORA,0.0,4)
        CALL SYMBOL(5.0,5.50,0.10,IPSI,0.0,5)
        CALL NUMBER(6.2,5.50,0.10,PSI,0.0,4)
        CALL PLOT(0.0,0.0,999)
        CALL PLOT(8.5,0.0,-3)
12      CONTINUE
        JJ=JJ+10
        READ(12,120) NPOINT
        IF(NPOINT .EQ. 0) GO TO 8
        GO TO 16
```

BEST AVAILABLE COPY

```
15        WRITE(6,140)
120       FORMAT(I4)
130       FORMAT(9E15.8)
140       FORMAT(1X,'MORE THAN 1000 POINTS')
16        STOP
          END
C
C
C  SUBROUTINE CLIPDI PARAMETERS
C   H IS DELTA T
C   X IS T(TIME)
C   NOEQ IS THE NUMBER OF EQUATINS
C   Y IS AN ARRAY CONTAINING INITIAL VALUES OF VARIABLES
C   XMAX IS THE END VALUE OF T (CLIPDI IS EXITED WHEN T=TMAX)
C   EMAX IS THE UPPER BOUND OF CONVERGENCE CRITERION
C   EMIN IS THE LOWER BOUND OF CONVERGENCE CRITERION
C   E=(EMAX+EMIN)/2
C   PRNDEL IS USED JUST FOR THE PURPOSE OF DETERMINING WHEN TO CALL PRINT SUN
          SUBROUTINE CLIPDI(H,X,NOEQ,Y,XMAX,EMAX,EMIN,E,PRNDEL)
          COMMON/LABS/PARAM,IER,RC1,TC1,TC2,TC3,ZC1,RESC1,LLG,PSI,PZ,LOL,
         !   LORA,PI2,T,Z,NPOINT,DZ,ENERO,RSUBM2,FIOMRA,ZSUBE,RSUBB,EPS,
         !   GAMMAC,ERERW2,RABO,IDATE,RA,A1,GAM,LOVLAM,SCRIPR
          REAL LLG,LOL,LORA,LOVLAM
          DIMENSION DY(6),Y1(6),DY1(6),DY1C(6),HY(6),DHY(6),HYC(6),Y1C(6),
         !   IDATE(3),Y(6),PARAM(110),FIOMRA(15),T(1000),Z(1000)
          INTEGER BOOL,BOOLH
          CALL F(X,Y,DY)
10        DELTA=0.0
          IF(NPOINT .GE. 1000) GO TO 150
          CALL PRNT(X,H,NOEQ,Y,DY)
C  <SAGHER>PROGS.FOR;21    TUE 21-DEC-76 10:54AM                    PAGE 1;4

15        IF((Y(1).GE. SCRIPR) .OR. (Y(1).LE.0.0)) GO TO 110
          KOUNT=0
          KOUNTH=0
          BOOL=0
          IF((X+H) .GT. XMAX) GO TO 100
20        DO 21 I=1,NOEQ
21        Y1(I)=DY(I)*H+Y(I)
          CALL F(X+H,Y1,DY1)
          DO 22 I=1,NOEQ
22        HY(I)=0.5*(Y(I)+Y1(I))+0.125*H*(DY(I)-DY1(I))
30        CALL F(X+0.5*H,HY,DHY)
          DO 31 I=1,NOEQ
31        Y1C(I)=((4.0*DHY(I)+DY(I)+DY1(I))*H)/6.0+Y(I)
          CALL F(H+X,Y1C,DY1C)
          IF(IER.GT.0) RETURN
          DO 32 I=1,NOEQ
32        HYC(I)=0.5*(Y(I)+Y1C(I))+0.125*H*(DY(I)-DY1C(I))
          DO 52 I=1,NOEQ
          CO=0.0
          IF((Y1C(I) .EQ. 0.0) .AND. (Y1(I) .NE. 0.0)) GO TO 70
          IF((Y1C(I) .NE. 0.0) .AND. (Y1(I) .EQ. 0.0)) CO=10.0
          IF((Y1C(I) .NE. 0.0) .AND. (Y1(I) .NE. 0.0)) CO=ABS((Y1C(I)-
         !      Y1(I))/Y1(I))
          IF(BOOL.EQ.1) GO TO 50
          IF(CO.LE.EMAX) GO TO 33
          BOOLH=1
          H=0.5*H
          KOUNT=KOUNT+1
          IF(KOUNT.LE.10) GO TO 20
          WRITE(6,130)
          GO TO 140
```

BEST AVAILABLE COPY

```
33      IF(BOOLH.EQ.1) GO TO 50
        IF((I.NE.1).OR.(CO.GE.EMIN).OR.((H+H+X).GE.XMAX)) GO TO 40
        DO 34 J=2,NOEQ
        CO=0.0
        IF((Y1C(J) .EQ. 0.0) .AND. (Y1(J) .NE. 0.0)) GO TO 70
        IF((Y1C(J) .NE. 0.0) .AND. (Y1(J) .EQ. 0.0)) CO=10.0
        IF((Y1C(J) .NE. 0.0) .AND. (Y1(J) .NE. 0.0)) CO=ABS((Y1C(J)-
     !       Y1(J))/Y1(J))
        IF(CO .EQ. 0.0) GO TO 40
        IF(CO.LT.EMIN) GO TO 34
        GO TO 40
34      CONTINUE
        H=H+H
        GO TO 20
40      BOOL=1
50      IF(CO.LE.E) GO TO 52
        DO 51 J=1,NOEQ
        HY(J)=HYC(J)
        Y1(J)=Y1C(J)
        DY1(J)=DY1C(J)
51      CONTINUE
        GO TO 30
52      CONTINUE
        X=X+H
        DO 60 I=1,NOEQ
        Y(I)=Y1C(I)
60      DY(I)=DY1C(I)
        DELTA=DELTA+H
        IF(DELTA.LT.PENDEL) GO TO 15
        GO TO 10
100     CONTINUE
        RETURN
110     WRITE(6,120)
120     FORMAT(1X,'H IS GREATER THAN SCRIPR OR LESS THAN 0')
130     FORMAT(1X,'HALVED H 10 TIMES, NO CONVERGENCE')
140     CONTINUE
        RETURN
150     WRITE(6,160)

C  <SAGHER>PROG5.FOR;21    TUE 21-DEC-76 10:54AM                    PAGE 1:5

160     FORMAT(1H ,'NUMBER OF POINTS EXCEEDED 1000'/
     !          1H ,'INCREASE DIMENSION OF T AND Z')
        RETURN
70      WRITE(6,170)
170     FORMAT(1H ,'PROGRAM CAN NOT CONVERGE,Y1C=0,Y1 NOT 0')
        RETURN
        END
C
C
C MODIFIED BESSEL FUNCTION OF ORDER 0
C X IS THE INPUT, RIO IS THE OUTPUT
        SUBROUTINE RIO(X,RIO)
        RIO=ABS(X)
        IF(RIO-3.75)1,1,2
1       Z=X*X*7.111111E-2
        RIO=(((((4.5813E-3*Z+3.607688E-2)*Z+2.659732E-1)*Z+1.206749)*Z
     1    +3.089942)*Z+3.515623)*Z+1.0
        RETURN
2       Z=3.75/RIO
        RIO=EXP(RIO)/SQRT(RIO)*(((((((3.92377E-3*Z-1.647633E-2)*Z
     1       +2.635537E-2)*Z-2.05770GE-2)*Z+9.16281E-3)*Z-1.57565E-3)*Z
     "       +2.25314E-3)*Z+1.328592E-2)*Z+3.989423E-1)
        RETURN
        END
```

BEST AVAILABLE COPY

```
C
C
C  MODIFIED BESSEL FUNCTIO OF ORDER 1
C  X AND ZI ARE INPUT, RI1 IS OUTPUT
C  X IS THE ARGUMENT
C  ZI IS THE OUTPUT OF MODIFIED BESSEL FUNCTION OF ORDER 0 FOR
C  THE SAME ARGUMENT X.
      SUBROUTINE BI1(X,ZI,RI1)
      Q1=0.5*X
      IF(ABS(X)-5.0E-4) 6,6,2
2     A0=1.0
      A1=0.0
      B0=0.0
      B1=1.0
      FI=2.0
3     FI=FI+2.0
      AN=FI/ABS(X)
      A=AN*A1+A0
      B=AN*B1+B0
      A0=A1
      B0=B1
      A1=A
      B1=B
      Q0=Q1
      Q1=A/B
      IF(ABS((Q1-Q0)/Q1)-1.0E-6) 4,4,3
4     IF(X) 5,6,6
5     Q1=-Q1
6     Q1=X/(2.0+X*Q1)
      RI1=Q1*ZI
10    RETURN
      END
C
C
C  Z AND R ARE INPUT, F1 AND F2 ARE OUTPUT.
C  F1 AND F2 ARE COMPUTED FROM A SUMMATION EQUATION WHICH HAS A
C  MODIFIED BESSEL FUNCTION. THE SUMMATION IS SUMMED UP TO 12 TERMS.
C  IF IT DOES NOT CONVERGE WITHIN 12 TERMS AN ERROR MESSAGE IS PRINTED.
C  THE SUMMATION IS TERMINATED AT TERM 12 BECAUSE AT TERM 13 AND ON
C  THE MODIFIED BESSEL FUNCTION RESULTS IN UNDERFLOW. EPS ISTHE
C  CONVERGENCE CRITERION SET TO 10E-5 IN MAIN PROGRAM,IF NO CONVERGENCE

C  <SAGEEE>PROGS.FOR;21    TUE 21-DEC-76 10:54AM                    PAGE 1:6

C  THEN CHANGE EPS TO 10E-4.
      SUBROUTINE F1F2(ZEE,R,F1,F2)
      DIMENSION FIOMRA(15),PARAM(110),Z(1000),T(1000),IDATE(3)
      COMMON/LABS/PARAM,IER,RC1,TC1,TC2,TC3,ZC1,BESC1,LLG,PSI,PZ,LOL,
     !   LORA,PI2,T,Z,NPOINT,DZ,ENERO,RSUBB2,FIOMRA,ZSUBE,RSUBB,EPS,
     !   GAMMAC,ERFRW2,BARO,IDATE,RA,A1,GAM,LOVLAM,SCRIPR
      REAL LLG,LOL,LORA,LOVLAM
      I=0
      SUM1=0.0
      SUM2=0.0
      FM=-1.0
1     I=I+1
      IF(I .GE. 13) GO TO 2
      FM=FM+2.0
      ARG1=FM*(ZEE-ZSUBE)
      ARG2=FM*RSUBB*R
      CALL BI0(ARG2,RI0)
      CALL BI1(ARG2,RI0,RI1)
      TERMI0=FIOMRA(I)*COS(ARG1)*RI0
      TERMI1=FIOMRA(I)*SIN(ARG1)*RI1
      SUM1=SUM1+TERMI0
      SUM2=SUM2+TERMI1
```

BEST AVAILABLE COPY

```
      IF(I.EQ.1) GO TO 3
      IF(ABS(SUM1-S1) .GT. EPS) GO TO 3
      IF(ABS(SUM2-S2) .LE. EPS) GO TO 4
3     S1=SUM1
      S2=SUM2
      GO TO 1
4     F1=SUM1+1.0
      F2=SUM2
      RETURN
2     WRITE(6,100)
100   FORMAT(1X,'F1 OR F2 DID NOT CONVERGE WITHIN 12 TERMS')
      IER=1
      RETURN
      END
C
C
C  T AND Y ARE INPUT, DY IS OUTPUT
C  Y IS AN ARRAY CONTAINING THE CURRENT VALUES OF THE 6 VARIABLES
C  UPON EXIT DY WILL CONTAIN THE DERIVATIVES OF THE 6 VARIABLES
      SUBROUTINE F(TEE,Y,DY)
      DIMENSION IDATE(3),FIOMRA(15),T(1000),Z(1000),PARAM(110),DY(6),
     !   Y(6)
      REAL LLG,LOL,LORA,LOVLAM
      COMMON/LABS/PARAM,IER,RC1,TC1,TC2,TC3,ZC1,BESC1,LLG,PSI,PZ,LOL,
     !  LORA,PI2,I,Z,NPOINT,DZ,ENERO,RSUBB2,FIOMRA,ZSUBF,RSUBB,EPS,
     !  GAMMAC,EREBW2,BABO,IDATE,RA,A1,GAM,LOVLAM,SCRIPR
      IF(IER.GT.0)RETURN
      CALL FIF2(Y(3),Y(1),F1,F2)
      IF(IER.GT.0)RETURN
      ARG=T-PSI-LLG*Y(3)
      IF(ARG .LT.0.0) GO TO 21
20    IF(ARG .LE. PI2) GO TO 22
      ARG=ARG-PI2
      GO TO 20
21    IF(ARG .GE. -PI2) GO TO 22
      ARG=ARG+PI2
      GO TO 21
22    CONTINUE
      SINE=SIN(ARG)
      COSINE=COS(ARG)
      ARG=BESC1*Y(1)
      CALL BESJ(ARG,0,BR0,0.0001,IER)
      IF(IER .GT. 0) GO TO 10
      CALL BESJ(ARG,1,RB1,0.0001,IER)
      IF(IER .GT. 0) GO TO 10
      ADD1=RC1*RB0*Y(1)*Y(5)*SINE
      ADD2=1.18E-4*(TC1*RB1*Y(6)*COSINE-TC2*RB0*Y(4)*SINE-TC3*RB1*

C   <SAGHER>PROGS.FOR;21    TUE 21-DEC-76 10:54AM                PAGE 1:7

     !          COSINE)
      ADD3=-ZC1*RB1*Y(1)*Y(5)*COSINE
      DY(1)=Y(4)
      DY(2)=Y(5)
      DY(3)=Y(6)
      A2=Y(1)*Y(5)
      A8=Y(4)*Y(5)
      A3=GAMMAC*RSUBB*A2*F2+ADD3
      A4=RSUBB2*Y(4)
      A9=RSUBB2*A2
      A6=A9*A8
      A7=GAM+A1*Y(6)*Y(6)
      A5=A9*Y(1)
```

BEST AVAILABLE COPY

```
      B1=-GAMMAC*(F2*Y(6)/RSUBB-F1*Y(4))+ADD2
      B2=2.0*GAM*A8
      B3=GAM*Y(1)
      B13=A1*A2
      B4=B13*A4
      B5=B13*A6
      B6=B13*A5
      B14=A1*Y(6)*Y(6)/A7
      B7=B3+B6*(1.0-B14)
      B8=B1-B2-B5
      B9=B4*(1.0-B14)
      B10=B13*A3*Y(6)/A7-B5*B14
      B11=(B8-B10)/B7
      B12=B9/B7
      C1=-GAMMAC*A2*F1*EREBW2+ADD1
      C2=GAM+A1*A4*Y(4)
      C6=A1*Y(4)
      C3=-B3*Y(5)*Y(5)+C6*A6
      C4=C6*A5
      C5=C6*Y(6)
      D1=A1*A5
      D2=C4*B11
      D3=A1*Y(6)
      D4=C5/A7
      DY(4)=(C1-C3-D2-D4*(A3-D3*A6-D1*Y(6)*B11))/
     !        (C2-C4*B12-D4*D3*A4+D4*D1*Y(6)*B12)
      DY(5)=B11-B12*DY(4)
      DY(6)=(A3-A1*(A4*DY(4)+A6+A5*DY(5))*Y(6))/A7
      GAM=1.0/SQRT(1.0-LOVLAM*LOVLAM*(RSUBB2*(DR*DR+R*R*DTHETA*DTHETA)
     !        +DZ*DZ))
      A1=GAM*GAM*GAM*LOVLAM*LOVLAM
      RETURN
10    WRITE(6,1000)
1000  FORMAT(1H ,'BESSEL FUNCTION DID NOT CONVERGE')
      STOP
      END
C
C
C  SUBROUTINE PRNT IS CALLED BY SUBROUTINE CLIPDI WHENEVER DELTA T BECOMES
C  GREATER OR EQUAL TO PRNDEL
C    X IS THE CURRENT VALUE OF T
C    H IS THE CURRENT VALUE OF DELTA T
C    NOEQ IS THE NUMBER OF EQUATIONS
C    Y IS AN ARRAY CONTAINING THE 6 VARIABLES
C    DY IS AN ARRAY CONTAINING THE DERIVATIVES OF THE 6 VARIABLES
      SUBROUTINE PRNT(X,H,NOEQ,Y,DY)
      DIMENSION T(1000), Z(1000),FIOMRA(15),PARAM(110),IDATE(3),Y(1),
     !    DY(1)
      REAL LLG,LOL,LORA,LOVLAM
      COMMON/LAB5/PARAM,IER,PC1,TC1,TC2,TC3,ZC1,BESC1,LLG,PSI,PZ,LOL,
     !    LORA,PI2,T,Z,NPOINT,DZ,ENERO,RSUBB2,FIOMRA,ZSUBE,RSUBB,EPS,
     !    GAMMAC,EREBW2,BARO,IDATE,PA,A1,GAM,LOVLAM,SCRIPR
      ZMDZ1=Y(3)-PZ*X
      ENER1=RSUBB2*(DY(1)*DY(1)+Y(1)*Y(1)*DY(2)*DY(2))+DY(3)*DY(3)
      ENER=(ENER1-ENERO)/ENERO
      NPOINT=NPOINT+1
      WRITE(12,50)NPOINT

C  <SAGMER>PROG5.FOR;21    TUE 21-DEC-76 10:58AM                    PAGE 1:8

50    FORMAT(I4)
      WRITE(12,60) X,(Y(I),I=1,NOEQ),ZMDZ1,ENER
60    FORMAT(9E15.8)
      T(NPOINT)=X
      Z(NPOINT)=Y(3)
```

```
      WRITE(10,10)X,H,ZMDZT
10    FORMAT(3H X=,E14.8,' H=',E15.8,' Z-DZ*T=',E15.8)
      WRITE(10,20)
20    FORMAT(/9X,'I',10X,'Y',17X,'DY')
      DO 40 I=1,NOEQ
      WRITE(10,30)I,Y(I),DY(I)
30    FORMAT(I10,2E17.8)
40    CONTINUE
      RETURN
      END
C  <SAGHER>RTHETA.FOR;15    THU 18-NOV-76 2:00PM                    PAGE 1

C PROGRAM RTHETA TO PLOT R VERSUS THETA
      DIMENSION DUMMY(4)
      DIMENSION IDATE(3),IPROG(2)
      REAL LOVLAM
      DIMENSION IBARO(2),IGAMC(2),ILOVLM(2),IDTH(2)
      DIMENSION H(14),LLINE(16),R(1002),THETA(1002)
      DOUBLE PRECISION INFILE,OUTPUT
      DATA IBARO,IRSUBA,IGAMC,IZSUBE,ILOVLM,IDTH/
     !  'BA/RO','=','RA=','GAMMA','C=','ZE=','L/LAM',
     !    'RDA=','THETA',' R='/
      DATA IXAXIS,IYAXIS/'THETA','R'/
      OPEN(UNIT=6,DEVICE='TTY')
      WRITE(5,11)
11    FORMAT(1H ,'HOW MANY CASES: ',$)
      READ(5,21) NCASES
21    FORMAT(I1)
      DO 65 K=1,NCASES
      WRITE(5,10)
10    FORMAT(1H ,'NAME OF INPUT FILE: ',$)
      READ(5,20) INFILE
20    FORMAT(A10)
      OPEN(UNIT=20,FILE=INFILE)
      OUTPUT=INFILE
      CALL RMOVE('R',0,OUTPUT,3,1)
      OPEN(UNIT=21,FILE=OUTPUT)
      READ(20,26)IPROG(1),IPROG(2),IDATE(1),IDATE(2),IDATE(3),RR,TETA,
     !  Z0,DR,DTHETA,DZ,
     !    LOVLAM,BARO,RA,GAMMA,ZSUBE
26    FORMAT(1X,2A5/1X,3A5/3X,E15.8,8X,E15.8,4X,E15.8/5X,E15.8,9X,
     !  E15.8,5X,
     !    E15.8/11X,E15.8,8X,E15.8,5X,E15.8/7X,E15.8,8X,E15.8)
      N=0
30    READ(20,35,END=50)(LLINE(I),I=1,16)
35    FORMAT(16A5)
      DECODE(80,37,LLINE)AX
37    FORMAT(A5)
      IF(AX .NE. ' X=') GO TO 30
      N=N+1
      READ(20,35) (LLINE(I),I=1,16)
      READ(20,35) (LLINE(I),I=1,16)
      READ(20,40) R(N),X
      READ(20,40) THETA(N),X
40    FORMAT(10X,2E17.8)
      GO TO 30
50    IF(N .LE. 1) GO TO 70
      RMAX=R(1)
      RMIN=RMAX
      TMAX=THETA(1)
      TMIN=TMAX
```

```
      DO 51 I=2,N
      IF(R(I) .GT. RMAX) RMAX=R(I)
      IF(R(I) .LT. RMIN) RMIN=R(I)
      IF(THETA(I) .GT. TMAX) TMAX=THETA(I)
      IF(THETA(I) .LT. TMIN) TMIN=THETA(I)
51    CONTINUE
      DUMMY(1)=RMIN
      DUMMY(2)=RMAX
      CALL SCALE(DUMMY,7.0,2,1)
      R(N+1)=DUMMY(3)
      R(N+2)=DUMMY(4)
      DUMMY(1)=TMIN
      DUMMY(2)=TMAX
      CALL SCALE(DUMMY,7.0,2,1)
      THETA(N+1)=DUMMY(3)
      THETA(N+2)=R(N+2)
      IF(R(N+2) .GT. DUMMY(4)) GO TO 52
      THETA(N+2)=DUMMY(4)
      R(N+2)=DUMMY(4)
```

C <SAGHER>RTHETA.FOR;15 THU 18-NOV-76 2:00PM PAGE 1:1

```
52    CONTINUE
      CALL PLOTF(30,21)
      CALL PLOT(0.0,0.0,3)
      CALL AXIS(0.0,0.0,IYAXIS,1,7.0,90.0,R(N+1),R(N+2),2)
      CALL AXIS(0.0,0.0,IXAXIS,-5,7.0,0.0,THETA(N+1),THETA(N+2),2)
      CALL PLOT(0.0,0.0,999)
      CALL LINE(THETA,R,N,1,0,0)
      CALL PLOT(0.0,0.0,999)
      CALL SYMBOL(5.0,8.00,0.1,IPROG,0.0,10)
      CALL SYMBOL(5.0,7.75,0.1,IDATE,0.0,12)
      CALL SYMBOL(5.0,7.50,0.1,IBARO,0.0,6)
      CALL NUMBER(6.2,7.50,0.1,BARO,0.0,4)
      CALL SYMBOL(5.0,7.25,0.1,IGAMC,0.0,7)
      CALL NUMBER(6.2,7.25,0.1,GAMMA,0.0,4)
      CALL SYMBOL(5.0,7.00,0.1,IZSUBE,0.0,3)
      CALL NUMBER(6.2,7.00,0.1,ZSUBE,0.0,5)
      CALL SYMBOL(5.0,6.75,0.1,IRSUBA,0.0,3)
      CALL NUMBER(6.2,6.75,0.1,RA,0.0,4)
      CALL SYMBOL(5.0,6.50,0.1,ILOVLM,0.0,9)
      CALL NUMBER(6.4,6.50,0.1,LOVLAM,0.0,4)
      CALL SYMBOL(5.0,6.25,0.1,IDTH,0.0,8)
      CALL NUMBER(6.4,6.25,0.1,DTHETA,0.0,5)
      CALL PLOTF(0.0,0.0,999)
      CALL PLOT(8.5,0.0,-3)
65    CONTINUE
      GO TO 80
70    WRITE(6,71)
71    FORMAT(1H ,'NUMBER OF POINTS IS LESS THAN 2')
80    STOP
      END
```

```
C PROGRAM CORREL
C THIS PROGRAM REQUERES TWO INPUT FILES,FILE M1M2FL AND FILE PIIYJJ.
C FILE M1M2FL CONTAINS 3 PARAMETERS M1,M2,FL, IT IS CREATED BY THE USER.
C FILE PIIYJJ IS THE OUTPUT OF PROGRAM 2 OR 5. FILE PIIYJJ CONTAINS
C N VALUES OF THE 6 VARIABLES R,THETA Z, DR/DT,DTHETA/DT,DZ/DT,
C PROGRAM CORREL READS FROM FILE PIIYJJ ALL N VALUES OF R,Z, DTHETA/DT,
C THEN INTEGRATES THE MATHEMATICAL EQUATION. THE RESULT OF INTEGRATION
C IS SAVED ON FILE TTYOUT. THE RESULT IS ALSO PLOTTED AND SAVED ON FILE
C BFNM. THE THETA LIMITS OF INTEGRATION IS 0 TO 360 DEGREES IN STEPS OF
C 5 DEGREES. THE Z LIMITS OF INTEGRATION IS 0 TO 61 IN STEPS OF Z/60.
C IN BOAT, THE STEP SIZE IS FIXED AND IS NOT INPUT
C
      DOUBLE PRECISION INFILE,OUTPUT
      DIMENSION IDATE(3),IPROG(2),LLINE(16),R(1000),DTHETA(1000),
     !     Z(1000),COSINE(73),RESS(1000),QQ(73),RM2(1000),
     !   BFNM(62),YY(73),IRABO(2),IGAMC(2),ILOVLM(2),IDTH(2),
     !   ZAXIS(62),RDTH(1000)
      REAL LOVLAM
      DATA IXAXIS,IYAXIS/'Z','BFNM'/
      DATA IRABO,IRSUBA,IGAMC,IZSUBE,ILOVLM,IDTH/'BA/BO','=','RA=',
     !   'GAMMA','C=','ZE=','L/LAM','BDA=','THETA',' P='/
      OPEN(UNIT=6,DEVICE='TTY')
      OPEN(UNIT=11,DEVICE='DSK',FILE='TTYOUT.DAT')
      OPEN(UNIT=13,DEVICE='DSK',FILE='M1M2FL.DAT')
      READ(13,5) M1,M2,FL
5     FORMAT(I2,I2,F5.2)
      WRITE(5,10)
10    FORMAT(1H ,'NAME OF INPUT FILE: ',$)
      READ(5,20)INFILE
20    FORMAT(A10)
      OPEN(UNIT=20,FILE=INFILE)
      READ(20,26)IPROG(1),IPROG(2),IDATE(1),IDATE(2),IDATE(3),
     !   RR,THETA,ZO,DR,DTETA,DZ,LOVLAM,RABO,RA,GAMMA,ZSUBE
26    FORMAT(1X,2A5/1X,3A5/3X,E15.8,8X,E15.8,4X,E15.8/5X,E15.8,9X,
     !   E15.8,5X,E15.8/11X,E15.8,8X,E15.8,5X,E15.8/7X,E15.8,8X,E15.8)
      RAD=1.74532925E-2
      DO 13 J=1,73
13    YY(J)=0.0
      NDEG=5
      NDEL=360/NDEG+1
      N=0
30    READ(20,35,END=50)(LLINE(I),I=1,16)
35    FORMAT(16A5)
      DECODE(80,37,LLINE)AX
37    FORMAT(A3)
      IF(AX .NE. ' X=') GO TO 30
      N=N+1
      READ(20,35) (LLINE(I),I=1,16)
      READ(20,35) (LLINE(I),I=1,16)
      READ(20,40) R(N),DUMMY
      READ(20,40) DUMMY,DTHETA(N)
      READ(20,40)Z(N),DUMMY
40    FORMAT(10X,2E17.8)
      GO TO 30
50    INTER=N/60
      DO 17 J=1,NDEL
      FK=(J-1)*NDEG
      ZPRIME=FK*RAD
17    COSINE(J)=COS(ZPRIME*FL)
      IF(M2 .EQ. 0) GO TO 14
      DO 15 J=1,N
```

BEST AVAILABLE COPY

```
15          RM2(J)=R(J)**M2
14          CONTINUE
            WRITE(11,51)N,INTER
51          FORMAT(1H ,'N=',I3,'  INTERVAL=',I2/)
            DO 60 K=1,N
            ARG=1.91585*R(K)
            CALL BESJ(ARG,1,RB1,0.0001,IER)
            IF(IER .GT. 0) GO TO 1000
            BESS(K)=RB1*RB1
C   <SAGHER>CORREL.FOR;1    TUE 21-DEC-76 3:15PM                    PAGE 1:1

60           RDTH(K)=R(K)*DTHETA(K)
            I=0
            I1=1
            I2=INTER+1
            DENOLD=0.0
61          CONTINUE
            DO 68 K=1,NDEL
            FK=(K-1)*NDEG
            ZPRIME=FK*RAD
            J=0
            K2=I1
            ZZP=Z(I1)+ZPRIME
62          IF(Z(I1+J) .GT. ZZP) GO TO 63
            J=J+1
            K2=K2+1
            GO TO 62
63          K1=K2-1
            VZ=RDTH(I1)-CVZVZZ
            COEF=(ZZP-Z(K1))/(Z(K2)-Z(K1))
            RZZP=COEF*(R(K2)-R(K1))+R(K1)
            DTHZZP=COEF*(DTHETA(K2)-DTHETA(K1))+DTHETA(K1)
            VZZP=RZZP*DTHZZP-CVZVZZ
            F1=BESS(I1)*VZ*VZZP
            IF(M1 .NE. 0) F1=F1*R(I1)**M1
            I3=I1+1
            SUM=0.0
            DO 64 J=I3,I2
            ZZP=Z(J)+ZPRIME
65          IF(Z(K2) .GT. ZZP) GO TO 66
            K2=K2+1
            GO TO 65
66          K1=K2-1
            COEF=(ZZP-Z(K1))/(Z(K2)-Z(K1))
            RZZP=COEF*(R(K2)-R(K1))+R(K1)
            DTHZZP=COEF*(DTHETA(K2)-DTHETA(K1))+DTHETA(K1)
            VZ=RDTH(J)-CVZVZZ
            VZZP=RZZP*DTHZZP-CVZVZZ
            F2=BESS(J)*VZ*VZZP
            IF(M1 .NE. 0) F2=F2*R(J)**M1
            SUM=SUM+0.5*(F2+F1)*(Z(J)-Z(J-1))
            F1=F2
64          CONTINUE
            YY(K)=YY(K)+SUM
            QQ(K)=YY(K)*COSINE(K)
68          CONTINUE
            SUM=0.0
            RADN=NDEG
            RADN=RADN*RAD
            KK=NDEL-1
            DO 74 J=1,KK
```

```
74        SUM=SUM+0.5*(QQ(J+1)+QQ(J))*RADN
          FNUM=SUM
          SUM=0.0
          IF(M2 .EQ. 0) GO TO 76
          DO 75 J=I1,I3
75        SUM=SUM+0.5*(RM2(J)+RM2(J+1))*(Z(J+1)-Z(J))
          GO TO 77
76        SUM=Z(I2)-Z(I1)
77         DENOLD=DENOLD+SUM
          I=I+1
          ZAXIS(I)=Z(I2)
          BFNM(I)=FNUM/DENOLD
          I1=INTER+I1
          I2=INTER+I2
          IF(I .LT. 54) GO TO 61
          WRITE(11,54) (ZAXIS(I),BFNM(I),I=1,54)
C  <SAGHER>CORREL.FOR;1    TUE 21-DEC-76 3:15PM                    PAGE 1:2

54        FORMAT(1H ,'Z,BFNM'/(2E17.8))
          OPEN(UNIT=12,DEVICE='DSK',FILE='BFNM.DAT')
          CALL PLOTF(30,12)
          CALL CPLOT1(1,ZAXIS,7.0,IXAXIS,1,54,BFNM,6.0,IYAXIS,4)
          CALL PLOT(0.0,0.0,999)
          CALL SYMBOL(5.0,8.00,0.1,IPROG,0.0,10)
          CALL SYMBOL(5.0,7.75,0.1,IDATE,0.0,12)
          CALL SYMBOL(5.0,7.50,0.1,IBAR0,0.0,6)
          CALL NUMBER(6.2,7.50,0.1,BAR0,0.0,4)
          CALL SYMBOL(5.0,7.25,0.1,IGAMC,0.0,7)
          CALL NUMBER(6.2,7.25,0.1,GAMMA,0.0,4)
          CALL SYMBOL(5.0,7.00,0.1,IZSUBE,0.0,3)
          CALL NUMBER(6.2,7.00,0.1,ZSUBE,0.0,5)
          CALL SYMBOL(5.0,6.75,0.1,IRSUBA,0.0,3)
          CALL NUMBER(6.2,6.75,0.1,RA,0.0,4)
          CALL SYMBOL(5.0,6.50,0.1,ILOVLM,0.0,9)
          CALL NUMBER(6.4,6.50,0.1,LOVLAM,0.0,4)
          CALL SYMBOL(5.0,6.25,0.1,IDTH,0.0,8)
          CALL NUMBER(6.4,6.25,0.1,DTETA,0.0,5)
          CALL PLOT(0.0,0.0,999)
          CALL PLOT(8.5,0.0,-3)
          GO TO 81
1000      WRITE(6,1001)
1001       FORMAT(1H ,'BESSEL FUNCTION DID NOT CONVERGE')
81        STOP
          END

:  <SAGHER>P20Y40.DAT;2    TUE 21-DEC-76 11:56AM                  PAGE 1

 PROGRAM #2,DC EQ. EXACT RELATIVISTIC,NO SPACE CHARGE
 DEC. 17,1976
 R= 0.10000000E+01  THETA= 0.00000000E+00  Z= 0.00000000E+00
   DR= 0.00000000E+00  DTHETA= 0.75522911E-02  DZ= 0.39688436E+00
   BAR0= 0.74500000E+00  GAMMAC= 0.20845330E+00  ZSUBE= 0.15707960E+01
   FGHZ= 0.94000000E+02  VKV= 0.30000000E+03  C= 0.88500000E+00
   SCRIPR= 0.23300000E+01  B0= 0.70000000E+04  SRA= 0.30867352E-02
   L= 0.62379600E-02  RA= 0.31091140E+01

 X= .00000000E+00 H= 0.10000000E-01 Z-DZ*T= 0.00000000E+00
```

BEST AVAILABLE COPY

I	Y	DY
1	0.10000000E+01	0.00000000E+00
2	0.00000000E+00	0.75522911E-02
3	0.00000000E+00	0.39688436E+00
4	0.00000000E+00	-0.93491184E-03
5	0.75522911E-02	0.58287609E-02
6	0.39688436E+00	-0.19749332E-03

X= .30100009E+01 H= 0.20000000E-01 Z-DZ*T=-0.12814403E-02

I	Y	DY
1	0.99227383E+00	-0.61367165E-02
2	0.45076448E-01	0.20036984E-01
3	0.11933409E+01	0.39604020E+00
4	-0.61367165E-02	-0.28546694E-02
5	0.20036984E-01	0.12729206E-02
6	0.39604020E+00	-0.18067657E-03

X= .60099995E+01 H= 0.20000000E-01 Z-DZ*T=-0.38232803E-02

I	Y	DY
1	0.96138408E+00	-0.13880997E-01
2	0.59618902E-01	0.12657683E-01
3	0.23814515E+01	0.39624741E+00
4	-0.13880997E-01	-0.17328177E-02
5	0.12657683E-01	-0.59192291E-02
6	0.39624741E+00	0.21269948E-03

X= .90099967E+01 H= 0.20000000E-01 Z-DZ*T=-0.52405000E-02

I	Y	DY
1	0.91627485E+00	-0.14743042E-01
2	0.10547778E+00	-0.94416578E-02
3	0.35706863E+01	0.39635651E+00
4	-0.14743042E-01	0.10979157E-02
5	-0.94416578E-02	-0.72604328E-02
6	0.39635651E+00	-0.18041985E-03

X= .12009994E+02 H= 0.20000000E-01 Z-DZ*T=-0.76680779E-02

I	Y	DY
1	0.87981608E+00	-0.88612827E-02
2	0.51925240E-01	-0.23172108E-01
3	0.47583107E+01	0.39590259E+00
4	-0.88612827E-02	0.25010798E-02
5	-0.23172108E-01	-0.12227018E-02
6	0.39590259E+00	0.19867318E-04

X= .15009991E+02 H= 0.20000000E-01 Z-DZ*T=-0.98714828E-02

I	Y	DY
1	0.88442641E+00	-0.16592925E-02
2	-0.12550914E-01	-0.16687422E-01
3	0.59473592E+01	0.39653923E+00
4	-0.16592925E-02	0.19825988E-02
5	-0.16687422E-01	0.48781494E-02
6	0.39653923E+00	0.28969924E-03

X= .18009988E+02 H= 0.20000000E-01 Z-DZ*T=-0.99866590E-02

I	Y	DY
1	0.88573479E+00	0.16512177E-02
2	-0.38973549E-01	-0.14778663E-02
3	0.71378960E+01	0.39700252E+00
4	0.16512177E-02	0.20090345E-03
5	-0.14778663E-02	0.38357002E-02
6	0.39700252E+00	0.17556169E-04

X= .21009985E+02 H= 0.20000000E-01 Z-DZ*T=-0.96503225E-02

APPENDIX B

DERIVATION OF SMALL SIGNAL RELATIVISTIC GAIN PARAMETER

The derivation presented here parallels that given by Bacon, Enderby, and Phillips (herein denoted as the "G. E. work"). * Because the derivation is given in detail in the reference cited, we have abbreviated the presentation here to emphasize only the main differences due to relativistic corrections.

The derivation begins with the relativistically correct force equation. **

$$\frac{d(m\vec{v})}{dt} = \vec{f}(\text{vector force}) = e(\vec{E} + \vec{v} \times \vec{B}) \tag{1}$$

Treating mass as a variable, we can differentiate to obtain

$$\frac{d(m\vec{v})}{dt} = \left(\frac{dm}{dt}\right)\vec{v} + m\frac{d\vec{v}}{dt} = e(\vec{E} + \vec{v} \times \vec{B}) \tag{2}$$

From the special theory of relative relativity, dm/dt can be expressed in terms of the three-vector force and velocity to be**

$$\frac{dm}{dt} = \frac{1}{c^2}(\vec{f} \cdot \vec{v}) = \frac{e}{c^2}(\vec{E} \cdot \vec{v} + \vec{v} \times \vec{B} \cdot \vec{v}) = \frac{e}{c^2}(\vec{E} \cdot \vec{v}) \tag{3}$$

---

*L. C. Bacon, E. E. Enderby, and R. M. Phillips, "V-Band Ubitron Amplifier Development," prepared by G. E. Company under Contract AF 33(616)-8356, April 1962.

**W. Rindler, Special Relativity, Oliver & Boyd, London, 1966, p. 95.

Putting this into equation 2 and solving for dv/dt gives

$$\frac{d\vec{v}}{dt} = \frac{e}{m}\left[\vec{E} + \vec{v} \times \vec{B} - \left(\frac{\vec{E}\cdot\vec{v}}{c^2}\right)\vec{v}\right] \tag{4}$$

This relativistically correct equation shows the added effects of a new force term expressed in terms of the field quantities.

If we now express relativistic mass in terms of velocity,

$$\left(\text{i.e.}\quad m = m_o\left(1 - \frac{\vec{v}\cdot\vec{v}}{c^2}\right)^{-1/2} \equiv \gamma m_o\right)$$

equation (4) takes the final form

$$\frac{d\vec{v}}{dt} = \frac{e}{\gamma m_o}\left(\vec{E} + \vec{v} \times \vec{B} - \frac{1}{c^2}(\vec{E}\cdot\vec{v})\,\vec{v}\right) \tag{5}$$

This equation is the beginning point for the small signal derivation. Note that if $\vec{E}$ and $\vec{B}$ are parallel to $\vec{v}$, that the equation reduces to

$$\frac{d\vec{v}_{\parallel}}{dt} = \frac{e}{\gamma m_o}\,\vec{E}_{\parallel}\left(1 - \frac{v_{\parallel}^2}{c^2}\right) = \frac{e}{\gamma^3 m_o}\,\vec{E}_{\parallel}$$

and if $\vec{E}$ is transverse to $\vec{v}$ we get

$$\frac{d\vec{v}_{\perp}}{dt} = \frac{e}{\gamma m_o}\,(\vec{E}_{\perp} + \vec{v} \times \vec{B})$$

This illustrates the concepts of "longitudinal" and "transverse mass" where the "effective mass" is $\gamma^3 m_o$ and γm_o respectively. In general, however, when both longitudinal and transverse forces are present, equation (5) must be used to determine the applicable relativistic corrections.

In the planar model used in the G. E. work, the following field variables are assumed to exist

$$\vec{v} = v_y \hat{y} + v_z \hat{z} \tag{6}$$

$$\vec{E} = E_y y$$

$$\vec{B} = B_x \hat{x}$$

Of these field variables $\vec{v}$ is assumed to have both dc and ac components, $\vec{E}$ is only an ac variable, and $\vec{B}$ is only a dc variable with sinusoidal variations in z. The electron beam is assumed to be travelling in the $\hat{z}$ direction. ($\hat{x}$, $\hat{y}$ and $\hat{z}$ are unit vectors in a rectangular coordinate system.)

Using these field variables, in equation (5) we get the following $\hat{y}$ and $\hat{z}$ component equations.

$$\ddot{y} = \frac{\eta}{\gamma}\left(E_y + v_z B_x - \frac{E_y v_y^2}{c^2}\right) \tag{7}$$

$$\ddot{z} = \frac{\eta}{\gamma}\left(- v_y B_x - \frac{E_y v_y v_z}{c^2}\right) \tag{8}$$

(Each dot over a variable indicates differentiation with respect to time. $\dot{y} = dy/dt$, $\ddot{y} = d^2y/dt^2$, etc.) Consistent with the G. E. work, we neglect all terms which are of order $(v_y/v_z)^2$, the ratio of the transverse to longitudinal velocity.

$$\text{i.e.} \left(\frac{v_y}{v_z}\right)^2 \ll 1$$

Thus the third term on the RHS of equation (7) can be neglected. (The effects of this term have been carried through the complete derivation and shown to be negligible.)

We now multiply equation (7) by $\dot{y}$ and equation (8) by $\dot{z}$ and add the resulting equations to eliminate the B_x terms. The result is

$$\dot{y}\,\ddot{y} + \dot{z}\,\ddot{z} = \frac{\eta E_y \dot{y}}{\gamma^3} \tag{9}$$

where we have used

$$\gamma^{-2} \simeq \left(1 + \frac{v_z^2}{c^2}\right), \left(\text{i.e.} \quad v^2 = v_z^2\left(1 + \frac{v_y^2}{v_z^2}\right) \simeq v_z^2\right).$$

Recognizing the LHS of equation (9) as $v\dot{v}$, and separating equation (9) into dc and ac parts we get the following ac small-signal relationship.

$$v_o \tilde{\dot{v}} = \frac{\eta \tilde{E}_y \dot{y}_o}{\gamma^3} \tag{10}$$

Here we have used the usual small-signal linearization technique of neglecting terms which are products of ac variables. (ac variables are designated by "~", and dc variables are designated by the subscript "o".)

AD-A040 043 HUGHES RESEARCH LABS MALIBU CALIF F/G 9/5
MILLIMETER WAVE UBITRON DEVELOPMENT PHASE I.(U)
APR 77 J M BAIRD, S SENSIPER, K AMBOSS F30602-76-C-0215
UNCLASSIFIED RADC-TR-77-133 NL

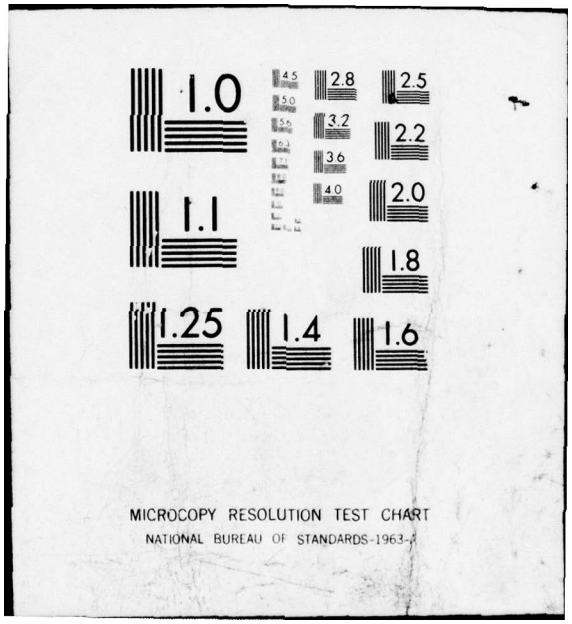
4 OF 4
AD
A040043





END

DATE
FILMED
6-77


1.0
1.1
1.25
1.4
1.6
1.8
2.0
2.2
2.5
2.8
3.2
3.6
4.0
4.5
5.0
5.6
6.3
MICROCOPY RESOLUTION TEST CHART
NATIONAL BUREAU OF STANDARDS-1963-A

The variable $\dot{y}_o$ on the RHS of equation (10) exists because the dc magnetic field is a sinusoidally varying function of space. This is obtained from the dc part of equation (7)

$$\ddot{y}_o = \frac{\eta}{\gamma} v_{zo} B_x$$

If we define $B_x = B_1 \cos \beta_m z$ and integrate this equation once we get for $\dot{y}_o$

$$\dot{y}_o = \frac{\eta B_1}{\gamma} \int \cos \beta_m z \frac{dz}{dt} dt = \frac{\eta B_1}{\gamma \beta_m} \sin \beta_m z \qquad (11)$$

Substitution of $\dot{y}_o$ from equation (11) into equation (10) and subsequent division by v_o gives a differential equation relating the time derivative of the ac velocity $\tilde{v}$ and the ac electric field $\tilde{E}_y$.

$$\dot{\tilde{v}} = \frac{\eta \tilde{E}_y}{\gamma^3} \left(\frac{\eta B_1}{\gamma v_o \beta_m} \right) \sin \beta_m z \equiv \frac{\eta \tilde{E}_y}{\gamma^3} \Lambda \sin \beta_m z \qquad (12)$$

The definition of Λ in this equation can be shown to be the ratio of the peak transverse dc velocity to the longitudinal dc velocity v_o. Thus, terms of order

$$\Lambda^2 \simeq \left(\frac{v_y(\text{peak})}{v_z} \right)^2$$

are neglected in this small-signal derivation.

Using the relationship $(v_y/v_z)^2 \ll 1$, the current continuity equation becomes

$$\frac{\partial \tilde{i}}{\partial z} = - j\omega\tilde{\rho} \tag{13}$$

where the time variation is assumed to be $\partial/\partial t = j\omega$, $\tilde{i}$ is the ac current density in the beam, and $\tilde{\rho}$ is the ac space charge density. Using this in the small-signal, linearized definition of current density

$$\tilde{i} = \rho_o \tilde{v} + v_o \tilde{\rho} \tag{14}$$

we get the following relationship between the ac velocity and current.

$$\tilde{v} = \frac{1}{j\beta_e \rho_o}\left(\frac{\partial}{\partial z} + j\beta_e\right) \tilde{i} \equiv \frac{1}{j\beta_e \rho_o} D_1 \tilde{i} \tag{15}$$

The differential operator D_1 defined by this equation is $D_1 \equiv \partial/\partial z + j\beta_e$.

Expanding the total differential with respect to time in equation (12) as

$$\frac{d}{dt} \cong \frac{\partial}{\partial t} + v_o \frac{\partial}{\partial z} = v_o\left(\frac{\partial}{\partial z} + j\beta_e\right) = v_o D_1$$

and substituting from equation (15) for $\tilde{v}$, we get the electronic equation relating small signal current and electric field

$$D_1^2 \tilde{i} = \frac{j\beta_e}{\gamma^3}\left(\frac{\eta\rho_o}{v_o}\right)(\Lambda \sin \beta_m z)\, \tilde{E}_y \tag{16}$$

To put this equation into final form, we now re-write the factor $(\eta\rho_o/v_o)$ in terms of the dc beam current I_o and voltage V_o. This is done by recognizing

$$\frac{\eta\rho_o}{v_o} = \frac{e\,\rho_o v_o}{m_o v_o^2} = -\frac{|e|\,I_o}{m_o v_o^2} \tag{17}$$

Then from the relativistic definition of kinetic energy

$$|e|\,V_o = m_o c^2(\gamma - 1) \tag{18}$$

we get

$$m_o v_o^2 = m_o c^2\left(\frac{\gamma^2 - 1}{\gamma^2}\right) = \frac{m_o c^2(\gamma - 1)(\gamma + 1)}{\gamma^2} = |e|\,V_o\left(\frac{\gamma + 1}{\gamma^2}\right) \tag{19}$$

Thus,

$$\frac{\eta\rho_o}{v_o} = -\frac{I_o}{\left(\frac{\gamma + 1}{\gamma^2}\right)V_o} \equiv -\left(\frac{\gamma^2}{\gamma + 1}\right)\frac{1}{R_o} \tag{20}$$

and the final form of the electronic equation is

$$D_1\,\tilde{i} = -\left(\frac{j\beta_e\,\Lambda \sin\beta_m z}{\gamma(\gamma + 1)\,R_o}\right)\,\tilde{E}_y \tag{21}$$

where R_o is the beam impedance, $R_o = V_o/I_o$.

Equation (21) differs from the G. E. work in the following three ways. (1) The dc velocity in the β_e and Λ factors must be the relativistic velocity, (2) as shown by equation (12), the definition of Λ has an additional factor of $1/\gamma$ as compared to the G. E. work, and (3) the RHS of equation (21) is multiplied by the additional factor of $2/\gamma(\gamma + 1)$.

The rf circuit equation derived in the G. E. work is unaltered by relativistic effects and therefore the derivation will not be repeated here. This circuit equation is

$$D_2 \tilde{E}_y \equiv \left(\frac{\partial^2}{\partial z^2} + \beta_o^2 \right) \tilde{E}_y = j\beta_o K i_y \tag{22}$$

where D_2 is the differential operator $D_2 \equiv \partial^2/\partial z^2 + \beta_o^2$, β_o is the circuit propagation constant, and K is an arbitrary coupling constant between the transverse current density $\tilde{i}_y$ and the rf electric field $\tilde{E}_y$.

Because the circuit equation is in terms of the transverse ac current density $\tilde{i}_y$ and the electronic equation (21) is in terms of the total ac current density $\tilde{i}$, it is now necessary to determine the relationship between these two variables. This is done by using the approximate relationship

$$i_y \cong i \frac{\dot{y}}{\dot{z}} \cong (I_o + \tilde{i})(\dot{y}_o + \tilde{y})/v_o \tag{23}$$

which is true for the case of $(\dot{y}/\dot{z})^2 \ll 1$.

A small-signal linearization of equation (23) gives an ac part

$$\tilde{i}_y = \frac{I_o \tilde{\dot{y}}}{v_o} + \frac{\dot{y}_o \tilde{i}}{v_o} \tag{24}$$

An expression for y_o in this equation has already been derived in equation (11), but we must return to equation (7) to obtain an expression for $\tilde{\dot{y}}$.

The small signal portion of equation (7) (again neglecting the third term on the RHS because $(v_y/v_z)^2 \ll 1$) is as follows.

$$\tilde{\ddot{y}} = \frac{\eta}{\gamma} \left(\tilde{E}_y + B_x \tilde{v}_z\right) \tag{25}$$

The desired expression for $\tilde{\dot{y}}$ can be obtained by integrating this equation in time, with the following result.

$$\tilde{\dot{y}} = v_o \Lambda \sin \beta_m z + \frac{\eta}{\gamma} \int \tilde{E}_y \, dt \tag{26}$$

Putting equations (11) and (26) into equation (24), and taking the total derivative with respect to time (to eliminated the integral) gives the desired relationship between $\tilde{i}_y$ and $\tilde{i}$.

$$D_1 \tilde{i}_y = \Lambda D_1(\tilde{i} \sin \beta_m z) - \left(\frac{\gamma}{\gamma + 1}\right) \frac{1}{R_o} \tilde{E}_y \tag{27}$$

In equation (27) we have again used the relativistic definition of kinetic energy (equation 19) to eliminate $m_o v_o^2$ from the second term on the RHS.

Combining equations (22) and (27) to eliminate $\tilde{i}_y$ we get the final circuit equation

$$\left[D_1 D_2 + \frac{j\beta_o K}{R_o} \left(\frac{\gamma}{\gamma + 1}\right)\right] \tilde{E}_y = j\beta_o K \Lambda D_1(\tilde{i} \sin \beta_m z) \tag{28}$$

This equation, combined with the electronic equation (21)

$$D_1^2 \tilde{i} = - \frac{j\beta_e \Lambda \sin \beta_m z}{\gamma(\gamma + 1) R_o} \tilde{E}_y \tag{21}$$

gives a relativistic, small-signal description of the Ubitron neglecting space charge.

Equations (21) and (28) are a fifth-order set of differential equations with periodic coefficients. The procedure for solving these equations is identical to that given in the G. E. work and will not be repeated here in detail. Basically it requires choosing a form for the solutions which satisfies Floquet's theorem* for periodic structures, and then substituting and averaging over one period. The result is a dispersion relationship given by

$$\xi^2 \left[2j\Delta - \frac{A_2}{\beta_o(\beta_e - \beta_o)} \right] = - \frac{A_1 A_3}{4\beta_o} \tag{29}$$

where

$$A_1 = - \frac{\beta_e \Lambda}{\gamma(\gamma + 1) R_o}$$

$$A_2 = - \frac{\beta_o K}{R_o} \left(\frac{\gamma}{\gamma + 1} \right) \tag{30}$$

$$A_3 = \beta_o K \Lambda$$

---

*C C. Johnson, Field and Wave Electrodynamics, McGraw-Hill, N. Y., 1965, pp. 244-245.

and ξ and Δ come from the assumed form of the solutions

$$i = \mathscr{I}\, e^{-j\beta_e z - \xi z}$$

$$E_y = \mathscr{E}\, e^{-j\beta_e z - \Delta z} \tag{31}$$

With the further definitions

$$C_u^3 \equiv \frac{K' \Lambda^2}{16 R_o} \left(\frac{2}{\gamma(\gamma + 1)}\right)$$

$$K' \equiv \frac{K}{\beta_e^2}$$

$$\xi \equiv -\beta_e C_u \delta \tag{32}$$

$$\Delta \equiv -\beta_e C_u \varepsilon$$

$$jb \equiv \varepsilon - \delta$$

$$b' \equiv b + \frac{4C_u^2 \gamma^2}{\Lambda^2} \left(\frac{\beta_e}{\beta_o - \beta_e}\right)$$

equation (29) can be rewritten in the familiar TWT form for conditions of zero-loss, zero-space-charge, and small-C.

$$\delta^3 + jb'\delta^2 + j = 0 \tag{33}$$

As in the case of the TWT, equation (33) provides small-signal solutions for the propagation and gain (or attenuation) of the three forward waves in the Ubitron. The other two waves are not important for the amplifier case being considered here.

One remaining definition needs to be given here for completeness. The variable K' in the definitions (32) is the interaction impedance of the Ubitron. Its value is given by

$$K' = \frac{E_y^2}{2\beta_e^2 P} \tag{34}$$

where E_y is the peak value of the transverse electric field and P is the power being carried by the circuit.

A summary of the relativistically correct, small-signal Ubitron parameters is given in Table I along with the corresponding TWT and non-relativistic parameters from the G. E. work. The comparison shows that for large beam voltages (i. e. large γ) that the gain parameter C is reduced by a relatively large factor from the classical values.

When all of the relativistic factors shown in Table 1 are combined in the evaluation of the small-signal gain parameter C_u, we get the following results.

$$C_u^3(\text{relativistic}) = C_u^3(\text{classical}) \times \frac{2}{\gamma^3(\gamma + 1)}$$

The relativistic factor on the RHS of this equation has been plotted as a function of voltage in Figure 1.

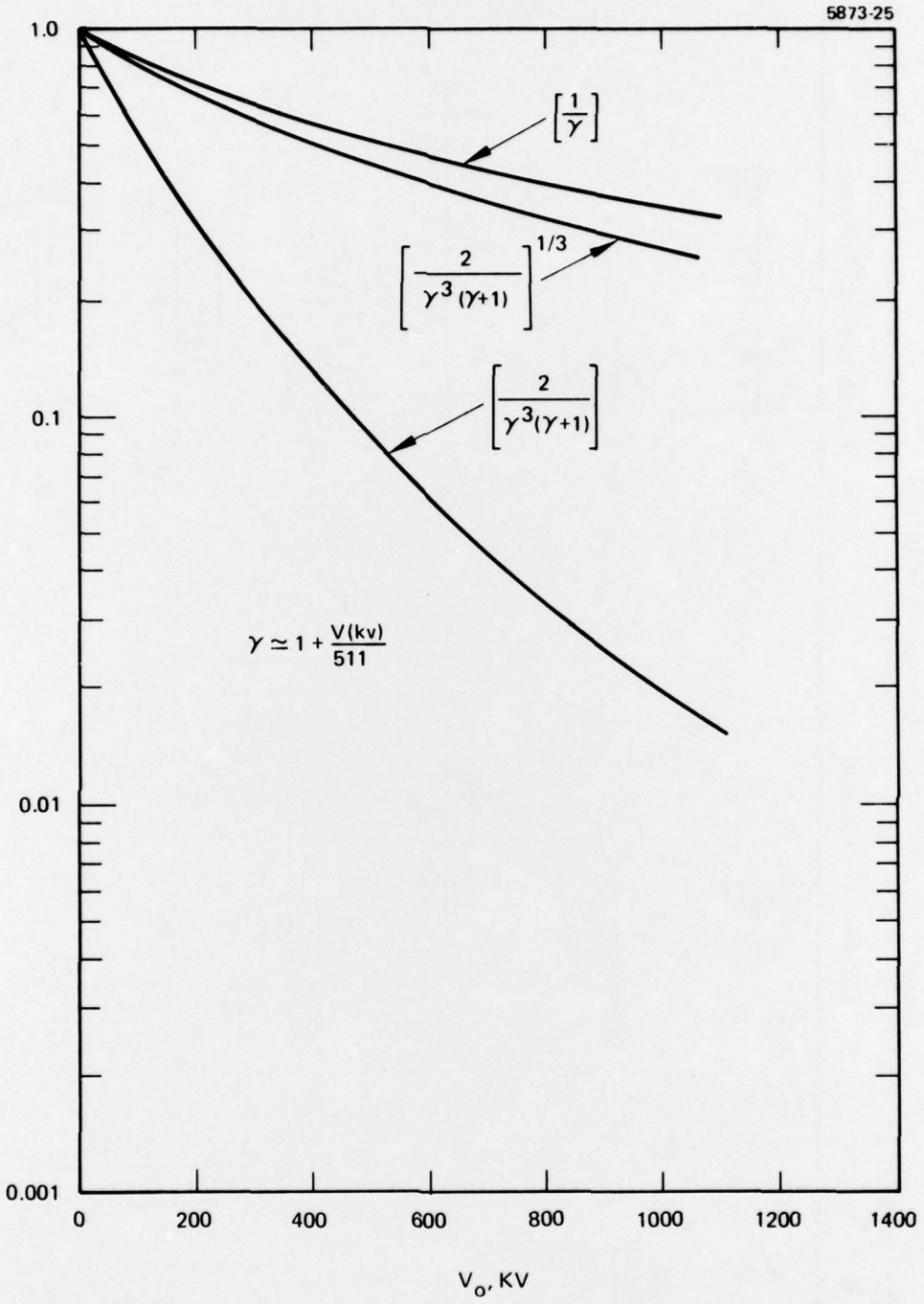


Figure 1. Plots of relativistic correction factors associated with C^3 and C compared to $1/\gamma$.

Table I. Comparison of Small Signal Parameters for TWT, Classical Ubitron and Relativistic Ubitron (Planar Geometry)

TWT	Classical Ubitron	Relativistic Ubitron
$C^3 = \frac{K}{4R_o}$	$C_u^3 = \frac{K' \Lambda^2}{16 R_o}$	$C_u^3 = \frac{K' \Lambda^2}{16 R_o} \left(\frac{2}{\gamma(\gamma + 1)}\right)$
$K = \frac{E_z^2}{2\beta_o^2 P}$	$K' = \frac{E_y^2}{2\beta_e^2 P}$	$K' = \frac{E_y^2}{2\beta_e^2 P}$
$b = b$	$b' = b + \frac{4C^2}{\Lambda^2}\left(\frac{\beta_e}{\beta_o - \beta_e}\right)$	$b' = b + \frac{4C_u^2\gamma^2}{\Lambda^2}\left(\frac{\beta_e}{\beta_o - \beta_e}\right)$
	$\Lambda = \frac{\eta B_1}{\beta_m v_o}$	$\Lambda = \frac{\eta B_1}{\beta_m v_o}\left(\frac{1}{\gamma}\right)$
		$v_o = c\left(\frac{\sqrt{\gamma^2 - 1}}{\gamma}\right)$
		$\beta_e = \frac{\omega}{c}\left(\frac{\gamma}{\sqrt{\gamma^2 - 1}}\right)$

APPENDIX C

MATHEMATICAL DESCRIPTION OF PERIODIC MAGNETIC FIELDS

One of the outputs of the magnetic analysis computer code used during this program is the magnetic field on the axis. This field can be used to describe the magnetic field throughout the region of the electron beam. In the following we outline the derivation of the mathematical relationships which have been used in this work.

Because both the divergence and the curl of the vector magnetic field $\vec{B}$ are zero throughout the volume of interest, B must satisfy the equation $\nabla^2 \vec{B} = 0$.

If azimuthal symmetry is assumed, this becomes

$$\nabla^2 (B_r \hat{r}) = 0$$

and

$$\nabla^2 (B_z \hat{z}) = 0$$

where $\hat{r}$ and $\hat{z}$ are unit vectors in a cylindrical coordinate system (r, θ, z). Using the relationship $\nabla^2 \hat{r} = -\hat{r}/r^2$ and separating the variables into

$$B_r(r, z) = R_r(r)\, R_z(z) \tag{1}$$

$$B_z(r, z) = Z_r(r)\, Z_z(z) \tag{2}$$

gives the following set of differential equations.

$$\frac{d^2 R_{zn}}{dz^2} + \gamma_n^2 R_{zn} = 0 \tag{3}$$

$$\frac{d^2 R_{rn}}{dr^2} + \frac{1}{r}\frac{dR_{rn}}{dr} - \left(\gamma_n^2 + \frac{1}{r^2}\right) R_{rn} = 0 \tag{4}$$

$$\frac{d^2 Z_{zn}}{dz^2} + \gamma_n^2 Z_{zn} = 0 \tag{5}$$

$$\frac{d^2 Z_{rn}}{dr^2} + \frac{1}{r}\frac{dZ_{rn}}{dr} - \gamma_n^2 Z_{rn} = 0 \tag{6}$$

These equations were obtained by using the separation constant γ_n^2 which is related to the magnetic period length L by the relationship

$$\gamma_n = \frac{2\pi n}{L} \tag{7}$$

General solutions for equations (3) through (6) are as follows. For the case of $\gamma_o = 0$ we get

$$\begin{aligned} Z_{zo}(z) &= A_{zo} + B_{zo} z \\ R_{ro}(r) &= A_{ro} r + \frac{B_{ro}}{r} \\ Z_{zo}(z) &= C_{zo} + D_{zo} z \\ Z_{ro}(r) &= C_{ro} + D_{ro} \ln r \end{aligned} \tag{8}$$

For $\gamma_n \neq 0$

$$
\begin{aligned}
R_{zn}(z) &= A_{zn} \cos(\gamma_n z) + B_{zn} \sin(\gamma_n z) \\
R_{rn}(r) &= A_{rn} I_1(\gamma_n r) + B_{rn} K_1(\gamma_n r) \\
Z_{zn}(z) &= C_{zn} \cos(\gamma_n z) + D_{zn} \sin \gamma_n(z) \\
Z_{rn}(r) &= C_{rn} I_o(\gamma_n r) + D_{rn} K_o(\gamma_n r)
\end{aligned}
\tag{9}
$$

where $I_i(\gamma_n r)$ and $K_i(\gamma_n r)$ are modified Bessel functions of the first and second kinds.

The final solutions for the magnetic field are obtained as follows. First, the field components from equations (1), (2), (8), and (9) are found for each γ_n and all terms which are either infinite at the axis or do not satisfy Maxwell's equations are eliminated.

The field components can then be summed to provide a complete description of the magnetic field in terms of the axial Fourier coefficients B_n and the periodicity L. The final result is as follows.

$$
B_z(r, z) = B_o + \sum_{n=1}^{\infty} B_n I_o(\gamma_n r) \cos[\gamma_n(z - z_n)] \tag{10}
$$

$$
B_r(r, z) = - \sum_{n=1}^{\infty} B_n I_1(\gamma_n r) \sin[\gamma_n(z - z_n)] \tag{11}
$$

Here, B_o is a constant axial magnetic field, B_n is the peak amplitude of the nth harmonic at the axis (r = 0), $\gamma_n = 2\pi n/L$ (L = magnetic period length), and z_n is the position of the peak axial field of the nth harmonic.

An alternative formulation which is useful for computational purpose is

$$B_z(r, z) = B_o + \sum_{n=1}^{\infty} I_o(\gamma_n r)[B_{cn} \cos(\gamma_n z) + B_{sn} \sin(\gamma_n z)] \tag{12}$$

$$B_r(r, z) = - \sum_{n=1}^{\infty} I_1(\gamma_n r)[B_{cn} \sin(\gamma_n z) - B_{sn} \cos(\gamma_n z)] \tag{13}$$

The relationships between constants in the two different formulations are

$$\begin{aligned} B_{cn} &= B_n \cos \gamma_n z_n \\ B_{sn} &= B_n \sin \gamma_n z_n \end{aligned} \tag{14}$$

and

$$\begin{aligned} B_n &= \sqrt{B_{cn}^2 + B_{sn}^2} \\ Z_n &= \frac{1}{\gamma_n} \tan^{-1}\left(\frac{B_{sn}}{B_{cn}}\right) \end{aligned} \tag{15}$$

The procedure for using the above mathematical formulation in Ubitron analysis is as follows. A magnetic circuit is designed and optimized using the magnetic circuit analysis computer code. The resulting tabulated function of axial magnetic field is then Fourier analyzed to give the B_{cn}, and B_{sn} harmonic amplitudes for the first few harmonic components. Finally, these amplitudes are used in equations (10) through (15) to determine the magnetic field for use in the beam and rf analysis. Thus, realistic periodic magnetic fields are used to determine beam focusing and rf gain for Ubitron design.

METRIC SYSTEM

BASE UNITS:

Quantity	Unit	SI Symbol	Formula
length	metre	m	...
mass	kilogram	kg	...
time	second	s	...
electric current	ampere	A	...
thermodynamic temperature	kelvin	K	...
amount of substance	mole	mol	...
luminous intensity	candela	cd	...

SUPPLEMENTARY UNITS:

plane angle	radian	rad	...
solid angle	steradian	sr	...

DERIVED UNITS:

Acceleration	metre per second squared	...	m/s
activity (of a radioactive source)	disintegration per second	...	(disintegration)/s
angular acceleration	radian per second squared	...	rad/s
angular velocity	radian per second	...	rad/s
area	square metre	...	m
density	kilogram per cubic metre	...	kg/m
electric capacitance	farad	F	A·s/V
electrical conductance	siemens	S	A/V
electric field strength	volt per metre	...	V/m
electric inductance	henry	H	V·s/A
electric potential difference	volt	V	W/A
electric resistance	ohm		V/A
electromotive force	volt	V	W/A
energy	joule	J	N·m
entropy	joule per kelvin	...	J/K
force	newton	N	kg·m/s
frequency	hertz	Hz	(cycle)/s
illuminance	lux	lx	lm/m
luminance	candela per square metre	...	cd/m
luminous flux	lumen	lm	cd·sr
magnetic field strength	ampere per metre	...	A/m
magnetic flux	weber	Wb	V·s
magnetic flux density	tesla	T	Wb/m
magnetomotive force	ampere	A	...
power	watt	W	J/s
pressure	pascal	Pa	N/m
quantity of electricity	coulomb	C	A·s
quantity of heat	joule	J	N·m
radiant intensity	watt per steradian	...	W/sr
specific heat	joule per kilogram-kelvin	...	J/kg·K
stress	pascal	Pa	N/m
thermal conductivity	watt per metre-kelvin	...	W/m·K
velocity	metre per second	...	m/s
viscosity, dynamic	pascal-second	...	Pa·s
viscosity, kinematic	square metre per second	...	m/s
voltage	volt	V	W/A
volume	cubic metre	...	m
wavenumber	reciprocal metre	...	(wave)/m
work	joule	J	N·m

SI PREFIXES:

Multiplication Factors	Prefix	SI Symbol
1 000 000 000 000 = 10^{12}	tera	T
1 000 000 000 = 10^{9}	giga	G
1 000 000 = 10^{6}	mega	M
1 000 = 10^{3}	kilo	k
100 = 10^{2}	hecto*	h
10 = 10^{1}	deka*	da
0.1 = 10^{-1}	deci*	d
0.01 = 10^{-2}	centi*	c
0.001 = 10^{-3}	milli	m
0.000 001 = 10^{-6}	micro	μ
0.000 000 001 = 10^{-9}	nano	n
0.000 000 000 001 = 10^{-12}	pico	p
0.000 000 000 000 001 = 10^{-15}	femto	f
0.000 000 000 000 000 001 = 10^{-18}	atto	a

* To be avoided where possible.